PSL UNIVERSITÉ PARIS

THÈSE DE DOCTORAT
DE L'UNIVERSITÉ PSL

Préparée à l'École Pratique des Hautes Études

# Accretion récifale, protection côtière et fonctionnement récifal face aux changements globaux

# Reef accretion, coastal protection and reef functioning in the face of global change


Soutenue par
**Jérémy T. Carlot**
Le 09 Décembre 2021


École doctorale n° 472
**École doctorale de l'École Pratique des Hautes Études**

Spécialité
**67 - Biologie des populations et écologie**

Composition du jury :

| | |
|---|---|
| Jean-Pierre Gattuso<br>Directeur de recherches, CNRS | *Président* |
| Joaquim Garrabou<br>Directeur d'études, CSIC | *Rapporteur* |
| Fanny Houlbreque<br>Chargée de recherches, IRD | *Rapporteuse* |
| Lucie Penin<br>Maitresse de conférences, IRD | *Examinatrice* |
| Lorenzo Bramanti<br>Chargé de recherches, CNRS | *Invité* |
| Maggy Nugues<br>Maitresse de conférences, EPHE | *Invitée* |
| Laetitia Hedouin<br>Chargée de recherches, CNRS | *Co-directrice de thèse* |
| Valeriano Parravicini<br>Directeur d'études, EPHE | *Directeur de thèse* |

École Pratique des Hautes Études | PSL

# Reef accretion, coastal protection and reef functioning in the face of global change

Jeremy Carlot

‘Cause the most important is not who you are,
but who you’ve chosen to be.
Quentin Postel

# Acknowledgements

First of all, I would like to thank my supervisor, Valeriano Parravicini, without whom none of this would have been possible. I still remember our first meeting during my MSc thesis. During these last six years, you have always been there, present, for any problem, no matter how small. During the field, calling the fishermen because the boat was drifting away. During the collaboration set up in England, when my English understanding was so insignificant that I could not even understand "Was it useful?". It feels odd to end this adventure after so many years. Thank you for everything. I would also like to thank my co-director Laetitia Hédouin, without whom the setting up of my *in situ* studies could never have started. Thank you for having spent several evenings sewing these plastic sheets to build incubation chambers. Thank you also for the time spent in French Polynesia to teach me coral taxonomy. I particularly remember a post-larvae evening with Héloïse. It seems so far away but remains engraved. Thank you.

Of course, during this thesis, I was assisted by a wonderful team. Although this team focused on fish (nobody is perfect) while I focused on corals, you were always very supportive and helpful. Of course, my thesis would not be what it is without my roommate/work colleague Nina Schiettekatte. Just like Valé, I can't tell you how much I thank you enough through this paragraph. You have been an inspiration throughout my thesis, and your skills are terrific. I am sure you will become a great researcher, and I wish you all the best in Hawaii. Of course, I would like to thank Simon Brandl and Jordan Casey as well. You guys are amazing. I have learned so much, especially by writing with you. Thank you so much for the time you took to help me with proofreading, conceptualizing, or doing extra activities (looking for mushrooms was great, and I wish we did it more with you guys). Of course, I would like to thank Alexandre Mercière. The field would not have been the same without you. I naturally keep in mind the moray eel attack during the fish catching with the clove oil. Now that you have the position, I have every intention of coming back and having a barbecue on this dear motu. Finally, my thanks also go to Fabien Morat. Your thoughtful advice has constantly improved my thinking and I thank you very much for the advice on coral cuttings. I would also like to thank my co-authors who helped me throughout my thesis: Mehdi, Alessio, Manu, Diego, Hunter, Maggy, Ulisse et *al*.

My thanks also go to the whole Mo'orea staff. The first thanks go to Yann and Adeline. Thank you for having stood by me in the field, in my early days,

patience was needed. I particularly remember a dive with you, Yann, where we finished the hammers, the chisels, the incubation chambers, sharing a tank to decompress before reaching the surface. These are memories engraved forever. Thanks to both of you. Also, I would like to thank Camille Gache for having been an outstanding pilot and taught me how to navigate between the coral bommies. A true captain! I would like to thank all those who helped me on the field, Daphinou, Marco. It was great to help each other with our respective fieldwork. I'll keep in mind the clownfish monitoring. Samantha, Hendrikje, Anaïs, Kim, Jennie, Ian, Sam, Robin, Remi, Thomas, Laurianne, Estelle, Robin and Mathilde, thank you for helping to mark the colonies. I have a memory where we were frozen with Robin after 3 hours of staining corals. Of course, I also want to thank the CRIOBE staff. Thanks to Benoit for spending so much time in the lab to define my samples' alkalinity and share some enjoyable reggae nights. Thanks to Pascal for helping cut corals skeleton, Franck for driving the boat, and Fréderic and Anne for the field dives. Thanks also to Gilles for the lab station management, no hard feelings.

I would also like to thank the Perpignan Lab. First, I would like to thank Héloïse, who has been the most supportive friend you can wish for. Thank you for the nights at Banyuls and the different collaborations we have to start together. I would also like to thank Guillaume, who helped me cut the coral piece with this terrific saw. I would also like to thank my three students, without whom nothing could have been done in such a short time, Hmeniko and Martin for the growth analysis and Cyril for the definition of the accretion rates at Mo'orea. Thank you, Nath' for helping me out so many times administratively. Thanks to Peter for the help with my laptop, and there were some! Thanks to Jérémy and Nina Jr, even if you switched to another team, the moments of sport, baking, or outdoor activities were a truly enjoyable break. Thanks to Titouan for the photogrammetric analysis. You saved me a lot of time! Thanks to Jason for being there to talk about all these theories and coral reefs. You are a valuable friend. Thanks to Gonzalo for the discussions and reflections in Spanish/French/English. Thanks to Charles for the relaxing moments and the scientific discussions (especially when it comes to Malthusian debates) after 5 pints of beer. I would like to take this opportunity to thank Fanette for being a great partner to beat the great Charles at the "palet Breton". Thanks, of course, to Claire, Céline, Chloé, and Clara, who were always available for outdoor activities or to go drinking beers at the Fla'. Thank you to the staff with whom we share moments of conviviality such as drinks, "galettes des rois" or PhD defenses: the entire chemistry lab,

Slimane, Benoit, Camille, Émilie, Serge, Pierre, Marilou, and Aurelie. Thanks to the interns and to the people passing by Perpignan for the enriching reflections or simply for drinking a beer when it was more than necessary: Flavio, Hugo, Nao, Lauric, Antoine, Maeva, Laura-Li, Romain, Fanny, Léa, Joana, or James. Thank you to my several roommates for bringing so much life into this cozy tiny apartment. Thank you, Chachou, for all your support, Raquel for coming to run with me, the DIY in the flat and your huge smile, Victor for your philosophical thoughts and lovely songs, Catherine and Arthur for your music or simply your good mood and of course Marion, for your good mood, your good food, and for supporting 2 PhD students writing their final manuscript.

Finally, I would not be the person I am today without the people surrounding me every day. I would like to thank my Spanish friends where I did my three COVID-19 lock-downs. Thanks to you, Pinche Dieguito. It has been highly enriching to have been able to "supervise" your scientific advances and I hope we will have the opportunity to meet again soon. I would like to thank Dani, Eva, Lydia, Saul, Carla and Robert, Maria and Jordi for including me so warmly. These moments in Spain have been very rich in learning about the spanish culture. Speaking Spanish, by the way, would never have been possible without Helena and Pablo; thank you both! Thank you also to the friends from university or top-school that I've seen again during this thesis: Clément, Marine, Morane, or Lola. It was great to see you again, and I hope we will have the opportunity to meet again! Finally, I would like to thank my French friends who have always been present and supportive. No, corals are not rocks, guys! But thank you for being curious, for being as present as Valeriano was. 4 more years and nothing has changed. You guys are fantastic! Thanks to Jérémy and Anaïs, Charlène and Romain, Victor (special thanks for the scientific support), Quentin and Marine, Kevin, Laurie, Kevin and Marion, Morgane, Stellou, Clairette, Jade, Cédric, Ferdi, Marc, and Dany. I hope to see you all very soon.

Finally, I would like to thank my family, Dad, Mom, Valentin. I know I have not always been very present, but thank you for letting me live my passion and making my own choices. Thanks to my cousins Fanny and Chloe for hosting me in Papeete and Barcelona respectively. To my family - Mamie, Papy, Nanou, Patou, Martine, Loulou, Nico, Flo, Cacal, Tatie - for always trying to understand what I was doing. Finally, I would like to thank Eli, with whom I shared my life (and my thesis) every day and night. You always knew how to support me. Thank you for everything Cariñito.

# Broad summary – English

In 1990, the Intergovernmental Panel on Climate Change (IPCC) highlighted that, from the last 100 years, the Earth has warmed between 0.3°C and 0.6°C due to an unprecedented increase in anthropogenic activity. This increase in global surface temperatures has acted as a snowball effect, reducing the ice sheet and thus increasing the global mean sea level (GMSL). More worryingly, the combined rise in temperature and sea level threatens many ecosystems, the most threatened of which would undoubtedly be coral reefs. Coral reefs are home to incredible biodiversity and provide shelter and food for over 500 million people worldwide. Although the reef barrier of many tropical islands protects coastal populations from ocean waves, their effectiveness is being reduced by global change. Coral cover is being reduced by various stresses such as the crown of thorns starfish outbreaks (*Acanthaster* cf. *solaris*), cyclones and bleaching events. The latter are becoming increasingly frequent and intense, acting on large scales. As a result, coral reefs are, in the worst case, depopulated or, in the best case, severely reduced, with far fewer three-dimensionally complex individuals (*i.e.,* those with the greatest potential to reduce wave energy) than before, threatening the future of coastal populations. In this Ph.D., I quantify the impact of climate change on coral reefs in Mo'orea (French Polynesia). I define 1) how the topography (also called structural complexity) evolves and 2) the potential accretion rate of coral reefs between 2005 and 2016. I also investigate coral demographic dynamics to better predict future coral assemblages. My results show that average structural complexity in Mo'orea recovered to pre-disturbance levels by 2016. These observations are encouraging since during extreme events (such as cyclones), and in the absence of high structural complexity, the energy of waves hitting the coast is significantly higher than previously estimated. Unfortunately, I also demonstrate that accretion rates remain below the IPCC's predictions for sea-level rise (scenario 4.5), threatening Mo'orea's coastal populations by 2100 if our carbon emissions do not decrease drastically.

Keywords: Coastal protection, sea level rise, coral reefs, French Polynesia, accretion rate, IPCC scenarios, global changes.

# Résumé large – Français

En 1990, le Groupe d'experts intergouvernemental sur l'Évolution du Climat (GIEC) démontre que, dans les 100 dernières années, la Terre s'est réchauffée entre 0.3 °C et 0.6 °C dû à une augmentation sans précédent de l'activité anthropique. Cette augmentation des températures à la surface du globe a agi comme un effet boule de neige, réduisant la calotte glaciaire et donc, augmentant le niveau moyen de la mer à l'échelle mondiale. Plus inquiétant encore, l'augmentation combinée de la hausse des températures et du niveau de la mer constitue une menace réelle pour bon nombre d'écosystèmes dont les plus menacés seraient certainement les récifs coralliens. Ces derniers abritent une biodiversité incroyable tout en fournissant refuge et nourriture à plus de 500 millions de personnes autour du globe. Bien que la barrière récifale d'un grand nombre d'îles tropicales protège les populations côtières des vagues océaniques, leur efficacité se voit réduite dû aux changements globaux. Le couvert corallien se voit réduit dû à divers stress tels que les invasions d'acanthaster pourpre (*Acanthaster* cf. *solaris*), les cyclones ou bien encore les évènements de blanchissement. Ces derniers se font de plus en plus fréquents, et sont de plus en plus intenses, agissant à de grandes échelles. Ainsi, le parterre corallien se voit, dans le pire des cas, dépeuplé, ou dans le meilleur, fortement réduit, arborant bien moins d'individus tridimensionnellement complexes (c.-à-d. les individus ayant le plus fort potentiel pour réduire l'énergie houlomotrice) qu'auparavant et menaçant ainsi le futur des populations côtières. Durant cette thèse, je quantifie l'impact du changement climatique sur les récifs coralliens de Polynésie française en me basant sur l'île de Mo'orea. Entre autres, je définis 1) comment évolue le relief (aussi appelé complexité structurelle) et 2) quel est le potentiel accrétionnaire des récifs coralliens entre 2005 et 2016. Je m'interroge également quant aux dynamiques démographiques coralliennes dans le but de prédire au mieux les assemblages coralliens futurs. Mes résultats démontrent que Mo'orea a récupéré des niveaux de relief en 2016 comparables à 2005. Ces observations sont encourageantes dû au fait que durant les événements extrêmes (tels que les cyclones), et en absence d'une forte complexité structurelle, l'énergie des vagues se heurtant aux côtes est nettement plus importante que précédemment estimée. Malgré cela, les taux d'accrétion restent en dessous des prédictions de montée des eaux du GIEC (scénario 4.5), menaçant ainsi les populations côtières de Mo'orea d'ici 2100 si nos émissions carbones ne diminuent pas drastiquement.

Mots clés : Protection côtière, montée des eaux, récifs coralliens, Polynésie française, taux d'accrétion, scénarios du GIEC, changements globaux.

# Resumen largo – Español

En 1990, el Grupo Intergubernamental de Expertos sobre el Cambio Climático (IPCC) destacó que, desde los últimos 100 años, la Tierra se ha calentado entre 0.3°C y 0.6°C debido a un aumento sin precedentes de la actividad antropogénica. Este aumento de las temperaturas superficiales globales ha actuado como una bola de nieve, reduciendo la capa de hielo y aumentando así el nivel medio del mar. Lo más preocupante es que el aumento combinado de la temperatura y el nivel del mar amenaza a muchos ecosistemas, de los cuales los más amenazados serían sin duda los arrecifes de coral. Los arrecifes de coral albergan una increíble biodiversidad proporcionando a la biota marina refugio y alimento a más de 500 millones de personas en todo el mundo. Aunque la barrera de arrecife de muchas islas tropicales protege a las poblaciones costeras de las olas del mar, su eficacia se está reduciendo por el cambio global. La cubierta de coral se está reduciendo por diversas presiones, como las invasiones de estrellas de mar coralívoras (*Acanthaster* cf. *solaris*), los ciclones y los eventos de blanqueamiento. Estos últimos son cada vez más frecuentes e intensos y actúan a gran escala. Como consecuencia, los arrecifes de coral se ven, en el peor de los casos, despoblados o, en el mejor, muy reducidos, con muchos menos individuos tridimensionales complejos (es decir, los que tienen mayor potencial para reducir la energía de las olas) que antes, lo que amenaza el futuro de las poblaciones costeras. En este doctorado, cuantifico el impacto del cambio climático en los arrecifes de coral de Mo'orea (Polinesia Francesa). Defino 1) cómo evoluciona la topografía (también llamada complejidad estructural) y 2) la tasa de acreción potencial de los arrecifes de coral entre 2005 y 2016. También, investigo la dinámica demográfica de los corales para predecir mejor los futuros conjuntos coralinos. Mis resultados muestran que la complejidad estructural media en Mo'orea se recuperó hasta los niveles anteriores a las perturbaciones en 2016. Estas observaciones son alentadoras, ya que durante los eventos extremos (como los ciclones), en ausencia de una alta complejidad estructural, la energía de las olas que golpean la costa es significativamente mayor de lo que pensábamos. Desgraciadamente, también demuestro que las tasas de acreción se mantienen por debajo de las predicciones del IPCC sobre el aumento del nivel del mar (escenario 4.5), amenazando a las poblaciones costeras de Mo'orea para el año 2100 si nuestras emisiones de carbono no disminuyen drásticamente.

Palabras clave: Protección costera, aumento del nivel del mar, arrecifes de coral, Polinesia Francesa, tasa de acreción, escenarios del IPCC, cambios globales.

# TABLE OF CONTENTS

**CHAPTER 1 – GENERAL INTRODUCTION 1**

**1.1 AN UNCERTAIN FUTURE 2**
1.1.1 AWARENESS OF CLIMATE CHANGE 2
1.1.2 TOWARDS A CHANGING WORLD 4
1.1.2.1 Increased anthropogenic activity 4
1.1.2.2 Climate change 6
1.1.2.3 Decline of ecosystems and associated species 9
**1.2 CORAL REEFS 11**
1.2.1 GENERALITIES 11
1.2.2 KEY FUNCTIONS 12
1.2.2.1 At the holobiont scale 12
1.2.2.2 At the reef scale 14
**1.3 THREATS TO CORAL REEFS AND THEIR IMPLICATIONS 16**
1.3.1 THREATS 16
1.3.1.1 *Acanthaster* cf. *solaris* threat 16
1.3.1.2 Bleaching events 17
1.3.1.3 Tropical storms 18
1.3.2 CORAL REEF DECLINE 18
1.3.2.1 Changes in coral reef functioning 18
1.3.2.2 Low reef accretion rates 20
**1.4 PH.D. OBJECTIVES 21**

**CHAPTER 2 – COMMUNITY COMPOSITION PREDICTS PHOTOGRAMMETRY-BASED STRUCTURAL COMPLEXITY ON CORAL REEFS 25**

**2.1 INTRODUCTION 27**
**2.2 MATERIAL AND METHODS 29**
2.2.1 STUDY AREA 29
2.2.2 STRUCTURAL COMPLEXITY MEASUREMENTS 30
2.2.3 BENTHIC COMMUNITY DESCRIPTION AND ASSESSMENT 32
2.2.4 STATISTICAL ANALYSIS 33
**2.3 RESULTS 35**
**2.4 DISCUSSION 38**
**2.5 ACKNOWLEDGEMENTS 40**
**2.6 DATA AVAILABILITY 40**
**2.7 SUPPLEMENTARY INFORMATION 41**
**2.8 ANNEX 41**
2.8.1 SURVEY DATA 42
2.8.2 CAMERA CALIBRATION 43
2.8.3 GROUND CONTROL POINTS 44
2.8.4 DIGITAL ELEVATION MODEL 45
2.8.5 PROCESSING PARAMETERS 46

**CHAPTER 3 – JUVENILE CORALS UNDERPIN CORAL REEF CARBONATE PRODUCTION AFTER DISTURBANCE 49**

**3.1 INTRODUCTION 51**
**3.2 MATERIAL AND METHODS 54**
3.2.1 $CaCO_3$ PRODUCTION USING *IN SITU* ALIZARIN RED-S STAINING 54
3.2.2 $CaCO_3$ PRODUCTION USING ALKALINITY ANOMALY EX SITU INCUBATIONS 55
3.2.3 PHOTOGRAMMETRY-BASED SIZE AREA RELATIONSHIPS 56
3.2.4 BAYESIAN $CaCO_3$ PRODUCTION MODELS 57
3.2.5 CORAL COMMUNITY $CaCO_3$ PRODUCTION 57
3.2.6 RECRUITMENT LOSS MODEL 60
**3.3 RESULTS 61**
**3.4 DISCUSSION 64**
**3.5 ACKNOWLEDGEMENTS 67**
**3.6 DATA AVAILABILITY 68**
**3.7 SUPPLEMENTARY INFORMATION 68**

**CHAPTER 4 – SCALING UP CALCIFICATION, RESPIRATION, AND PHOTOSYNTHESIS RATES OF SIX PROMINENT CORAL TAXA 77**

**4.1 INTRODUCTION 79**
**4.2 MATERIAL AND METHODS 81**
4.2.1 CORAL SPECIES SELECTION, PREPARATION, AND ACCLIMATION 81
4.2.2 TANK PREPARATION 82
4.2.3 RESPIRATION AND PHOTOSYNTHESIS 83
4.2.4 CALCIFICATION 84
4.2.5 COLONY-SIZE ESTIMATION USING PHOTOGRAMMETRY 85
4.2.6 STATISTICAL ANALYSIS 85
**4.3 RESULTS 87**
**4.4. DISCUSSION 90**
**4.5 ACKNOWLEDGEMENTS 94**
**4.6 DATA AVAILABILITY 95**
**4.7 SUPPLEMENTARY INFORMATION 95**

**CHAPTER 5 – LOSS OF STRUCTURAL COMPLEXITY FROM CORAL REEFS IMPLIES A LACK OF EFFICIENCY IN DISSIPATING WAVE ENERGY IN THE FACE OF GLOBAL CHANGES 101**

**5.1 INTRODUCTION 103**
**5.2 MATERIEL & METHODS 104**
5.2.1 FIELDWORK MEASURES 104
5.2.2 STRUCTURAL COMPLEXITY DEFINITION 105
5.2.3 NIKURADSE DEFINITION 105
5.2.4 HYDRODYNAMIC MODEL 106
5.2.5 STATISTICAL ANALYSES 108
**5.3 RESULTS AND DISCUSSION 109**
**5.4 DATA AVAILABILITY 113**
**5.5 SUPPLEMENTARY INFORMATION 113**

**CHAPTER 6 – MO'OREA'S REEFS MIGHT NOT KEEP UP WITH SEA LEVEL RISE IN THE NEAR FUTURE 117**

**6.1 INTRODUCTION 119**
**6.2 MATERIEL & METHODS 120**
6.2.1 $CaCO_3$ PRODUCTION FROM CORALS AND CORAL CRUSTOSE ALGAE 121
6.2.2 FISH BIOEROSION DETERMINATION 122
6.2.3 URCHIN BIOEROSION DETERMINATION 123
6.2.4 REEF ACCRETION DEFINITION 124
**6.3 RESULTS AND DISCUSSION 124**
6.3.1 POPULATION DEMOGRAPHICS TRENDS 124
6.3.2 MO'OREA'S CARBONATE BUDGET AND FOLLOWING REEF ACCRETION 126
6.3.3 RISKS IN THE NEAR FUTURE 128
**6.4 DATA AVAILABILITY 129**
**6.5 SUPPLEMENTARY INFORMATION 129**

**CHAPTER 7 – GENERAL DISCUSSION 133**

**7.1 MAIN ADVANCES 134**
**7.2 LIMITS AND FUTURES DIRECTIONS 137**
7.2.1 MANAGEMENT LIMITS 137
7.2.2 INCREASE SPATIAL RESOLUTION 137
7.2.3 CONSIDERING NUTRIENT RELEASES 138
7.2.4 PREDICTIONS 139
**7.3 SOLUTIONS AND RECOMMENDATIONS 140**
7.3.1 ARTIFICIALISATION 140
7.3.2 NATURAL PROTECTION 140
7.3.3 SCIENTIFIC ENGINEERING 142
**7.4 GENERAL CONCLUSION 143**

**REFERENCES 145**

**ANNEXES 171**

**8.1 OTHOLITOMETRY STUDY 172**
**8.2 GUT CONTENTS STUDY 182**
**8.3 SCIENCE POPULARISATION (FRENCH) 202**

# LIST OF FIGURES

**FIGURE 1.1 |** MAJOR INTERNATIONAL EVENTS ON CLIMATE CHANGE OR SUSTAINABLE DEVELOPMENT IN THE LAST FIFTY YEARS. 3

**FIGURE 1.2 |** CLIMATE TRENDS FROM 1880 TO 2019. A. CHANGE IN ATMOSPHERIC CO2 CONCENTRATION (PPM) B. CHANGE IN TEMPERATURE ANOMALY (°C) C. CHANGE IN GLOBAL MEAN SEA LEVEL (GMSL) (MM). THE REFERENCE YEAR WAS ARBITRARILY CHOSEN AS 1880. 7

**FIGURE 1.3 |** GLOBAL DISTRIBUTION OF CORAL REEFS IN TROPICAL AND SUBTROPICAL REGIONS. THIS DATASET WAS COMPILED FROM A NUMBER OF SOURCES BY UNEP WORLD CONSERVATION MONITORING CENTRE (UNEP-WCMC) AND THE WORLDFISH CENTRE, IN COLLABORATION WITH THE WORLD RESOURCES INSTITUTE (WRI) AND THE NATURE CONSERVANCY (TNC). 11

**FIGURE 1.4 |** A. POCILLOPORA MEANDRINA HOSTING HUNDREDS OF DAMSELFISHES (CHROMIS VIRIDIS) © LAURIC THIAULT B. SPIROBRANCHUS GIGANTEUS (A TUBE WORM OF THE FAMILY SERPULIDAE) LIVING IN CORALS OF THE GENUS PORITES C. CORAL POLYPS FEEDING AT NIGHT D. BLEACHED CORAL POLYPS FEEDING ON PHYTOPLANKTON. B,C AND D: © TUMBLR 13

**FIGURE 1.5 |** A. BUTTERFLYFISH FEEDING ON A CORAL OF THE GENUS ACROPORA B. ONE OF THE MOST ABUNDANT AND WIDESPREAD ECHINOIDS (I.E., DIADEMA SP.) IN MO'OREA'S WATERS C. SCHOOL OF PARROTFISH (CHLORURUS SORDIDUS) © ALAMY STOCK PHOTOS 15

**FIGURE 2.1 |** LOCATION OF THE THIRTEEN LONG-TERM MONITORING SITES SURVEYED EACH YEAR FROM 2004 UNTIL 2017 AROUND MO'OREA IN THE SOCIETY ARCHIPELAGO, FRENCH POLYNESIA. 30

**FIGURE 2.2 |** EVOLUTION OF ONE OF THE TWENTY QUADRATS USED TO DEFINE CORAL COVER IN HAAPITI (ON THE SOUTHWESTERN SIDE OF THE ISLAND) BEFORE (2004), IMMEDIATELY AFTER (2010) AND SEVERAL YEARS AFTER (2017) CYCLONE OLI. 30

**FIGURE 2.3 |** EXAMPLE OF UNDERWATER PHOTOGRAMMETRY. **A.** ORTHORECTIFIED PHOTOMOSAIC. THE BLACK DOTS INDICATE THE RANDOM POINTS WITH SHAPE CLASSIFICATION. **B.** DIGITAL ELEVATION MODEL REPRESENTING DEPTH VALUES (THE PHOTOMOSAIC IS KEPT TRANSPARENT IN THE BACKGROUND). **C.** DETAIL OF THE PHOTOMOSAIC. 31

**FIGURE 2.4 |** PRINCIPAL COMPONENTS ANALYSIS (PCA) OF THE 11 MORPHO-SPECIES FROM 2004 TO 2017. CORAL COVER (CC) IS WRITTEN AT THE BOTTOM RIGHT OF EACH BOX. ON EACH PLOT, THE CORAL COMMUNITY IN 2004 IS INCLUDED AS A BASELINE IN BLACK DASHED LINES. ABBREVIATIONS ARE AS FOLLOW: ACR - ACROPORA SPP; CCA - CRUSTOSE CORALLINE ALGAE; DEA - DEAD CORAL; ENC - ENCRUSTING CORALS; MAC – MACROALGAE; MAS - MASSIVE CORALS; OER - OTHER ERECTS FORMS; OTH - OTHERS (SPONGES OR BENTHIC SPECIES); PAV - PAVEMENT; AND POC - POCILLOPORA SPP; RUB – RUBBLES; SMU - SAND OR MUD. 35

**FIGURE 2.5 |** RUGOSITY RECONSTRUCTIONS FROM 2004 TO 2017 ACCORDING TO THE AVERAGE OF THE MODELS (CROSS VALIDATED GENERATED TREES BOOSTED MODEL ON THE LEFT AND CROSS VALIDATED LASSO GENERALIZED LINEAR MODEL ON THE RIGHT) ON EACH OF THE THREE SIDES OF MO'OREA. THE COTS OUTBREAK AND CYCLONE OLI ARE SHOWN IN 2006 AND 2010, RESPECTIVELY. 36

**FIGURE 2.6 |** DIFFERENCE BETWEEN ACROPORA AND POCILLOPORA COVER (%), AS WELL AS THE DIFFERENCE IN RUGOSITY INDEX. DARK BLUE BARS REPRESENT 2004, AND RED BARS REPRESENT 2017. ASTERISK INDICATE SIGNIFICANT DIFFERENCES ($P<0.05$) WHILE N.S INDICATE NON-SIGNIFICANT DIFFERENCES ($P>0.05$). 37

**FIGURE S2.1 |** CAMERA LOCATIONS AND IMAGE OVERLAP. COLORS REPRESENT THE NUMBER OF PHOTOS OVERLAPPED. 42

**FIGURE S2.2 |** IMAGE RESIDUALS FOR HERO4 BLACK (3 MM). 43

**FIGURE S2.3 |** GROUND CONTROL POINTS (GCP) OVERVIEW 45

**FIGURE S2.4 |** RECONSTRUCTED DIGITAL ELEVATION MODEL. RESOLUTION: 1.06MM/PIX AND POINT DENSITY: 889956 PTS/$M^2$ 45

**FIGURE 3.1 |** CONCEPTUAL DIAGRAM DESCRIBING ISOMETRIC VERSUS ALLOMETRIC $CACO_3$ PRODUCTION CURVES. SIZE DEPENDENT METABOLIC PRODUCTION CHARACTERIZED BY (A) A LINEARLY INCREASING MODEL WITH CORAL SURFACE AREA (ISOMETRIC METABOLIC CURVE IN ORANGE; EQUATION $Y = \alpha X + 0$), AND (B) A LOGARITHMIC ASYMPTOTE (ALLOMETRIC METABOLIC CURVE IN BLUE; EQUATION $Y = \alpha X^B + 0$). THE DASHED LINE INDICATES THE SIZE AT WHICH THE TWO CURVES CROSS (I.E., THIS THRESHOLD POINT DEPENDS ON BOTH THE INTERCEPTS AND THE ALLOMETRIC SCALING SLOPES). COMPARED TO THE ALLOMETRIC MODEL, THE ISOMETRIC MODEL MAY UNDERESTIMATE $CACO_3$ PRODUCTION BELOW THIS THRESHOLD AND OVERESTIMATE $CACO_3$ PRODUCTION AT LAGER CORAL SIZES. 53

**FIGURE 3.2 |** AVERAGE LIVE CORAL COVER IN MO'OREA, FRENCH POLYNESIA, FROM 2005 TO 2016. PERTURBATIONS INCLUDED A PREDATORY SEA STAR (ACANTHASTER CF. SOLARIS) OUTBREAK FROM 2006 TO 2009 AND A CYCLONE IN 2010. PHOTOGRAPHS ILLUSTRATE THE REEFSCAPE IN **A.** 2006, **B.** 2010 AND **C.** 2015. 58

**FIGURE 3.3 |** $CACO_3$ PRODUCTION RATES OF THE THREE REEF-BUILDING CORAL SPECIES. ON THE LEFT. CHANGES IN LINEAR EXTENSION FOR THE CORAL SPECIES A. HYACINTHUS, P. VERRUCOSA AND P. LUTEA AS A FUNCTION OF COLONY SIZE. ON THE RIGHT, CHANGES IN $CACO_3$ PRODUCTION RATES AS A FUNCTION OF COLONY SIZE. $CACO_3$ PRODUCTION WAS ESTIMATED USING TWO GROWTH MEASUREMENT METHODS (IN SITU ALIZARIN RED-S STAINING AND EX SITU METABOLIC INCUBATIONS). 62

**FIGURE 3.4 |** CORAL COMMUNITY $CACO_3$ PRODUCTION ESTIMATES OF A $10M^2$ PORTION OF REEF SUBSTRATE IN MO'OREA FROM 2005 TO 2016 ACCORDING TO THE ISOMETRIC VERSUS ALLOMETRIC CORAL $CACO_3$ PRODUCTION MODELS. **A.** $CACO_3$ PRODUCTION RATE (KG $M^{-2}$ $YR^{-1}$), **B.** CUMULATIVE $CACO_3$ PRODUCTION (KG $YR^{-1}$). ESTIMATES ARE BOUNDED BY A 95% CONFIDENCE INTERVAL. CORAL SYMBOLS ON TOP INDICATE CHANGES IN AVERAGE CORAL COLONY SIZE, AND NUMBERS INDICATE CORAL COLONY DENSITY PER $10M^2$ OF REEF SURFACE AREA. 63

**FIGURE 3.5** | NORMALIZED $CACO_3$ PRODUCTION TRAJECTORIES ACCORDING TO FOUR SCENARIOS OF CORAL RECRUITMENT OVER FIVE YEARS DURING REEF RECOVERY. A MULTI-SPECIES, OPEN-POPULATION INTEGRAL PROJECTION MODEL WAS USED TO PREDICT THE RECOVERY DYNAMICS OF AN ASSEMBLAGE OF THREE CORAL GENERA (ACROPORA, POCILLOPORA AND PORITES) BASED ON CORAL DEMOGRAPHIC PERFORMANCE (IN RECRUITMENT, GROWTH, AND SURVIVAL) MEASURED IN MO'OREA. THE FOUR SCENARIOS PREDICTED DIFFERENT RATES OF CORAL RECRUITMENT REDUCTION AS COMPARED TO CURRENT LEVELS (0%, 25%, 50% AND 75% REDUCTIONS). $CACO_3$ PRODUCTION RATES WERE ESTIMATED FROM MODEL PREDICTIONS OF CORAL ABUNDANCE, COMPOSITION AND SIZE DISTRIBUTION (FIGURE S5, COMBINED WITH THE ALLOMETRIC $CACO_3$ PRODUCTION FUNCTIONS ESTIMATED IN MO'OREA (FIG. 1). $CACO_3$ PRODUCTION RATES WERE NORMALIZED RELATIVE TO THE HIGHEST VALUE (SCENARIO 0% REDUCTION AT YEAR 5; GREEN CURVE). 64

**FIGURE S3.1 |** MAP OF STUDY SITES FOR THE IN SITU ALIZARIN RED-S STAINING. ALIZARIN RED-S STAINING WAS CONDUCTED ON THE REEF SLOPES AROUND MO'OREA, FRENCH POLYNESIA, AND INCLUDED 175 COLONIES (NUMBERED FROM 1 TO 175 UNDER THE GRAY LABELS). THE GREY LABELS INDICATE

THE SAMPLING SITES. THE CORALS USED IN THE EX-SITU INCUBATIONS WERE COLLECTED AT VAIPAHU, ON THE NORTH SHORE OF THE ISLAND. 68

**FIGURE S3.2 |** ALIZARIN RED-S STAINING EXAMPLE. THE PHOTOGRAPHS ILLUSTRATE A 0.7 MM THICK SLICE FROM ONE OF THE POCILLOPORID COLONIES 131 DAYS AFTER STAINING. **A.** INTROSPECTED IMAGE OBSERVED UNDER MICROSCOPE, AND **B.** THE SAME SLICE OBSERVED UNDER A FLUORESCENT MICROSCOPE. **C.** A SUPERPOSITION OF THE TWO IMAGES TO DEFINE THE MAXIMUM LINEAR EXTENSION OF THE CORAL. FOR THIS CORAL FRAGMENT, THE LINEAR EXTENSION WAS 0.57 CM OVER 131 DAYS, WHICH CORRESPONDS TO A $CACO_3$ PRODUCTION RATE OF 3.1 KG $M^{-2}$ $YR^{-1}$. 69

**FIGURE S3.3 |** PHOTOGRAMMETRY-BASED SIZE-AREA RELATIONSHIPS. FOR EACH OF THE THREE CORAL SPECIES, WE FITTED A POWER-LAW REGRESSION FOR THE MEAN DIAMETER (I.E., THE MEAN OF THE LENGTH, WIDTH AND HEIGHT OF EACH COLONY) AND THE LIVE SURFACE AREA OF THE CORAL COLONIES. WE ALSO ESTIMATED AN AVERAGE TRENDLINE ACROSS THE THREE CORAL SPECIES (DASHED POINTS) ($R^2$=0.97). CORAL SYMBOLS INDICATE THE GROWTH MORPHOLOGIES OF THE THREE CORAL SPECIES. 70

**FIGURE S3.4 |** COMPILATION OF THE ALIZARIN RED-S AND THE INCUBATION DATASETS. THE BAYESIAN ALLOMETRIC $CACO_3$ MODEL WAS FIRST CHARACTERIZED FOR THE THREE CORAL GENERA (ACROPORA, POCILLOPORA AND PORITES) WITH ONLY THE ALIZARIN RED-S DATASET (N=130 TOP PLOTS). WE THEN MERGED BOTH ALIZARIN RED-S AND INCUBATION DATASETS FOR DEFINING A MORE COMPLETE ALLOMETRIC $CACO_3$ PRODUCTION MODEL (N=200, BOTTOM PLOT). THE POWER-LAW EQUATIONS FROM EACH SPECIES AND EACH DATASET WERE WRITTEN ON THE TOP OF EACH PLOT. FOR EACH OF THE THREE SPECIES, NO SIGNIFICANT DIFFERENCE IN CALCIFICATION ESTIMATES WERE FOUND BETWEEN THE ALIZARIN RED-S ONLY AND BOTH THE ALIZARIN RED-S AND INCUBATION COMBINED DATASETS (TWO-TAILED T-TEST; P = 0.93, 0.61 AND 0.17 FOR RESPECTIVELY ACROPORA HYACINTHUS, POCILLOPORA VERRUCOSA AND PORITES LUTEA). 71

**FIGURE S3.5 |** ROBUSTNESS OF THE CORAL COMMUNITY SIZE DISTRIBUTIONS DATA. TO TEST WHETHER OUR ISLAND-SCALE ESTIMATIONS OF CORAL SIZE-DISTRIBUTIONS MATCHED THE DATA FROM LOCALLY PERFORMED SURVEYS AT SPECIFIC SITES AROUND MO'OREA (SEE METHODS SECTION CORAL COMMUNITY SIZE DISTRIBUTIONS), WE COMPARED OUR PREDICTIONS TO THE CORAL SIZE-DISTRIBUTION DATASET OBSERVED IN KAYAL ET AL. (2015) FROM THE YEAR 2009 AND FOR THE GENUS POCILLOPORA. THUS, ON THE LEFT PLOT, WE REPRESENTED THE MODELED SIZE-DISTRIBUTION DATASET WHILE WE DESCRIBED ON THE RIGHT PLOT, THE CURRENT OBSERVED SIZE-DISTRIBUTION DATASET. FOR BOTH DATASETS, WE OBSERVED A PEAK OF SEVERAL INDIVIDUALS BETWEEN 0 AND 4 CM OF DIAMETER. DESPITE A SLIGHT INCREASE FOR SMALL COLONIES IN THE DATASET MODELED, BOTH PATTERNS ARE SIMILAR, AND WE FOUND NO SIGNIFICANT DIFFERENCE BETWEEN BOTH SIZE-DISTRIBUTION DATASETS (TWO-TAILED T-TEST; P = 0.08). 72

**FIGURE S3.6 |** RECRUITMENT LOSS MODEL. CORAL COMMUNITY TRAJECTORIES PREDICTED UNDER FOUR RECRUITMENT SCENARIOS OVER THE COURSE OF FIVE YEARS (2010-2015). THE POPULATION DYNAMICS OF THE THREE CORAL TAXA ARE EXPRESSED IN TERMS OF CHANGES IN CORAL ABUNDANCE (Y-AXIS) ACROSS COLONY SIZES (X-AXIS) WITH TIME (YEARS) AND SCENARIOS (0%, 25%, 50% AND 75% REDUCTIONS IN RECRUITMENT RATES). THE PREDICTED CORAL ABUNDANCES, COMPOSITIONS, AND SIZE STRUCTURES WERE USED TO ESTIMATE COMMUNITY CALCIFICATION UNDER THE FOUR SCENARIOS (SEE FIGURE 3.4). 73

**FIGURE 4.1 |** SCALING RELATIONSHIPS BETWEEN THE THREE PHYSIOLOGICAL PROCESSES (I.E., CALCIFICATION, RESPIRATION, AND PHOTOSYNTHESIS RATES, RESPECTIVELY, FROM TOP TO BOTTOM) AND LIVE CORAL SURFACE AREA FOR SIX CORAL SPECIES (ACROPORA HYACINTHUS, ASTREA CURTA, MONTIPORA VERRILLI, NAPOPORA IRREGULARIS, POCILLOPORA CF. VERRUCOSA

AND PORITES SPP.) WITH A ± 95% BAYESIAN CREDIBLE INTERVAL. ALL RELATIONSHIPS ARE DEPICTED WITH DOTS REPRESENTING THE RAW DATA AND REGRESSION LINES REPRESENTING POSTERIOR PREDICTIONS FROM THE BAYESIAN LINEAR MODEL (± 95% CREDIBLE INTERVALS). CORAL SILHOUETTES REPRESENT THE MATURE CORAL MORPHOLOGY. 88

**FIGURE 4.2 |** REPRESENTATION OF HYPOTHETICAL CORAL ASSEMBLAGES AND THEIR CORRESPONDING ENERGY RATIOS (NET PHOTOSYNTHESIS RATE/CALCIFICATION RATE). **A.** PERCENTAGE OF LIVE CORAL COVER OF THE 6 CORAL SPECIES FROM 2004 TO 2017. REEFSCAPES ARE REPRESENTED ON THE RIGHT FOR THREE YEARS (I.E., 2005, 2010, AND 2015) **B.** RELATIONSHIP BETWEEN CALCIFICATION AND NET PHOTOSYNTHESIS, WHICH UNDERPIN THE COMMUNITY-WIDE MODELS. ESTIMATES FROM PREVIOUS BAYESIAN MODELS (UNFILLED POINTS) WERE ADDED TO OUR OBSERVATIONS (FILLED POINTS). **C.** MATRICES REPRESENTING ENERGY RATIOS (NET PHOTOSYNTHESIS RATE/CALCIFICATION RATE) ACCORDING TO DIFFERENT SCENARIOS OF POCILLOPORA CF. VERRUCOSA COVER (0 TO 100% COVER) VS. THE COVER OF THE FIVE OTHER SPECIES (0 TO 100% COVER; A. HYACINTHUS, A. CURTA, M. VERRILLI, N. IRREGULARIS, AND PORITES SPP.) AFTER THE CYCLONE IN 2010 (I.E., WHICH RESULTED IN THE DOMINANCE OF SMALL CORAL COLONIES). 89

**FIGURE S4.1 |** TANK SET UP. A. CORAL COLONIES IN TWO TANKS CONDITIONED TO REFLECT IN SITU ENVIRONMENTAL PARAMETERS. IN THE LEFT TANK, THE CORAL COLONIES ARE **A.** HYACINTHUS, AND IN THE RIGHT TANK, THEY ARE N. IRREGULARIS. **B.** P. VERRUCOSA IN AN INCUBATION CHAMBER USED TO DEFINE CALCIFICATION AND GROSS PHOTOSYNTHESIS RATES. **C.** PHOTOS OF THE 6 DIFFERENT CORAL SPECIES (A. A. HYACINTHUS; B. A. CURTA; C. M. VERRILLI; D. N. IRREGULARIS; E. P. VERRUCOSA AND F. PORITES SPP.) FROM BOSSERELLE ET AL. (2014) 96

**FIGURE S4.2 |** TRACE PLOTS DEPICTING THE MONTE CARLO CHAINS FROM THE THREE BAYESIAN MODELS. EACH MODEL (I.E., CALCIFICATION, RESPIRATION, AND PHOTOSYNTHESIS) WAS RUN WITH THREE CHAINS OF 5,000 ITERATIONS, WITH THE FIRST 2,500 STEPS DISCARDED. THE SCATTERPLOTS REPRESENT POSTERIOR PREDICTIVE CHECKS WITH THE RESPECTIVE $R^2$ VALUES ESTIMATED FROM THE MODEL. 97

**FIGURE S4.3 |** RELATIONSHIP BETWEEN THE SURFACE AREA-SPECIFIC PHYSIOLOGICAL PROCESSES (CALCIFICATION, RESPIRATION, AND PHOTOSYNTHESIS RATES, RESPECTIVELY, FROM THE TOP TO THE BOTTOM) AND LIVE CORAL SURFACE AREA FOR SIX CORAL SPECIES (ACROPORA HYACINTHUS, ASTREA CURTA, MONTIPORA VERRILLI, NAPOPORA IRREGULARIS, POCILLOPORA CF. VERRUCOSA, AND PORITES SPP.) WITH A ± 95% BAYESIAN CREDIBLE INTERVAL. ALL RELATIONSHIPS ARE DEPICTED WITH DOTS REPRESENTING THE RAW DATA POINTS AND REGRESSION LINES REPRESENTING POSTERIOR PREDICTIONS FROM THE BAYESIAN LINEAR MODEL (± 95% CREDIBLE INTERVALS). CORAL SILHOUETTES REPRESENT THE MATURE CORAL MORPHOLOGY 98

**FIGURE 5.1 |** EVOLUTION OF THE STRUCTURAL COMPLEXITY FROM 2005 TO 2016 ON THE WEST SIDE OF MO'OREA ISLAND (FRENCH POLYNESIA). PERTURBATIONS INCLUDED A PREDATORY SEA STAR (ACANTHASTER CF. SOLARIS) OUTBREAK FROM 2006 TO 2009 AND A CYCLONE IN 2010. PHOTOGRAPHS ILLUSTRATE THE REEFSCAPES IN **A.** 2005, **B.** 2011 AND **C.** 2016. 110

**FIGURE 5.2 | A.** SCATTERPLOT BETWEEN THE WAVE HEIGHT NEAR THE SHORE ($H_{S, SHORE}$), THE STRUCTURAL COMPLEXITY (SC) AND THE WAVE HEIGHT OFFSHORE ($H_{S, REEF}$). COLORS REPRESENT ONE YEAR OF MONITORING. THE AVERAGE REGRESSION IS EXPRESSED AS $H_{S, SHORE} = 0.11 - 0.01 \times SC + 0.13 \times H_{S, REEF} - 0.01 \times SC: H_{S, REEF}$ ($R^2 = 0.46$). FOR EACH YEAR (2005 AND 2008 TO 2016), 1000 WAVES HEIGHT NEAR THE SHORE WERE ESTIMATED. **B.** INCREASE OF THE WAVE HEIGHT NEAR THE SHORE ACCORDING TO THE STRUCTURAL COMPLEXITY LOSS AND THE MAGNITUDE OF THE EVENT. FOR EACH 1M WAVE HEIGHT OFFSHORE, WE USED THE SAME REGRESSION MODEL AS BEFORE (I.E., $H_{S, SHORE}$ = INTERCEPT + SC + $H_{S, REEF}$ + SC: $H_{S, REEF}$) AND $H_{S, SHORE}$ WAS ESTIMATED FOR EACH SET OF WAVE HEIGHT OFFSHORE. DRAWING ON THIS MODEL, WE DETERMINED THE LIKELY INCREASE OF THE

SIGNIFICANT WAVE HEIGHT NEAR THE SHORE ACCORDING TO THE LOSS OF THE STRUCTURAL COMPLEXITY. 112

**FIGURE S5.1 |** TRANSECT ALONG WHICH WAVE ATTENUATION WAS ESTIMATED FROM SENSOR 1 TO SENSOR 2, 3 AND 4. **A.** AERIAL VIEW OF HAAPITI, MO'OREA (FRENCH POLYNESIA) (WORLDVIEW-3 IMAGERY). **B.** CROSS-SECTION OF THE TRANSECT HIGHLIGHTING THE 3 DIFFERENT ENVIRONMENT AND SENSOR LOCATIONS WITHIN THE VERY SAME TRANSECT AT HAAPITI, MO'OREA (FRENCH POLYNESIA). 113

**FIGURE S5.2 |** WAVE CONDITIONS AT HAAPITI, MO'OREA (FRENCH POLYNESIA). **A.** DENSITY PLOT OF THE WAVE HEIGHT OFFSHORE (M) AT HAAPITI, MO'OREA (FRENCH POLYNESIA) IN 2016. FOR EACH DAY FROM 2016 AT NOON (GMT+12:00), THE WAVE HEIGHT HAS BEEN DEFINED THANKS TO THE MARC-WW3 ESTIMATES IN FRENCH POLYNESIA. **B.** REPRESENTATION OF THE MOST COMMON RANGE OF WAVE SIZE AT HAAPITI (HS ~ 1.5M). **C.** REPRESENTATION OF HIGHER WAVE CONDITIONS AT HAAPITI (HS ~ 3M) 114

**FIGURE S5.3 |** REPRESENTATION OF THE THREE DIFFERENT CORAL SPECIES (**A.** ACROPORA HYACINTHUS, **B.** POCILLOPORA CF. VERRUCOSA, **C.** PORITES LUTEA) 114

**FIGURE S5.4 |** REPRESENTATION OF THE HAAPITI TRANSECT WITH RANDOM LOCATION OF THE 3 SPECIES ALONG A TRANSECT FROM A 0M DEPTH TO 20M DEPTH. THE DIFFERENT CORAL SPECIES ARE REPRESENTED IN THREE COLORS (ACROPORA HYACINTHUS IN RED, POCILLOPORA CF. VERRUCOSA IN GOLD AND PORITES LUTEA IN BLUE) 115

**FIGURE S5.5 |** DEFINITION OF THE NIKURADSE ESTIMATES ($K_N$) **A.** DEFINITION OF THE AVERAGE CORAL HEIGHT WITHIN A $10M^2$ TRANSECT AND ILLUSTRATION OF THE $K_N$ ESTIMATES EQUIVALENT ABOVE. ACROPORA HYACINTHUS WERE REPRESENTED IN RED, POCILLOPORA CF. VERRUCOSA IN ORANGE AND PORITES LUTEA IN BLUE **B.** CHANGE IN COMPLEXITY FROM 2005 TO 2016. THE STANDARD YEAR HAS BEEN SELECTED FOR 2016 BECAUSE THE HIGHEST STRUCTURAL COMPLEXITY ESTIMATES WERE DEFINED THIS YEAR. RED POINTS REPRESENT THE AVERAGE FOR EACH YEAR. **C.** SCATTERPLOT BETWEEN $K_N$ ESTIMATES DEFINED BY THE 'TOPOGRAPHIC APPROACH' AND $K_N$ ESTIMATES DEFINED BY THE 'HYDRODYNAMICAL APPROACH'. **D.** RELATIONSHIP BETWEEN STRUCTURAL COMPLEXITY AND $K_N$ ESTIMATES. THE RELATIONSHIP IS WRITTEN AS $K_N$ = 0.25 X LOG(STRUCTURAL COMPLEXITY). 115

**FIGURE 6.1 | A.** EVOLUTION OF LIVE CORAL COVER (%) FROM 2005 TO 2016 ON MO'OREA. **B.** EVOLUTION OF THE PARROTFISHES' DENSITY (IND $M^{-2}$) FROM 2005 TO 2016 ON MO'OREA. **C.** $CACO_3$ GAINS AND THE LOSSES (KG $M^{-2}$ $YR^{-1}$) FROM 2005 TO 2016 AT MO'OREA, WITH $CACO_3$ PRODUCTION FROM CORALS IN GOLD, $CACO_3$ PRODUCTION FROM CCA IN ORANGE, BIOEROSION FROM PARROTFISHES IN BLUE AND BIOEROSION FROM SEA-URCHINS IN PURPLE. RED DOTS REPRESENT THE $CACO_3$ BUDGET FOR EACH YEAR (±SE). **D.** EVOLUTION OF OVERALL ACCRETION RATE (MM $YR^{-1}$) FROM 2005 TO 2016 ON MO'OREA (±SE). HORIZONTAL LINES REPRESENT THE GLOBAL MEAN SEA LEVEL (GMSL) UNDER 4 IPCC'S SCENARIOS (I.E., SSP1-1.9 IN YELLOW, SSP1-2.6 IN ORANGE, SSP2-4.5 IN LIGHT RED AND SSP3-7.0 IN DARK RED) 126

**FIGURE S6.1 | A.** EVOLUTION OF THE AVERAGE PARROTFISH SIZE (CM) FROM 2005 TO 2016 ON MO'OREA (±SE). **B.** CONTRIBUTION (%) OF FIVE MAIN PARROTFISH SPECIES TO BIOEROSION FROM 2005 TO 2016 ON MO'OREA. **C.** AVERAGE ABUNDANCE OF PARROTFISH WITHIN A $50M^2$ TRANSECT FROM 2005 TO 2016 ON MO'OREA. 130

# LIST OF TABLES

**TABLE 2.1 |** SHAPE CLASSIFICATION CATEGORIES DEFINED TO ESTIMATE RUGOSITY. TEN VARIABLES ARE MORPHOLOGICAL, BUT THE GENUS LEVEL IS GIVEN FOR ACROPORA SPP. AND POCILLOPORA SPP. 32

**TABLE S2.1 |** POST HOC (TUKEY HSD) MATRIX FOR TESTING THE RUGOSITY DIFFERENCE ACCORDING TO EACH YEAR COMBINATION. THE P-VALUE (THRESHOLD: 0.05) FOR EACH COMBINATION IS WRITTEN IN THE MATRIX DATA AS FOLLOWS. THE RED VALUES ARE SIGNIFICANTLY DIFFERENT AND THE BLUE VALUES ARE NOT. 41

**TABLE S2.2 |** COEFFICIENTS AND STANDARD ERROR FOR EACH PARAMETER ACCORDING TO BEST MODEL DEFINED: RUGOSITY ~ DIM 1 + DIM 3 + DIM 5 + FACTOR(SITE) (R2 = 0.81). THE P-VALUE REPRESENTS THE SIGNIFICANCE OF EACH PARAMETER ACCORDING TO THE R CODE (*** HIGHLY SIGNIFICANT (<0.001), **VERY SIGNIFICANT (<0.01), * SIGNIFICANT (<0.05), . ALMOST SIGNIFICANT (<0.1), N.S NON-SIGNIFICANT; THRESHOLD: P-VALUE = 0.05) 41

**TABLE S2.3 |** CAMERAS' INFORMATION 42

**TABLE S2.4 |** HERO4 BLACK PARAMETERS (157 IMAGES) 43

**TABLE S2.5 |** GROUND CONTROL POINTS (GCP) STATISTICS 44

**TABLE S2.6 |** PROCESSING PARAMETERS 46

**TABLE S3.1 |** COMPILATION OF ALL ESTIMATED VARIABLES OVER THE COURSE OF TEN YEARS. THE FIRST THREE VARIABLES CORRESPOND WITH DEMOGRAPHIC PERFORMANCE WITHIN A $10M^2$ TRANSECT (NUMBER OF INDIVIDUALS, AVERAGE CORAL DIAMETER, AND LIVE CORAL SURFACE AREA). THE NEXT SIX VARIABLES CORRESPOND WITH ESTIMATES OF $CACO_3$ PRODUCTION ($CACO_3$ PRODUCTION, AREA-NORMALIZED $CACO_3$ PRODUCTION, AND CUMULATIVE $CACO_3$ PRODUCTION FOR BOTH ISOMETRIC AND ALLOMETRIC $CACO_3$ PRODUCTION MODELS) 74

**TABLE 4.1 |** POINT ESTIMATES AND 95% CREDIBLE INTERVALS FOR FITTED PARAMETERS BASED ON BAYESIAN LINEAR MODELS ESTIMATING CALCIFICATION, RESPIRATION, AND PHOTOSYNTHESIS RATES ACCORDING TO COLONY SIZE FOR SIX CORAL SPECIES. THE COEFFICIENTS $\alpha$ AND ß ARE CALCULATED AS: METABOLIC RATE = $\alpha\ S_A^{ß}$ WHERE $S_A$ IS THE CORAL SURFACE AREA ($CM^2$) AND THE METABOLIC RATE IS EXPRESSED IN ($MG.H^{-1}$). WHEN ß IS LOWER THAN ONE, THE METABOLIC RATE SCALES HYPO-ALLOMETRICALLY WITH $S_A$, WHEREAS WHEN ß EQUALS 1, THE METABOLIC RATE SCALE ISOMETRICALLY WITH $S_A$. 88

**TABLE S4.1 |** POINT ESTIMATES AND 95% CREDIBLE INTERVALS FOR FITTED PARAMETERS BASED ON BAYESIAN LINEAR MODELS ESTIMATING CALCIFICATION, RESPIRATION, AND PHOTOSYNTHESIS RATES BASED ON COLONY SIZE AND SPECIES IDENTITY. 95

**TABLE 6.1 |** DENSITY, GROWTH RATE AND GAF OF THE 4 CCA SPECIES OBSERVED AT MO'OREA. DENSITY AND GROWTH ADJUSTMENT FACTOR (GAF) WERE RESPECTIVELY EXTRACTED AND DEFINED FROM LEWIS ET AL. (2017) 122

# Chapter 1

# General introduction


*Coral reefs in Temae (Mo'orea, French Polynesia), with one of many sunsets*

# 1.1 An uncertain future

## 1.1.1 Awareness of climate change

The first world conference that explicitly consider the anthropogenic degradation of the environment as a major issue was the 1972 United Nations Conference on the Human Environment in Stockholm (Linnér and Selin, 2013). Several principles for a sustainable use of environmental resources (including the Stockholm Declaration and Action Plan for the Human Environment) were adopted in that occasion. For the first time, the Stockholm Declaration placed environmental issues at the forefront of international concerns and started a dialogue between industrialized and developing countries on topics such as economic growth, air pollution, or even water and oceans (United Nations, 1972). At the end of this conference, participants created the United Nations Environment Program (UNEP) Najam, 2005).

Eighteen years later, in 1990, the Intergovernmental Panel on Climate Change (IPCC) published the first report (IPCC, 1990). They reported that emissions produced by human activities were gradually increasing the atmospheric concentrations of greenhouse gases (GHG). They highlighted that $CO_2$ had been responsible for over half of the enhanced greenhouse effect. They also observed that global mean surface air temperature had increased by *ca*.0.3 to 0.6 °C over the last 100 years.

Two years later, in June 1992, the Earth Summit (officially known as the United Nations Conference on Environment and Development – UNCED) was held in Rio de Janeiro (Brazil). During this conference, the United Nations produced a broad agenda (*i.e.,* the Agenda 21) calling for new investment strategies in the 21$^{st}$ century to achieve overall sustainable development (United Nations, 1992). The Earth Summit concluded that sustainable development was an attainable goal for all the people of the world and that integrating and

balancing economic, social, and environmental concerns is crucial for sustaining human life.

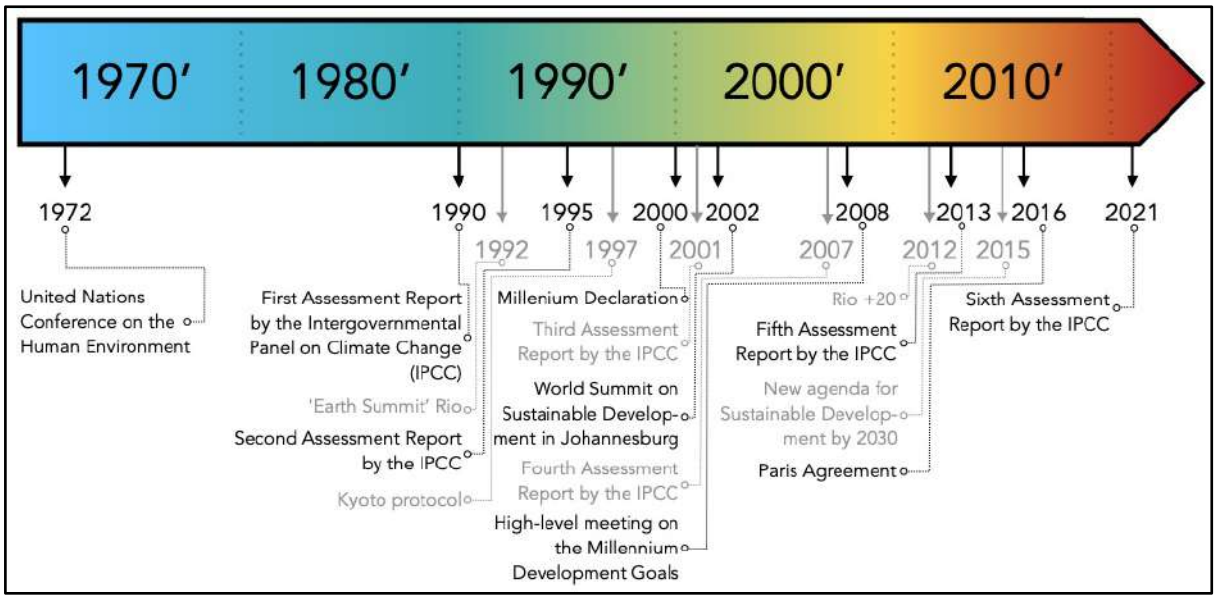


*Figure 1.1 | Major international events on climate change or sustainable development in the last fifty years.*

Overall, it was not until the 1990s that the number of environmental councils, working groups or declarations increased (**Figure 1.1**). From among the most noteworthy events to date, it is important to highlight that the IPCC has had six assessment cycles and delivered six Assessment Reports – the most comprehensive scientific reports – about climate change produced worldwide (https://www.ipcc.ch). Another landmark moment came in 2000 when the Millennium Summit established the eight Millennium Development Goals (MDGs) (United Nations, 2010), reviewed further at high-level meetings in New York, in 2005, 2008, and 2010. Later, in 2002, the World Summit on Sustainable Development in Johannesburg gave birth to a new Action Plan (Doran, 2002). A decade later, in 2012, the United Nations Conference on Sustainable Development (also called Rio +20) positively assessed the efforts made by the participating countries (United Nations, 2012). Finally, in 2015, the United Nations Summit on Sustainable Development gave birth to Agenda 2030 and its seventeen sustainable development goals (UN General Assembly, 2015).

## 1.1.2 Towards a changing world

### 1.1.2.1 Increased anthropogenic activity

• Human overpopulation

During the second half of the twenty-first century, the world population reached historically unprecedented demographic levels, exceeding 7.8 billion people in March 2020 (World Population Data Sheet, 2020). It has been shown that once humans reached a population of over 6 billion, their biomass exceeded that of all other major terrestrial animal species that have ever existed by more than 100 times (Cafaro and Crist, 2012). As a result, over 15 000 scientists worldwide issued a warning to humanity which asserted that rapid human population growth is the main driver behind many ecological and even societal threats (Ripple *et al.*, 2017).

• Overfishing

One of the main problems of fisheries science remains the growing gap between the number of fish available - defined by fishing quotas - and humanity's desire to catch them, a problem that is getting worse as the world's population increases (World Population Data Sheet, 2020). Therefore, as the 2019 report of the Intergovernmental Science-Policy Platform on Biodiversity and Ecosystem Services (IPBES) states, overfishing is the main driver of mass species extinction in the oceans (IPBES, 2019), despite efforts toward more sustainable practices. In fact, the Food and Agriculture Organization (FAO) stated that regulated fishery production has remained constant for the last two decades whilst unsustainable overfishing has increased to 33% of the world's fisheries. In parallel, they also noted that aquaculture has increased from nearly 120 million tonnes per year in 1990 to more than 170 million tonnes in 2018 (http://www.fao.org/home/en/).

• Irrigation

The agricultural sector is, undoubtedly, the main consumer of water worldwide, accounting for about 70% of withdrawal and 90% of consumption (https://www.worldbank.org). In several developing countries, irrigation accounts for up to 95% of all water use and is a major contributor to food production and security (http://www.fao.org/home/en/). Unfortunately, although irrigation projects can have large benefits, the negative side effects are often overlooked (de Fraiture and Giordano, 2014). Agricultural irrigation technologies (*e.g.,* high-powered water pumps, pipelines) are responsible for the large-scale depletion of freshwater resources (*e.g.,* rivers, lakes, aquifers). As a result, water resources are running dry, contributing, in turn, to the extinction of many aquatic species (Pearce, 2018).

• Agricultural land loss

Land degradation is a process partly caused by a combination of human-induced processes acting upon the land (Edwards, 1991). Global loss of agricultural land by degradation and abandonment is estimated to be from 6 (Bridges and Oldeman, 2019) to 12 (Edwards, 1991) million hectares per year since the mid-1940s. Such losses are attributable to soil erosion and salinization, loss of nutrients and organic matter, acidification, compaction, water logging, and subsidence (Bridges and Oldeman, 2019). Human-induced land degradation tends to be particularly serious in dry regions (Eswaran, Lal and Reich, 2001). Despite estimated losses of agricultural land, the amount of arable land used in crop production globally increased by *ca.* 9% from 1961 to 2012 (http://www.fao.org/home/en/). Worryingly, it is estimated that a third of the world's agricultural land is seriously degraded (Cameron *et al.*, 2015).

• Meat production

Around 26% of the planet's terrestrial surface is devoted to livestock grazing (http://www.fao.org/home/en/), resulting in an increase in the use of fossil energies, a decrease in water and land resources, and a significant rise in GHG emissions (Steinfeld *et al.*, 2006). The continuous increase of demand for meat is contributing to biodiversity loss as it is one of the main drivers of deforestation and habitat destruction (see section 1.1.2.3) (Machovina, Feeley and Ripple, 2015).

### 1.1.2.2 Climate change

Many indicators (*e.g.,* the increase in the Earth's surface temperature or the rise in average sea level) point to a change in climate over the course of at least the last century (https://www.ipcc.ch). There is now a consensus on the role of human activities in this change: the climatic balance is essentially disturbed by anthropogenic GHG emissions.

• Carbon dioxide

$CO_2$ emissions into the atmosphere can be of natural or anthropogenic origin. The anthropogenic source has been growing rapidly in recent decades (Myhre *et al.*, 2013). Once released, the gas is partly absorbed by natural carbon sinks and has doubled between 1960 and 2010. Half of the $CO_2$ released by human activities is stored in the atmosphere (Blunden and Boyer, 2021), reaching over 410ppm in 2019, whereas it was around 280ppm prior to the Industrial Revolution (**Figure 1.2**). According to the latest data from the Emissions Database for Global Atmospheric Research (EDGAR, https://edgar.jrc.ec.europa.eu), released in 2019, global $CO_2$ emissions increased by 1.9% in 2018, a bigger increase than in the previous year (*i.e.,* +1.2%). Rising emissions in Asia account for more than half of this growth. Emissions are also increasing in North America (+2.2%), while they are decreasing in the European Union (-1.9%). Indeed, in 2018, China remained the world's largest $CO_2$ emitter (29.7%), ahead of the

United States (13.9%), the European Union (8.1%) and India (6.9%). Between 1990 and 2018, overall emissions increased by 67.4% (*i.e.*, 15.2 Gt $CO_2$). Over this period, the biggest contributors to this increase were China (+370%, 8.9 Gt $CO_2$), India (+340%, 2.0 Gt $CO_2$) and the Middle East and North Africa (+210%, 2.2 Gt $CO_2$). Over the same period, emissions from the United States increased slightly (+2.9%), while those from the European Union decreased (-19.3%). This overall increase intensifies the greenhouse effect, which causes global warming.

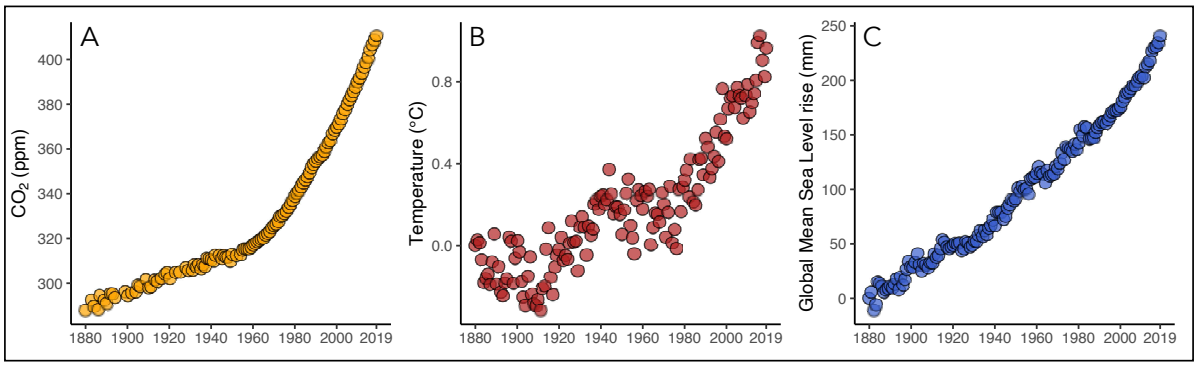


*Figure 1.2 | Climate trends from 1880 to 2019. A. Change in atmospheric CO2 concentration (ppm) B. Change in temperature anomaly (°C) C. Change in global mean sea level (GMSL) (mm). The reference year was arbitrarily chosen as 1880.*

• Temperature

The deviation of global average surface temperature from the pre-industrial reference period 1850-1900 is negligible until the mid-1930s, and then becomes essentially positive until about 1980 (**Figure 1.2**). Since the beginning of the 1980s, global warming has become more pronounced, with a continuous increase in the decadal surface temperature average (Allen *et al.*, 2018). The decade 2010-2019 (0.66°C above the 1961-1990 average) was 0.19°C warmer than the previous decade (0.47°C above the 1961-1990 average) (**Figure 1.2**). Moreover, the last five years observed are also the five warmest since 1850, with in 2016, the highest temperature anomaly of +0.86°C above the 1961-1990 average since 1850 (https://www.ncdc.noaa.gov/). Since the end of the 19$^{th}$ century, the global average temperature has risen by nearly 1°C (**Figure 1.2**).

• Acidification

Oceans absorb $CO_2$ and release it into the atmosphere, changing the carbonate chemistry and acidity of seawater (Doney *et al.*, 2009). This process has become a major global issue in the last decade because of the effects it could have on marine organisms and biogeochemical cycles (Hoegh-Guldberg, 2011). Indeed, under low pH and low carbonate concentration, water tend to dissolve calcium carbonate, threatening many organisms that use it to build their shells and skeletons (*e.g.*, scleractinian corals; DeCarlo et al., 2015). In addition, the energy needs required to adapt to a more acidic environment may reduce the amount of energy available for other physiological processes (*e.g.*, reproduction, growth) for several species (see chapter 4).

• Sea level rise

The polar regions are losing ice, and this loss has accelerated in the 2000s (Rignot *et al.*, 2008). Between 2002 and 2019, the mass of the Greenland ice sheet shrank by *ca.* 268 ± 14 Gt $year^{-1}$ (Moon *et al.*, 2020). More precisely, during the exceptionally warm Arctic summer of 2019, Greenland lost 600 Gt of ice, which is equivalent to a sea level rise of 2.2mm. The average sea level rose by 1.7 ± 0.3 mm $year^{-1}$ over the period 1901-2010 and has continued to rise with an average rise of 3.3 ± 0.4 mm $yr^{-1}$ over the period 1993-2019 (**Figure 1.2;** Moon et al., 2020). About 30% of the sea level rise is due to the expansion caused by the increase in water temperature (Church *et al.*, 2013).

• Increase of extreme weather events

Extreme weather events (*e.g.*, hurricanes, typhoons, heatwaves) are, by definition, rare events. They are therefore difficult to take into account in climate models, which tends to predict averages (Perera *et al.*, 2020). However, there are

indications that an increase in the frequency and magnitude of these events is very likely. More precisely, observations over the past 50 years show a trend towards warmer weather, an intensification of the water cycle, and, more randomly, an increase in storminess (Le Treut, Cubasch and Allen, 2005). Although there is still significant uncertainty concerning the increase in frequency of extreme sea storms (*e.g.*, those driven by tropical cyclones), there is consensus on the fact that warmer ocean temperatures and higher sea levels will increase their impacts (Christensen *et al.*, 2013), threatening coastal societies (see section 1.3.2).

## 1.1.2.3 Decline of ecosystems and associated species

Human activity is responsible for the deterioration of the environment through the depletion of resources (such as air, water and soil), ecosystem destruction, wildlife extinction, and pollution. Overall, 87% of the oceans and 77% of land surface (excluding Antarctica) have been altered by anthropogenic activity, whereas only 23% of the planet's landmass remains considered as "wilderness areas" (Watson *et al.*, 2018) and only 3% of the planet's terrestrial surface is not yet impacted by human activity (*i.e.*, little to no human footprint) (Plumptre *et al.*, 2021).

• Mass extinction

Through human history, there are many well documented cases of human-induced species extinctions (Robert, 1988; De Vos *et al.*, 2015). Today, the rate of extinctions has increased so much that it may be equivalent to the past mass extinctions (De Vos *et al.*, 2015), making our time the sixth mass extinction crisis. As a result, several scientists suggest that humans are the cause of this mass extinction crisis, the most serious environmental threat to the persistence of civilization due to its irreversibility (Ceballos, Ehrlich and Raven, 2020).

• Habitat Fragmentation

Habitat fragmentation is the reduction of a large area leading to habitat loss. Habitat fragmentation is considered to be one of the main cause of biodiversity loss and ecosystem degradation worldwide (Wilson *et al.*, 2016). Human pressures are highly responsible for habitat fragmentation, which alters the connectivity and quality of habitats (Wilson *et al.*, 2016). Some consequences include the reduction of pollination, as well as crop yield, with important consequences for food production worldwide.

• Decline in biodiversity and ecosystem collapse

Between 1970 and 2016, *ca.* 68% of the world's wildlife was destroyed due to human activity (Almond, Grooten and Petersen, 2020). More precisely, 83% of wild mammals, 80% of marine mammals, 50% of plants and 15% of fish have disappeared since the dawn of human civilization. Overall, one million species of plants and animals have gone extinct, putting many species populations at risk of vanishing over the next few decades (De Vos *et al.*, 2015). As a result, biodiversity loss represents a threat to the productivity of any ecosystem worldwide (Liang *et al.*, 2015), impacting natural ecosystem functioning (see section 1.3.2.1). Moreover, it has been highlighted that ecosystems could abruptly collapse if GHG emissions continue to rise, and that at the current rate of warming, ocean ecosystems could reach a tipping point as early as 2030, followed by tropical terrestrial ecosystems around 2050 (Trisos, Merow and Pigot, 2020). Indeed, the erosion of biodiversity is unlikely to occur gradually and would instead result in a succession of sudden collapses once a certain temperature threshold has been exceeded. As a result, if the global temperature rises by more than 4°C above pre-industrial levels, 15% of the world's ecosystems could face collapse. One of the main ecosystems at risk of collapse would be coral reefs.

# 1.2 Coral Reefs

## 1.2.1 Generalities

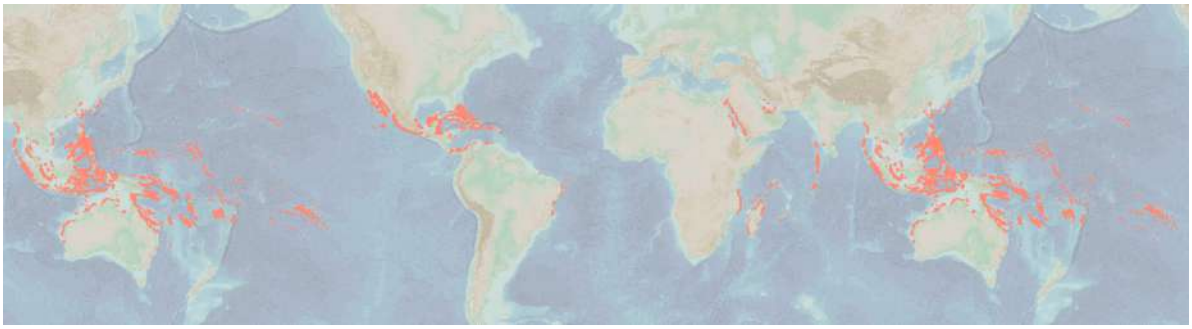

*Figure 1.3 | Global distribution of coral reefs in tropical and subtropical regions. This dataset was compiled from a number of sources by UNEP World Conservation Monitoring Centre (UNEP-WCMC) and the WorldFish Centre, in collaboration with the World Resources Institute (WRI) and The Nature Conservancy (TNC).*

Coral reefs are among the most diverse and productive ecosystems worldwide (Reaka-Kudla, 1997), delivering valuable ecosystem services to millions of coastal people (Hoegh-Guldberg, Pendleton and Kaup, 2019). They cover a mere 0.1% of the ocean but support one quarter of all marine species (Burke *et al.*, 2011). They are present in over 100 countries, including more than 80 developing countries (**Figure 1.3**). They are important sources of food and income, tourism and also protect shorelines from storms (see section 1.3.2.2) (Woodhead *et al.*, 2019). At least 275 million people depend directly on reefs for livelihoods and sustenance. Reef-dependence is particularly high in small-island states, especially in developing countries (Burke *et al.*, 2011). Therefore, coral reefs, along with mangroves and sea-grass beds, provide among the highest ecosystem services of all marine ecosystems on the planet. As an example, a healthy square kilometer of coral reef can yield over 15 tonnes of fish and other seafood every year (Hilmi, Safa and Reynaud, 2012). The Economics of Ecosystems and Biodiversity (TEEB) estimates that coral reefs generate *ca.* US$1.25 million per hectare thanks to tourism, coastal protection and fisheries (http://teebweb.org).

## 1.2.2 Key functions

One of the most remarkable facts about coral reefs is that tropical reef-building corals commonly flourish in nutrient-poor environments (Darwin, 1839) despite the high biodiversity and productivity that coral reefs may support. This phenomenon is called Darwin's paradox and, over a century later, it has continued to puzzle scientists. To answer this paradox, scientists have looked at coral reef functioning (Brandl, Rasher, *et al.*, 2019). They have highlighted that the solution to this paradox lies in the diverse set of multi-level functions that coral reefs dispose of.

### 1.2.2.1 At the holobiont scale

First, as the primary bio-constructors of reefs, scleractinian corals are foundation species that play a unique role in creating the habitats for thousands of other taxa (Stachowicz, 2001; Graham and Nash, 2013). At a reef scale, corals produce calcium carbonate ($CaCO_3$) and act as ecosystem engineers contributing to the structural complexity of the habitat (Graham and Nash, 2013) (**Figure 1.4**). This structural complexity plays an important ecological role in community regulation processes, promoting the formation of micro-habitats that serve as refuges against different types of environmental stresses (Lenihan *et al.*, 2008), as well as facilitating the overlapping of ecological niches and the maintenance of high biodiversity (Bruno, Stachowicz and Bertness, 2003). Coral colonies are home to a diverse endolithic and boring fauna, composed mainly of worms, molluscs, sponges, arthropods and echinoderms. Other species live as epifauna on the colonies, such as worms, molluscs, crustaceans and fish (Castro, 1988) (**Figure 1.4**).

Second, corals also play a major role in the primary production and transmission of energy through the food web. Indeed, through the photosynthetic activity of their symbiotic *zooxanthellae*, corals participate in a

significant part of primary production among reefs (Scott and Jitts, 1977). The assimilation of this energy by the polyps in the form of organic compounds allows energy to be transmitted from the *zooxanthellae* to the coral, and to higher trophic levels through predation. In addition to its photosynthetic activity which contributes to *ca.* 90% of the coral needs (*e.g.*, for growth or survival) when light conditions are good (Muscatine, 1990), the coral host can also secure some of its energy needs through heterotrophy (**Figure 1.4**). However, when conditions are unfavorable (*i.e.,* low light), the heterotrophy may represent up to 66% of the fixed carbon incorporated into the coral skeleton, reversing the balance between autotrophy and heterotrophy (Grottoli and Wellington, 1999).

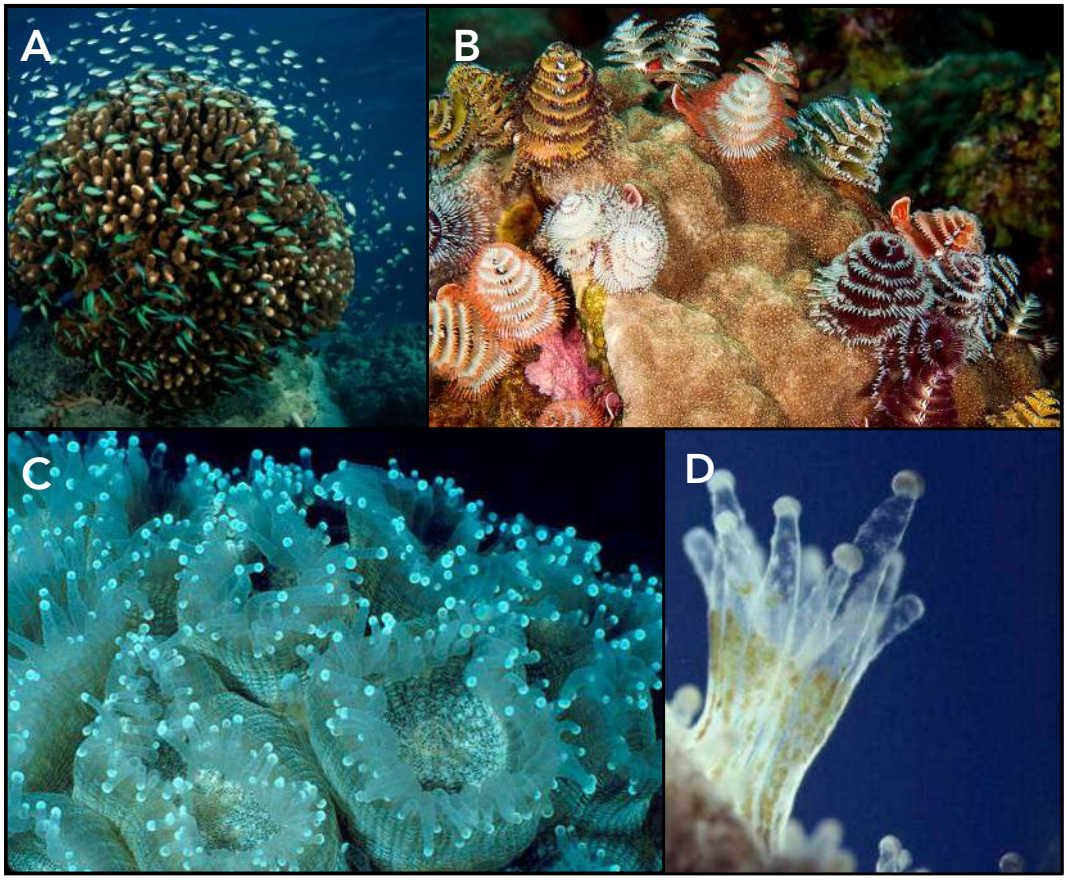


***Figure 1.4 |*** *A. Pocillopora meandrina hosting hundreds of damselfishes (Chromis viridis) © Lauric Thiault B. Spirobranchus giganteus (a tube worm of the family Serpulidae) living in corals of the genus Porites C. Coral polyps feeding at night D. Bleached coral polyps feeding on phytoplankton. B,C and D: © tumblr*

Third, coral reefs are net sources of fixed nitrogen (Rädecker *et al.*, 2015). Nitrogen fixation – in other words the conversion of elemental dinitrogen ($N_2$) into ammonium ($NH_4^+$) – contributes to the sustaining of net productivity under oligotrophic conditions (Cardini *et al.*, 2014). However, nitrogen fixation activity in corals is highly dynamic and can be rapidly changed according to environmental conditions (Wiebe, Johannes and Webb, 1975). Consequently, nitrogen fixation may counteract availability shortages of environmental nitrogen to maintain a constant nitrogen supply for symbiont-based primary production in corals. Nevertheless, the overall contribution from corals to the nitrogen budget, although non-negligible, remains relatively low (Rädecker *et al.*, 2015).

### 1.2.2.2 At the reef scale

Coral colonies also have a relatively large number of predators, both among fish taxa and among benthic invertebrates (Rotjan and Lewis, 2008). These corallivores can be classified into two categories according to the nature of their predation (Penin *et al.*, 2007). Strict corallivores remove living tissue from colonies without altering their calcareous skeleton (Cole *et al.*, 2011). Conversely, non-specialist predators exert accidental predation on colonies targeting epi- or endofauna or flora (Rotjan and Lewis, 2008). In general, this type of predation also affects the skeletal structure of corals, which predators ingest along with living tissue and epiphytic and endolithic species (Chazottes *et al.*, 2002). Other organisms such as gastropods, polychaetas, or reef fishes from other families (*e.g.*, *Balistidae*) may also exhibit significant predation on scleractinian populations (Rotjan and Lewis, 2008). Survival of specialist coral predators is significantly linked to coral health (*e.g., Chaetodontidae* (**Figure 1.5**). The presence of specialised predators is generally a good indicator of reef health, and any variation in their health tends to have an impact on these populations (Berumen and Pratchett, 2006).

Non-strict corallivores include a relatively large number of grazing organisms that predate on corals incidentally. This is the case of echinoids (*i.e.*, sea urchins) and on the other hand parrotfishes (**Figure 1.5**; Chazottes et al., 2002). These herbivores are generally known to play a role in regulating algal communities that are major competitors of corals (Mumby and Harborne, 2010). They have specialized mouthparts that allow them to scrape the surface of the substrate and ingest the algae growing on it (Viviani, 2019). In the process, these grazers also ingest some inorganic substrate, and by discharging it as finer particles, they participate in bioerosion and carbonate cycling on the reef (Chazottes *et al.*, 2002).

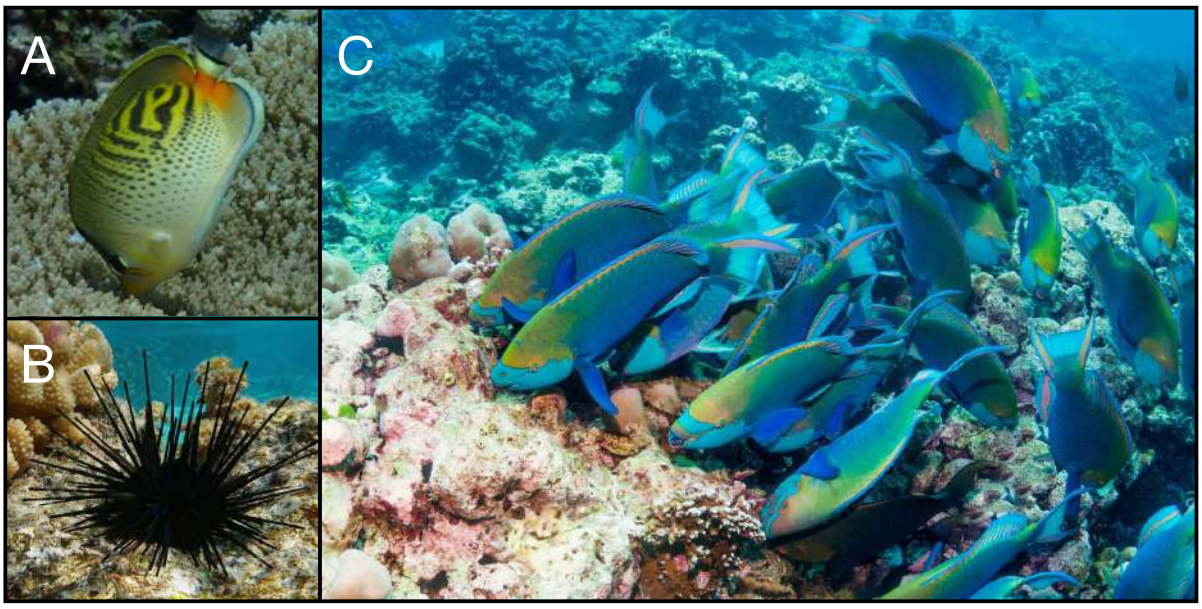


***Figure 1.5 |*** *A. Butterflyfish feeding on a coral of the genus Acropora B. One of the most abundant and widespread echinoids (i.e., Diadema sp.) in Mo'orea's waters C. School of parrotfish (Chlorurus sordidus) © Alamy stock photos*

Although, in general, accidental predation by grazers affects all corals, it mainly has a harmful effect on two stages of coral development. First, accidental predation by grazers affects coral recruitment through the abrasion or ingestion of new recruits on the substrate (Penin *et al.*, 2011), and at high intensities, grazing can locally limit coral recruitment (Penin *et al.*, 2010). Second, at the adult stage, bites from grazing species only partially affect colonies, which generally

survive such injuries (Mumby, 2009). At this stage of development, it is mainly the bioerosive hyperactivity exercised by high densities of grazers that can affect colonies, notably by weakening the calcareous structure at the base of colonies, leading in turn to a collapse of coral communities (Bellwood *et al.*, 2004).

## 1.3 Threats to coral reefs and their implications

### 1.3.1 Threats

Coral reefs are severely threatened by both natural and anthropogenic disturbances, including extreme rain events that dilute seawater, waves associated with super-storm, and thermal stress from unusually warm water (Hughes, Barnes, *et al.*, 2017). Although the list above corresponds to the main threats, coral reefs may also face other damaging activities such as coral mining or pollution, cyanide and blast fishing. Overall, these disturbances seldom destroy entire reefs (although they are amplified in intensity and frequency by human activity), but the increase in frequency of these disturbances could lead to the absolute decline of coral reefs by 2050 (Heron *et al.*, 2017).

#### 1.3.1.1 *Acanthaster* cf. *solaris* threat

One of the most emblematic coral predators is the Crown-of-Thorns starfish (*Acanthaster* cf. *solaris*, also called COTS; Kayal *et al.*, 2012). The effects of COTS outbreaks are highly variable. For example, 8 to 9 years after the start of an invasion, up to 60% of about 400 km of the Great Barrier Reef (GBR) was still affected, especially in the outer part, and up to 10% was lost (Moran, 1988). Coral cover in some areas fell from 78% to 2% in six months (Moran, 1988). COTS are one of the main cause of coral mortality in Indonesia (Baird *et al.*, 2013), with mortality rates exceeding 50% at many sites. In French Polynesia, the island of Mo'orea lost more than 96% of its initial coral cover between 2005 and 2010 (Pratchett *et al.*, 2017). Recovery after these outbreaks is slow (Moran, 1988)), with young corals being more vulnerable than large colonies (Leray *et al.*, 2012).

The consequences are not limited to corals: it has been observed that during a COTS outbreak, corallivorous fish populations decline, to the benefit of herbivorous species (Moran, 1988), thus permanently modifying the composition of the ecosystem (Kayal *et al.*, 2012) (see section 1.3.2.1).

### 1.3.1.2 Bleaching events

One of the direct effects of anthropogenic climate change is the increase in seawater temperature, which leads to the breakdown of the symbiosis between host coral and *zooxanthellae* (Hughes *et al.*, 2003). As a result, the microscopic *zooxanthellae* can no longer transform light energy into organic compounds, which leads to the production of oxygen radicals (Fitt *et al.*, 2001). The corals, unable to tolerate the presence of these substances in large quantities, then expel the *zooxanthellae*, leaving the coral tissues transparent.

In the last two decades, bleaching events have become an annual phenomenon (Kwiatkowski *et al.*, 2015). The risk of bleaching has increased most in Australia, the Middle East, and parts of Asia, with the first mass bleaching observed in 1998 (Wilkinson, 2008). It was considered the most severe on record, with bleaching affecting every biogeographical region of the world. Mass bleaching events became more frequent, with a second event recorded in 2010, (https://www.aims.gov.au) followed six years later by the most severe mass bleaching event ever recorded, in 2016 (Hughes *et al.*, 2018). As a result, 67% of corals have been impacted in Australia's northern part of the Great Barrier Reef (GBR). The fourth mass bleaching event was recorded only one year later, in 2017, causing widespread damage (Hughes, Kerry, *et al.*, 2017). These mass bleaching events result from the periodic occurrence of the warm equatorial Pacific El Nino current, which was particularly intense in 2015 and 2016 (https://www.ncdc.noaa.gov/). Recently, in 2020, the latest and fifth mass bleaching event was recorded (Pratchett *et al.*, 2021). This event was considered the second most serious on record, just behind the 2016 mass bleaching event.

Severe levels of bleaching occurred in all three sections of the GBR (*i.e.*, northern, central, and southern), damaging severely, once again, the GBR. Since 1980, 30% of bleaching events have been classified as "severe" and the risk of bleaching worldwide has increased by 4% per year, causing an estimated 16% of the worlds' coral reefs to die (Heron *et al.*, 2017).

#### 1.3.1.3 Tropical storms

Finally, one of the most serious impact on coral reefs is due to tropical storms. For example, at the GBR, tropical storms and cyclones account for 48% of estimated losses of coral cover, followed by coral predation by COTS (42% of coral loss) and coral bleaching (10% of coral loss) (De'ath *et al.*, 2012). The latter, however, has recently increased dramatically (Hughes *et al.*, 2018) (see previous section 1.3.1.2). Indeed, wave forces generated by winds, particularly by tropical storms and cyclones, are often the dominant process acting to limit coral colony size (Madin *et al.*, 2014) and strongly influence coral cover change (De'ath *et al.*, 2012). Colony dislodgment by frequent storms results mainly in mortality – although, in rare cases, unattached colonies may live for several days (Knowlton *et al.*, 1981) and may even reattach to become part of the reef again (Smith and Hughes, 1999). In addition, the biomechanical vulnerability of corals to storms differs among species and individuals due to their shape and size, with susceptible species typically becoming more vulnerable to dislodgment as they grow (Madin and Connolly, 2006).

### 1.3.2 Coral reef decline

#### 1.3.2.1 Changes in coral reef functioning

• Overall community changes

Some predictions suggest that about 70% to 90% of all coral reefs may be severely impacted over the next 20 years due to the several threats mentioned

above (see section 1.3.1) (Setter et *al.*, *in review*). Currently, 19% of the existing area of functional coral reefs have been lost and about 60% of the world's reefs may be at risk (Wilkinson, 2008). If these stresses continue, the ecology and productivity of coral reefs will be affected worldwide. As a result, the fifth Global Environment Outlook predicts that many tropical coral reefs could be severely damaged by 2050 (Heron *et al.*, 2017). Coral reef decline will have devastating effects on coastal communities that depend on them. More precisely, loss of coral cover and shifts from coral-dominated to algal-dominated reefs would lead to the loss of many ecosystem functions and services on which people rely.

• Coral reef flattening

One of the direct implications of the threats mentioned above is the flattening of coral reefs. Indeed, increasing evidence suggests that many reefs will become low-complexity systems, dominated by turf algae (Jouffray *et al.*, 2015; Smith *et al.*, 2016; Arias-González *et al.*, 2017; Bellwood *et al.*, 2018). Coral reefs have changed in structure and shape over the past few decades: they have flattened, and many complex reefs have almost been destroyed. For example, the structural complexity of Caribbean reefs has declined in a non-linear trend with the nearly total disappearance of the most complex coral reefs over the past 40 years (Alvarez-Filip *et al.*, 2009). More precisely, the flattening of Caribbean reefs was first observed in the early 1980s. This process slowed down between 1985 and 1998 before structural complexity began declining again more rapidly until now. The reason behind the flattening of the Caribbean coral reefs lies in a disease which spread in the waters between Florida and the Caribbean, where 90% of the Elkhorn and Staghorn reefs were destroyed. When corals were able to recover and grow again, the first mass bleaching event struck Caribbean coral reefs, resulting in a permanent change in their structural complexity. The decrease of structural complexity may threaten coastal societies due to lower efficiency in dissipating wave energy from oceanic waves (see section 1.3.2.2).

• Decrease in coral reef functioning

Despite decreased coral cover due to various disturbances, some regions have recovered equivalent or even greater coral cover post-disturbance. However, coral reefs may have lost several key species, resulting in a functional deficit. This point has been elucidated by McWilliam et al. (2020), who studied three geographically distant coral regions (*i.e.*, French Polynesia, Jamaica and Australia). For all of these regions, a perturbation occurred which drastically reduced the coral cover. After some time, the coral cover in each region increased again until it reached a pre-disturbance level of coral cover (although in Jamaica, the coral cover remained low). The researchers highlighted that, despite a good recovery, the coral reefs lost functionality.

## 1.3.2.2 Low reef accretion rates

• Reef accretion rate

On the one hand, corals produce $CaCO_3$ (see section 1.2.2.1) which is used to maintain both their three-dimensional physical structures and their vertical growth potential. On the other hand, increasing temperatures and $CO_2$ levels are considered a key factor in coral reef degradation (see section 1.1.2.2). It has been established that the combined action of global warming and acidification reduces scleractinian coral calcification by 20% when $pCO_2$ levels exceed 700 ppm and temperature increases by 3°C (Kornder, Riegl and Figueiredo, 2018). As a result, carbonate budgets (*i.e.*, carbonate gains from calcareous organisms such as scleractinian corals minus carbonate losses from processes such as bioerosion by parrotfishes) are reduced, implying, in turn, lower accretion rates (*i.e.*, vertical growth). These results are supported by Perry & Morgan (2017) who point out that repeated coral bleaching events result in drastic reductions in carbonate budgets.

• Flooding risk

Coastal societies will be exposed to wave action unless coral reefs are able to keep up with the rising sea level by maintaining high standards of both vertical growth and structural complexity (Harris *et al.*, 2018; Perry *et al.*, 2018). Some islands from the Pacific have already suffered from sea level rise due to a low carbonate budget. Indeed, in 2016, researchers revealed that five of the Solomon Islands had disappeared into the Pacific during the second half of the 20$^{th}$ century (Albert *et al.*, 2016). Later, in 2017, this information was supported by (Nunn, Kohler and Kumar, 2017), and 8 new islands were reported as having sunk. Although relatively small (*i.e.*, 100 m$^2$ each), they are likely to have sunk between 2007 and 2014. Finally, other Pacific islands, such as the Kiribati Islands, suffered terrible flooding events in 2018, due to reduced structural complexity and low accretion rates resulting from the fourth mass bleaching event (see section 1.3.1.2). These islands are now at risk of being submerged by 2100 as well.

## 1.4 Ph.D. objectives

The aim of this multidisciplinary Ph.D. is to define how coral assemblages respond to expected global changes, especially in terms of functioning and coastal protection. My work is based in Mo'orea (French Polynesia) where the experimental station of the Centre de Recherches Insulaires et Observatoire de l'Environnement (CRIOBE) is located. My Ph.D. is divided into 7 chapters; the first corresponds to the general introduction you have read and the last to my general discussion and recommendations. The other chapters are described below:

Chapter 2. In this chapter, I define both the structural complexity and the coral cover in 2016 to hindcast structural complexity from 2004 to 2017 at Mo'orea and quantify how structural complexity is impacted by two types of disturbance (*i.e.*, a COTS outbreak and a cyclone).

Chapter 3. In this chapter, I highlight the extent to which juvenile corals are important for reef recovery, and define the $CaCO_3$ production from corals at Mo'orea from 2005 to 2016.

Chapter 4. In this chapter, I define calcification, respiration and photosynthesis rates for the six main coral species living at Mo'orea. I suggest that interspecific functional efficiency may explain the reshuffling of species that occurred in Mo'orea after a major disturbance.

Chapter 5. In this chapter, I demonstrate that the loss of structural complexity impairs the coastal protection service in a non-linear way, highlighting the devastating implications of extreme events.

Chapter 6. In this chapter, I quantify the $CaCO_3$ budget and the reef accretion at Mo'orea from 2005 to 2016, and I question Mo'orea's efficiency to protect coastal societies in the future according to the sixth IPCC assessment.

# Chapter 2

# Community composition predicts photogrammetry-based structural complexity on coral reefs

This chapter is published in *Coral Reefs*.

## Authors

J. Carlot, A. Rovère, E. Casella, D. Harris, C. Grellet-Muñoz, Y. Chancerelle, E. Dormy, L. Hedouin, V. Parravicini

## Citation

Carlot, J., Rovère, A., Casella, E. *et al.* Community composition predicts photogrammetry-based structural complexity on coral reefs. *Coral Reefs* **39,** 967–975 (2020). **https://doi.org/10.1007/s00338-020-01916-8**

# Abstract

The capacity of coral reefs to provide ecosystem services is directly related to their three-dimensional structural complexity. This parameter is also correlated with total fish biomass, reef resilience to external stresses and the dissipation of wave energy. However, information on structural complexity (*i.e.,* reef rugosity) has not always been assessed in historical monitoring programs, and long-term trends are sometimes unavailable. In this study, we show that it is possible to predict and hindcast the three-dimensional complexity of coral reefs by combining photogrammetry, statistical modelling and historical benthic community data. We calibrated lasso generalized linear models and boosted regression trees to predict structural complexity from photogrammetry transects around Mo'orea (French Polynesia). Our models were able to predict structural complexity with high accuracy (cross-validated $R^2$ ranges between 0.81 and 0.9). We then used our models to hindcast historical trends in 3D structural complexity using community composition data collected in Mo'orea from 2004 to 2017. The temporal analysis highlighted the severe impact of a crown-of-thorns (COTS) outbreak from 2006 to 2009 and Cyclone Oli in 2010. In conjunction, these two events reduce coral cover from *ca.* 50% to almost zero. While the collection of actual data is always to be preferred, our model captured these effects, confirming the capacity of this modelling technique to predict structural complexity on the basis of assemblage composition.

# 2.1 Introduction

The increasing frequency of coral mass mortality associated with bleaching events raises global concerns (Van Oppen and Lough, 2009; Heron *et al.*, 2016; Hughes, Kerry, *et al.*, 2017). These disturbances are associated with severe habitat destruction, which reduces the structural complexity of coral reefs (Newman *et al.*, 2015). Structural complexity is the three-dimensional spatial arrangement of an ecosystem (McCormick, 1994; Chazdon, 2014), and on coral reefs this is represented by the multitude of growth forms and distribution of hard corals. According to the habitat heterogeneity hypothesis, the more complex the structure of an ecosystem, the greater the diversity and abundance of associated organisms (MacArthur and Wilson, 1967). On coral reefs, the 3D structural complexity of the habitat is correlated with the biomass and diversity of fishes (Willis and Anderson, 2003; Gratwicke and Speight, 2005; Alvarez-Filip *et al.*, 2009; Rogers, Blanchard and Mumby, 2014), the reef's capacity to recover from disturbances (Graham *et al.*, 2015) and the reef's ability to dissipate wave energy, thus protecting the shoreline from extreme inundations (Harris *et al.*, 2018). Broad-scale declines in the complexity of coral reefs have been observed in the Caribbean and the Indo-Pacific as a result of both human impacts and climate changes (Hoegh-Guldberg, 1999; Hughes *et al.*, 2003; Hoegh-Guldberg *et al.*, 2007; Perry *et al.*, 2018). While several monitoring programs (*e.g.*, NOAA coral reef monitoring plan) regularly assess structural complexity, this is not the case in across all regions such as French Polynesia.

In the context of spatial analysis in geomorphology, Risk (1972) and Hobson (2019) highlighted the importance of selecting surface complexity metrics that are 1) readily understandable and interpreted, 2) capable of being measured in the field, and 3) comparable among studies and locations. In early studies, it was proposed that rugosity could be recorded by draping a steel chain over the reef surface, then measuring the ratio between the total length of the

chain and the planar distance between the ends of the chain. The higher the ratio, the more complex the substratum (Hill and Wilkinson, 2004; Graham and Nash, 2013). Despite the ease of use of such metric, laying a chain represents a bi-dimensional measure which does not capture three-dimensional (3D) habitats such as coral reefs. Although some time-consuming 3D metrics have been proposed (*e.g.*, Parravicini *et al.*, 2006), recent progress in underwater photogrammetry only recently provided the opportunity to capture the three-dimensionality of coral reefs. Examples of studies that employ photogrammetry include the use of a Remote Operated Vehicle (ROV) equipped with a downward-looking camera (Friedman *et al.*, 2012), extracting the species-level complexity index for six species along a transect (Burns *et al.*, 2015), defining new metrics to estimate complexity such as tortuosity and fractal dimension (Leon *et al.*, 2015; Naughton *et al.*, 2015) and measuring the small-scale three-dimensional features of a shallow-water corals with drones (Casella *et al.*, 2017). The growing prevalence of photogrammetry in studies on structural complexity has led some researchers to question the chain-tape method (Storlazzi *et al.*, 2016).

Whatever the metric employed (chain-tape or photogrammetry), ample data demonstrates that corals contribute to the overall complexity of a reef, but the mechanism by which corals contribute to this complexity is still a matter of debate. Some authors claim that it is driven by the presence of branching species such as *Acropora* spp. and overall coral cover is not as important (Aronson and Precht, 2006; Alvarez-Filip *et al.*, 2009, 2011). Others claim that coral cover is significantly and highly correlated to rugosity (Halford *et al.*, 2004; Graham and Nash, 2013) and/or species composition (Richardson, Graham and Hoey, 2017). In both cases, there is a consensus that structural complexity is related to coral community structure.

In this study, we combined statistical modelling with the reconstruction of 3D reef transects via photogrammetry in order to test our capacity to predict

coral reef structural complexity on the basis of benthic community composition. Using benthic time series data, we back-calculated reef structural complexity since 2004. We were able to retrace two relevant episodes of habitat destruction: the COTS outbreak from 2006 to 2009 and cyclone Oli in 2010.

# 2.2 Material and Methods

## 2.2.1 Study area

Mo'orea (French Polynesia) is located in the Pacific Ocean between 17.4714° and 17.6058° south and 149.7522° and 149.9269°' west. The island has three coastlines which face to the north, southwest and southeast (**Figure 2.1**). The island is encircled by a coral reef, which is 500 to 700 m wide. The only exception is the northeast extremity where the lagoon width is limited to a few tens of meters. Tides are semidiurnal with an amplitude of less than 0.3 m (Chazottes, Campion-Alsumard and Peyrot-Clausade, 1995; Leichter *et al.*, 2013). The swell direction is from the southwest to northeast during the entire year. The three sides of the islands can thus be used as a proxy of wave exposure (Carroll, Harrison and Adjeroud, 2006).

The reefs in Mo'orea are threatened by several biotic and abiotic disturbances (Adjeroud *et al.*, 2018). The most devastating biotic disturbances were the 1979 and 2006 COTS outbreaks, each of which reduced average coral cover from 50% to 10% or less (Berumen and Pratchett, 2006; Lamy *et al.*, 2016). Cyclones are the primary abiotic disturbances that affect reefs around Mo'orea. In 1991, Cyclone Wasa reduced coral cover around Mo'orea from 20% to 5%, while Cyclone Oli reduced coral cover, which was still recovering from the COTS outbreak, from 7% to 3% in 2010 (Lamy *et al.*, 2016; Adjeroud *et al.*, 2018) (**Figure 2.2**).

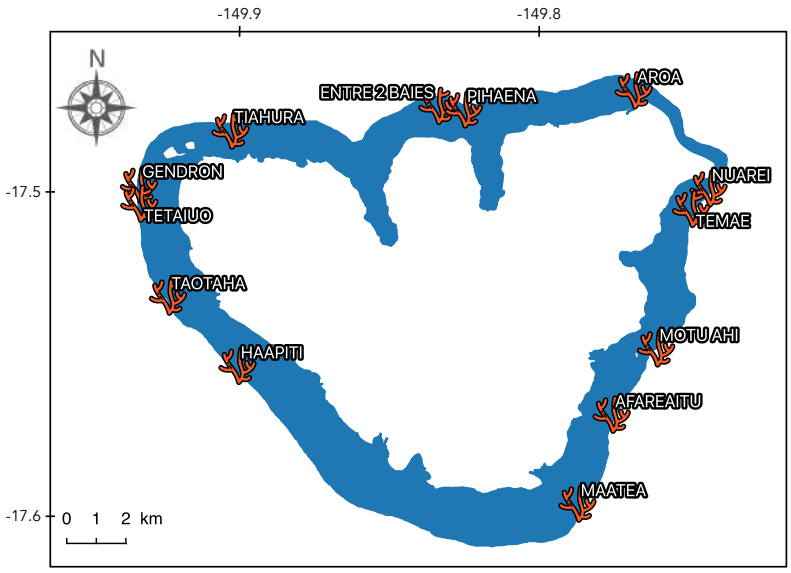


*Figure 2.1 | Location of the thirteen long-term monitoring sites surveyed each year from 2004 until 2017 around Mo'orea in the Society archipelago, French Polynesia.*

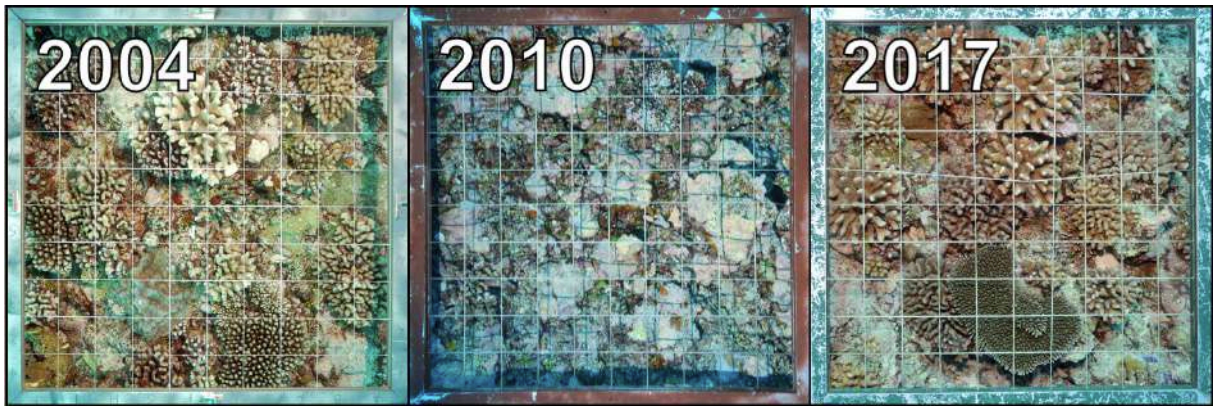


*Figure 2.2 | Evolution of one of the twenty quadrats used to define coral cover in Haapiti (on the southwestern side of the island) before (2004), immediately after (2010) and several years after (2017) Cyclone Oli.*

## 2.2.2 Structural complexity measurements

In Mo'orea, 57 photogrammetric transects were surveyed from the end of 2015 through the beginning of 2016 at three different sites that correspond to three wave exposures: Tiahura (North Coast, 21 transects), Haapiti (Southwest

coast, 20 transects) and Temae (Southeast coast, 16 transects) (**Figure 2.1**). Surveys were run as 20m × 2m belt transects, and all transects were conducted on the outer reef between 5 and 8m depth. For each transect, a 2m long chain was placed perpendicularly to a 20m transect, then a diver swam *ca.* 2m above the benthos along the transect at a constant speed as constant while collecting images with a GoPro Hero4 camera pointed toward the benthos. The camera was set to collect photos (12 megapixels) in time-lapse mode (2 pictures per second). For each transect, we collected approximately 300 photos with a forward overlap of *ca.* 90%, with the diver swimming over the length of the entire transect four times to allow optimal side overlap. After the photo collection, the diver noted the depth of each extremity of the chain and transect tape so that they may be used as Ground Control Points (GCPs). In the case of an in situ self-calibration, the camera calibration is derived from image coordinates measured in the mapping photography and including the camera calibration parameters as unknowns in a self-calibrating bundle adjustment (Harwin, Lucieer and Osborn, 2015).

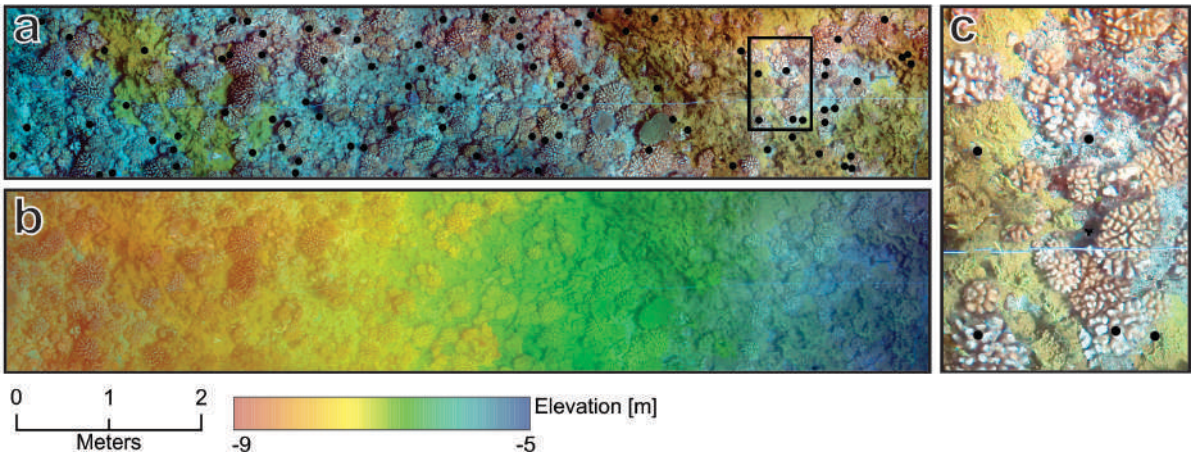


*Figure 2.3 | Example of underwater photogrammetry. **A.** Orthorectified photomosaic. The black dots indicate the random points with shape classification. **B.** Digital Elevation Model representing depth values (the photomosaic is kept transparent in the background). **C.** Detail of the photomosaic.*

The photos and the GCPs were input into Agisoft Photoscan (www.agisoft.com), a photogrammetry software based on the Structure from Motion (SfM) method (Ullman, 1979; Westoby *et al.*, 2012). We used Agisoft to build the orthophotomosaic and the Digital Elevation Model (DEM) of each transect, as explained by Storlazzi *et al.*, (2016). For the 57 transects, we estimated an average horizontal error of 0.1±0.06m and an average vertical error of 0.04±0.04m. Only the vertical error influenced the estimation of rugosity, but given the range of the error, it was considered negligible. Details of the photogrammetric process are detailed in the section 2.8. Subsequently, we imported the DEM in ArcGIS v10.2 and calculated reef rugosity by dividing the surface of the DEM area by the area of its planar projection (approximately 40$m^2$) (Figure 2.3).

## 2.2.3 Benthic community description and assessment

***Table 2.1 |*** *Shape classification categories defined to estimate rugosity. Ten variables are morphological, but the genus level is given for Acropora spp. and Pocillopora spp.*

| | |
|---|---|
| ACR | *Acropora* spp. |
| CCA | Crustose coralline algae |
| DEA | Dead corals |
| ENC | Encrusting corals |
| SMU | Sand and mud |
| RUB | Rubble |
| MAC | Macroalgae |
| MAS | Massive corals |
| OER | Corals with other erects forms |
| OTH | Other (like echinoid) |
| PAV | Pavement, bare rock and turf covering rock |
| POC | *Pocillopora* spp. |

In order to predict structural complexity as a function of benthic community structure, the orthophotomosaics produced by Agisoft Photoscan were imported into the software Coral Point Count v4.1 (Kohler and Gill, 2006). We assessed benthic cover by placing 100 random points on the photomosaic and described 8 distinct benthic cover categories (**Table 2.1)**.

In order to hindcast structural complexity for the three sites surveyed around Mo'orea, data from the MPA network long-term monitoring program was used. This dataset consists of benthic surveys from 2004 to 2017 using 25m line-point intercept transects collected around the island across three habitats (fringing reef, back reef and outer reef) (**Figure 2.1**). For comparability among datasets, we used only the long-term monitoring data collected on the outer reef.

## 2.2.4 Statistical analysis

All the statistical analyses were run on R version 3.5.3 (R Core Team, 2019). Our main goal was to calibrate a model that predicts structural complexity according to benthic community composition. In order to achieve this, we built a database that includes the time series data and data from our photogrammetry transects without transforming the data to perform multivariate analysis. Thus, the Euclidean distance on untransformed data was used to generate a principal component analysis (PCA) using the *vegan* package in R. The first 5 orthogonal axes, which accounted for more than 75% of the variance, were then extracted as predictor variables. To account for spatial variability in exposure, we included island side (north, southwest, southeast) as a parameter in our model.

In our models, we used lasso generalized linear models (using the *caret* package in R) and boosted regression trees (BRT; Elith, Leathwick and Hastie, 2008). With both methods, model selection was done to maximize the deviance explained with a ten-fold cross-validation procedure (CV-$R^2$). More precisely, the dataset is split into ten sections, nine of which are used for the calibration, and

the last one is used for the evaluation of model performance. CV-$R^2$ represents the expected performance of the model when fitted to new data (Elith, Leathwick and Hastie, 2008).

In the model coral reef structural complexity was predicted by the five PCA axes and island side as a proxy of wave exposure. In addition, BRT were fitted using the R functions provided by Elith, Leathwick and Hastie (2008). This technique requires the specification of four main parameters: bag fraction (bf), learning rate (lr), tree complexity (tc) and the number of trees (nt), where bf is the proportion of samples used at each step, lr is the contribution of each fitted tree to the final model, tc is the number of nodes of each fitted tree, and nt represents the number of trees corresponding to the number of boosting iterations. Optimal parameters were selected by CV-$R^2$ maximization (Parravicini *et al.*, 2013). The models were calibrated using 1000 bootstrap replicates of the original dataset to estimate uncertainty and provide 95% confidence interval around predicted values.

Both models were then used to hindcast structural complexity since 2004 using time series data. In order to estimate whether predicted structural complexity was able to identify the effect of major past perturbations (*i.e.,* COTS and cyclone Oli), we generated PCAs for each year using the Euclidean distance on untransformed data. We chose running PCAs to emphasize the patterns driven by the most abundant species/taxa (*i.e.,* the ones with the highest percent cover) since PCAs are more sensitive to variations in abundance than other ordination analyses (Van den Boogaart and Tolosana-Delgado, 2013). For the purpose of this study, we conducted a CA to verify that results are consistent. We ran an analysis of variance with year and island side as fixed factors to test for differences in structural complexity. A Tukey post-hoc analysis was then used to compare structural complexity across individual years (Table S2.1).

# 2.3 Results

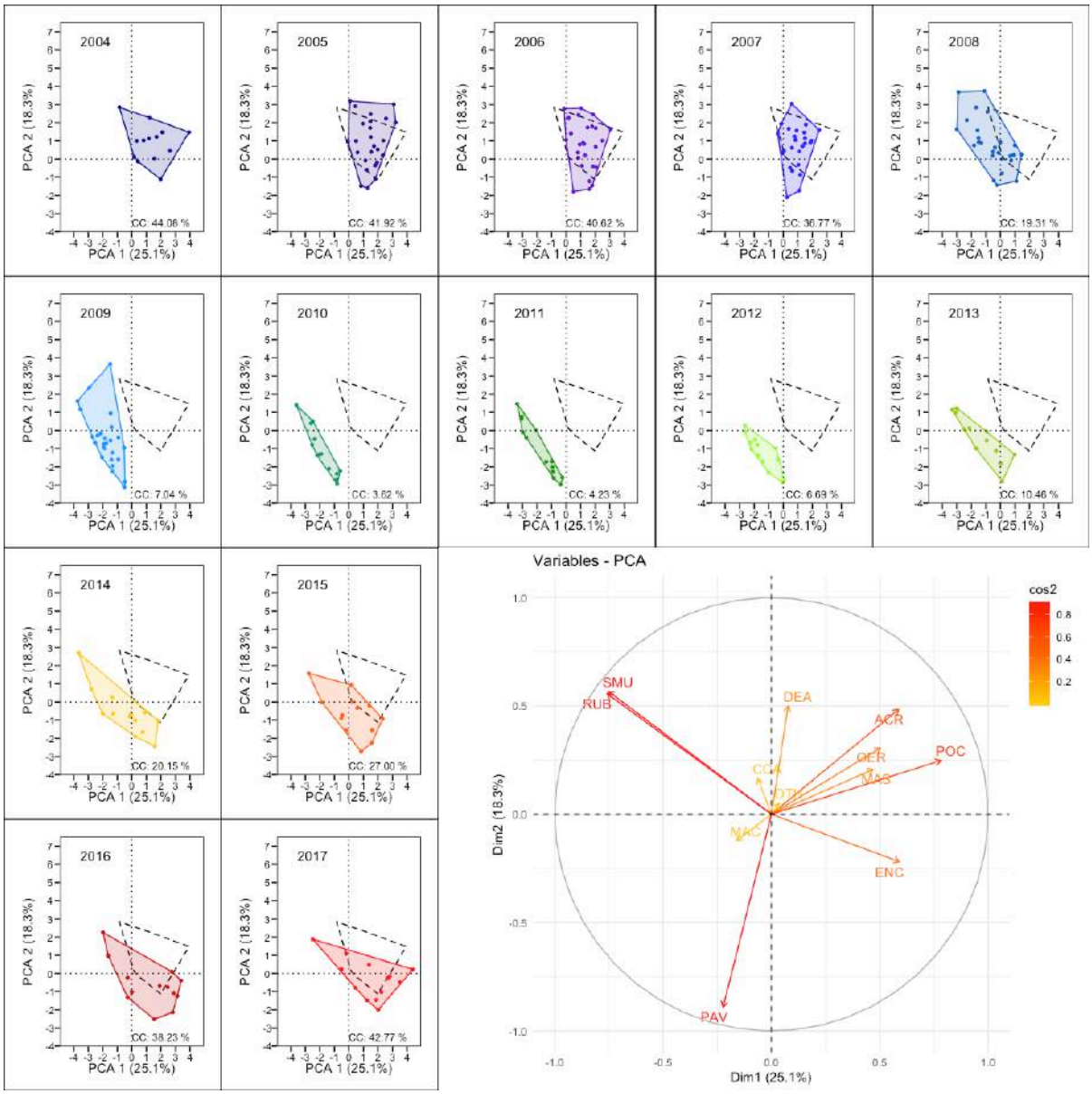


*Figure 2.4 | Principal components analysis (PCA) of the 11 morpho-species from 2004 to 2017. Coral cover (CC) is written at the bottom right of each box. On each plot, the coral community in 2004 is included as a baseline in black dashed lines. Abbreviations are as follow: ACR - Acropora spp; CCA - crustose coralline algae; DEA - dead coral; ENC - encrusting corals; MAC – macroalgae; MAS - massive corals; OER - other erects forms; OTH - others (Sponges or benthic species); PAV - pavement; and POC - Pocillopora spp; RUB – rubbles; SMU - sand or mud.*

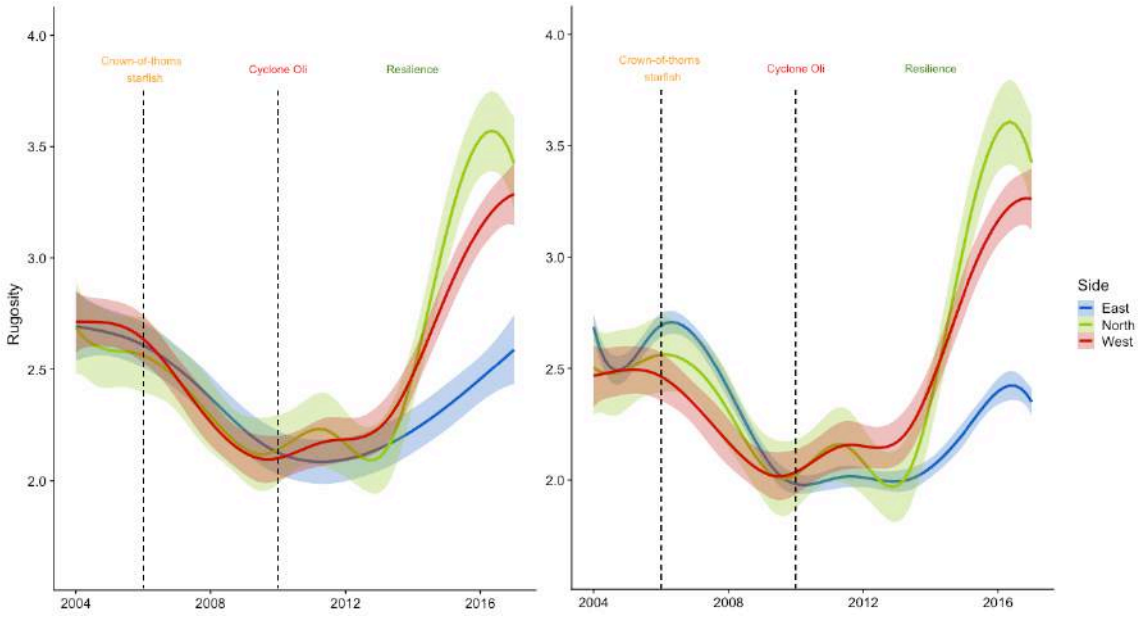


*Figure 2.5 | Rugosity reconstructions from 2004 to 2017 according to the average of the models (cross validated generated trees boosted model on the left and cross validated lasso generalized linear model on the right) on each of the three sides of Mo'orea. The COTS outbreak and Cyclone Oli are shown in 2006 and 2010, respectively.*

The time series data revealed that coral diversity was higher in 2004, with an average percent coral cover (CC) of 44.08% (**Figure 2.4**). The CC decreased from 2004 to 2010, reaching a minimum of 3.62% CC, which corresponds to cyclone Oli. After that, the CC increased through 2017, with a final value of 42.77%. In 2004, the coral reefs around Mo'orea also showed a higher diversity of coral morphologies (massive, branching, columns and encrusting). The assemblages remained fairly stable despite a slow decline of CC from 2004 to 2006 (44.08% to 40.62%). Then, a first COTS outbreak occurred in early 2006 and continued until 2009 (Kayal *et al.*, 2012). The following year, Cyclone Oli hit the island, further decreasing CC. After these events and until 2014, the substrate predominantly consisted of rubble. From 2015, the CC recovered to a state similar to that of 2004. However, compared to 2004, the coral cover in 2017 had a lower percent cover of *Acropora* spp. (9.76 ± 5.61% in 2004 vs 2.53 ± 1.90% in

2017). In contrast, the percent cover of *Pocillopora* spp. remained fairly stable (20.10 ± 6.78% in 2004 vs 26.61 ± 14.52% in 2017).

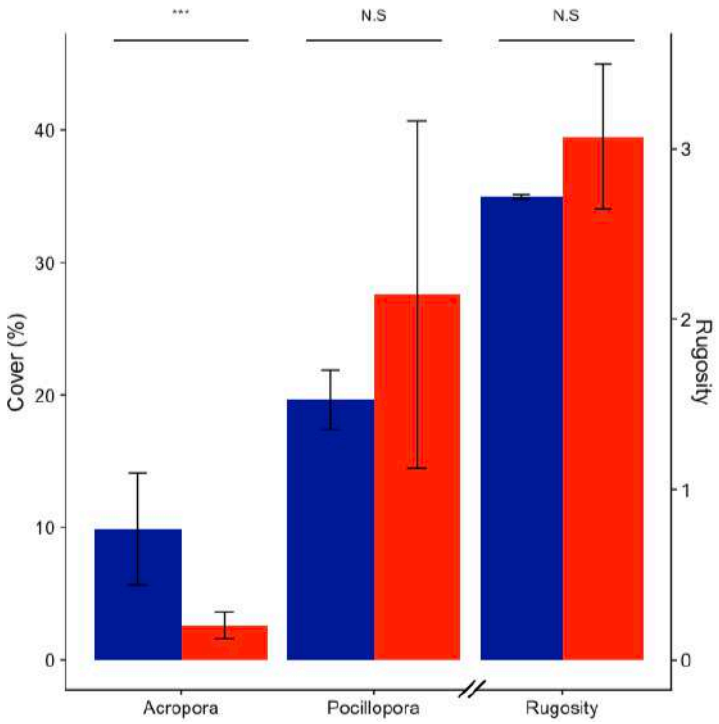


*Figure 2.6 | Difference between Acropora and Pocillopora cover (%), as well as the difference in rugosity index. Dark blue bars represent 2004, and red bars represent 2017. Asterisk indicate significant differences (p<0.05) while N.S indicate non-significant differences (p>0.05).*

The cross-validated $R^2$ (CV-$R^2$) from our models reached 0.81 for the lasso GLM and 0.9 for the BRT. After model selection, the first three PCA axes and island side were retained by the lasso GLM and the BRT (Table S2.2). The back calculation of structural complexity captured all major shifts in community structure described above. All sites were predicted to lose complexity in synchrony with COTS outbreaks and Cyclone Oli (Figure 2.5). Further, structural complexity also differs according to wave exposure.

Finally, rugosity reached pre-disturbance levels in 2015. Then, at the scale of Mo'orea, structural complexity remained fairly stable. Indeed, despite local

differences, when we compare the first year of monitoring (2004) with the last year of monitoring (2017), no significant differences were detected (**Figure 2.6, Table S2.1**).

## 2.4 Discussion

Utilizing a combination of photogrammetry and statistical modeling, we were able to use long-term species composition data to predict the structural complexity of coral reef assemblages around Mo'orea over the course of 14 years. Our hindcasted metric of structural complexity captured the significant changes in coral cover observed on Mo'orea's coral reefs (Berumen and Pratchett, 2006; Adjeroud *et al.*, 2018). *Acropora* spp. and *Pocillopora* spp. were dominant in 2003 and 2004 (Berumen and Pratchett, 2006). Subsequently, the populations of these genera were affected by both COTS outbreaks (2006-2010) and Cyclone Oli (2010) (Kayal *et al.*, 2012). *Acropora* was primarily susceptible to these disturbance events, but *Pocillopora* spp. also eventually collapsed, followed by *Montipora* spp. and *Porites* spp. During these events, predicted structural complexity dropped across all sites, demonstrating that statistical models can produce reasonable predicted values when accrual data are not available.

The use of photogrammetry allowed us to obtain a three-dimensional metric of structural complexity, which contrasts to the traditional chain transect method (Burns *et al.*, 2015). Alvarez-Filip *et al.* (2009) reviewed 464 records of rugosity among 200 reefs, which were predominantly performed with the chain method. None of the reported measures exceeded a rugosity of 4, however, 7% of our measurements exceeded this value. This may simply be attributed to the specific characteristics of our study, or, more likely, it may result from the higher resolution of photogrammetry compared to the chain method. Although a higher resolution (pixel size of 1.73µm x 1.73µm) does not translate to higher accuracy, it is important to also be aware of the limitations of photogrammetry (Figueira *et al.*, 2015; Lavy *et al.*, 2015; Bryson *et al.*, 2017). For example, the use of

photogrammetry performs better on planar segments of the reef where the diver can easily maintain a fixed distance from the benthos.

Our approach assumes that the confidence with which a model predicts structural complexity depends on several factors: i) the calibrating dataset covers all the potential combinations of benthic community structure, ii) the predicted values are insensitive to the employed modeling technique, iii) the model performs well on new data not included in the calibration, and iv) the model performance is insensitive to small variations in the input dataset. Statistical techniques allow us to address the last three points. Here we accounted for the uncertainty related to the statistical technique (*i.e.,* comparing BRT vs. GLM) and the effects of small variations in the input dataset using bootstrapping, and we evaluated the performance of our model on new data with cross validation. Upon doing this, uncertainty can be estimated and propagated into further analyses if structural complexity is used as a covariate in subsequent models.

Although the collection of actual data is preferred to hindcasting, when structural complexity information is not available and 'reference' or historical conditions need to be determined, statistical modeling can be used with caution to complement to existing data. However, predicted values from models cannot be blindly accepted. First, while the space-for-time approach is frequently used in ecological research (Pickett, 1989; Mcclanahan and Graham, 2005; Done *et al.*, 2010; Woesik *et al.*, 2011), it is prone to potential biases (Kappes, Sundermann and Haase, 2010). For example, dead coral can dominate benthic communities after a COTS outbreak as well as after a cyclone, but the 3D structure of the assemblage will be different in these two cases. Indeed, in both cases, live coral cover will be low, but after a COTS outbreak, the 3D structure of corals will be maintained; on the contrary, after a cyclone, the community will be flattened. Unfortunately, our calibrating dataset did not include data collected during perturbed conditions, such as after cyclone Oli. Second, our calibrating dataset

only included 5% acroporid cover, while in 2004, *Acropora* cover was, on average, 10%. Therefore, while we are able to delineate the general temporal trend, our capacity to accurately predict rugosity during these conditions is limited. Finally, topography may vary across time as a result of the balance between accretion and erosion, and topographic change may influence structural complexity in a way that cannot be accounted for in statistical models.

Structural complexity is negatively correlated with algal cover and strongly related to fish biomass, and it is also the main predictor of coral reef recovery after an acute disturbance (Graham and Nash, 2013; Graham *et al.*, 2015). Given the importance of structural complexity for the ecological functioning of coral reefs, the reconstruction of this variable from long-term benthic monitoring data may help us to better understand and predict changes in coral reefs. Today more than ever, global coral reefs are witnessing the effects of climate change and other human impacts (Hughes *et al.*, 2018). Coral bleaching is occurring on coral reefs with an unprecedented frequency, and future coral reefs are expected to lose diversity and productivity by these perturbations and effectively become flattened (Alvarez-Filip *et al.*, 2009). Long and reliable time-series are one of the best ways to obtain reference conditions for ecological indicators. When this information is not available, modeling represents a valuable alternative to track and anticipate the long-term loss of structural complexity.

## 2.5 Acknowledgements

We thank Jordan Casey for constructive comments and assistance with writing. This research was supported by grants Reef Services and RisqueRecif from the BNP Foundation and French Polynesian government. Valeriano Parravicini is supported by the Institut Universitaire de France.

## 2.6 Data availability

Code and data are available on my Github folder "Structural Complexity": https://github.com/JayCrlt/Structural_complexity.git

## 2.7 Supplementary information

*Table S2.1 | Post Hoc (Tukey HSD) matrix for testing the rugosity difference according to each year combination. The P-value (threshold: 0.05) for each combination is written in the matrix data as follows. The red values are significantly different and the blue values are not.*

| | 2004 | 2005 | 2006 | 2007 | 2008 | 2009 | 2010 | 2011 | 2012 | 2013 | 2014 | 2015 | 2016 | 2017 |
|---|---|---|---|---|---|---|---|---|---|---|---|---|---|---|
| 2004 | 1,00 | | | | | | | | | | | | | |
| 2005 | 0.98 | 1.00 | | | | | | | | | | | | |
| 2006 | 0.96 | 1.00 | 1.00 | | | | | | | | | | | |
| 2007 | 1.00 | 0.87 | 0.80 | 1.00 | | | | | | | | | | |
| 2008 | 0.04 | 0.00 | 0.00 | 0.00 | 1.00 | | | | | | | | | |
| 2009 | 0.00 | 0.00 | 0.00 | 0.00 | 0.93 | 1.00 | | | | | | | | |
| 2010 | 0.00 | 0.00 | 0.00 | 0.00 | 0.96 | 1.00 | 1.00 | | | | | | | |
| 2011 | 0.00 | 0.00 | 0.00 | 0.00 | 0.95 | 1.00 | 1.00 | 1.00 | | | | | | |
| 2012 | 0.00 | 0.00 | 0.00 | 0.00 | 0.98 | 1.00 | 1.00 | 1.00 | 1.00 | | | | | |
| 2013 | 0.01 | 0.00 | 0.00 | 0.00 | 1.00 | 1.00 | 1.00 | 1.00 | 1.00 | 1.00 | | | | |
| 2014 | 0.11 | 0.00 | 0.00 | 0.03 | 1.00 | 1.00 | 0.99 | 0.99 | 1.00 | 1.00 | 1.00 | | | |
| 2015 | 0.91 | 0.05 | 0.04 | 0.81 | 1.00 | 0.20 | 0.31 | 0.30 | 0.35 | 0.51 | 0.98 | 1.00 | | |
| 2016 | 1.00 | 1.00 | 0.99 | 1.00 | 0.01 | 0.00 | 0.00 | 0.00 | 0.00 | 0.00 | 0.05 | 0.80 | 1.00 | |
| 2017 | 1.00 | 1.00 | 1.00 | 1.00 | 0.00 | 0.00 | 0.00 | 0.00 | 0.00 | 0.00 | 0.00 | 0.34 | 1.00 | 1.00 |

*Table S2.2 | Coefficients and standard error for each parameter according to best model defined: Rugosity ~ Dim 1 + Dim 3 + Dim 5 + factor(Site) (R2 = 0.81). The p-value represents the significance of each parameter according to the R code (*** highly significant (<0.001), **very significant (<0.01), * significant (<0.05), . almost significant (<0.1), N.S non-significant; threshold: p-value = 0.05)*

| | Estimate | Standard Error | p-value |
|---|---|---|---|
| Intercept | 1.65970 | 0.14616 | 1.08e-15 (***) |
| Dimension 1 | 0.53283 | 0.08602 | 9.48e-08 (***) |
| Dimension 3 | 0.41917 | 0.07003 | 2.03e-07 (***) |
| Dimension 5 | -0.15003 | 0.06090 | 1.71e-02 (*) |

## 2.8 Annex

The following Annex details the settings from Agisoft Photoscan used for the processing of underwater photos for one site.

## 2.8.1 Survey Data

*Table S2.3 | Cameras' information*

| | | | |
|---|---|---|---|
| Number of images: | 157 | Camera stations: | 157 |
| Flying attitude: | 2.56m | Tie points: | 139.838 |
| Ground resolution: | 0.53 mm/pix | Projections: | 383.598 |
| Coverage area: | 56.3 sq m | Reprojection error: | 1.88 pix |
| Camera Model | Resolution | Focal Length | Pixel Size |
| HERO4 Black (3 mm) | 4000 x 3000 | 3mm | 1.73 x 1.73 um |

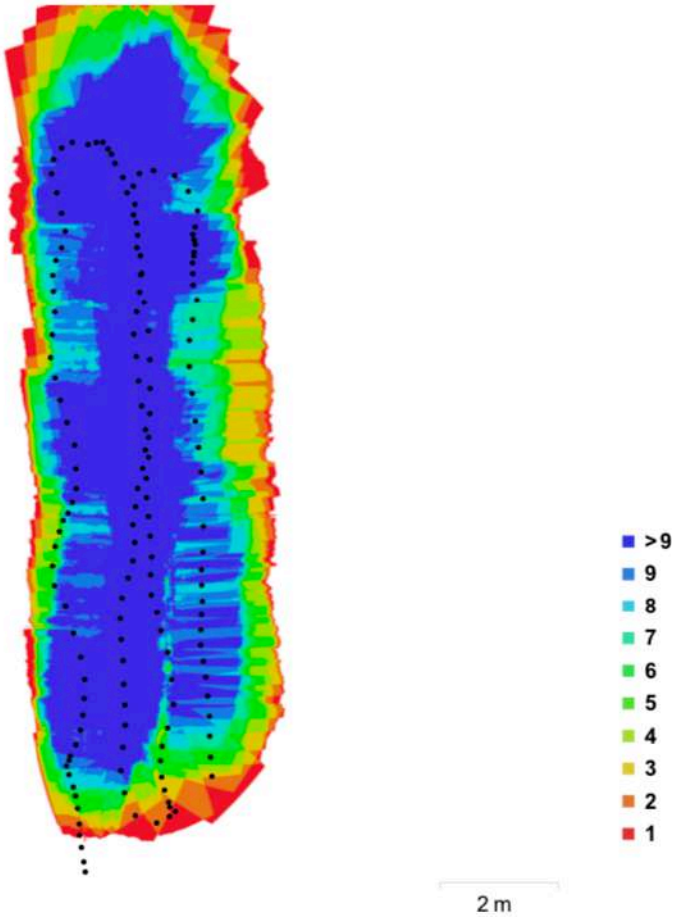


*Figure S2.1 | Camera locations and image overlap. Colors represent the number of photos overlapped.*

## 2.8.2 Camera calibration

*Table S2.4 | HERO4 Black parameters (157 images)*

| Resolution | Focal length | Pixel size | Precalibrated |
|---|---|---|---|
| **4000x3000** | **3 mm** | **1.73 x 1.73 µm** | **No** |
| Type: | Frame | Skew: | 0 |
| Fx: | 4666.42 | Cx: | 2005.25 |
| Fy: | 4666.42 | Cy: | 1486.48 |
| K1: | 0.223613 | P1: | 0.00194777 |
| K2: | 0.373779 | P2: | -0.00200162 |
| K3: | 1.24196 | P3: | 0 |
| K4: | 0 | P4: | 0 |

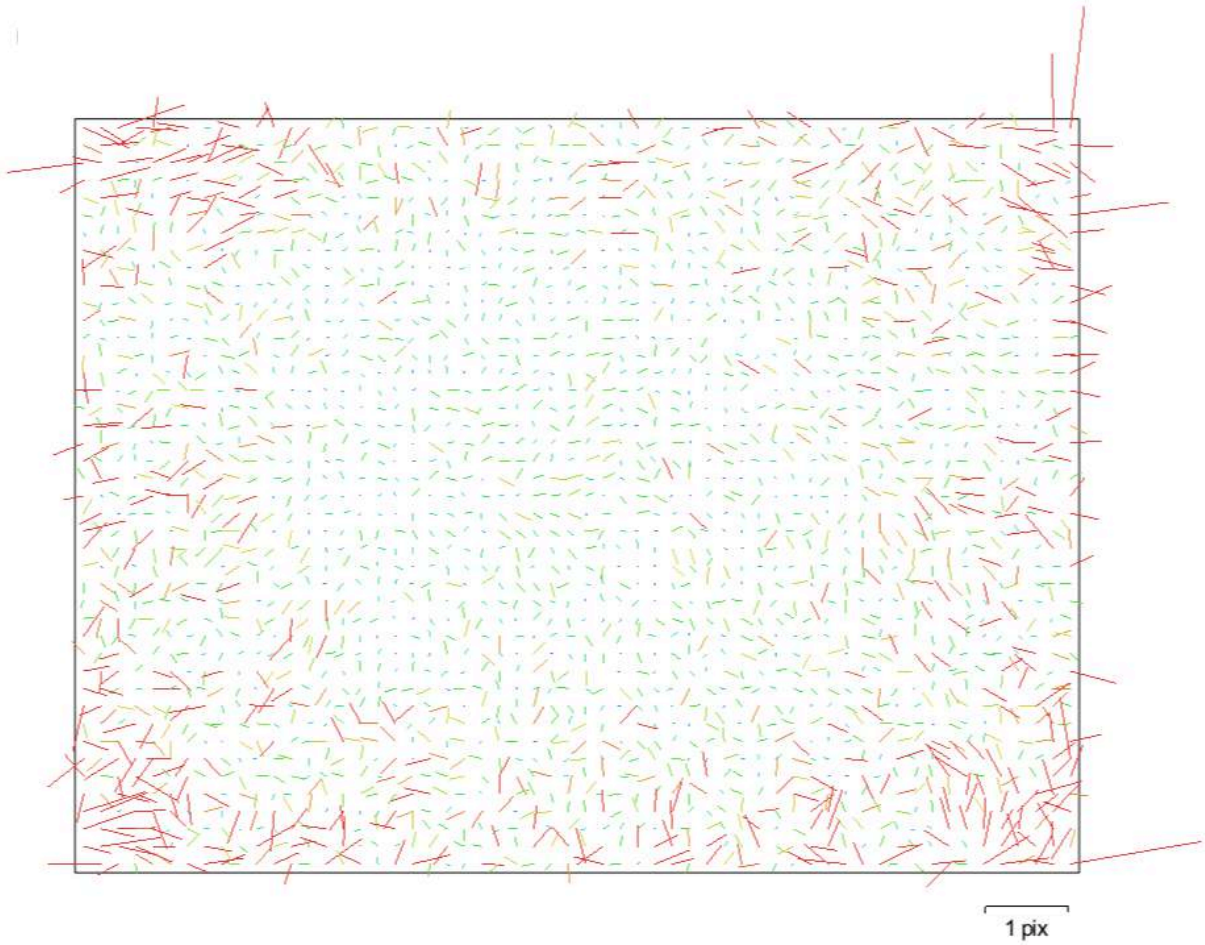


*Figure S2.2 | Image residuals for HERO4 Black (3 mm).*

## 2.8.3 Ground Control Points

*Table S2.5 | Ground Control Points (GCP) statistics*

| Label | XY error(m) | Z error (m) | Error (m) | Projections | Error (pix) |
|---|---|---|---|---|---|
| point1 | 0.206298 | -0.0677987 | 0.217153 | 13 | 1.992 |
| point2 | 0.0963633 | 0.0426041 | 0.105361 | 16 | 1.153 |
| point3 | 0.039409 | 3.96756e-05 | 0.039409 | 17 | 0.051 |
| point4 | 0.205045 | 0.0251539 | 0.206582 | 9 | 0.044 |
| **Total** | **0.154468** | **0.0419657** | **0.160067** | | **1.151** |


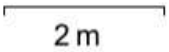

*Figure S2.3 | Ground control Points (GCP) overview*

## 2.8.4 Digital Elevation Model

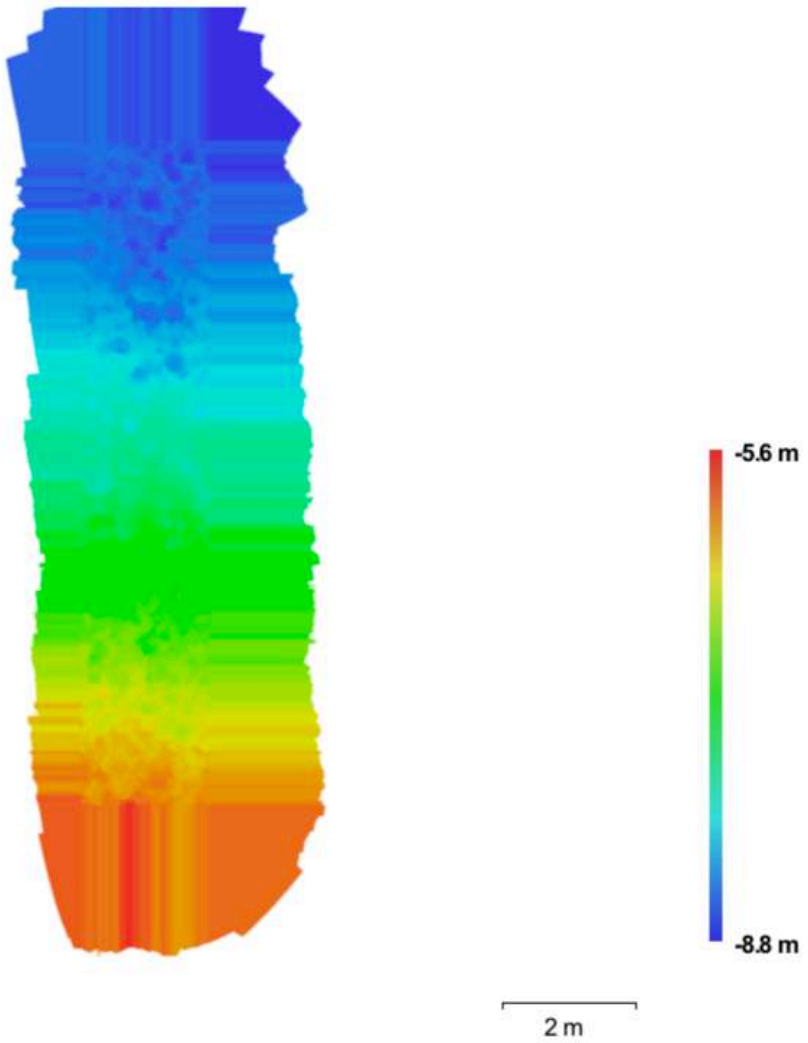


*Figure S2.4 | Reconstructed digital elevation model. Resolution: 1.06mm/pix and point density: 889956 pts/m$^2$*

## 2.8.5 Processing parameters

*Table S2.6 | Processing parameters*

| | |
|---|---|
| **General** | |
| Cameras | 157 |
| Aligned cameras | 157 |
| Markers | 4 |
| Coordinate system | Local Coordinates |
| **Point Cloud** | |
| Points | 139,838 of 221,231 |
| RMS reprojection error | 0.382302 (1.88392 pix) |
| Max reprojection error | 6.30304 (30.1948 pix) |
| Mean key point size | 5.32459 pix |
| Effective overlap | 2.94411 |
| **Alignment parameters** | |
| Accuracy | High |
| Pair preselection | Disabled |
| Key point limit | 40,000 |
| Tie point limit | 4,000 |
| Constrain features by mask | No |
| Matching time | 17 minutes 46 seconds |
| Alignment time | 3 minutes 10 seconds |
| **Optimization parameters** | |
| Parameters | f, cx, cy, k1-k3, p1, p2 |
| Optimization time | 5 seconds |
| **Dense Point Cloud** | |
| Points | 72,229,238 |
| **Reconstruction parameters** | |
| Quality | High |
| Depth filtering | Aggressive |
| Processing time | 8 minutes 29 seconds |
| **Model** | |
| Faces | 4,815,282 |
| Vertices | 2,417,898 |
| **Reconstruction parameters** | |
| Surface type | Arbitrary |
| Source data | Dense |
| Interpolation | Enabled |
| Quality | High |
| Depth filtering | Aggressive |
| Face count | 4,815,282 |
| Processing time | 4 hours 29 minutes |
| **DEM** | |
| Size | 1,886 x 9,433 |
| Coordinate system | Local Coordinates |
| **Reconstruction parameters** | |
| Source data | Dense cloud |
| Interpolation | Enabled |
| **Orthomosaic** | |
| Size | 3,773 x 18,867 |
| Coordinate system | Local Coordinates |
| Channels | 3, unit8 |
| Blending mode | Mosaic |
| **Reconstruction parameters** | |
| Surface | Mesh |
| Enable color correction | No |

# Chapter 3

# Juvenile corals underpin coral reef carbonate production after disturbance

This chapter is published in *Global Change Biology*.

## Authors

Jérémy Carlot, Mohsen Kayal, Hunter S. Lenihan, Simon J. Brandl, Jordan M. Casey, Mehdi Adjeroud, Ulisse Cardini, Alexandre Merciere, Benoit Espiau, Diego R. Barneche, Alessio Rovere, Laetitia Hédouin, Valeriano Parravicini

## Citation

Carlot, J., Kayal, M., Lenihan, H.S. *et al.* Juvenile corals underpin coral reef carbonate production after disturbance. *Global Change Biology* **27**, 2623-2632 (2021) https://doi.org/10.1111/gcb.15610

# Abstract

Sea-level rise is predicted to cause major damage to tropical coastlines. While coral reefs can act as natural barriers for ocean waves, their protection hinges on the ability of scleractinian corals to produce enough calcium carbonate ($CaCO_3$) to keep up with rising sea levels. As a consequence of intensifying disturbances, coral communities are changing rapidly, potentially reducing community-level $CaCO_3$ production. By combining colony-level physiology and long-term monitoring data, we show that reefs recovering from major disturbances can produce 40% more $CaCO_3$ than currently estimated due to the disproportionate contribution of juvenile corals. However, the buffering effect of highly productive juvenile corals is compromised by recruitment failures, which have been more frequently observed after large-scale, repeated bleaching events. While the size structure of corals can bolster a critical ecological function on reefs, climate change impacts on recruitment may undermine this buffering effect, thus further compromising the persistence of reefs and their provision of important ecosystem services.

# 3.1 Introduction

The Intergovernmental Panel on Climate Change (IPCC) predicts a climate-driven sea-level rise of 0.43m to 0.84m by 2100 (Oppenheimer *et al.*, 2019), thus increasing the risk of coastal flooding, especially during tropical storms (Tebaldi, Strauss and Zervas, 2012; Nunn, Kohler and Kumar, 2017; Ellison, Han and Lewis, 2019). Sea-level rise will be amplified in the tropics, where vulnerable ecosystems such as mangroves and coral reefs act as natural barriers to protect more than 500 million people from oceanic waves (Hoegh-Guldberg *et al.*, 2007). For coasts protected by coral reefs, their future exposure to oceanic waves will largely depend on the ability of scleractinian corals to produce enough calcium carbonate ($CaCO_3$) for reefs to grow vertically at a rate equivalent to sea-level rise. However, reefs are increasingly threatened by both climate change and local anthropogenic disturbances (Hughes, Kerry, *et al.*, 2017; Darling *et al.*, 2019). Climate-induced coral bleaching is expected to become an annual phenomenon for most coral reefs within the next twenty years (van Hooidonk *et al.*, 2016), inducing a state of constant disturbance that decreases the likelihood of recovery. Whether reefs and their services will persist is presently unknown and requires the assessment of reef $CaCO_3$ production across disturbance-recovery cycles (Harris *et al.*, 2018; Perry *et al.*, 2018).

The quantification of $CaCO_3$ production (kg $m^{-2}$ $yr^{-1}$) for reefscapes is traditionally based on species-specific linear extension rates of corals combined with the proportional substratum cover of the species. In most cases, this is applied to each colony regardless of their size (Perry, Lange and Januchowski-Hartley, 2018). Depending on the coral growth form, this scaling process relies on the assumption that species-specific $CaCO_3$ production rates are constant throughout coral ontogeny. However, this may not always be the case as $CaCO_3$ production rates may be either allometric or isometric (**Figure 3.1**). In the case of isometry, $CaCO_3$ production rate scales linearly with colony size; conversely, in

the case of allometry, $CaCO_3$ production rate either accelerates or decelerates as colonies grow. While it is often assumed that the coral colony-level production of $CaCO_3$ is isometric, recent work suggests that coral growth (expressed as an increase in planar area) is allometric, either because large colonies experience higher rates of partial-mortality (Madin *et al.*, 2020) and/or because coral colonies allocate less energy to $CaCO_3$ production in favor of reproduction once they reach a certain size (Kayal *et al.*, 2015). Whether coral growth is indeed isometric or allometric remains poorly resolved, but may significantly influence our community-wide estimates of $CaCO_3$ production (Figure 3.1). If corals grow allometrically, assuming isometry may lead to an underestimation of the production by small colonies and significantly obscure overarching estimates of $CaCO_3$ production patterns across reefscapes.

Recent climate-driven disturbances, especially catastrophic coral-bleaching events and major storms, can substantially alter the size-distribution of coral assemblages (Dietzel *et al.*, 2020). Large perturbations often remove a substantial proportion of large coral colonies and leave the remaining assemblage dominated by small corals (Alvarado *et al.*, 2016; Holbrook *et al.*, 2018). In these situations, isometric approaches may lead to a severe underestimation of overall $CaCO_3$ production, thus inhibiting our ability to infer a reef's ability to regain coral cover. Yet, the loss of large corals may also significantly reduce overall fecundity, leading to reduced coral recruitment and thus inhibiting coral recovery (Hughes and Tanner, 2000). This negative feedback loop can diminish the overall productivity of reefs over time (Hughes *et al.*, 2019). According to recent estimates, most coral reefs have a net production of $CaCO_3$ close to zero (Woodroffe and Webster, 2014; Perry *et al.*, 2018). Therefore, even slight differences in $CaCO_3$ production may have major implications for the capacity of reefs to survive despite sea-level rise.

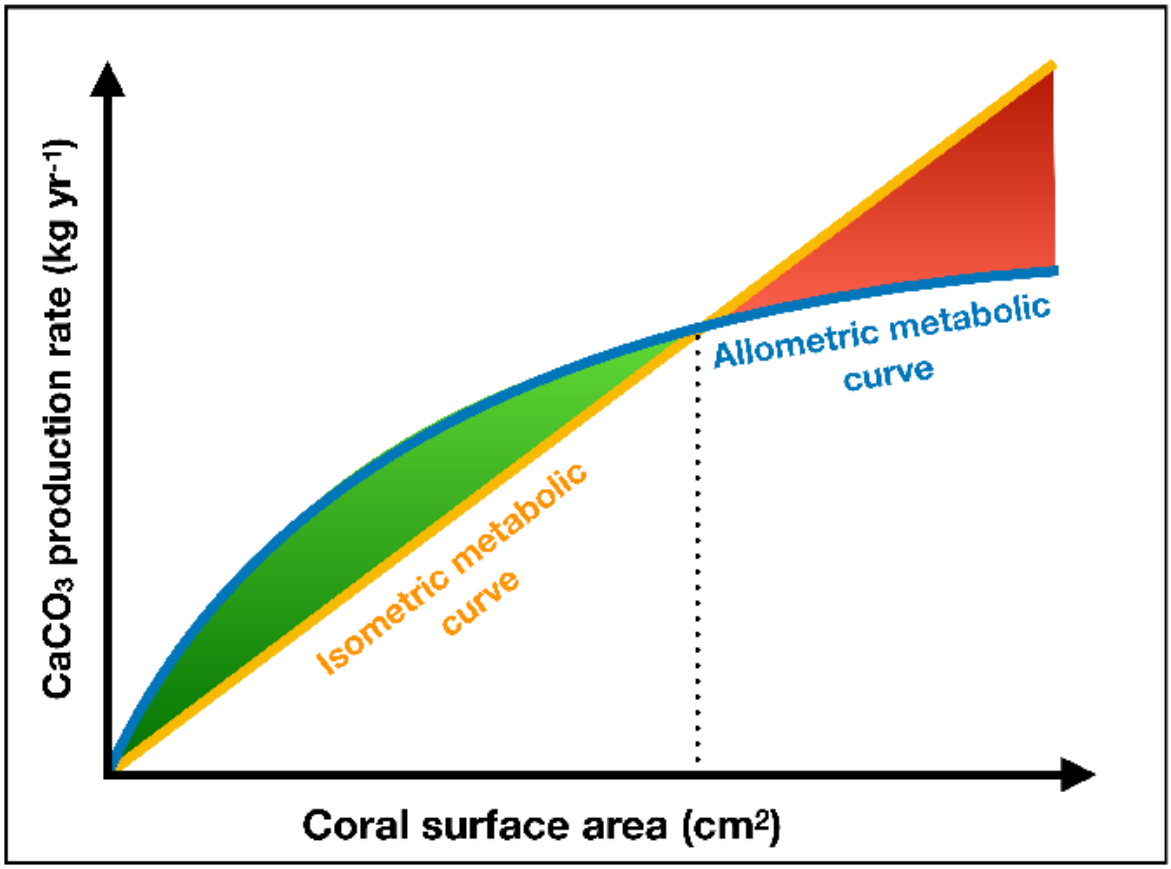


*Figure 3.1 | Conceptual diagram describing isometric versus allometric $CaCO_3$ production curves. Size dependent metabolic production characterized by (a) a linearly increasing model with coral surface area (isometric metabolic curve in orange; equation $y = \alpha x + 0$), and (b) a logarithmic asymptote (allometric metabolic curve in blue; equation $y = \alpha x^{\beta} + 0$). The dashed line indicates the size at which the two curves cross (i.e., this threshold point depends on both the intercepts and the allometric scaling slopes). Compared to the allometric model, the isometric model may underestimate $CaCO_3$ production below this threshold and overestimate $CaCO_3$ production at lager coral sizes.*

Here we estimate $CaCO_3$ production rates of three prominent coral genera over a range of colony sizes and test whether $CaCO_3$ production follows an allometric or isometric growth pattern. We then use an empirical time-series dataset from French Polynesia that reports the size of individual coral colonies across a ten-year disturbance-recovery cycle to examine whether the conventional isometric approach leads to an incorrect estimation of community-

level $CaCO_3$ production. Finally, we evaluate the outcome of large-scale disturbances, such as a major bleaching event, simulating the effect of recruitment loss on $CaCO_3$ production over five years.

# 3.2 Material and Methods

## 3.2.1 $CaCO_3$ production using *in situ* alizarin red-S staining

In June 2018, we used the approach described by Dustan (1975) to stain 175 coral colonies of *Acropora hyacinthus* (n = 50)*, Pocillopora* cf*. verrucosa* (n = 75)*,* and *Porites lutea* (n = 50) *in situ* at a depth of 10 to 15 m on the outer reef slopes around the island of Mo'orea (French Polynesia, **Figure S3.1**). Before staining, we measured the length, width, and height of each coral colony. We stained colonies with a surface area ranging from 140 $cm^2$ (*i.e.,* ~5 cm diameter) to 3,850 $cm^2$ (*i.e.,* ~80 cm diameter), which broadly matches the range of coral colony sizes observed in Mo'orea (Kayal et al., 2018; coral colonies observed *in situ* ranged from <1 $cm^2$ to ~5000 $cm^2$). We enclosed each coral in a 5, 10, or 20 L transparent plastic bag, filled with 10 mg $L^{-1}$ of alizarin red-S, for 72 hours. All colonies were tagged and mapped for future retrieval. To minimize the confounding effects of competition on growth, we chose colonies that were not in direct contact with other corals. In December 2018, 74% of colonies (n = 130) were recovered and three fragments were collected from each coral for growth measurements. We reasoned that a 6 month period was representative of the mean annual growth rate, since it covered the average temperatures typical for the cooler (26°C) and warmer (29°C) seasons in Mo'orea (cf. Smith, Barshis and Birkeland, 2007). Samples were dried for 48 hours and placed into transparent epoxy for 24 hours before slicing three 0.7 mm thick slices from each colony using a diamond-tipped saw, perpendicular to the major axis of growth. We took high-resolution photos of each colony slice using fluorescence, and calculated linear extension as the average of three measurements (*i.e.,* length, width, and height)

per colony (Figure S3.2). We also measured the longest linear extension from the edge of the stain to the periphery of the skeleton to the nearest 0.1mm using Image J software (Schneider, Rasband and Eliceiri, 2012). Finally, we calculated the $CaCO_3$ production rate using the equation C = (LE × D) × AC, where C represents the $CaCO_3$ production rate (g $cm^{-2}$ $yr^{-1}$), LE represents the linear extension (cm $yr^{-1}$), D represents the skeletal density, measured by the buoyed weight displacement method (respectively 1.4, 1.5 and 1.3 g $cm^{-3}$ for *A. hyacinthus, P. verrucosa* and *P. lutea*), and AC represents the adjustment coefficient (between 0 and 1), depending on the growth form of the colony (Morgan and Kench, 2012). We used an AC of 0.4, 0.5, and 1 for *A. hyacinthus, P. verrucosa,* and *P. lutea,* respectively.

### 3.2.2 $CaCO_3$ production using alkalinity anomaly ex situ incubations

To characterize $CaCO_3$ production in smaller colonies, for which the Alizarin red-S approach was not feasible, we removed 96 coral colonies (*A. hyacinthus* (n = 25)*, P. verrucosa* (n = 25) and *P. lutea* (n = 46)) with surface areas of 35–1,000 $cm^2$ (*i.e.,* ∼3–15 cm diameter) from the north shore of Mo'orea (depth = 12m) using a hammer and chisel. Before each collection, we recorded relevant environmental parameters (mean ambient seawater temperature, salinity, and photosynthetically active radiation). Upon return to the surface, we placed colonies in seawater tanks under the same environmental conditions for recovery and acclimation. Sponges, crustose coralline algae (CCA), macro-algae, epiphytes, and small crustaceans were carefully removed from the corals. We measured the length, width, and height of each colony, then tagged and kept the corals in the acclimation tank for 7 days. 73% of the colonies (n = 70) did not show any obvious adverse reactions to collected and handled, so we retained them for $CaCO_3$ production measurements. Coral colonies were grouped into three different size classes (<100 $cm^2$, 100–400 $cm^2$, and 400–1000 $cm^2$—see section 3.2.3). Size

selection for the incubation chambers was based on providing sufficient water volume for each coral colony, while ensuring traceability of changes in water chemistry (Kolb, 2018). Consequently, colonies were incubated in chambers of three different volumes (0.5, 1, and 4 L, respectively) to maintain a relatively constant incubation volume to colony size ratio. Four additional incubation chambers were used as blank controls. Each week, we assessed four controls and four corals of each size class. Water samples of 50 mL were collected from the incubation controls and each chamber after three hours of incubation for total alkalinity analysis. We made sure that coral colonies did not experience O2 reductions of more than 80% (Kolb, 2018), in which case observations were removed from the dataset. We defined net $CaCO_3$ production by assuming a mole of $CaCO_3$ is produced when the alkalinity measure ($\Delta AT$) drops by two moles for a fixed time ($\Delta t$) (Smith and Key, 1975). By multiplying these parameters ($-\Delta AT/2\Delta t$) by seawater density ($\rho_{sw}$), we defined the global $CaCO_3$ production rate, which was then normalized with live coral surface area and converted to g $cm^{-2}$ $yr^{-1}$ based on the molar $CaCO_3$ mass (Dickson, Sabine and Christian, 2007).

## 3.2.3 Photogrammetry-based size area relationships

To examine the relationship between $CaCO_3$ production and colony size, we used a 3D surface area to avoid underestimating coral $CaCO_3$ production, as surface folding and branching increase the coral surface area. Following the coral incubation protocol, 100 to 200 overlapping high-resolution photos were taken for each colony (**Figure S3.3**). The photos were used to construct 3D models using Agisoft PhotoScan (Agisoft, 2016). We defined volume and live surface area from the final 3D model (*i.e.,* outside area of the coral minus the base). We fitted a power-law regression between coral colony mean diameter (*i.e.,* mean of the 3 dimensions defined for each colony) and coral live surface area ($R^2 = 0.97$) (Kayal *et al.*, 2015). This relationship was used to estimate the surface area of the coral

colonies measured during the alizarin red-S staining, incubation experiments, and size distribution surveys.

## 3.2.4 Bayesian $CaCO_3$ production models

To test whether $CaCO_3$ production of the three coral genera followed an allometric or isometric pattern, we first verified that the $CaCO_3$ production from *in situ* alizarin red-S staining and *ex situ* incubations were analogous. Alizarin red-S staining has the advantage of providing data from corals *in situ* (*i.e.,* growing under normal environmental conditions). However, given the potential for toxicity in juvenile corals (Dustan, 1975), $CaCO_3$ production of juveniles is better estimated with *ex situ* incubations. In our study, alizarin red-S staining and alkalinity anomaly incubation yielded similar results for $CaCO_3$ production (**Figure S3.4**); therefore, we merged the datasets to estimate isometric and allometric relationships with Bayesian inference as follows:

$$C_i \sim N(\mu_i, \sigma^2), \text{ Allometric model: } \mu_i = \alpha x_i^{\beta}$$
$$\text{Isometric model: } \mu_i = \alpha x_i + \beta$$

where $C_i$ is the $CaCO_3$ production rate (g $yr^{-1}$) and $x_i$ the live coral surface area ($cm^2$). We specified the same priors for both models ($\alpha \sim$ Normal (10,10) and $\beta \sim$ Normal (0.5,0.5)) with a weakly-informative variance ($\sigma^2 \sim$ Student (3,0,450)). We fitted our models with 3000 iterations across four chains, and discarded the first 1500 warm-up iterations of each chain. We verified chain convergence with visual inspection and confirmed that Rhat (the potential scale-reduction factor) was less than 1.05. Using the model summary parameters, we then predicted both $CaCO_3$ production and area-normalized $CaCO_3$ production rates (± 95% Bayesian credible interval).

## 3.2.5 Coral community $CaCO_3$ production

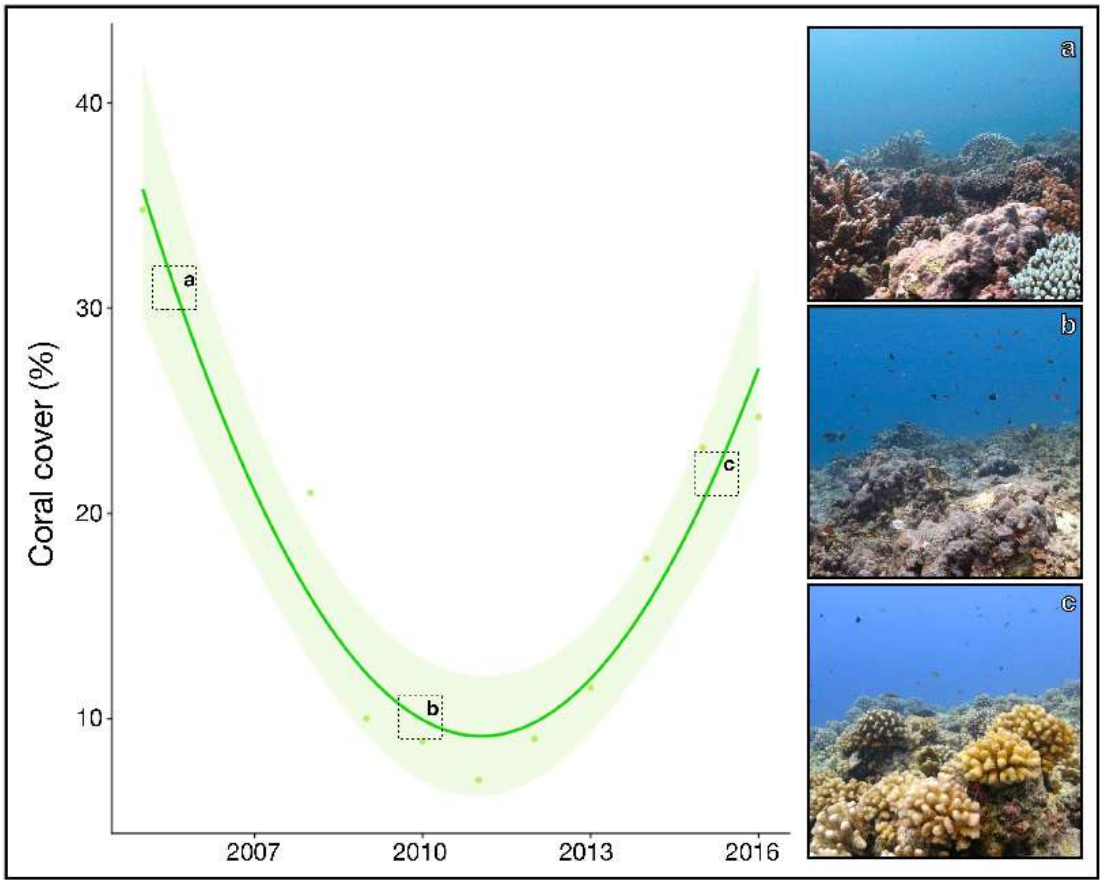


*Figure 3.2 | Average live coral cover in Mo'orea, French Polynesia, from 2005 to 2016. Perturbations included a predatory sea star (Acanthaster cf. solaris) outbreak from 2006 to 2009 and a cyclone in 2010. Photographs illustrate the reefscape in* ***A.*** *2006,* ***B.*** *2010 and* ***C.*** *2015.*

We used both isometric and allometric functions for quantifying community wide $CaCO_3$ production to test whether the two approaches yielded different results when coral size distribution changes over time. Between 2005 and 2016, Mo'orea experienced an outbreak of the predatory sea star *Acanthaster* cf. *solaris* (2006-2009), followed by a cyclone (2010). The two disturbances reduced live coral cover from approximately 50% in 2005 to 3% in 2010 (Kayal *et al.*, 2012; Carlot *et al.*, 2020). Following the disturbances, coral cover recovered to pre-disturbance levels by 2016 (Kayal *et al.*, 2018; Figure 3.2). The change in coral cover was accompanied by considerable variations in coral size distributions. Large colonies were dominant in 2005 (Table S3.1) but were dramatically outnumbered by small recruits in 2011 (Adjeroud *et al.*, 2018). We

applied both $CaCO_3$ production models (*i.e.,* isometric versus allometric) at the community level by combining data from three studies that recorded temporal changes in size distributions of the three major reef-building corals around Mo'orea. The first study evaluated coral size distributions in 2005 (Adjeroud, Mauguit and Penin, 2015), the second study took place from 2008-2010 (Kayal *et al.*, 2015) and the third study was conducted from 2011-2016 (Kayal *et al.*, 2018) as part of the Mo'orea Coral Reef Long Term Ecological Research program (LTER; http://mcr.lternet.edu). All surveys were conducted at a minimum of three different sites around Mo'orea at a depth of approximatively 12m.

Due to heterogeneity among datasets (*i.e.*, differences in survey protocols, efforts, sites and observers), we standardized the data by pooling all transects for a given year to obtain an island-scale coral size distribution for each taxon, from which we estimated population abundances matching the percent cover of the species at each site. To do so, we assumed that the planar shape of our three species is approximated by a circle when observed from above. We then calculated individual colony planar areas from visually-determined length and width (*i.e.,* $((\text{length} + \text{width})/4)^2\pi$). In some of the studies, coral size distribution was evaluated without recording the sampling effort (*e.g.,* by recording the size of the 50 first colonies intercepted along a transect). Therefore, we evaluated coral density per $10m^2$ substrate by randomly sampling individuals from our island-scale size distribution dataset until matching the percent cover of the species in each year. We repeated this process 100 times to obtain an average island-scale coral size distribution per taxa per year. We compared our coral size-distributions estimates with empirical data collected in 2009 by Kayal *et al.* (2015) for the three coral species and found no significant difference (Figure S3.4). Annual changes in coral cover for the three coral genera were estimated as part of the "*Service d'Observatoire CORAIL*" monitoring (SO CORAIL monitoring; http://observatoire.criobe.pf). We then assigned $CaCO_3$ production to each colony and summed them to yield total production per $10m^2$ of reef.

## 3.2.6 Recruitment loss model

To estimate how large-scale disturbance events may impact reef $CaCO_3$ production, we used a multi-species, open-population, integral projection model (IPM) developed to characterize coral community dynamics around Mo'orea (Kayal *et al.*, 2018). The IPM predicted recovery dynamics in the abundance, composition, and size distribution of coral assemblages (*i.e., Acropora*, *Pocillopora,* and *Porites*) after the 2006-2010 disturbances (**Figure S3.5**). For each population, the model is governed by the following:

$$\mathrm{n}\,(z', \mathrm{t}+1) = \int_{Low}^{Up} s\,(z)\mathrm{G}\,(z, z')\mathrm{n}\,(z, \mathrm{t})\mathrm{d}z + R\,(\gamma, z')$$

where the distribution of individuals n (*z'*, *t*+1) of final-size *z'* at time *t*+1 is predicted as a function of the distribution of the individuals n (*z*, *t*) of sizes *z*, bounded to the size-range interval [*Low*, *Up*], at time *t*. The functions *s*, *G,* and *R* describe empirically estimated size (*z*) dependent survival and growth, and density (γ) dependent recruitment, respectively.

We used the IPM to simulate the recovery of coral assemblages from 2010 to 2015 according to different recruitment scenarios. Specifically, we compared reef recovery under the observed recruitment rates (present-day scenario R×1) *versus* different scenarios of decline where recruitment was restricted to 75%, 50%, and 25% of the observed values (scenarios R×0.75, R×0.5, and R×0.25, respectively). The model was implemented with estimates of coral demographic parameters based on empirically measured coral survival, growth, and recruitment rates on the north shore of Mo'orea, where coral recruitment and recovery achieved maximum levels in 2010-2015 (Kayal *et al.*, 2018). Finally, the allometric Bayesian model was applied to the distribution of the coral colonies' surface area predicted under the four recruitment scenarios (**Figure S3.6**) to

estimate $CaCO_3$ production rates (**Figure 3.4**). All statistics and predictive models were run using the *brms* and *nlme* packages (Pinheiro *et al.*, 2013; Bürkner, 2017a, 2017b) in R version 3.5.3 (R Core Team, 2019).

## 3.3 Results

All three coral species exhibited an allometric linear extension pattern, with small coral colonies producing disproportionately larger amounts of $CaCO_3$ per unit surface area than larger colonies (**Figure 3.3**). For example, a fivefold increase in colony surface area from 100 to 500 $cm^2$ led to a 26% decline in linear extension for *Acropora* and *Pocillopora* and a 10% decrease for *Porites*.

According to the isometric model, reef-scale $CaCO_3$ production per unit area remained relatively constant (~7 kg $CaCO_3$ $m^{-2}$ $yr^{-1}$; **Figure 3.4** and **Table S3.1**) across the ten-year study period, despite fluctuations in coral cover (**Figure 3.2**). In contrast, the allometric model revealed marked variation in reef-scale $CaCO_3$ production over the same period. $CaCO_3$ production per unit area increased from 9 kg $CaCO_3$ $m^{-2}$ $yr^{-1}$ during pre-disturbance in 2005 to 17 kg $CaCO_3$ $m^{-2}$ $yr^{-1}$ in 2010 and 22 kg $CaCO_3$ $m^{-2}$ $yr^{-1}$ in 2013 during reef recovery (**Figure 3.4A** and **Table S3.1**). These peaks co-occurred with the recolonization of juvenile corals (Adjeroud *et al.*, 2018), initiated in 2006 in response to the *Acanthaster* outbreak, but it was interrupted by the cyclone in 2010 (Kayal *et al.*, 2012). After 2013, coral colonies grew steadily, leading to a gradual decline in the production of $CaCO_3$ per unit area. Overall, the isometric model led to a 40% underestimation of the total $CaCO_3$ produced over the ten-year period compared to our allometric model (**Figure 3.4B**).

To test how reduced coral recruitment impacts reef-scale $CaCO_3$ production, we simulated coral community composition and size structure across a five-year recovery period under four different scenarios of decline in coral recruitment (0%, 25%, 50%, and 75% declines). Recruitment declines

dramatically reduced $CaCO_3$ production, with a 68% reduction in $CaCO_3$ production when recruitment is reduced by 75% (**Figure 3.5**). Even a moderate decline of 25% in recruitment reduced post-disturbance $CaCO_3$ production by ~30% over a five-year period.

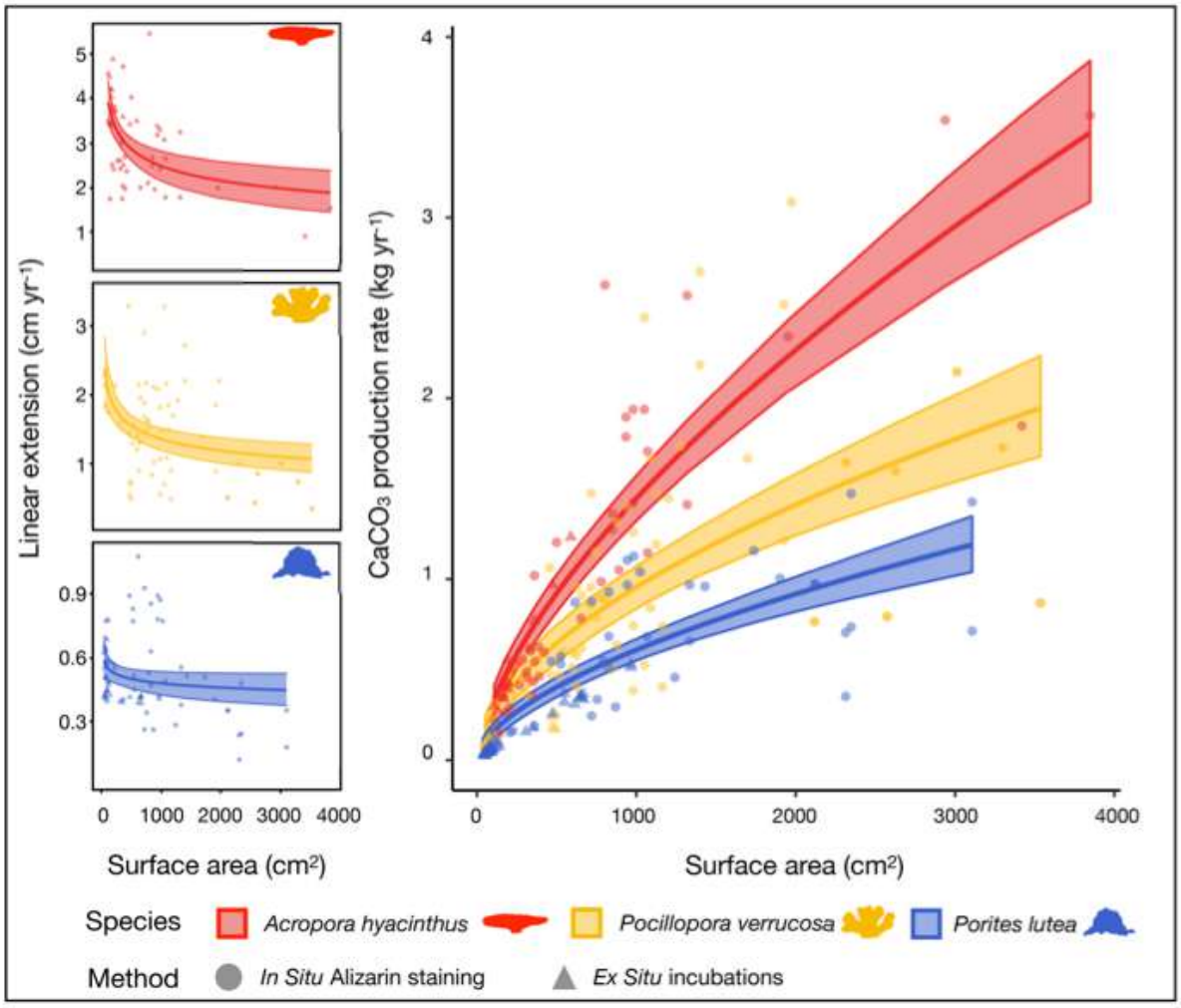


*Figure 3.3 | $CaCO_3$ production rates of the three reef-building coral species. On the left. changes in linear extension for the coral species A. hyacinthus, P. verrucosa and P. lutea as a function of colony size. On the right, changes in $CaCO_3$ production rates as a function of colony size. $CaCO_3$ production was estimated using two growth measurement methods (in situ alizarin red-S staining and ex situ metabolic incubations).*

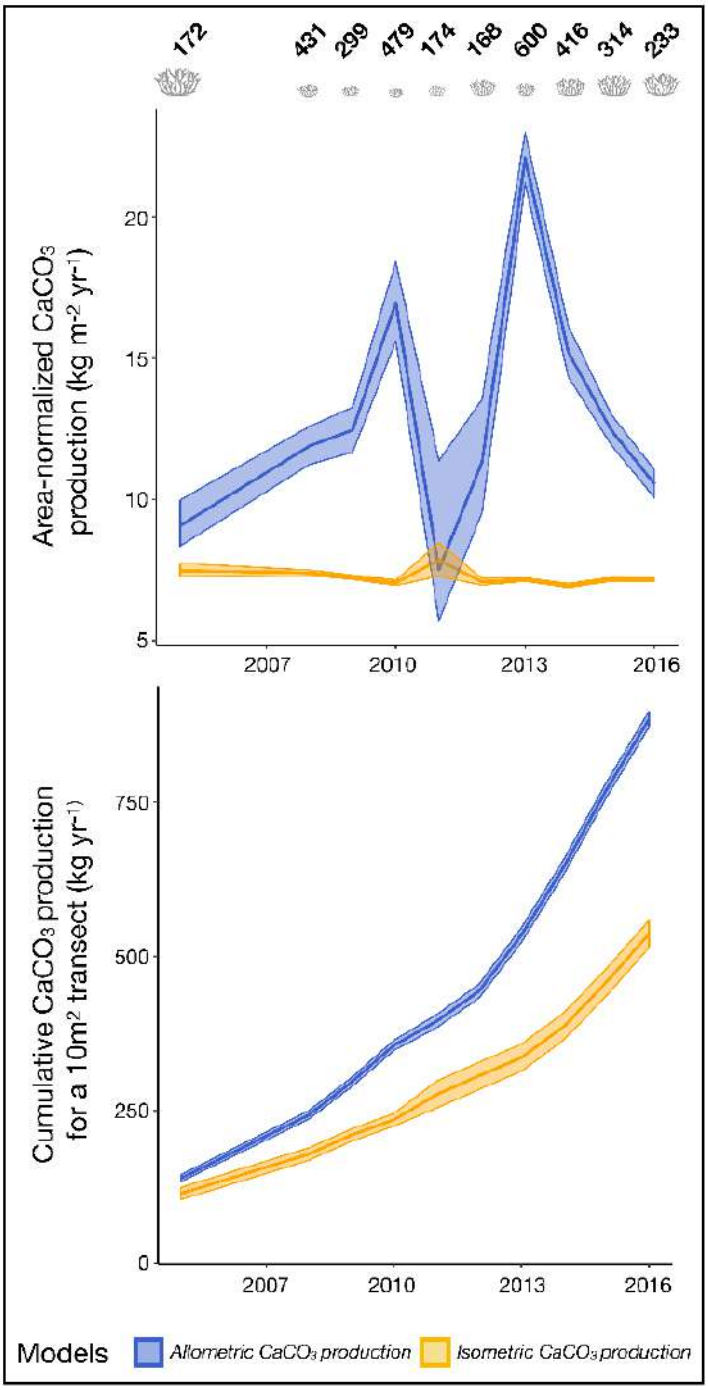


*Figure 3.4 | Coral community $CaCO_3$ production estimates of a 10m$^2$ portion of reef substrate in Mo'orea from 2005 to 2016 according to the isometric versus allometric coral $CaCO_3$ production models.* ***A.*** *$CaCO_3$ production rate (kg m$^{-2}$ yr$^{-1}$),* ***B.*** *cumulative $CaCO_3$ production (kg yr$^{-1}$). Estimates are bounded by a 95% confidence interval. Coral symbols on top indicate changes in average coral colony size, and numbers indicate coral colony density per 10m$^2$ of reef surface area.*

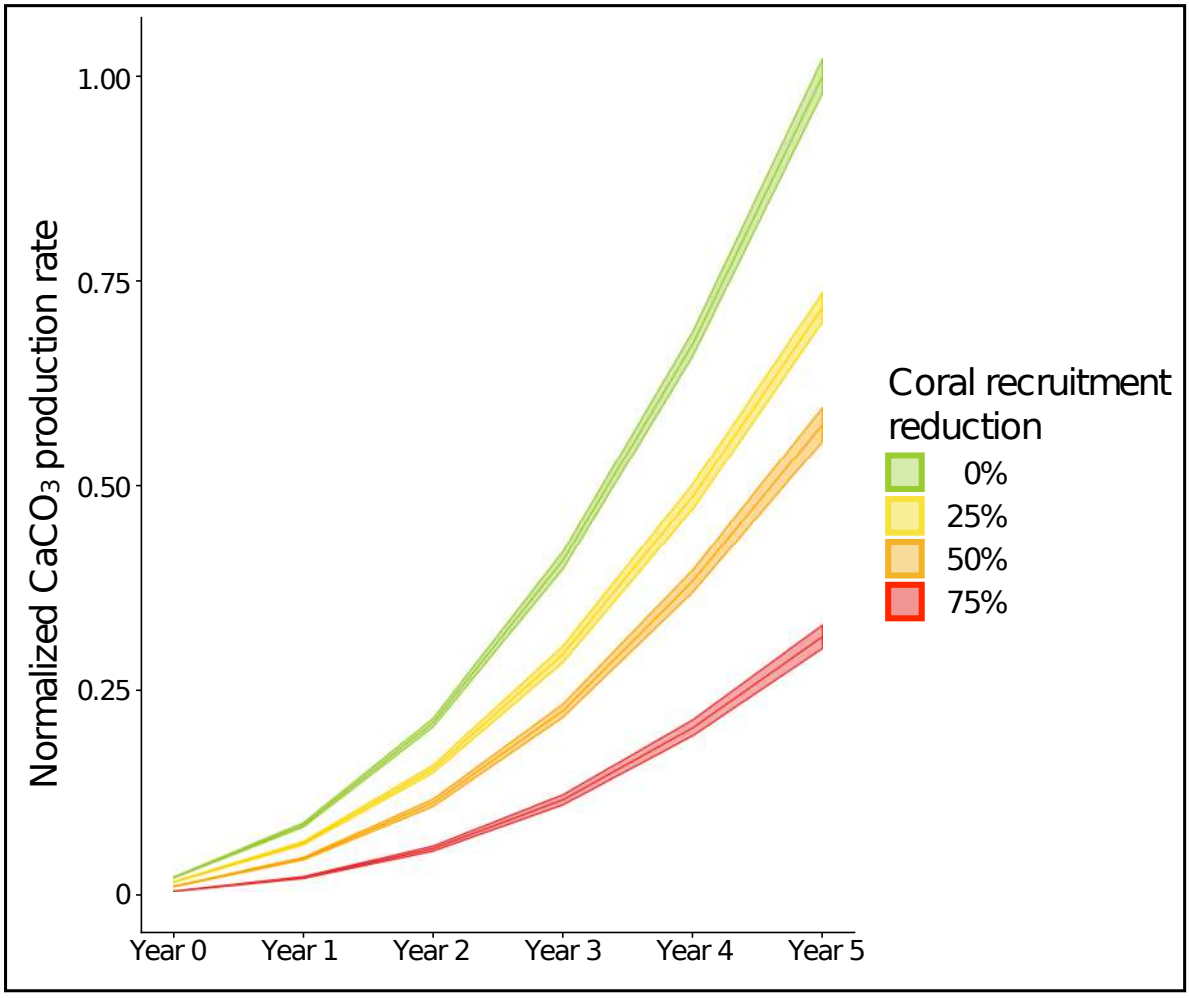


*Figure 3.5 | Normalized $CaCO_3$ production trajectories according to four scenarios of coral recruitment over five years during reef recovery. A multi-species, open-population integral projection model was used to predict the recovery dynamics of an assemblage of three coral genera (Acropora, Pocillopora and Porites) based on coral demographic performance (in recruitment, growth, and survival) measured in Mo'orea. The four scenarios predicted different rates of coral recruitment reduction as compared to current levels (0%, 25%, 50% and 75% reductions). $CaCO_3$ production rates were estimated from model predictions of coral abundance, composition and size distribution (Figure S5, combined with the allometric $CaCO_3$ production functions estimated in Mo'orea (Fig. 1). $CaCO_3$ production rates were normalized relative to the highest value (scenario 0% reduction at year 5; green curve).*

## 3.4 Discussion

Our study demonstrates that three major reef-building corals in Mo'orea (*Acropora hyacinthus*, *Pocillopora* cf. *verrucosa*, and *Porites lutea*) show allometric linear extension and $CaCO_3$ production patterns. Using the allometric patterns to quantify reef-scale $CaCO_3$ production from coral size structure time-series in Mo'orea indicates that the conventional isometric approach leads to a 40% underestimation of $CaCO_3$ production over a ten-year period. Our results imply that recovering reefs have exceptionally high calcification rates due to the fast growth of juvenile corals. Thus, static metrics of coral community assemblages, particularly percent of live coral cover, may mask dynamic processes that underpin the functioning of reefs, such as $CaCO_3$ production (Brandl, Rasher, *et al.*, 2019).

Over a 10-year-period in Mo'orea, assumption of isometry resulted in an average underestimation of 3 kg $m^{-2}$ $yr^{-1}$, which equals approximately half of the bioerosion caused by sea urchins and parrotfishes around Mo'orea per year (*i.e.*, *ca.* 6 kg $m^{-2}$ $yr^{-1}$; Peyrot-Clausade *et al.*, 2000; Alvarado *et al.*, 2016). Although allometric growth, when expressed as an increase in planar area, has been documented for corals (Dornelas *et al.*, 2017), this pattern most likely arose from the higher probability of partial mortality in larger colonies, and thus lower increases in planar area (Kayal *et al.*, 2015; Pratchett *et al.*, 2015; Madin *et al.*, 2020), rather than inherent differences in growth rate across ontogeny. Our *ex situ* estimates of $CaCO_3$ production were not sensitive to the potential effects of partial mortality for two reasons. First, they are nearly instantaneous measures (Gattuso *et al.*, 1998) on small colonies in which partial mortality is less prevalent. Second, partial mortality is often due to predation or overgrowth, which are easily excluded in controlled *ex situ* experiments. Although alizarin red-S staining was conducted in the field, where partial mortality can be observed, we carefully selected healthy branches that did not show signs of predation or overgrowth. Thus, allometric growth likely results from shifts in the energy allocated to $CaCO_3$ production across the colony size gradient. Indeed, larger colonies may invest

substantial energy in reproduction, which might reduce the energy available for calcification (Kayal *et al.*, 2015).

Our findings also have important implications for our understanding of system-wide reef accretion rates under climate change. Indeed, reef accretion depends on the net community production of $CaCO_3$ (Perry *et al.*, 2012) and our results suggest that, after a perturbation, small colonies may greatly bolster community-level $CaCO_3$ production (see also Gilmour *et al.*, 2013). However, the presence of juvenile corals strongly depends on the reproductive capacity of mature coral colonies (Edmunds, 2017; Holbrook *et al.*, 2018; Vercelloni *et al.*, 2019). Severe, large-scale, and repeated disturbances can dramatically erode the supply of coral recruits to large swaths of reefs. For example, coral recruitment on the Australian Great Barrier Reef in 2018 declined by 89% in response to the loss of corals during 2016 and 2017 bleaching events (Hughes *et al.*, 2019). Our results indicate that disruption and decline of coral recruitment may lead to a decrease in the production of $CaCO_3$ with a potentially profound impact on reef accretion. In fact, because juvenile corals play a disproportionate role in $CaCO_3$ production, reductions in coral recruitment following disturbances, such as extensive coral bleaching, may undermine the capacity of reef ecosystems to recover and, ultimately, endanger the persistence of reefs that protect tropical coasts (Oppenheimer *et al.*, 2019).

Area-normalized $CaCO_3$ production showed a nearly inverted profile (Figure 3.4A) compared to coral cover, emphasizing the deep divide between metrics of ecosystem function (*e.g.*, growth, $CaCO_3$ production) and their outcomes (*e.g.*, coral cover, structural complexity). As a consequence, much of coral reef monitoring is likely to evaluate outcomes of past reef configurations rather than current levels of functioning. To efficiently monitor and protect coral reefs in times of unprecedented anthropogenic and climatic impacts, our results emphasize the need to move beyond ecosystem assessments based solely on

static surveys (*e.g.*, coral cover or fish biomass) and consider metrics that quantify reef functioning as a dynamic process (Darling *et al.*, 2012; Madin *et al.*, 2016; Brandl, Rasher, *et al.*, 2019; Edmunds and Riegl, 2020).

Overall, we provide a novel perspective on coral reef $CaCO_3$ production that has direct implications for the security of coastal populations throughout the tropics (Arkema *et al.*, 2013; Perry *et al.*, 2018). With current projections of global change, reefs will face disturbances such as coral bleaching at increasing frequencies. After these disturbances, juvenile corals can buffer the decrease in community $CaCO_3$ production caused by live coral loss through their rapid growth. However, reductions in coral recruitment, as recorded after large-scale disturbances, will undermine this buffering capacity, ultimately hampering vertical reef accretion and consequently the protection of tropical coasts from oceanic waves. The buffering capacity of small colonies provides only a short-term boost (until colonies grow bigger) that may support a faster return to pre-disturbance levels of coral cover and reef structural complexity. Yet, vertical reef accretion happens over a much longer time frame and relies on several other factors such as substrate cementation by coralline algae and sediment input (Perry *et al.*, 2012; Perry, Lange and Januchowski-Hartley, 2018). Thus, despite the capacity of juvenile corals to temporarily accelerate reef recovery through rapid growth, long-term persistence of coral reefs and their services inevitably hinge on the preservation of coral populations across size classes.

## 3.5 Acknowledgements

We thank the "*Service d'Observatoire CORAIL*" (SO CORAIL) and the Mo'orea Coral Reef Long Term Ecological Research (LTER) programs. Thanks also to Yann Lacube and Adeline Goyaud for help with alizarin red-S staining, Martin Alessandrini and Hmeniko Tourancheau for help defining linear coral extension rates, technical support from the Université de Perpignan and the Banyuls sur

Mer Observatory (Fabien Morat, Guillaume Iwankow, Titouan Morage and David Pecqueur) and Joshua Madin for reviewing our manuscript before submission.

## 3.6 Data availability

Code and data are available on my Github folder "Allometric Coral Growth": https://github.com/JayCrlt/Allometric_coral_growth.git

## 3.7 Supplementary information

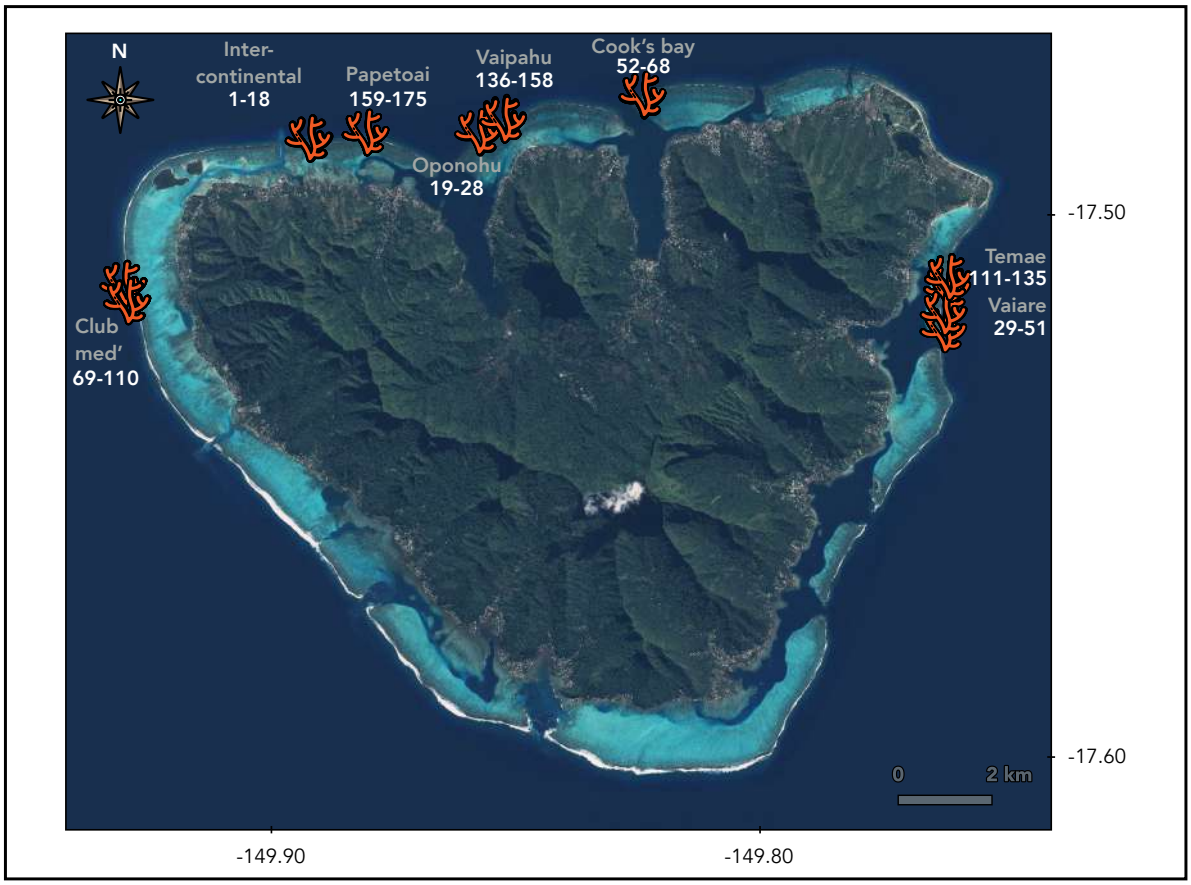


*Figure S3.1 | Map of study sites for the in situ alizarin red-S staining. Alizarin red-S staining was conducted on the reef slopes around Mo'orea, French Polynesia, and included 175 colonies (numbered from 1 to 175 under the gray labels). The grey labels indicate the sampling sites. The corals used in the ex-situ incubations were collected at Vaipahu, on the north shore of the island.*

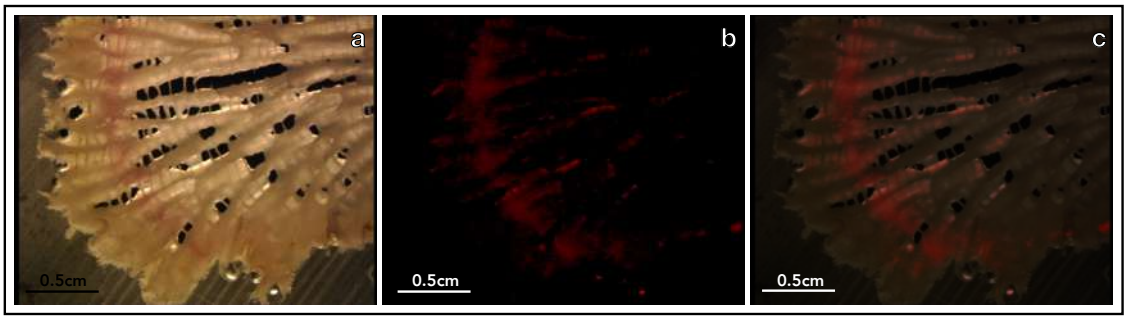


*Figure S3.2 | Alizarin red-S staining example. The photographs illustrate a 0.7 mm thick slice from one of the pocilloporid colonies 131 days after staining.* ***A.*** *Introspected image observed under microscope, and* ***B.*** *the same slice observed under a fluorescent microscope.* ***C.*** *A superposition of the two images to define the maximum linear extension of the coral. For this coral fragment, the linear extension was 0.57 cm over 131 days, which corresponds to a* $CaCO_3$ *production rate of 3.1 kg* $m^{-2}$ $yr^{-1}$.

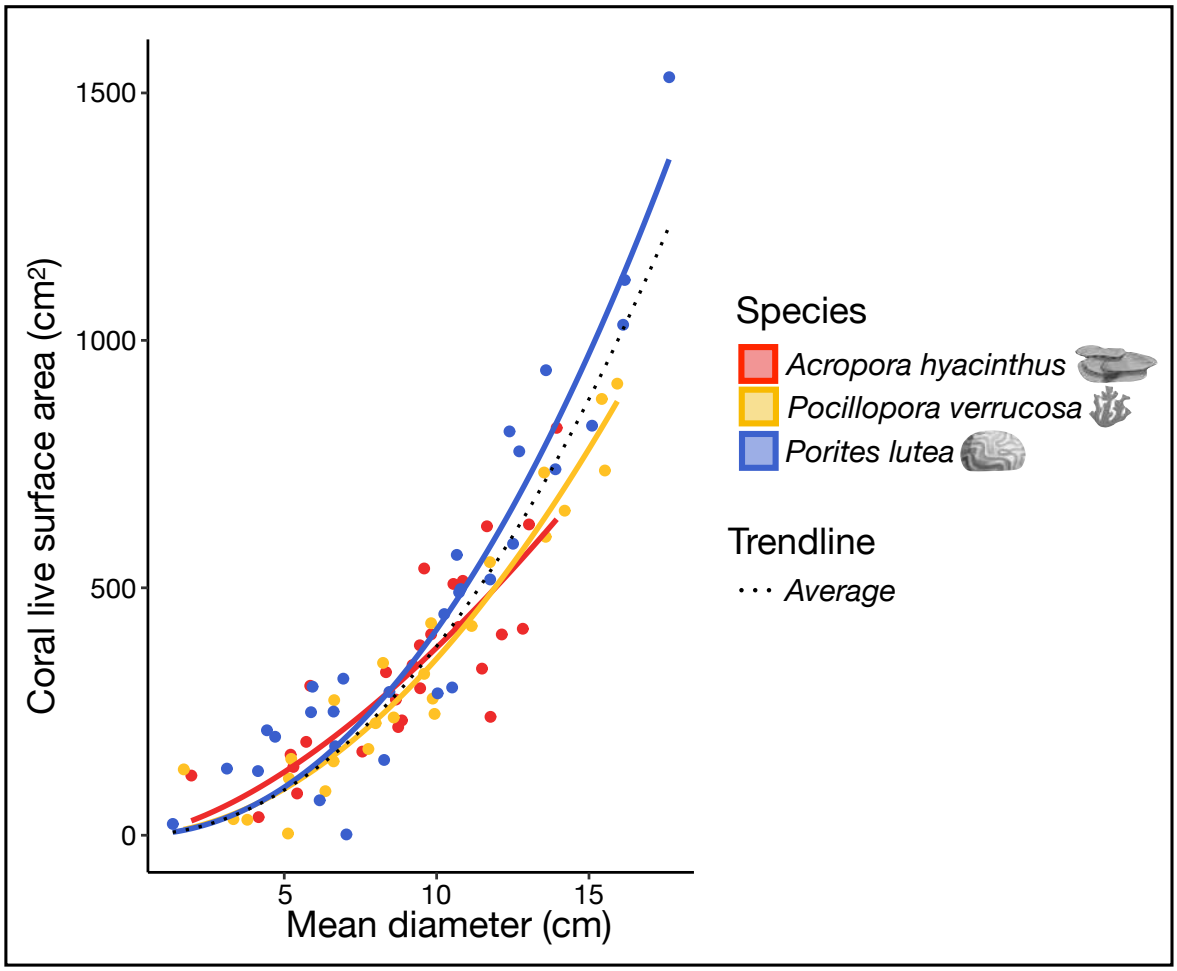


*Figure S3.3 | Photogrammetry-based size-area relationships. For each of the three coral species, we fitted a power-law regression for the mean diameter (i.e., the mean of the length, width and height of each colony) and the live surface area of the coral colonies. We also estimated an average trendline across the three coral species (dashed points) ($R^2$=0.97). Coral symbols indicate the growth morphologies of the three coral species.*

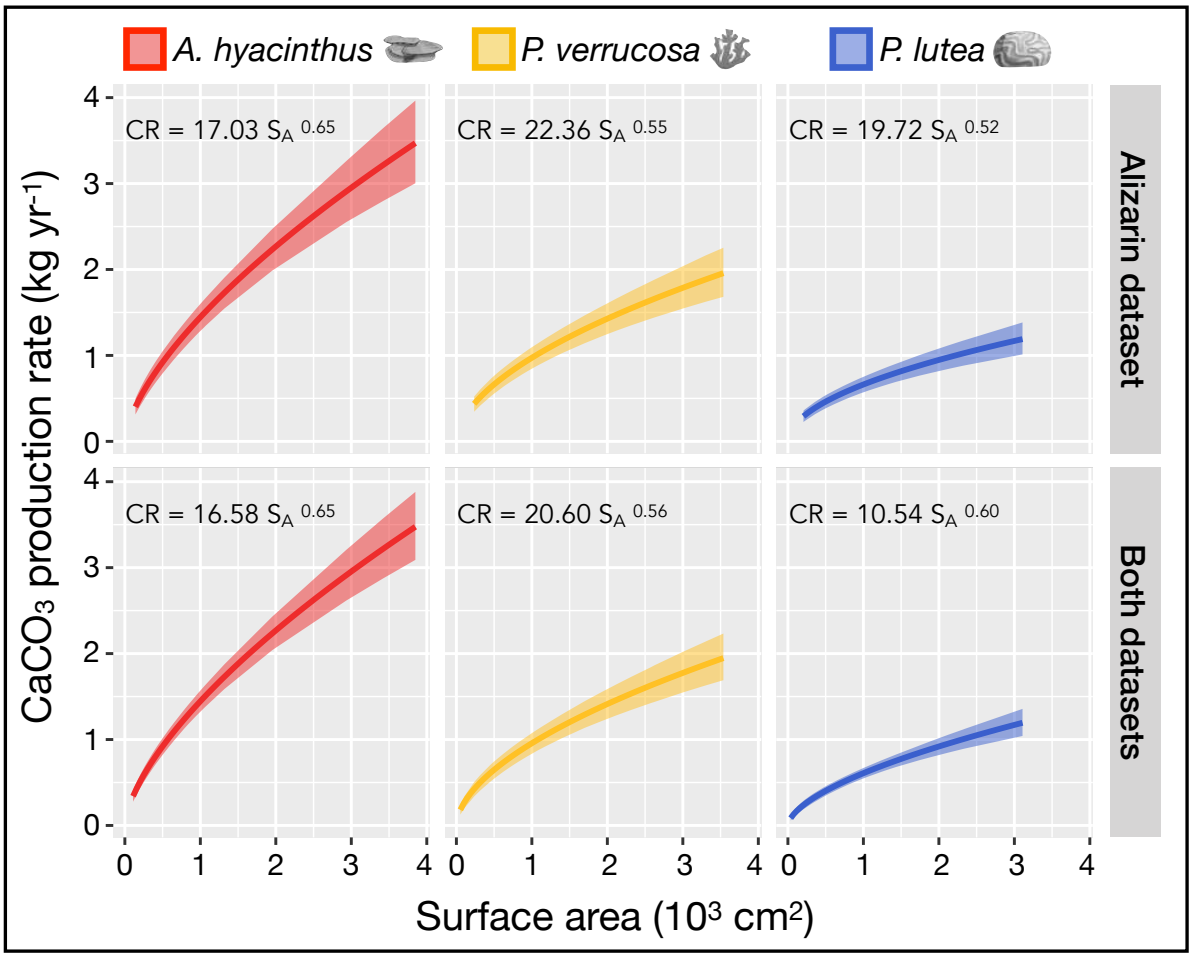


*Figure S3.4 | Compilation of the alizarin red-S and the incubation datasets. The Bayesian allometric $CaCO_3$ model was first characterized for the three coral genera (Acropora, Pocillopora and Porites) with only the alizarin red-S dataset (n=130 top plots). We then merged both alizarin red-S and incubation datasets for defining a more complete allometric $CaCO_3$ production model (n=200, bottom plot). The power-law equations from each species and each dataset were written on the top of each plot. For each of the three species, no significant difference in calcification estimates were found between the alizarin red-S only and both the alizarin red-S and incubation combined datasets (two-tailed t-test; p = 0.93, 0.61 and 0.17 for respectively Acropora hyacinthus, Pocillopora verrucosa and Porites lutea).*

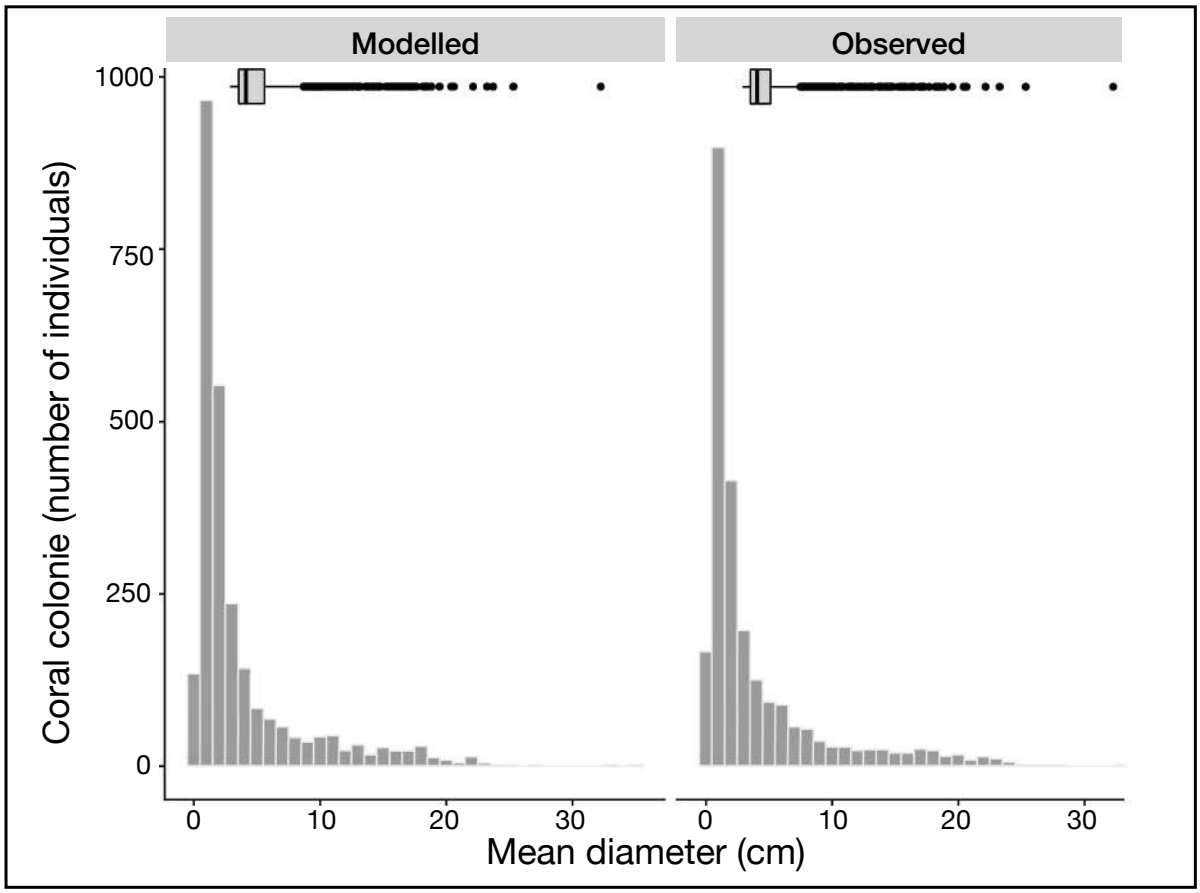


*Figure S3.5 | Robustness of the coral community size distributions data. To test whether our island-scale estimations of coral size-distributions matched the data from locally performed surveys at specific sites around Mo'orea (see Methods section Coral community size distributions), we compared our predictions to the coral size-distribution dataset observed in Kayal et al. (2015) from the year 2009 and for the genus Pocillopora. Thus, on the left plot, we represented the modeled size-distribution dataset while we described on the right plot, the current observed size-distribution dataset. For both datasets, we observed a peak of several individuals between 0 and 4 cm of diameter. Despite a slight increase for small colonies in the dataset modeled, both patterns are similar, and we found no significant difference between both size-distribution datasets (two-tailed t-test; p = 0.08).*

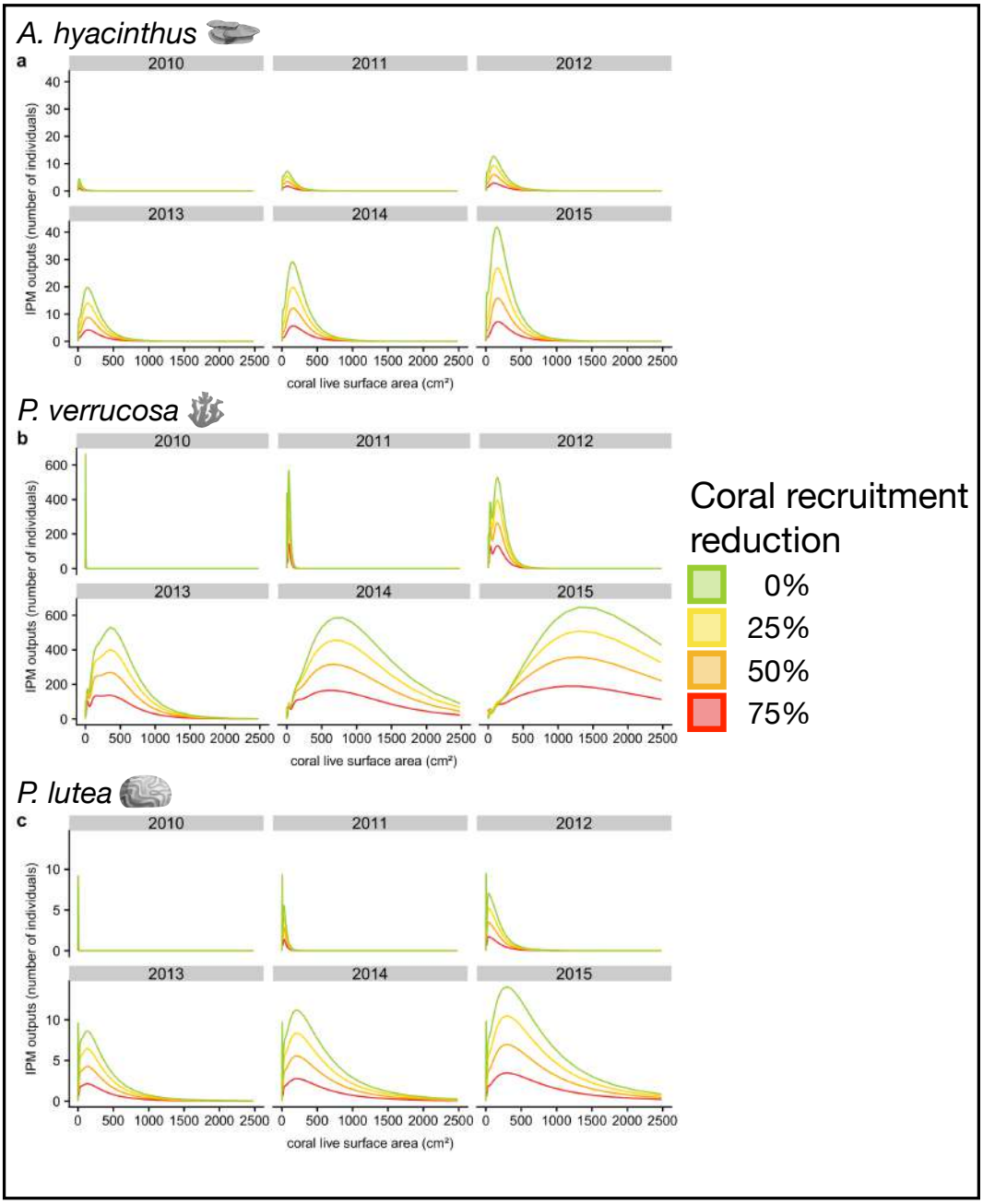


*Figure S3.6 | Recruitment loss model. Coral community trajectories predicted under four recruitment scenarios over the course of five years (2010-2015). The population dynamics of the three coral taxa are expressed in terms of changes in coral abundance (y-axis) across colony sizes (x-axis) with time (years) and scenarios (0%, 25%, 50% and 75% reductions in recruitment rates). The predicted coral abundances, compositions, and size structures were used to estimate community calcification under the four scenarios (see Figure 3.4).*

*Table S3.1 | Compilation of all estimated variables over the course of ten years. The first three variables correspond with demographic performance within a 10m² transect (number of individuals, average coral diameter, and live coral surface area). The next six variables correspond with estimates of $CaCO_3$ production ($CaCO_3$ production, area-normalized $CaCO_3$ production, and cumulative $CaCO_3$ production for both isometric and allometric $CaCO_3$ production models)*

| | | 2005 | 2006 | 2007 | 2008 | 2009 | 2010 | 2011 | 2012 | 2013 | 2014 | 2015 | 2016 |
|---|---|---|---|---|---|---|---|---|---|---|---|---|---|
| | Number of individuals | 172 | | | 431 | 299 | 479 | 174 | 168 | 600 | 416 | 314 | 233 |
| | Average coral diameter (cm) | 12,7 | | | 4,45 | 3,68 | 2,96 | 4,19 | 5,77 | 3,88 | 5,75 | 7,54 | 8,78 |
| | Coral live surface area sampled ($m^2$) | 15,6 | | | 8,60 | 4,20 | 3,50 | 5,20 | 4,30 | 4,10 | 7,30 | 10,0 | 10,8 |
| Isometric prediction | Production ($kg.yr^{-1}$) | 11,63 | | | 6,35 | 3,08 | 2,48 | 4,06 | 3,05 | 2,95 | 5,06 | 7,17 | 7,77 |
| | Cumulative production ($kg.yr^{-1}$) | 11,63 | | | 17,98 | 21,06 | 23,54 | 27,60 | 30,65 | 33,60 | 38,66 | 45,83 | 53,61 |
| | Area-normalised production ($kg.m^{-2}.yr^{-1}$) | 7,47 | | | 7,39 | 7,24 | 7,04 | 7,85 | 7,08 | 7,16 | 6,95 | 7,17 | 7,17 |
| Allometric prediction | Production ($kg.yr^{-1}$) | 14,10 | | | 10,22 | 5,29 | 5,98 | 3,88 | 4,88 | 9,10 | 11,07 | 12,44 | 11,42 |
| | Cumulative production ($kg.yr^{-1}$) | 14,10 | | | 24,32 | 29,61 | 35,58 | 39,47 | 44,34 | 53,44 | 64,51 | 76,95 | 88,37 |
| | Area-normalised production ($kg.m^{-2}.yr^{-1}$) | 9,07 | | | 11,9 | 12,4 | 17 | 7,51 | 11,3 | 22,1 | 15,2 | 12,44 | 10,53 |

# Chapter 4

# Scaling up calcification, respiration, and photosynthesis rates of six prominent coral taxa

This chapter is in the first stage of revision in Ecology and Evolution

## Authors

Jeremy Carlot, Héloïse Rouzé, Diego R. Barneche, Alexandre Mercière, Benoit Espiau, Ulisse Cardini, Simon J. Brandl, Jordan M. Casey, Gonzalo Pérez-Rosales, Mehdi Adjeroud, Laetitia Hédouin and Valeriano Parravicini

# Abstract

Coral reefs provide a range of important services to humanity, which are underpinned by community-wide ecological processes such as coral calcification. Estimating these processes relies on our knowledge of organismal physiology and species-specific abundances in the field. For colonial animals such as reef-building corals, abundance is frequently expressed as the percentage of live coral cover, a metric that does not account for demographic parameters such as coral size. This is problematic because many physiological processes exhibit non-linear scaling over ontogeny, and failure to account for these patterns may skew estimates of ecosystem functioning. In the present study, we characterise the ontogenetic scaling of three physiological rates — calcification, respiration, and photosynthesis — for six prominent, reef-building coral taxa in Mo'orea (French Polynesia). After a seven-day acclimation period in the laboratory, we defined coral physiological rates for three hours during daylight (*i.e.,* calcification and gross photosynthesis) and one hour during night light conditions (*i.e.,* dark respiration). Our results indicate that across all taxa, area-specific calcification rates are higher for smaller colonies. However, photosynthesis and respiration rates remain constant over the colony-size gradient. Furthermore, we identify considerable species-specific variation by revealing correlations between the ratio of net primary production and calcification and recent demographic dynamics of these six coral species. Therefore, intraspecific scaling of reef-building coral physiology not only alters our understanding of community-wide coral reef functioning, but it also explains species-specific responses to disturbances.

# 4.1 Introduction

Coral reefs are among the most diverse marine ecosystems and provide essential services to more than 500 million people worldwide (Hoegh-Guldberg, Pendleton and Kaup, 2019). Healthy coral reefs protect coastlines from wave energy, reduce the risk of coastal flooding (Harris *et al.*, 2018), and provide local populations with crucial food supplies (Cinner *et al.*, 2020). While there is broad agreement on which processes are fundamental for reef systems, our capacity to quantitatively define a 'functional' reef is still limited (Kennedy *et al.*, 2013; Hughes, Barnes, *et al.*, 2017; Brandl, Rasher, *et al.*, 2019). For example, coral nitrogen cycling may be crucial for primary productivity (*i.e.*, photosynthesis), but it is poorly documented and may vary greatly among reefs (Rädecker *et al.*, 2015). Similarly, coral calcification is key to reef accretion, but the rates of calcification necessary to keep up with sea level rise remain largely unquantified (Brandl, Rasher, *et al.*, 2019).

One reason why defining 'functional' reefs remains challenging is that functional studies on coral reefs traditionally employ qualitative, categorical traits as a proxy for functioning, but our capacity to directly quantify processes is still limited (Brandl, Rasher, *et al.*, 2019). Integrating empirically-measured processes into quantifications of reef functioning has been performed using two main approaches: i) the direct measurement of in situ elemental fluxes and ii) the scaling of individual-level physiological processes to the community level using an additive approach (Allen, Gillooly and Brown, 2005; Barneche *et al.*, 2014). Direct measurements of elemental fluxes are the most accurate method to quantify ecological functioning (Nakamura and Nakamori, 2009). However, direct assessments are labour intensive and subject to local, current conditions, and they are thus impractical for integrating research across large spatial and temporal scales. As an alternative, scaling up organismal physiological processes to community-wide fluxes has been used to estimate large-scale biomass

production and nutrient cycling in coral reef fishes (Allgeier *et al.*, 2014; Brandl, Tornabene, *et al.*, 2019; Morais, Connolly and Bellwood, 2020; Schiettekatte *et al.*, 2020) as well as calcification and accretion in coral assemblages (Perry *et al.*, 2012). While this method can leverage widely-available datasets of fish or coral community structure, reliable estimates inevitably depend on the availability and accuracy of physiological measurements conducted at both species and individual levels (Edmunds and Riegl, 2020).

At the physiological level, corals consume dioxygen ($O_2$) through respiration and produce $O_2$ due to their symbiotic association with photosynthetic microalgae from the Symbiodiniaceae family (LaJeunesse *et al.*, 2018). The coral host provides their symbiotic algae with a protected environment and essential compounds such as respiratory carbon dioxide ($CO_2$) and nitrogenous waste, which are necessary for the symbiotic algae to photosynthesize (Muscatine and Porter, 1977; Barnes, 1987; Birkeland, 1997). In turn, the coral host receives photosynthetically fixed carbon that may support up to 95% of its metabolism (Muscatine, 1990), including skeletal growth through biocalcification (*i.e.*, calcification rate) (Barnes, 1987; Muscatine, 1990; Birkeland, 1997; Barnes and Hughes, 1999). These basic physiological processes are essential to ecological functioning at the community level, since calcification, respiration, and photosynthesis are interconnected elemental fluxes that allow organsims and ultimately, the entire reef system, to persist and accrete (Howard *et al.*, 2017). Therefore, accurate quantifications of species-specific rates of calcification, respiration, and photosynthesis rate are necessary to extrapolate system-wide functioning based on coral community structure (Madin *et al.*, 2016).

Several studies on coral calcification have highlighted that coral growth may be allometric (*i.e.*, exhibiting varying rates according to colony size) (Jokiel and Morrissey, 1986; Vollmer and Edmunds, 2000; Edmunds and Burgess, 2016;

Dornelas *et al.*, 2017) instead of isometric (*i.e.*, exhibiting constant rates across colony size). Specifically, the growth rate of large colonies is substantially lower than that of smaller coral colonies, but the mechanisms behind this pattern remain unclear. For example, larger colonies may invest substantial energy in reproduction, which reduces the energy available for growth (Richmond, 1987). Likewise, larger colonies can experience higher partial mortality (*e.g.*, localized tissue necrosis, overgrowth by other organisms, and predation from parrotfishes), which may also reduce growth rates (Pratchett *et al.*, 2015; Madin *et al.*, 2020). Understanding whether and why organismal growth rates are isometric or allometric has important implications for our capacity to estimate community-level fluxes (Carlot *et al.*, 2021). Indeed, most community data report the substrate covered by each species without recording the size of individual colonies (Flower *et al.*, 2017; Edmunds and Riegl, 2020). Therefore, the estimation of ecosystem functions using the additive framework will be accurate only in the case of isometry. In the case of allometry, in turn, information on colony size distribution is necessary to calculate community-level fluxes. Thus, determining whether ecological functions are isometric or allometric is critical to accurately define community-level estimates and make management decisions (Edmunds and Riegl, 2020).

In the present study, we quantify three primary physiological functions (*i.e.,* calcification, respiration, and photosynthesis) for six coral taxa along a gradient of colony size to examine whether each species exhibits an isometric or allometric pattern.

# 4.2 Material and Methods

## 4.2.1 Coral species selection, preparation, and acclimation

In September 2018, we collected 384 coral colonies from six coral taxa: *Acropora hyacinthus (n = 72), Astrea curta (n = 60), Montipora verrilli (n = 48), Napopora irregularis (n = 48), Pocillopora* cf. *verrucosa (n = 84)* and massive

*Porites spp. (n = 72).* These taxa exhibit unique life-history strategies and are among the most abundant reef-building coral species in Mo'orea (Putnam *et al.*, 2012; Darling *et al.*, 2019). They also represent a large diversity of morphologies, such as tabular (*A. hyacinthus*), branched-corymbose (*N. irregularis* and *P. verrucosa*), encrusting (*M. verrilli*), and massive (*A. curta* and *Porites spp*.). Although we were able to identify five taxa to the level of species in the field, we were unable to distinguish massive *Porites* beyond the genus level because *P. lutea* and *P. lobata* are macro-morphologically indistinguishable. We sampled all coral colonies at a depth of 11–13 m on the outer reef of the northern coast of Mo'orea. Before each collection, we recorded mean ambient seawater temperature and salinity *in situ*, and we obtained measurements of photosynthetically active radiation (PAR: 400-700 nm) three times a week at 14:00 from sensors at 12m depth. We collected colonies from the substratum using a hammer and chisel and transported them to the lab in a cooler filled with unfiltered seawater. Transportation took approximately 15 minutes.

## 4.2.2 Tank preparation

In the laboratory, each colony was quickly cleaned with Milli-Q water and epibionts or epiphytes were carefully removed. We attributed each colony to a size class: (S1) <100 $cm^2$, (S2) 100-400 $cm^2$ and (S3) >400 $cm^2$ for further physiological measurements (n = 128 colonies for each size class). We placed all colonies into 4 tanks, each with the dimensions 80cm x 45cm x 20cm (Figure S4.1), which were conditioned to reflect *in situ* environmental parameters. 30 corals from the same species were kept in each tank (n = 10 for each size class). Prior to taking measurements, we gave the colonies 7 days to recover and acclimate. Following Edmunds and Burgess (2017), we incubated the coral colonies for one week and assumed that the acclimation was successful due to the low incidence of bleaching (only 2 coral colonies). Each week, when starting new coral acclimation trials, we alternated tanks for each coral species to avoid

tank effects. Every 3 days, the main water containers were re-filled with water from the forereef. The pH and water temperature were checked (and maintained between 8.1 to 8.3 and 25.5°C to 30.2°C, respectively). Light intensity was maintained with artificial lights above all tanks, simulating high light-intensity conditions without any clouds in the field at 12m depth (*i.e.,* 350 µmol quanta $m^{-2}$ $s^{-1}$; see Respiration and photosynthesis section; **Figure S3.1**). Corals were kept under artificial light for 12 hours per day during the entire acclimation period.

## 4.2.3 Respiration and photosynthesis

We assessed coral physiology using intermittent-flow respirometry, where colonies were immersed in chambers connected to both a closed recirculating pump system and an open flush-pump system to periodically record oxygen concentrations in the unfiltered seawater. The colonies were incubated in permeable chambers of three different volumes ranging from 0.5 L to 1 L to 4 L, which were selected according to the ratio between incubation volume and colony size. Incubation chambers were of variable sizes (0.5, 1, and 4L) and to achieve the same water renewal rates, the water pumps were set at different flow rates (0.6L $min^{-1}$, 2L $min^{-1}$, and 7.5L $min^{-1}$, respectively). The renewal rate was fixed at 1.25 to establish a low turbulent flow speed for each incubation chamber (*i.e.,* 0.5 cm $s^{-1}$; Edmunds and Burgess, 2017). Colonies smaller than 100 $cm^2$ were incubated in 0.5 L chambers, colonies between 100 and 400 $cm^2$ were incubated in 1 L chambers, and colonies larger than 400 $cm^2$ were incubated in 4 L chambers (**Figure S4.1**). For each respirometry trial, we assessed four controls and four corals of each size class (n = 12 colonies for each trial). Since we measured both photosynthesis and respiration, we measured $O_2$ concentrations in the chambers in both artificial light and dark conditions. For each trial, we exposed colonies to light for three hours, then we turned off the light and recorded $O_2$ consumption 30 minutes later. We limited the dark phase to 1 hour to prevent $O_2$ concentrations from falling below 80% saturation (Kolb, 2018). $O_2$

concentration was recorded with PyroScience FireSting optical oxygen meters (Pyroscience GmBH, Aachen, Germany), which were factory calibrated. We removed the first thirty minutes of each trial, which corresponded to the stabilization of the $O_2$ concentration slopes in the closed stage of the system. For each trial, we included a chamber that was not populated with a coral colony to account for background bacterial respiration. Using these blanks, we corrected $O_2$ concentrations for each trial, ultimately yielding two consumption profiles: one that corresponded to physiological activity in daylight (*i.e.,* non-distinction of the respiration and photosynthesis activities and corresponding to the net photosynthesis) and the other in nocturnal conditions (*i.e.,* respiration). All oxygen concentrations are described in mg ($O_2$) $h^{-1}$. The respirometry system was bleached after each trial to minimize background respiration by the accumulation of microorganisms.

## 4.2.4 Calcification

We collected 50 mL of water from each incubation chamber and the control chambers, both in light and dark conditions. We stored the samples in sealed, opaque vials in the dark at 4°C, then we allowed them to stabilize for 2 hours at room temperature (25°C) before processing. We carried out three titrations per sample to define total alkalinity using a Titrando 888 (Metrohm) and Titripur c(HCl) (with a concentration of 100 mmol $L^{-1}$). We defined titration controls with water samples collected before coral incubations. We calculated calcification rate based on the difference between total alkalinity measured at the beginning and end of each incubation period (ΔAT) (Dickson, Sabine and Christian, 2007). Specifically, we assumed that one mole of $CaCO_3$ is produced when alkalinity (ΔAT) drops by two moles across a fixed time period (Δt) (*i.e.*, - ΔAT/2Δt), then by multiplying these parameters by seawater density ($\rho_{sw}$). Finally, we converted the resulting value to g $cm^{-2}$ $yr^{-1}$ based on the molar mass of $CaCO_3$.

## 4.2.5 Colony-size estimation using photogrammetry

After each incubation, we took 100 to 200 overlapping high-resolution photos (300 dpi) of each colony. The photos were used to construct 3D models using the Agisoft PhotoScan software (Agisoft, 2016), which allowed us to define 3D live surface area of each colony (Harwin, Lucieer and Osborn, 2015). We worked with 3D surface area rather than planar area to avoid underestimating coral $CaCO_3$ production. High-resolution photos allowed us to capture coral complexity without killing the corals. We removed surface area under the coral base from our estimates so that we only measured live surface area. To ensure reproducibility, we also defined the Coral Shadow Area (Grottoli *et al.*, 2021) for the wider application of our estimates. All coral colonies (n = 384) were then placed in a large holding aquarium (for a maximum of 2 weeks) and ultimately returned to the outer reef.

## 4.2.6 Statistical analysis

Before analysing the data, we removed data points if 1) a coral colony exhibited a negative calcification rate (*i.e.,* dissolution), 2) the tank temperature dropped below 27°C (*i.e.,* failure of the tank heating system), or 3) the linear fit of $O_2$ concentrations over time to quantify respiration or net photosynthesis rates exhibited an $R^2$ value lower than 0.8 (Kolb, 2018). Following this quality control procedure, we retained 250 out of 384 (65 %) of data points for the analysis. We then applied Bayesian models to estimate the relationship between colony surface area and each physiological rate on the natural log scale using the R package *brms* (Bürkner, 2017a, 2017b). Our models were specified with the following structure:

$$\ln(R_{S,i}) \sim \mathcal{N}(\mu_{S,i}, \sigma)$$
$$\mu_{S,i} = (\ln(\alpha) + \zeta_{[S_i,1]}) + (\beta + \zeta_{[S_i,2]}) \ln(x_i)$$

$$\zeta = (\Omega\mathbb{Z})\delta_s$$
$$\text{diag}(\mathbb{Z}) = \sigma_\zeta$$
$$\beta \sim \mathcal{N}(0, 5);\ \ln(\alpha) \sim \mathcal{N}(0, 5);\ \sigma \sim \Gamma(2, 0.1);\ \delta_s \sim \mathcal{N}(0, 1);\ \Omega \sim \text{LKJ}(1);$$
$$\sigma_\zeta \sim \Gamma(2, 0.1)$$

where $\ln(R_{S,i})$ is the natural logarithm of the rate of calcification (kg $yr^{-1}$), $O_2$ consumption (mg $h^{-1}$), or $O_2$ production (mg $h^{-1}$) of species $S$ and individual $i$; $\ln(x_i)$ is the natural logarithm of live coral surface area ($cm^2$); $\ln(\alpha)$ is the among-species average intercept on the natural log scale; $\beta$ is the among-species average size scaling slope (*i.e.*, exponent on the natural scale); $S_i$ is a vector comprising $s$ levels of species ($n$ = 6), which, in turn, create a hierarchical matrix $\zeta$ of $s$ rows and two columns, respectively, representing species-level additive deviations from $\ln(\alpha)$ and $\beta$; $\Omega$ is the Cholesky factor of the correlation matrix between the hierarchical effects, $\mathbb{Z}$ is the two-by-two diagonal matrix, for which the diagonal is a vector of among-species standard deviations ($\sigma_\zeta$), and $\delta_s$ is an $s$-by-two matrix of standardised hierarchical effects. The prior sampling distributions were specified to follow Gaussian ($\mathcal{N}$(location, scale)), Gamma ($\Gamma$(shape, inverse scale)) and log-LKJ (LKJ(shape)). We ran our models with three chains, 5,000 draws per chain, and a warm-up period of 2,500 steps, thus retaining 7,500 draws to construct posterior distributions. We verified chain convergence with trace plots and confirmed that $R_{hat}$ (the potential scale-reduction factor) was lower than 1.05 (Gelman, Rubin and *al.*, 1992). We obtained $R^2$ values of 0.92, 0.77, and 0.77 for the calcification rate model, respiratory rate model, and photosynthetic rate model, respectively (**Table S4.1, Figure S4.2**). We then divided our raw data by the respective surface area of each colony to express rates on an area-specific basis. To calculate the posterior distribution of the scaling exponent of area-specific rates against colony area, we used 1-$\beta$ (**Figure S4.3**).

The ratio between net photosynthesis rate and calcification has been used as a proxy for how much energy is available to perform other functions (*e.g.*, reproduction) (Rinkevich, 1989). To do so, we performed simulations to evaluate the energy budget of monospecific assemblages. Specifically, we first defined average colony size for the six genera following cyclone Oli in 2010 (Carlot *et al.*, 2021), which resulted in the dominance of small colonies (within the same range as our ex situ coral estimates). On reefs around Mo'orea, a series of recent disturbances have shifted coral composition in favour of *Pocillopora* corals (Adjeroud *et al.*, 2018), so we chose to compare *Pocillopora vs.* the other genera. We randomly generated 100 size distributions which were used to calculate species- and size-specific photosynthesis and calcification rates. These estimates were used to compare population-wide estimates of *P. verrucosa* against each of the other five species (*i.e., A. hyacinthus, A. curta, M. verrilli, N. irregularis* and *Porites spp*.). Finally, we estimated the 'energetic ratio' for each population. All the statistical analyses were run in R version 4.0.3 (R Core Team, 2019).

## 4.3 Results

For all coral species, we observed an increase in calcification, respiration, and photosynthesis across the colony-size gradient (Figure 4.1). However, we identified both hypo-allometric and isometric relationships, depending on the physiological process. Calcification showed a hypo-allometric relationship with colony size, as evidenced by values of $\beta$ that were lower than 1 (Table 4.1, Table S4.1., Figure 4.1). Thus, juvenile corals calcify more efficiently than adults, relative to their surface area. Although massive *Porites* spp., massive *A. curta*, and encrusting *M. verrilli* had higher $\beta$ values than the other species, only 2% of the 5,000 posterior draws had a slope greater than 1 (*i.e.,* isometric trajectories, meaning that juveniles grow as fast as adults). On the other hand, respiration and photosynthesis increased isometrically with colony size, as demonstrated by $\beta$ values that did not differ from 1.

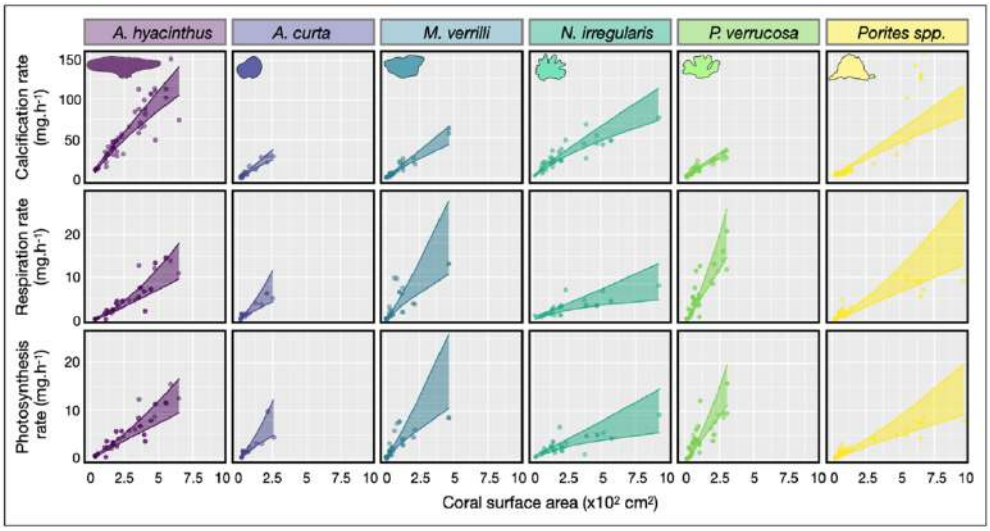


*Figure 4.1 | Scaling relationships between the three physiological processes (i.e., calcification, respiration, and photosynthesis rates, respectively, from top to bottom) and live coral surface area for six coral species (Acropora hyacinthus, Astrea curta, Montipora verrilli, Napopora irregularis, Pocillopora cf. verrucosa and Porites spp.) with a ± 95% Bayesian credible interval. All relationships are depicted with dots representing the raw data and regression lines representing posterior predictions from the Bayesian linear model (± 95% credible intervals). Coral silhouettes represent the mature coral morphology.*

*Table 4.1 | Point estimates and 95% credible intervals for fitted parameters based on Bayesian linear models estimating calcification, respiration, and photosynthesis rates according to colony size for six coral species. The coefficients $\alpha$ and ß are calculated as: Metabolic rate = $\alpha S_A^{ß}$ where $S_A$ is the coral surface area ($cm^2$) and the metabolic rate is expressed in ($mg.h^{-1}$). When ß is lower than one, the metabolic rate scales hypo-allometrically with $S_A$, whereas when ß equals 1, the metabolic rate scale isometrically with $S_A$.*

| | | Calcification | | | Respiration | | | Photosynthesis | | |
|---|---|---|---|---|---|---|---|---|---|---|
| Parameters | | Mean | 2.5% | 97.5% | Mean | 2.5% | 97.5% | Mean | 2.5% | 97.5% |
| *A. hyacinthus* | α | 0.26 | 0.15 | 0.48 | 0.01 | 0.01 | 0.06 | 0.02 | 0.01 | 0.06 |
| | ß | 0.85 | 0.77 | 0.94 | 1.29 | 1.00 | 1.41 | 1.11 | 0.87 | 1.32 |
| *A. curta* | α | 0.24 | 0.14 | 0.45 | 0.02 | 0.01 | 0.06 | 0.02 | 0.01 | 0.06 |
| | ß | 0.89 | 0.80 | 0.97 | 1.06 | 0.78 | 1.33 | 1.05 | 0.82 | 1.27 |
| *M. verilli* | α | 0.24 | 0.14 | 0.45 | 0.02 | 0.02 | 0.07 | 0.02 | 0.01 | 0.06 |
| | ß | 0.93 | 0.83 | 1.00 | 1.00 | 0.71 | 1.26 | 0.98 | 0.74 | 1.19 |
| *N. irregularis* | α | 0.24 | 0.14 | 0.45 | 0.01 | 0.01 | 0.06 | 0.02 | 0.01 | 0.05 |
| | ß | 0.82 | 0.75 | 0.91 | 0.76 | 0.47 | 1.02 | 0.80 | 0.56 | 1.01 |
| *P. verrucosa* | α | 0.24 | 0.14 | 0.44 | 0.02 | 0.02 | 0.07 | 0.02 | 0.01 | 0.06 |
| | ß | 0.86 | 0.78 | 0.95 | 1.20 | 0.91 | 1.46 | 1.20 | 0.96 | 1.41 |
| *Porites spp.* | α | 0.24 | 0.14 | 0.44 | 0.02 | 0.01 | 0.06 | 0.02 | 0.01 | 0.05 |
| | ß | 0.93 | 0.84 | 1.00 | 1.16 | 0.87 | 1.42 | 1.08 | 0.84 | 1.29 |

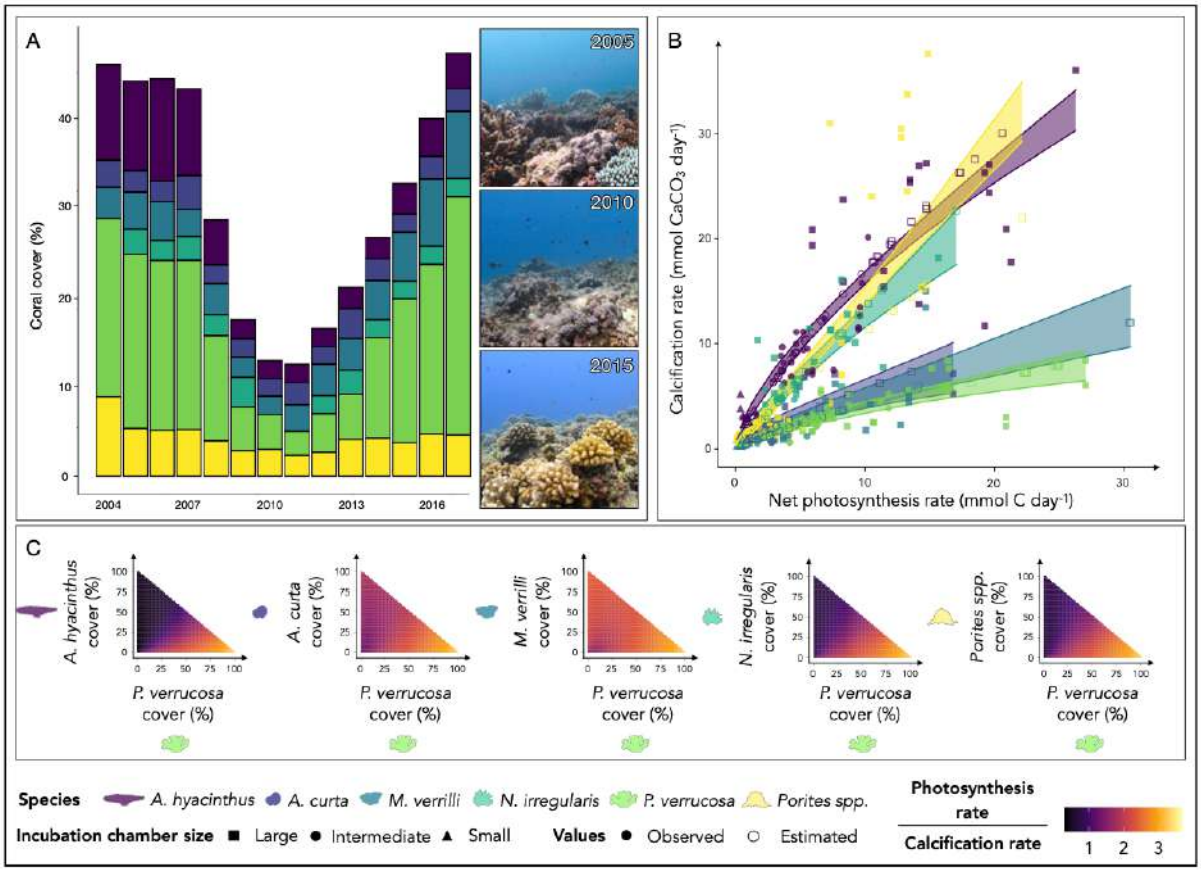


*Figure 4.2 | Representation of hypothetical coral assemblages and their corresponding energy ratios (net photosynthesis rate/calcification rate).* ***A.*** *Percentage of live coral cover of the 6 coral species from 2004 to 2017. Reefscapes are represented on the right for three years (i.e., 2005, 2010, and 2015)* ***B.*** *Relationship between calcification and net photosynthesis, which underpin the community-wide models. Estimates from previous Bayesian models (unfilled points) were added to our observations (filled points).* ***C.*** *Matrices representing energy ratios (net photosynthesis rate/calcification rate) according to different scenarios of Pocillopora cf. verrucosa cover (0 to 100% cover) vs. the cover of the five other species (0 to 100% cover; A. hyacinthus, A. curta, M. verrilli, N. irregularis, and Porites spp.) after the cyclone in 2010 (i.e., which resulted in the dominance of small coral colonies).*

Whole colony calcification rates were hypo-allometric; thus, calcification rates per unit surface area decreased as colony size increased for all species, while photosynthesis and respiration per unit area were not size dependent for all species. However, we detected substantial among-species variation in the $\alpha$ coefficients (*i.e.,* the species-specific intercepts) for all three physiological

processes (Figure 4.1, Table S4.1). These results highlight among-species performance variations across all three physiological processes. For example, *A. hyacinthus* showed the highest calcification, while *M. verrilli* exhibited the lowest calcification. Yet, this trend was reversed for both respiration and photosynthesis, where *M. verrilli* and *A. hyacinthus* showed the highest and lowest rates, respectively. Depending on the coral community composition around Mo'orea, these observations may have significant implications (Figure 4.2A). Furthermore, we detected we detected two main trends when examining species-specific relationships between photosynthetic rates and calcification rates (Figure 4.2B). *Porites* spp., *N. irregularis*, and *A. hyacinthus* showed higher calcification rates than net photosynthetic rates, while *A. curta, M. verrilli,* and *P. verrucosa* showed the opposite pattern. Using these ratios to model population-wide processes after cyclone Oli, we found that monospecific stands of *P. verrucosa* exhibited the highest rates of calcification vs. photosynthesis, regardless of population structure (*i.e.*, ratio ~ 3.5; Figure 4.2C).

## 4.4. Discussion

Organismal physiology underpins community-wide ecological processes that define ecosystem functioning. We analysed three fundamental physiological functions (*i.e.,* calcification, respiration, and photosynthesis) for six prominent coral taxa to test whether the relationships between these functions and colony size was isometric or allometric. Similar to recent results (Edmunds and Burgess, 2016; Dornelas *et al.*, 2017; Madin *et al.*, 2020), we found that calcification increases hypo-allometrically per unit area with live coral surface area across all six species. However, this was not the case for photosynthesis and respiration, which scaled isometrically with live coral surface area. This contrasts with previous work, which suggested that respiration and photosynthesis in *Pocillopora* sp. scale allometrically with colony size (Edmunds and Burgess, 2016). The prevalence of isometric relationships across the six species in our study

suggests that isometric scaling of respiration and photosynthesis rates may be common across corals, at least at comparable climatic conditions.

As opposed to the allometric scaling of calcification, the isometric scaling of photosynthesis emphasizes the importance of coral growth in early life stages, potentially due to tissue age (Elahi and Edmunds, 2007). Small, recently settled colonies generally experience intense mortality (Ritson-Williams *et al.*, 2009; Penin *et al.*, 2010; Wall and Stallings, 2018), and a rapid increase in colony size (through extensive calcification) may offer the best chance for survival (Heino and Kaitala, 1999; Doropoulos *et al.*, 2012). Thus, while it is beneficial for small coral colonies to disproportionally invest in calcification, there are no immediate benefits from increased photosynthesis. In fact, high photosynthesis per unit surface area may hamper early-life stage success through exposure to oxidative stress (Fitt *et al.*, 2001; Hoogenboom and Anthony, 2006). Thus, photosynthetic energy may be allocated to others processes such as nutrient cycling (Falkowski *et al.*, 1984) or it may be stored for reproduction at maturity (Leuzinger, Anthony and Willis, 2003).

Although we defined ex situ calcification rates (alkalinity anomaly method), our results are consistent with other methods, such as x-rays (Lough, 2008), community metabolism (Langdon and Atkinson, 2005), or in situ measurements (Kuffner, Hickey and Morrison, 2013). While the examined coral species showed comparable scaling relationships for calcification rates, *A. hyacinthus* had a consistently higher rate than the other species. These results are also consistent with the high calcification rates documented for corals in the genus *Acropora*, which are generally classified as fast-growing corals (Harriott, 1999; Anderson *et al.*, 2018). However, although *A. hyacinthus* had the highest calcification rate, its photosynthetic and respiratory rates were among the lowest in our experiments. This provides physiological evidence that *A. hyacinthus* tends to allocate most of its energy to growth, at least in the absence of spawning activity, during which

large amounts of energy may be dedicated to gamete development (Razak *et al.*, 2020). Conversely, *M. verrilli* and *P. verrucosa* had the highest photosynthetic rates (Figure 4.1, Figure S4.3) but markedly lower calcification rates than *A. hyacinthus*, which further highlights differences in the life-history strategies of the various species. For *Pocillopora*, at least, brooding sperm and egg bundles may require this investment and subsequently enhance the chances of *Pocillopora* offspring to survive (Hirose, Kinzie and Hidaka, 2001). Indeed, the high photosynthetic rate of *P. verrucosa* may explain the success of this species in Mo'orea, a reef system recently dominated by pocilloporids (Hédouin *et al.*, 2020). Although *M. verrilli* employs broadcast spawning, it is the second most abundant coral genus in Mo'orea (Bosserelle *et al.*, 2014), suggesting that higher photosynthesis rates are directly related to ecological success under the current environmental conditions in Mo'orea.

Notably, *M. verrilli* and *P. verrucosa* are also known for their lower *Symbiodinium* density (from 4 to 6-fold less than the genus *Acropora*) (Edmunds *et al.*, 2014), which further emphasizes their high photosynthetic rates. The distinct photosynthetic rates among coral taxa might arise from the different physiological and ecological attributes of associated symbiotic communities (Baird, Guest and Willis, 2009; Putnam *et al.*, 2012; Rouzé *et al.*, 2019) and their transmission. *P. verrucosa* generally shows a stable association with the genus *Cladocopium* (Stat, Morris and Gates, 2008; Baker *et al.*, 2018), which exhibits high photosynthetic efficiency and is transmitted vertically to offspring. *M. verrilli* shows a similar association and transmission dynamics (Stat, Yost and Gates, 2015). In contrast, *A. hyacinthus* exhibits flexible association with different Symbiodiniaceae genera, often obtained through horizontal transfer (Davies *et al.*, 2020). While this results in the dominance of acroporids in a variety of environmental conditions, the present community composition around Mo'orea suggests that the physiological profile of *A. hyacinthus* and its variable symbionts are disadvantageous under current conditions, as the genus has become rare as

compared to *P. verrucosa* or *M. verrilli* (Babcock *et al.*, 2003). The other three coral species (*i.e., A. curta, N. irregularis,* and massive *Porites spp.*) show intermediate physiological performance and likewise intermediate abundances around Mo'orea. Thus, the revealed differences in physiological profiles likely determine the energetic basis for processes unfolding at the population and community levels.

Our study focused on specific *in situ* conditions; therefore, additional work is required to strengthen the robustness of our findings and reaffirm our predictions for future coral community assemblages according to different environmental conditions. Indeed, light intensity and water flow highly impact physiological rates, and, as such, they may significantly affect calcification rates (Edmunds and Burgess, 2017; Cresswell *et al.*, 2020). In addition, although we assumed a proportional variation in physiological rates according to variations in light intensity, sea temperature (Venti, Andersson and Langdon, 2014), and water flow (Edmunds and Burgess, 2017), calcification rates may change disproportionately with decreases in light intensity and increases in ocean acidity (Dufault *et al.*, 2013), which further depends on coral species and life history stage (Kornder, Riegl and Figueiredo, 2018). Moreover, our findings are derived from a distinct range in the size spectrum of the studied species. Specifically, our work focused on relatively small coral colonies that are dominant after severe disturbances such as cyclone Oli (Carlot *et al.*, 2021), thus potentially biasing the obtained scaling relationships through the omission of larger, more mature colonies. Finally, due to heterogeneity in the shape of corals, additional work might reveal changes in physiological rates according to coral surface standard (*i.e.*, planar area vs contour area) (Jokiel, Jury and Kuffner, 2016), but we were unable to address this component in the present study.

Thoroughly understanding the nature of the investigated scaling relationships opens opportunities to estimate ecosystem-wide processes that are

critical for coral reef functioning. In the case of photosynthesis and respiration, isometric scaling permits relatively simple extrapolations of colony-level processes to entire communities. Specifically, if species identities and the relative combined surface areas of colonies are known, we may be able to compute reasonably accurate estimates of community-wide respiration and photosynthesis. In this case, standard coral survey methods that record the percent cover of different species (English, Wilkinson and Baker, 1997; Hill, Wilkinson and *al.*, 2004) allow the estimate of community-level photosynthetic capacity. In contrast, due to the size-dependency of calcification, an accurate estimation of community-level calcification would require information on the size distribution of individual colonies, which are seldom recorded in standard monitoring (Edmunds and Riegl, 2020). Given that calcification is a crucial function performed by coral assemblages, with direct implications for reef accretion (Perry *et al.*, 2018) and wave-energy attenuation (Harris *et al.*, 2018), the absence of colony size from most major coral reef monitoring programs may preclude us from inferring community-level processes with adequate accuracy.

Overall, our results expand our understanding of coral physiology and species-specific traits that can confer ecological advantages under changing environmental conditions. Further, our findings strengthen our capacity to predict community-wide rates of photosynthesis and respiration based on commonly collected coral survey data. Our results suggest that the lack of demographic data (*i.e.,* colony size) across the literature and many monitoring databases prevents us from precisely defining community-wide estimates of calcification. Therefore, including colony size would greatly enhance long-term monitoring efforts, since surface area dictates the total light, carbon, and nutrients that a coral can absorb.

## 4.5 Acknowledgements

This study was conducted under the authority of the Direction de environment de Polynésie française (DIREN) under the convention 681/MCE/ENV signed on 20 April 2018. We thank the Service d'Observatoire CORAIL (SO CORAIL).

## 4.6 Data availability

Code and data are available on my Github folder "Coral Physiology": https://github.com/JayCrlt/Coral_Physiology

## 4.7 Supplementary information

*Table S4.1 | Point estimates and 95% credible intervals for fitted parameters based on Bayesian linear models estimating calcification, respiration, and photosynthesis rates based on colony size and species identity.*

| | Calcification | | | Respiration | | | Photosynthesis | | |
|---|---|---|---|---|---|---|---|---|---|
| Parameters | Mean | 2.5% | 97.5% | Mean | 2.5% | 97.5% | Mean | 2.5% | 97.5% |
| **Fixed effects** | | | | | | | | | |
| ln(α) | -6.126 | -6.719 | -5.486 | -4.154 | -5.565 | -2.741 | -3.971 | -5.074 | -2.907 |
| ß | 0.881 | 0.792 | 0.966 | 1.074 | 0.796 | 1.351 | 1.033 | 0.800 | 1.256 |
| **Random effects** | | | | | | | | | |
| Std. Deviation of ln(α) | 0.613 | 0.228 | 1.408 | 1.437 | 0.624 | 3.006 | 1.081 | 0.383 | 2.376 |
| Std. Deviation of ß | 0.075 | 0.006 | 0.199 | 0.281 | 0.100 | 0.638 | 0.221 | 0.050 | 0.519 |
| Correlation of ln(α) and ß | -0.58 | -0.98 | 0.527 | -0.602 | -0.959 | 0.236 | -0.507 | -0.953 | 0.536 |

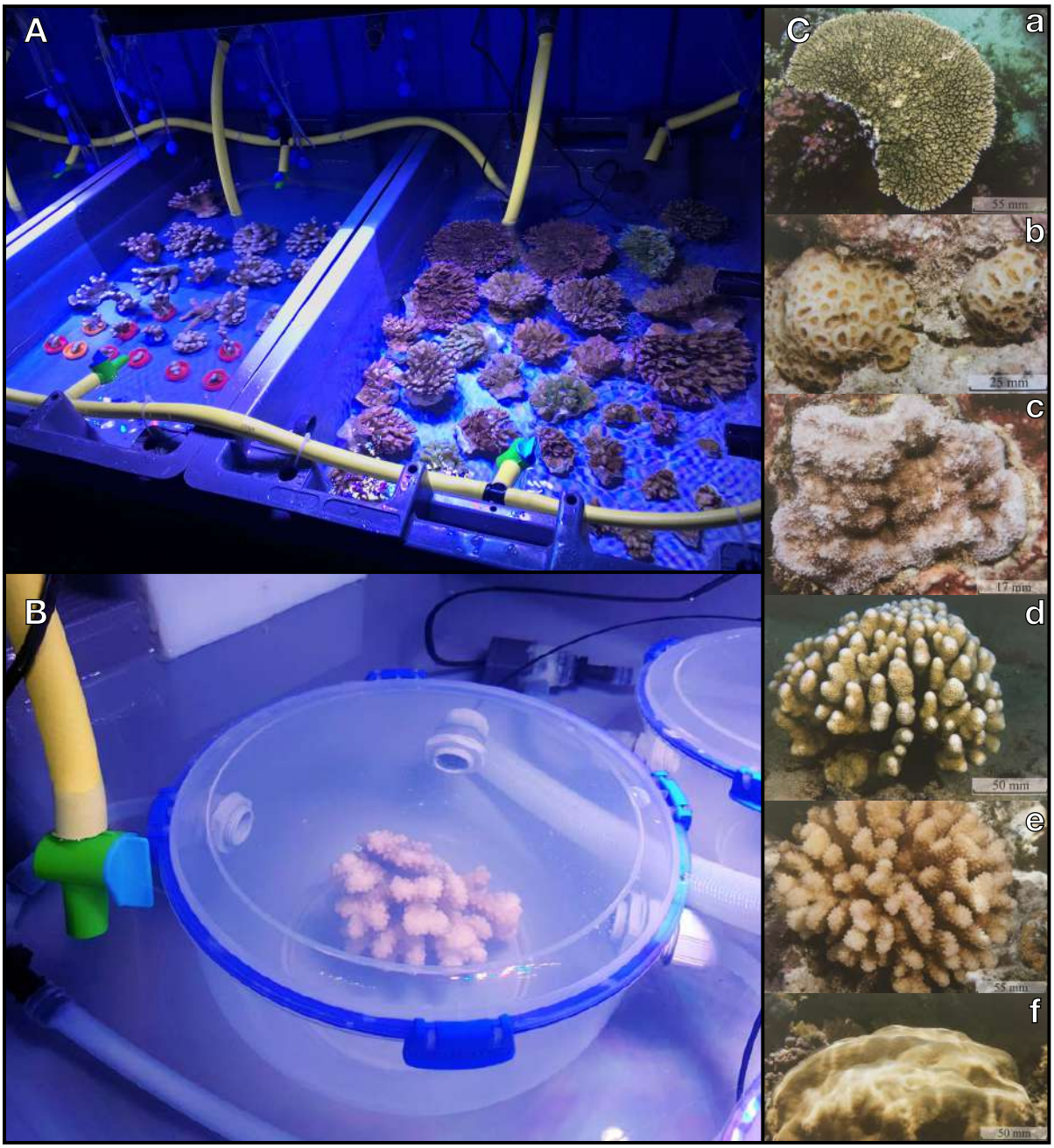


***Figure S4.1 |*** *Tank set up. A. Coral colonies in two tanks conditioned to reflect in situ environmental parameters. In the left tank, the coral colonies are* ***A.*** *hyacinthus, and in the right tank, they are N. irregularis.* ***B.*** *P. verrucosa in an incubation chamber used to define calcification and gross photosynthesis rates.* ***C.*** *Photos of the 6 different coral species (a. A. hyacinthus; b. A. curta; c. M. verrilli; d. N. irregularis; e. P. verrucosa and f. Porites spp.) from Bosserelle et al. (2014)*

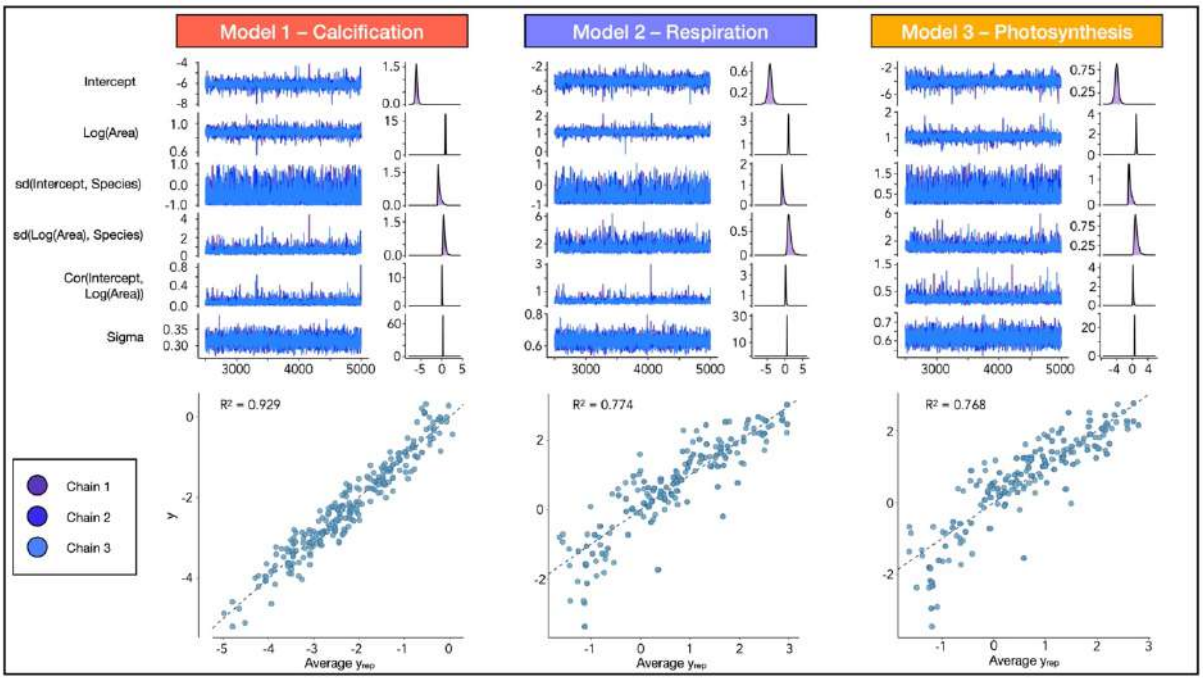


*Figure S4.2 | Trace plots depicting the Monte Carlo chains from the three Bayesian models. Each model (i.e., calcification, respiration, and photosynthesis) was run with three chains of 5,000 iterations, with the first 2,500 steps discarded. The scatterplots represent posterior predictive checks with the respective $R^2$ values estimated from the model.*

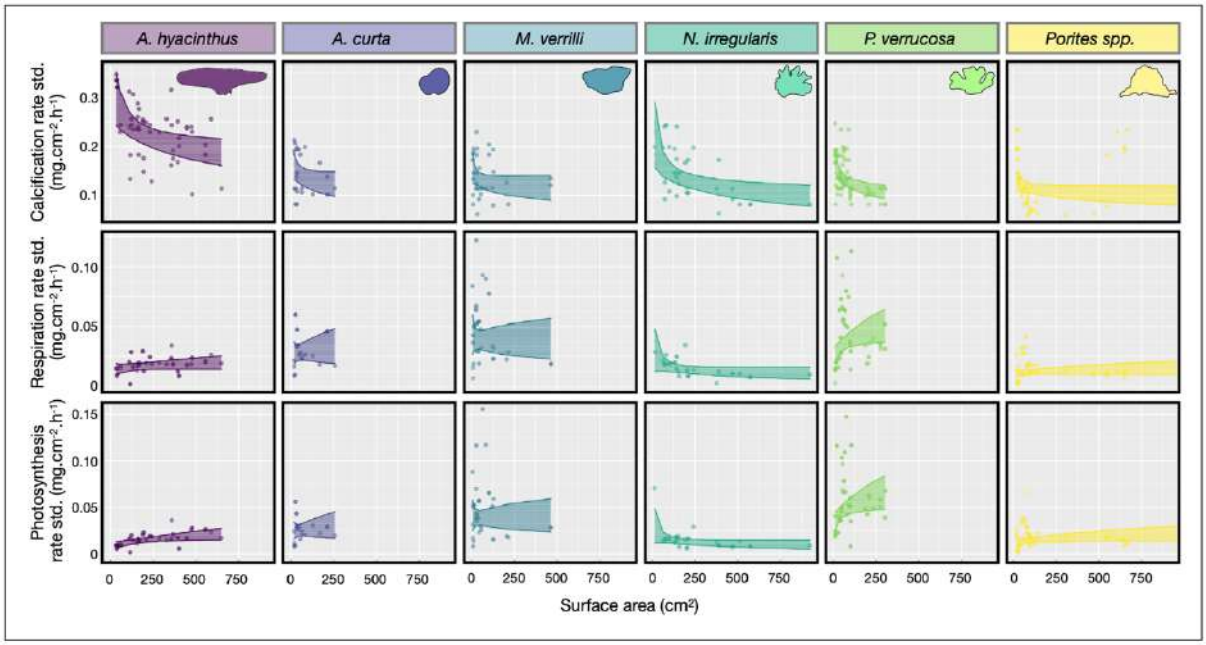


*Figure S4.3 | Relationship between the surface area-specific physiological processes (calcification, respiration, and photosynthesis rates, respectively, from the top to the bottom) and live coral surface area for six coral species (Acropora hyacinthus, Astrea curta, Montipora verrilli, Napopora irregularis, Pocillopora cf. verrucosa, and Porites spp.) with a ± 95% Bayesian credible interval. All relationships are depicted with dots representing the raw data points and regression lines representing posterior predictions from the Bayesian linear model (± 95% credible intervals). Coral silhouettes represent the mature coral morphology*

# Chapter 5

# Loss of structural complexity from coral reefs implies a lack of efficiency in dissipating wave energy in the face of global changes

This chapter is in preparation for Proceedings of the National Academy of Sciences of the United States of America

## Authors

Jérémy Carlot, Michalis Vousdoukas, Theofanis Karambas, Alessio Rovere, Hunter S. Lenihan, Mohsen Kayal, Mehdi Adjeroud, Laetitia Hedouin, Valeriano Parravicini

# Abstract

Coral reefs protect 500 million people from oceanic waves, but they are threatened by intensifying anthropogenic disturbances and climate change. These have the effect of reducing the structural complexity of coral assemblages, hence affecting the effective ability of reefs to break incoming waves. To forecast how tropical coastal populations will be affected by future flooding risks requires an understanding of the continued capacity of reefs to dissipate wave energy under ongoing global changes and large-scale bleaching events. In this work, we show that the relationship between coral reef structural complexity and waves dissipation increases heterogeneously according to the height of the waves. For example, we reveal that structural complexity has twice the potential to dissipate an offshore wave of 3m compared to an offshore wave of 1m. Our results are based on a unique field experiment that recorded the almost complete loss of structural complexity in French Polynesia in 2010, right after a cyclone. Thus, we surmise that, if structural complexity is compromised (as observed after dramatic large-scale disturbances), the expected rise of storm intensity in the near future may jeopardize the persistence of coastal societies along the tropics in the 21$^{st}$ century.

# 5.1 Introduction

During the second half of the twentieth century, the world population reached historically unprecedented demographic levels, exceeding 7.8 billion people in March 2020 (World Population Data Sheet, 2020). Because coastal zones are among the most developed areas worldwide (Barbier *et al.*, 2011; Temmerman *et al.*, 2013; Neumann *et al.*, 2015), these places tend to accommodate most of the demographic increase, gathering steadily more people and therefore resulting in high population densities (McGranahan, Balk and Anderson, 2007; Haslett, 2009). This is particularly true for coral reef islands where the livelihoods of more than 500 million people are linked to the highly valuable ecosystemic services of coral reefs (Hoegh-Guldberg, Pendleton and Kaup, 2019) (*e.g.*, food supplies tourism, coastal protection (Costanza *et al.*, 2014; Woodhead *et al.*, 2019). Coastal societies can develop on these areas thanks to natural coastal protection against ocean waves, provided by the reefs. Indeed, coral reefs absorb 97% of the incoming wave energy (Ferrario *et al.*, 2014), therefore effectively buffering shorelines from the risk of flooding during extreme storms (Spalding, Ruffo, *et al.*, 2014).

Although there is still significant uncertainty on whether climate change will lead to an increase in the frequency of extreme sea storms (*e.g.*, those driven by tropical cyclones), there is consensus on the fact that warmer ocean temperatures and higher sea levels will increase coastal flood and erosion risk (Hinkel *et al.*, 2019; Vousdoukas *et al.*, 2020). Unfortunately, coral reefs are also threatened by intensifying anthropogenic stressors, including global ocean warming, sea-level rise and local impacts such as pollution and sedimentation (Hughes, Barnes, *et al.*, 2017). These perturbations usually imply a decrease in living coral cover (De'ath *et al.*, 2012) and habitat structural complexity, especially when tropical storms hit coral assemblages that underwent massive mortalities, such as in the case of bleaching event (Madin and Connolly, 2006;

Alvarez-Filip *et al.*, 2009). The combination of coral mortality and loss of structural complexity leads to the flattening of reefs, a process that is becoming increasingly common worldwide (Gardner *et al.*, 2003; Bruno and Selig, 2007; Alvarez-Filip *et al.*, 2009; Rogers, Blanchard and Mumby, 2014). Decreasing structural complexity (Beck *et al.*, 2018; Roelvink *et al.*, 2021) will result in lower natural protective capacity and further magnification of the already high anticipated coastal risks (Christensen *et al.*, 2013). Despite the fact that the link between wave attenuation and structural complexity is widely accepted among scientists, studies which quantify the level of protection in real-world conditions are limited.

Here, we use field observations and numerical wave models to show that structural complexity offers natural protection which increases exponentially with wave height. For example, we find that the potential of coral roughness to dissipate incoming waves doubles as the significant wave height increases from 1 m to 3 m. Such natural protective capacity will be greatly reduced in view of bleaching events becoming an annual phenomenon for 90% of reefs since 2020 (Kwiatkowski *et al.*, 2015).

# 5.2 Materiel & Methods

## 5.2.1 Fieldwork measures

Mo'orea (French Polynesia) is encircled by coral reefs, which are 500–700 m wide with a dominant swell direction coming from the southwest to northeast. Thus, wave conditions were measured on the fore-reef slopes and reef flats of Ha'apiti (South-west coast), because this site was considered as a high-energy site (Harris et al. 2018) (**Figure S5.1**). Pressure records were measured in a cross-reef transect from the fore-reef slope to the reef flat using INW PT2X Aquistar and DHI SensorONE pressure transducers (PTs) both logging at 4 Hz. Pressure

records were corrected for pressure attenuation with depth (Tucker and Pitt 2001) and split into 15-min ensembles (Harris *et al.*, 2015).

## 5.2.2 Structural complexity definition

To define structural complexity, we took 100 to 200 overlapping high-resolution photos (300 dpi) of 30 coral colonies (n = 10 for *Acropora hyacinthus*, n = 10 for *Pocillopora* cf. *verrucosa* and n = 10 for *Porites lutea*). The photos were used to construct 3D models using the Agisoft PhotoScan software (Agisoft, 2016) (**Figure S5.3**). Thanks to a dataset that document changes in coral colony size (*i.e.,* width, length and height) distributions across a full disturbance-recovery cycle between 2005 and 2016 (Carlot *et al.*, 2021) we randomly resize coral 3D models and placed coral colonies 100 times within a transect from 20m depth to the reef crest (160m length, **Figure S5.4**). To ensure ecological variability we randomly rotate coral colonies between $-\pi/2$ and $\pi/2$. For example, for one trial (out of 100) in 2005, we randomly placed 1400 coral colonies within our $160m^2$ (n = 448 for *Acropora hyacinthus*, n = 912 for *Pocillopora* cf. *verrucosa* and n = 240 for *Porites lutea*). For each coral colony, a random rotation was defined and for each species, one of the ten 3D models was randomly selected. Finally, to quantify the complexity from corals we converted our transect as raster and used the function *rumple_index* of the *LidR package* (Roussel *et al.*, 2020; Roussel and Auty, 2021) in R 4.0.0 (R Core Team 2019). Our estimates are consistent with previous structural complexity at this location (Carlot *et al.*, 2020).

## 5.2.3 Nikuradse definition

To calibrate the hydrodynamic model, we defined the Nikuradse roughness ($k_n$) estimates based on our structural complexity estimates. In the 1930s, Nikuradse measured the hydraulic effects of uniform sand grain roughness on

the flow in cylindrical pipes (Nikuradse, 1933). Thus, to convert our structural complexity estimates to $k_n$ estimates, we assumed that coral colonies were distributed homogeneously within our 3D transect for each year. We defined the average coral height within the transect for each virtual 3D transect (one transect per year). This average height was considered as the radius of the theoretical Nikuradse's sand grain and was multiplied by 2 to obtain $k_n$ estimates (**Figure S5.5A**). To validate our approach, we first defined $k_n$ estimates from a hydrodynamical approach' for each pair of sensors (between sensor 1 and sensor 2, between sensor 2 and sensor 3 and between sensor 3 and sensor 4; **Figure S5.1**) in 2016. Second, to define $k_n$ estimates during the other past years, we delineated the structural complexity as the ratio between 2016 and the other past years and quantify how much the complexity has changed in percentage (**Figure S5.5B**). Third, we applied this percentage of change in complexity to the $k_n$ estimate defined in 2016 by the 'hydrodynamical approach'. We also used our dataset that documents changes in coral colony size (*i.e.,* width, length and height) from 2005 to 2016, to define the average coral height for each year of our 3D transects and thus quantify $k_n$ estimates by our 'topographic approach'. Consistently, we compared our $k_n$ estimates defined by the 'topographic approach' and our $k_n$ estimates defined by the 'hydrodynamical approach' by making a scatterplot and we defined a linear regression between both $k_n$ *i.e.,* $k_{n,hydrodynamical} = \alpha \cdot k_{n,topographic}$ (**Figure S5.5C**). The slope α was used as a factor of correction and was applied to our estimates obtained with the 'topographic approach'. To ensure reproducibility for further studies and break boundaries between hydro-physicists and ecologists, we traced the relationship between structural complexity and Nikuradse roughness estimates ($R^2$ = 68%; **Figure S5.5D**).

## 5.2.4 Hydrodynamic model

The present nonlinear wave model in the nearshore zone is based on the Boussinesq equations (Karambas and Koutitas, 2002) :

$$\frac{\partial U}{\partial t}+\frac{1}{h}\frac{\partial M_u}{\partial x}-\frac{1}{h}U\frac{\partial (Uh)}{\partial x}+g\frac{\partial \zeta}{\partial x}=\frac{(d^2+2d\zeta)}{3}\frac{\partial^3 U}{\partial x^2\partial t}+d_x h\frac{\partial^2 U}{\partial x\partial t}+$$
$$+\frac{d^2}{3}\left(U\frac{\partial^3 U}{\partial x^3}-\frac{\partial U}{\partial x}\frac{\partial^2 U}{\partial x^2}\right)+d\frac{\partial \zeta}{\partial x}\frac{\partial^2 U}{\partial x\partial t}+dd_x U\frac{\partial^2 U}{\partial x^2}+d_x\frac{\partial \zeta}{\partial x}\frac{\partial U}{\partial t}-$$
$$-\quad d\frac{\partial^2}{\partial x\partial t}\left(\delta\frac{\partial U}{\partial x}\right)+E-\frac{\tau_b}{\rho h}+ \qquad (1)$$
$$+Bd^2\left(\frac{\partial^3 U}{\partial x^2\partial t}+g\frac{\partial^3 \zeta}{\partial x^3}+\frac{\partial^2\left(U\frac{\partial U}{\partial x}\right)}{\partial x^2}\right)+2Bdd_x\left(\frac{\partial^2 U}{\partial x\partial t}+g\frac{\partial^2 \zeta}{\partial x^2}\right)$$

where, $U$ is the mean over the depth horizontal velocity, ζ is the surface elevation, d is the water depth, $u_o$ is the near bottom velocity, $h=d+\zeta$, $M_u=(d+\zeta)u_0^2+\delta(c^2-u_0^2)$, δ is the roller thickness determined geometrically according to Schäffer, Madsen and Deigaard (1993), E is an eddy viscosity, $\tau_b$ is the bed friction term and $B$=1/15. More details are found in Karambas and Koutitas (2002).

In this work the wave breaking mechanism is based on the surface roller concept (Schäffer, Madsen and Deigaard, 1993). However, in the swash zone, surface roller is not present and the eddy viscosity concept is used to describe the breaking process. The term E in equation (1) is written:

$$\mathrm{E_{b_x}}=\mathrm{B_b}\frac{1}{\mathrm{h}+\eta}\{\mathrm{v_c}[(\mathrm{h}+\eta)\mathrm{U}]_\mathrm{x}\}_\mathrm{x} \qquad (2)$$

where $v_e$ is the eddy viscosity coefficient:

$$\mathrm{v_e}=\ell^2\left|\frac{\partial \mathrm{U}}{\partial \mathrm{x}}\right| \qquad (3)$$

where $\ell$ is the mixing length $\ell$ = 3.5 $h$ και $B_b$ a coefficient according to Kennedy *et al.* (2000)

The 'dry bed' boundary condition is used to simulate runup (Karambas and Koutitas, 2002). The numerical solution is based on the fourth-order time predictor-corrector scheme proposed by Wei and Kirby (1995). Therefore, the bed friction term $\tau_b$ is calculated based on the following formula:

$$\tau_{bx} = \frac{1}{2}\rho f_w U|U| \quad (4)$$

where the bottom friction coefficient $f_w$ is given by the formula suggested by Swart (1974), (which is an explicit approximation to the implicit, semi-empirical formula given by Jonsson (2021)

$$f_w = \exp\left[5.213\left(\frac{k_n}{\alpha_0}\right)^{0.194} - 5.977\right] \quad (5)$$

Where $\alpha_o$ is the amplitude of the near-bed wave orbital motion and $k_s$ is the Nikuradse roughness height.

## 5.2.5 Statistical analyses

To quantify how much wave energy is dissipated by coral reef aiming to validate our model efficiency, we made a ratio between offshore wave height ($H_{s,\ reef}$) and wave height near the shore ($H_{s,\ shore}$) for each wave trial and each year (*i.e.,* 1000 waves per year). We then applied Bayesian models to estimate the relationship between $H_{s,\ shore}$, $H_{s,\ reef}$ and structural complexity using the R package *brms* (Bürkner, 2017a, 2017b). Our model was specified with the following structure:

$$H_{S,shore} \sim \mathcal{N}(\mu_S, \sigma)$$
$$\mu_S = (\alpha + \sigma_\zeta) \times H_{s,reef} + (\beta + \sigma_\zeta) \times SC + (\gamma + \sigma_\zeta) \times H_{s,reef} : SC$$
$$\alpha \sim \mathcal{N}(0,1); \beta \sim \mathcal{N}(0,1); \gamma \sim \mathcal{N}(0,1); \sigma \sim \Gamma(2, 0.1); \sigma_\zeta \sim \Gamma(2, 0.1)$$

where $H_{s,shore}$ is the significant wave height near the shore (m), SC is the structural complexity, and $H_{s,reef}$ is the significant wave height near the reef (m). The prior sampling was specified to follow a Gaussian ($\mathcal{N}$(location, scale)) and a Gamma ($\Gamma$(shape, inverse scale)) distribution. We ran our models with three chains, 5,000 draws per chain, and a warm-up period of 2,500 steps, thus retaining 7,500 draws to construct posterior distributions. We verified chain convergence (n=4) with trace plots and confirmed that $R_{hat}$ (the potential scale-reduction factor) was lower than 1.05 (Gelman, Rubin and al., 1992). We obtained a $R^2$ value of 0.46 (**Figure 5.2A**). Finally, drawing on our model, we defined the $H_{s,\ shore}$ according to the wave height on the outer reef from 1m to 6m. We defined the relationship between these estimates and structural complexity to extract the slope and predicted the potential rise of the wave height near the shore according to the loss of structural complexity (**Figure 5.2B**).

## 5.3 Results and discussion

We monitored the structural complexity in Mo'orea (French Polynesia) documenting changes in coral colony size and abundance along an area of 160 x 1m and for the most conspicuous taxa between 2005 and 2016 (*i.e., Acropora hyacinthus, Pocillopora* cf. *verrucosa* and *Porites lutea*) (Trapon *et al.*, 2013). In that period, an outbreak of the predatory sea star *Acanthaster* cf. *solaris* (2006-2009), followed by a cyclone (2010), reduced coral cover from 50% to 3% and halved structural complexity in 2010 (**Figure 5.1**). By the year 2016, coral cover recovered from these disturbances with a dominance of *Pocillopora* cf. *verrucosa* (Adjeroud *et al.*, 2018; Carlot *et al.*, 2021), presenting a higher complexity profile

from the three coral species and resulting as an increase of the overall reef structural complexity.

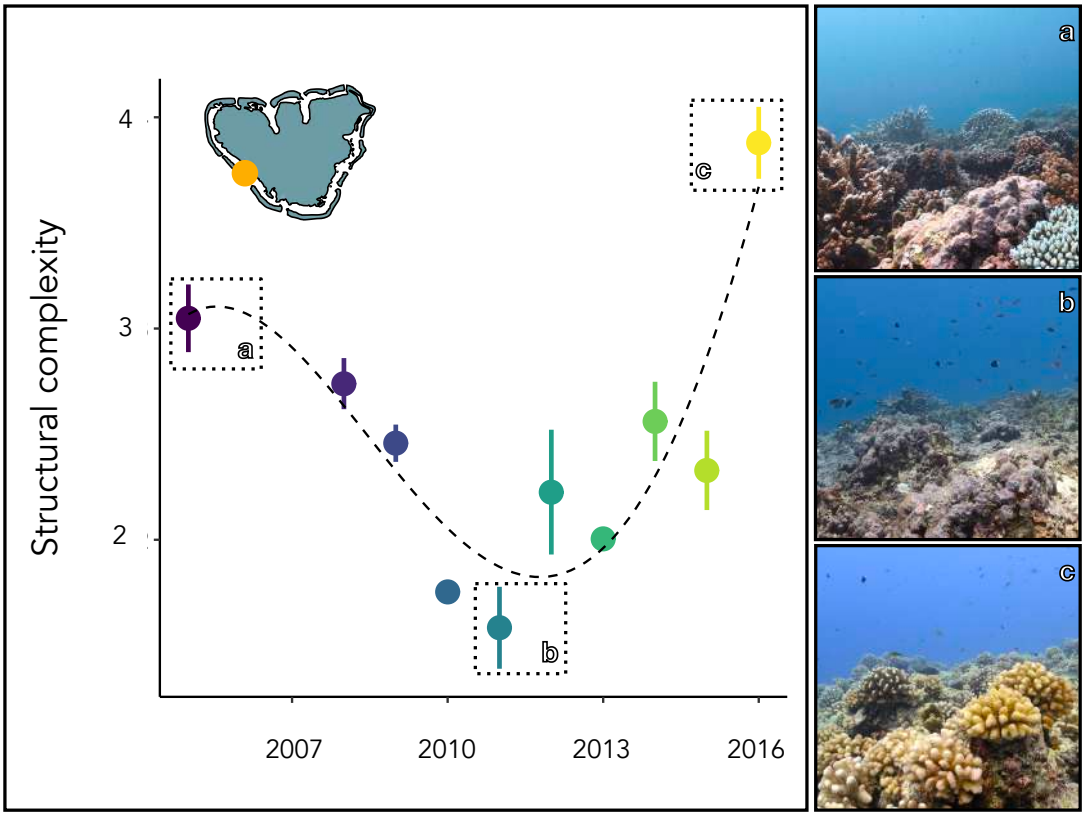


*Figure 5.1 | Evolution of the structural complexity from 2005 to 2016 on the west side of Mo'orea island (French Polynesia). Perturbations included a predatory sea star (Acanthaster cf. solaris) outbreak from 2006 to 2009 and a cyclone in 2010. Photographs illustrate the reefscapes in **A.** 2005, **B.** 2011 and **C.** 2016.*

For the same study period (2005-2016), we have collected water level data along a cross-shore transect and on-, off-shore and on the reef (**Figure S5.1**). The sampling location was selected because of its exposure to the dominant swell direction (Harris *et al.*, 2018). Using spectral analysis, we have quantified coral reef wave energy dissipation, as well as the Nikuradse roughness $k_n$ (Vousdoukas *et al.*, 2012). post-processing of the in situ physical roughness measurements along with the Nikuradse roughness from the hydrodynamic data, allowed generating $k_n$ values along the entire profile. The latter were used in a Boussinesque wave model which allowed up to quantify the capacity of structural

complexity to attenuate incoming wave energy on the study site. To make sure that the simulations represent the local wave climate we processed 30 years of wave data and extracted 1000 conditions discretizing the $0^{th}$ to $100^{th}$ percentile space in equal distances. We then run the wave model for all combinations of the 1000 wave conditions and 10 bed roughness profiles. We then build a Bayesian model to characterize the relationship between the wave height near the shore, structural complexity and wave height on the outer reef. Consistently with previous studies (Harris *et al.*, 2018), our results show that the lower the structural complexity, the lower is the wave dissipation, and hence the higher the waves close to the shore (Figure 5.2A). However, we detected that the effect of structural complexity in dissipating wave energy is strongest in the case of extreme events (Figure 5.2A).

We further exemplify our results calculating how the slope of the relationship between wave height on the shore and structural complexity differ according to the wave height on the outer reef (Figure 5.2B). We show that structural complexity has twice the potential to dissipate a wave of 3m (*i.e.*, which correspond to more than 97.5% of the wave height offshore observed in 2016), compared to a wave of 1m (*i.e.*, which correspond to less than 2.5% of the wave height offshore observed in 2016, Figure S5.2). Those results indicate that the loss of structural complexity will dramatically affect the capacity of reefs to protect coastlines, especially in the case of extreme events. To validate our hydrodynamic model, we quantify how much wave energy is dissipated by coral reefs, making a ratio between offshore wave height and wave height near the shore. We obtain results in line with previous works (Ferrario *et al.*, 2014), confirming that coral reefs absorb 95% to 97% of the waves' energy according to the structural complexity, which is most of the time, correlated with reefs' health (Graham and Nash, 2013).

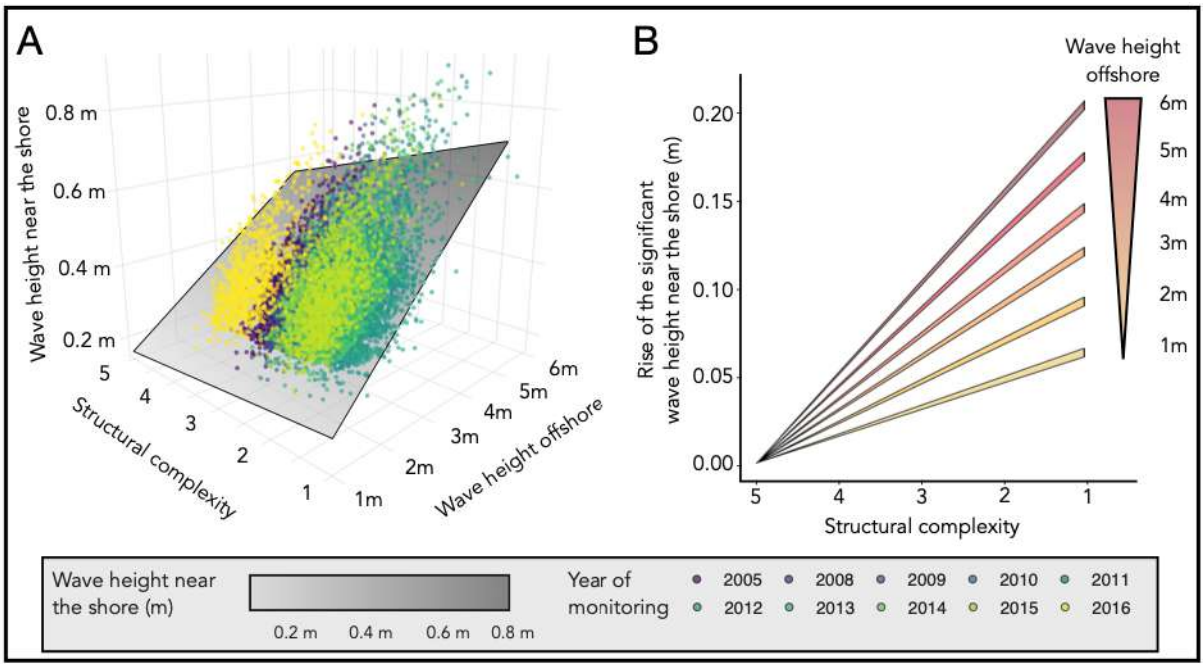


*Figure 5.2 | A. Scatterplot between the wave height near the shore ($H_{S,\ shore}$), the structural complexity (SC) and the wave height offshore ($H_{S,\ reef}$). Colors represent one year of monitoring. The average regression is expressed as $H_{S,\ shore}$ = 0.11 - 0.01 x SC + 0.13 x $H_{S,\ reef}$ - 0.01 x SC: $H_{S,\ reef}$ ($R^2$ = 0.46). For each year (2005 and 2008 to 2016), 1000 waves height near the shore were estimated. B. Increase of the wave height near the shore according to the structural complexity loss and the magnitude of the event. For each 1m wave height offshore, we used the same regression model as before (i.e., $H_{S,\ shore}$ = Intercept + SC + $H_{S,\ reef}$ + SC: $H_{S,\ reef}$) and $H_{S,\ shore}$ was estimated for each set of wave height offshore. Drawing on this model, we determined the likely increase of the significant wave height near the shore according to the loss of the structural complexity.*

Overall, our results paint a grim picture for the safety of coastal societies in the future because wave energy reduction relies mainly on reef accretion and structural complexity (Harris *et al.*, 2018). Under a worst-case scenario (Representative Concentration Pathway 8.5), accretion may cease for 94% of the reefs worldwide by 2050 (Cornwall *et al.*, 2021) and coral reefs worldwide may start to flatten due to ocean acidification and warming (Gardner *et al.*, 2003; Bruno and Selig, 2007; Alvarez-Filip *et al.*, 2009; Rogers, Blanchard and Mumby, 2014). Hence, our results further demonstrate the fundamental role of structural complexity in dissipating wave energy, especially in the case of extreme storm

expected for the near future. Our work attests the risk of coastal flooding in tropical regions if ongoing climate change and anthropogenic pressure that reduce structural complexity are not halted (Nunn, Kohler and Kumar, 2017).

## 5.4 Data availability

Code and data are available in my Github folder "Wave resistance": https://github.com/JayCrlt/Wave_resistance.git

## 5.5 Supplementary information

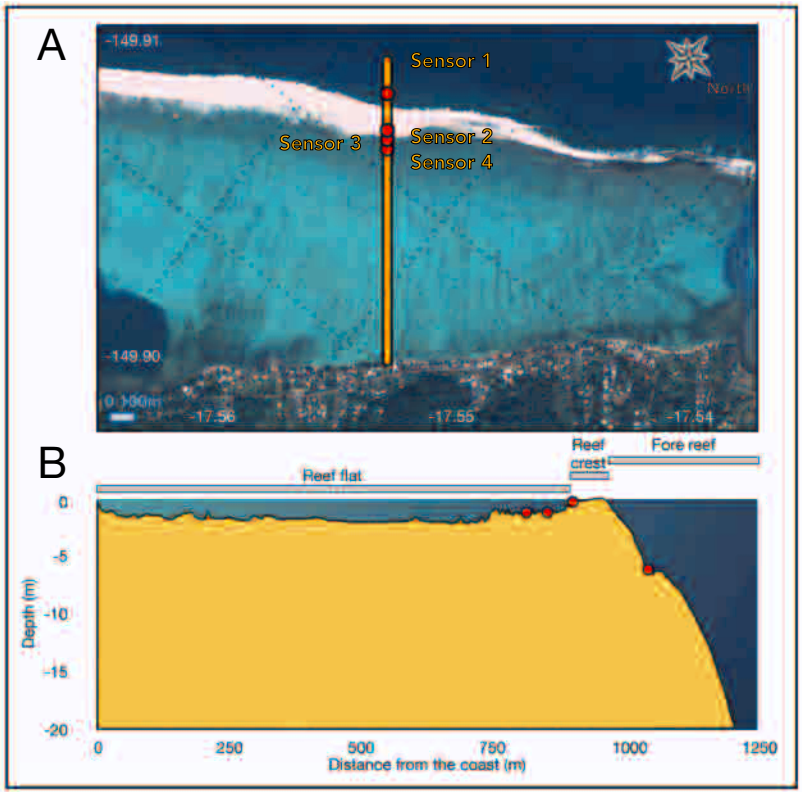


*Figure S5.1 | Transect along which wave attenuation was estimated from sensor 1 to sensor 2, 3 and 4. **A.** Aerial view of Haapiti, Mo'orea (French Polynesia) (WorldView-3 imagery). **B.** Cross-section of the transect highlighting the 3 different environment and sensor locations within the very same transect at Haapiti, Mo'orea (French Polynesia).*

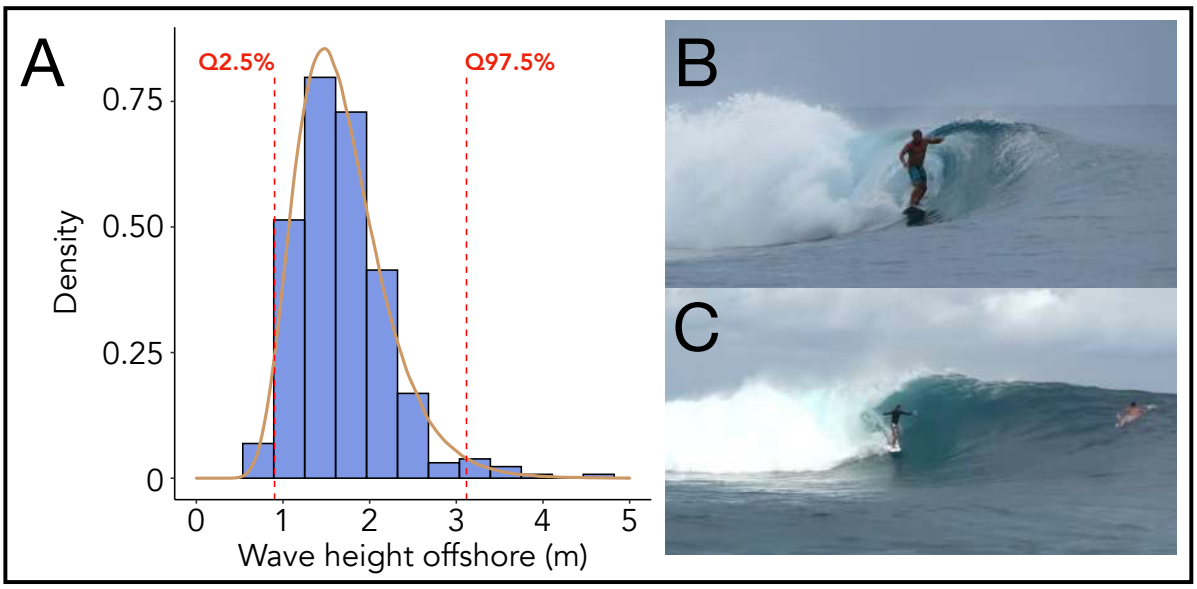


*Figure S5.2 | Wave conditions at Haapiti, Mo'orea (French Polynesia). **A.** Density plot of the wave height offshore (m) at Haapiti, Mo'orea (French Polynesia) in 2016. For each day from 2016 at noon (GMT+12:00), the wave height has been defined thanks to the MARC-WW3 estimates in French Polynesia. **B.** Representation of the most common range of wave size at Haapiti (Hs ~ 1.5m). **C.** Representation of higher wave conditions at Haapiti (Hs ~ 3m)*

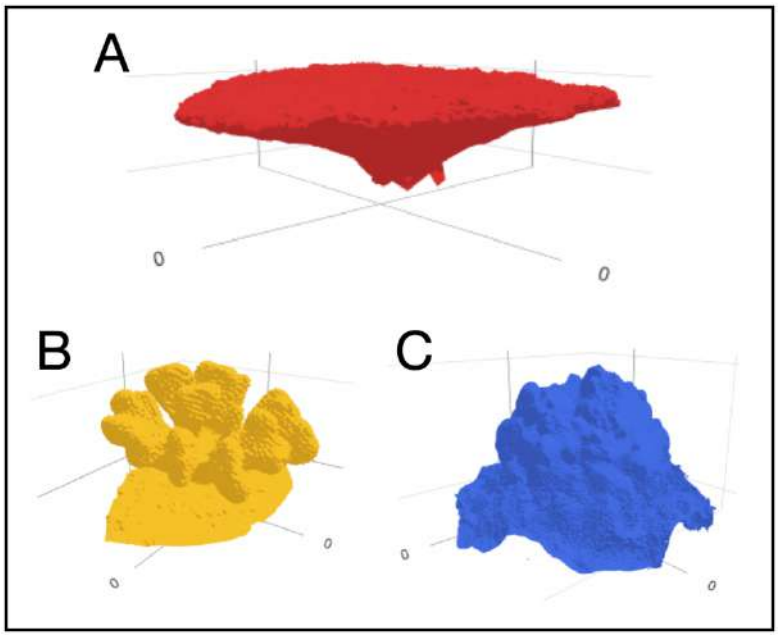


*Figure S5.3 | Representation of the three different coral species (**A.** Acropora hyacinthus, **B.** Pocillopora cf. verrucosa, **C.** Porites lutea)*

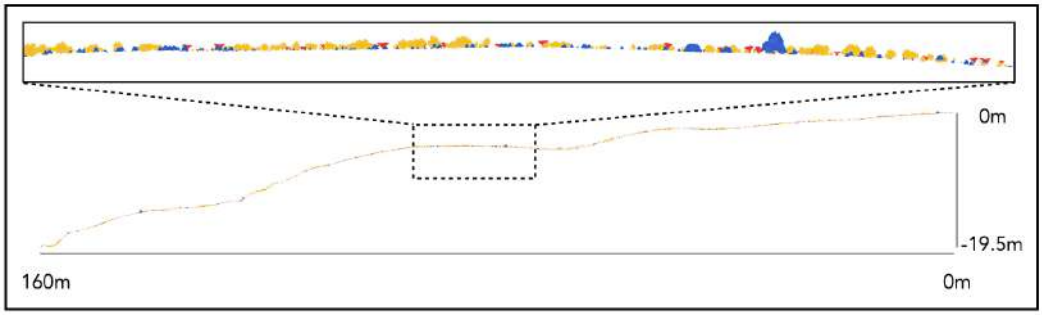


*Figure S5.4 | Representation of the Haapiti transect with random location of the 3 species along a transect from a 0m depth to 20m depth. The different coral species are represented in three colors (Acropora hyacinthus in red, Pocillopora cf. verrucosa in gold and Porites lutea in blue)*

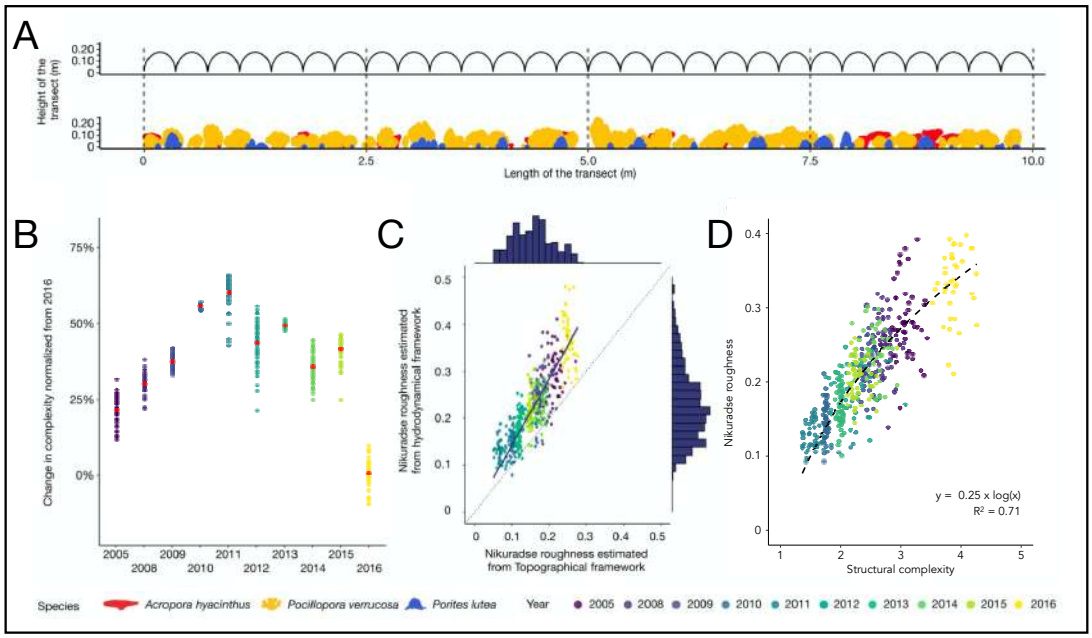


*Figure S5.5 | Definition of the Nikuradse estimates ($k_n$) **A.** Definition of the average coral height within a 10m$^2$ transect and illustration of the $k_n$ estimates equivalent above. Acropora hyacinthus were represented in red, Pocillopora cf. verrucosa in orange and Porites lutea in blue **B.** Change in complexity from 2005 to 2016. The standard year has been selected for 2016 because the highest structural complexity estimates were defined this year. Red points represent the average for each year. **C.** Scatterplot between $k_n$ estimates defined by the 'topographic approach' and $k_n$ estimates defined by the 'hydrodynamical approach'. **D.** Relationship between structural complexity and $K_n$ estimates. The relationship is written as $k_n$ = 0.25 x log(Structural complexity).*

# Chapter 6

# Mo'orea's reefs might not keep up with sea level rise in the near future

This chapter is in preparation for Coral Reefs

## Authors

Jérémy Carlot, Cyril Hautecoeur, Chris T. Perry, Hendrikje Jorissen, Maggy Nugues, Gonzalo Pérez-Rosales, Laetitia Hedouin, Valeriano Parravicini

# Abstract

Coral reefs protect coastal societies from oceanic waves but are threatened by intensifying anthropogenic disturbances and climate change resulting in lower accretion rates. Although there is an increased interest in defining reef accretion rate for reef islands, no studies from the last fifteen years estimated the accretion rate of coral reefs in French Polynesia. In this work, we defined the $CaCO_3$ budget of coral assemblages in Mo'orea (French Polynesia) over 10 years (*i.e.*, from 2005 to 2016). Our results highlight that the average accretion rate is lower than the Global Mean Sea Level (GMSL) under the SSP2-4.5 scenario, which is one of the most optimistic. Therefore, our study raises a global concern for coastal protection at Mo'orea and paints a grim picture for the island population by 2100.

# 6.1 Introduction

Coral reefs are among the most diverse ecosystems on earth and provide many valuable ecosystem services to more than 500 million people worldwide (Hoegh-Guldberg, Pendleton and Kaup, 2019). The capacity of these ecosystems to provide crucial services directly relies on coral reef functioning (Harborne *et al.*, 2017; Brandl, Rasher, *et al.*, 2019). For example, the production of the carbonate framework ($CaCO_3$) contributes to the structural complexity of the habitat and to the capacity of reefs to dissipate waves' energy, thus reducing the risk of flooding during extreme storms (Ferrario *et al.*, 2014; Spalding, Ruffo, *et al.*, 2014). Unfortunately, over the past few decades, these ecosystems experienced major declines in coral cover globally (Hughes, Kerry, *et al.*, 2017; Madin *et al.*, 2018), threatening essential services such as coastal protection. These declines are mainly due to anthropogenic stressors, including global ocean warming, sea-level rise and local impacts (*e.g.*, pollution and sedimentation) (Hughes, Barnes, *et al.*, 2017), which are continuously intensifying over time. As a result, coral reef decline is expected to increase in the near future as well as the frequency of large scale coral bleaching events (Kwiatkowski *et al.*, 2015). More precisely, coral bleaching and the associated coral mortality reduce the growth rates of many coral species (Kornder, Riegl and Figueiredo, 2018), affecting, in turn, potential reef accretion (Perry and Morgan, 2017a), with severe consequences for the safety of coastal societies. Indeed, the ability of reefs to protect coastlines from erosion and climate-driven disasters in the coming decades will depend on the interplay between the rates of sea-level rise and reef accretion in a more frequently disturbed marine environment (Harris *et al.*, 2018).

To define reef accretion and unravel whether corals reefs may keep up with ongoing sea-level rise or not, the Reef Budget Methodology (Perry, Lange and Januchowski-Hartley, 2018) has become an essential tool over the past

decade (Perry *et al.*, 2018; Cornwall *et al.*, 2021). The strength of this method lies in its capacity to accurately quantify gains and losses of $CaCO_3$ on the basis of standard monitoring data on several ecosystem components (*i.e.*, corals, reef fishes, encrusting algae and sea urchins). On coral reefs, corals are the main reef $CaCO_3$ producers (Vecsei, 2004; Perry *et al.*, 2012), with additional $CaCO_3$ being produced by crustose Coralline Algae (CCA), while other marine organisms such as parrotfishes, echinoid taxa (*e.g.*, sea-urchins), or endolithic organisms (*e.g.*, sponges), gradually erode the substrate (Peyrot-Clausade *et al.*, 2000; Vogel *et al.*, 2000; Perry and Hepburn, 2008). A $CaCO_3$ budget can be defined by considering both gains and losses, which might subsequently be converted into reef accretion potential (Perry *et al.*, 2015). As the estimation of reef accretion estimation relies on several biological compartments (*e.g.*, coral and reef fishes) which are threatened by intensifying anthropogenic disturbances (*e.g.*, bleaching events), it is expected that reef accretion rates will change over time (Perry and Morgan, 2017b).

Despite the increase of studies assessing reef accretion worldwide (Perry et al. 2018; Cornwall et al. 2021), no studies from the last fifteen years assess how much French Polynesia's reefs will accrete (Montaggioni, 2005). In this study, we used the Reef Budget Methodology, to determine how Mo'orea's (French Polynesia) potential accretion rate evolves in the face of global sea level rise projections for 2100 (IPCC, 2021). Using both benthic and fish time-series data, we defined the reef accretion from 2005 to 2016, highlighting how intensifying perturbations may threaten coastal societies in a near future.

## 6.2 Materiel & Methods

To define vertical reef accretion, we first determined net carbonate production (kg $CaCO_3$ $m^{-2}$ $yr^{-1}$) at Mo'orea from 2005 and 2008 to 2016, French Polynesia. To do so, we used the Reef Budget Methodology from Perry, Lange and Januchowski-Hartley (2018). Drawing on this method, we quantified both

producers and bioeroders of $CaCO_3$. More precisely, 1) we measured coral's and CCA's $CaCO_3$ production and 2) we define fish (especially parrotfishes) and urchin bioerosion. The amount of $CaCO_3$ production produced by both coral and CCA less the bioerosion from fish and urchin corresponds to the net $CaCO_3$ production. For this study, we considered only reefs from the forereef as they are the main hamper of oceanic waves (Ferrario *et al.*, 2014). All the statistical analyses were run in R version 4.0.3 (R Core Team, 2019).

## 6.2.1 $CaCO_3$ production from corals and Coral Crustose Algae

For $CaCO_3$ production from corals, we used published values from (Carlot *et al.*, 2021). These $CaCO_3$ production rates were obtained 1) by staining *in situ* 175 medium to large coral colonies with Alizarin Red-S and 2) by measuring water alkalinity, ex situ, of 96 small to medium coral colonies. Corals were sampled around Mo'orea, on the fore reef, between 10 and 15m depth (see Carlot et *aL* 2021)

Concerning $CaCO_3$ production from CCA, we used four published growth rates from Jorissen *et al.* (2020) (Table 6.1). Fragments of different CCA species were placed into Petri dishes in contact with coral recruit and placed in the same habitat where CCA fragments and coral were sampled. CCA surface areas were estimated by taking photos to estimate growth rates after 124 to 158 days. Then, we defined the $CaCO_3$ production from CCA by using the formula as follows:

$$\text{CCA production (kg } CaCO_3 \text{ m}^{-2} \text{ yr}^{-1}) = g \times d \times GAF \times 10000 / 1000$$

where g is the growth rate (cm $yr^{-1}$), d is the skeletal density (g $cm^{-3}$) and GAF is a growth adjustment factor which consider that growth is not homogeneous (*i.e.,* lateral growth rate higher than vertical growth) (Morgan and Kench, 2012). This factor was assessed by dividing the vertical accretion rate by the horizontal

accretion rate of each species from (Lewis, Kennedy and Diaz-Pulido, 2017). As the vertical accretion rate of *Neogoniolithon foslei* was not available, we estimated its GAF as the mean of the three others species (Table 6.1). In order to assess a CCA production per meter square we corrected the CCA production by the CCA cover (*i.e.,* by multiplying it).

*Table 6.1 | density, growth rate and GAF of the 4 CCA species observed at Mo'orea. Density and Growth Adjustment Factor (GAF) were respectively extracted and defined from Lewis et al. (2017)*

| Species | Density (g $cm^{-3}$) | Growth (cm $yr^{-1}$) | GAF |
|---|---|---|---|
| *Porolithon onkodes* | 2.58 | 1.4566 | 0.150 |
| *Lithophylum insipidum* | 2.71 | 2.5304 | 0.140 |
| *Neogoniolithon foslei* | 2.10 | 3.4648 | 0.112 |
| *Paragoniolithon conicum* | 2.10 | 2.2134 | 0.046 |

## 6.2.2 Fish bioerosion determination

Fish data was collected by the Centre de Recherches Insulaires et OBservatoire de l'Environnement (CRIOBE) from 2005 to 2016. Sampling was conducted within the 13 Marine Protected Areas (MPA) of Mo'orea. The Underwater Visual Census (UVC) technique used was deployed on a belt of 25 meters long and 2 meters wide. The delimited area is used to compute a number of fish per square meter. The fish are identified to the species level. Each census is achieved in the 50 m² belt transect (fixed distance sampling) where the size of each fish is estimated (in cm). We assessed the fish bioerosion rate drawing on Lange *et al.* (2020), which defined relationships between fish size and 1) bite volume, 2) proportion of bites leaving scars and 3) bite rate for each species. We considered only parrotfishes because they are the main bioeroders and we have selected only individuals bigger or equal to 10 cm (Lange *et al.*, 2020). Sixteen species were recorded in Mo'orea from 2 genus (*Chlorurus* genera and *Scarus* genera*).* Species were classified into two functional groups: "scrapers" (*Scarus*

species), or "excavators" (*Chlorurus* species), with excavators eroding more substrate than scrapers du to jaw morphological differences (Bellwood and Choat, 1990). Therefore, bioerosion rate was measured as:

$$\text{Bioerosion rate (kg ind}^{-1}\text{ yr}^{-1}\text{)} = v \times d/10^3 \times s_{prop} \times br \times 60 \times \text{hours of daylight} \times \text{proportion of daytime feeding} \times 365.25$$

where v is the bite volume ($cm^3$), $s_{prop}$ is the proportion of bites leaving scars, br is bite rate (bites $min^{-1}$) and d is substratum density (kg $cm^{-3}$). Mo'orea substratum density was defined by using skeletal density data from the Coral Trait Database (Madin *et al.*, 2016). We considered only coral species found in Mo'orea's outer reefs and we defined the mean coral skeletal density weighted by the coral species proportion (*i.e.,* d = 1.66 g $cm^{-3}$). We assumed 12 hours of daylight in Mo'orea (https://www.timeanddate.com/sun/@4034185) and the proportion of daytime feeding is a factor depending on the total length (TL) of fish species (Lange *et al.*, 2020). This factor is equal to 0.833 for large parrotfish (*S. rubroviolaceus* and *C. microrhinos*) and to 0.877 for smaller parrotfish (other species). The bioerosion rate equation gives us a rate per individual and per year. To convert bioerosion rates per surface area and per year, we multiplied for each species its bioerosion rate by its proportion within the transect and divided this product by the belt transect surface area (*i.e.*, $50m^2$). Then, we summed all bioerosion rates (*i.e.,* kg $CaCO_3$ $m^{-2}$ $yr^{-1}$) for each species and for each MPA. Finally, we averaged the bioerosion rates of the thirteen MPAs to get the average bioerosion rate at the Mo'orea-scale.

## 6.2.3 Urchin bioerosion determination

Urchin abundance data was collected by the CRIOBE from 2005 to 2016 in the very same belt-transect than fish monitoring. Because urchin length was not recorded, we used published urchin bioerosion rates on Mo'orea (Peyrot-

Clausade *et al.*, 2000). We considered only *Diadema* and *Echinothrix* species, as they are the main species in Mo'orea. For each bioerosion rate, urchin abundance was defined. Thus, we defined the bioerosion rate per individual. By using the same protocol for the fish, we multiplied our urchin abundance from the CRIOBE dataset monitoring by its individual bioerosion rate to estimate a bioerosion rate per transect. We divided this bioerosion rate per transect by the belt transect surface area (*i.e.,* 50$m^2$). Finally, we averaged the bioerosion rates from each MPA and get an urchin bioerosion rate in kg $CaCO_3$ $m^{-2}$ $yr^{-1}$ at Mo'orea-scale.

### 6.2.4 Reef accretion definition

Vertical reef accretion (mm $yr^{-1}$) is defined as a function of the net $CaCO_3$ production and relies on the assumption that a proportion of bioeroded $CaCO_3$ is reincorporated into the reef framework. Thus, 50% of $CaCO_3$ sediment derived from parrotfish and urchin bioerosion is not considered as it is defecated by these organisms. Other sources of sediment production have not been considered. Moreover, the porosity of the reef framework was not considered as homogeneous because it depends on the coral assemblage. Thus, we applied a factor of 0.7, because Mo'orea's reefs are dominated by branched/tabular colonies (Perry *et al.*, 2015).

## 6.3 Results and discussion

### 6.3.1 Population demographics trends

Mo'orea is located in the Pacific Ocean and belongs to French Polynesia. This island has suffered from several disturbances during the last two decades. The first disturbance documented with our time series data is related to an outbreak of the predatory *Acanthaster* cf. *solaris* starfish from 2006 to 2009, which reduced coral cover from 50% to less than 10% (Lamy *et al.*, 2016). In 2010, Oli, a category 4 cyclone with peak sustained winds of 132 mph, hit the reefs of

Mo'orea reducing living coral cover from 7% to 3% (Lamy *et al.*, 2016; Adjeroud *et al.*, 2018) (Figure 6.1A). After these disturbances, coral cover recovered to pre-disturbance levels by 2016. However, the *Acropora* genus, which was the most prominent genus on the north side of Mo'orea before 2010, was replaced by *Pocillopora* (Holbrook *et al.*, 2018). On top of this, considerable variations in coral size distributions were observed (Carlot *et al.*, 2021). Indeed, the reefs of Mo'orea's did not recover to pre-disturbances levels in terms of coral size, which changed from 12.5 (median colony diameter in 2006) to 8.5cm (median coral diameter in 2016).

As coral reefs are the structures which provides habitat and nutrients to several organisms such as reef fishes (Brandl, Tornabene, *et al.*, 2019), parrotfishes' demographics were threatened indirectly as well by both perturbations. Overall, the parrotfish density within Mo'orea's reefs remained constant from 2005 to 2013, with approximatively 17 ± 5 parrotfishes per $50m^2$ (Figure 6.1B). However, the average parrotfish size has decreased by nearly 5cm (Figure S6.1A), having important implications for human food supplies and for the $CaCO_3$ framework (Lange *et al.*, 2020). Specifically, the bioerosion rates from parrotfishes are driven mainly by two species in Mo'orea: *Chlorurus sordidus* and *Scarus psittacus* (Figure S6.1B). Except for 2005 with highest abundance observations, *C. sordidus* populations remained relatively constant with approximatively 7 ± 3 individuals per $50m^2$ (Figure S6.1C). Similarly, *S. psittacus* populations consist of 8 ± 2 individuals per $50m^2$, with a decreasing trend from 2013 to 2016 (*i.e.*, the abundance of *S. Psittacus*, has been nearly halved from 2013 to 2016). Unfortunately, *Chlorurus microrhinos*, the main bio-eroding species in French Polynesia, was too rare to evaluate the impact of disturbances on this species. Finally, the abundance of others parrotfish species remained stable from 2005 to 2013. However, from 2013, parrotfishes abundance decreased, resulting in half of the overall abundance of the 5 most abundant parrotfish bioeroders by 2016 (Figure S6.1C).

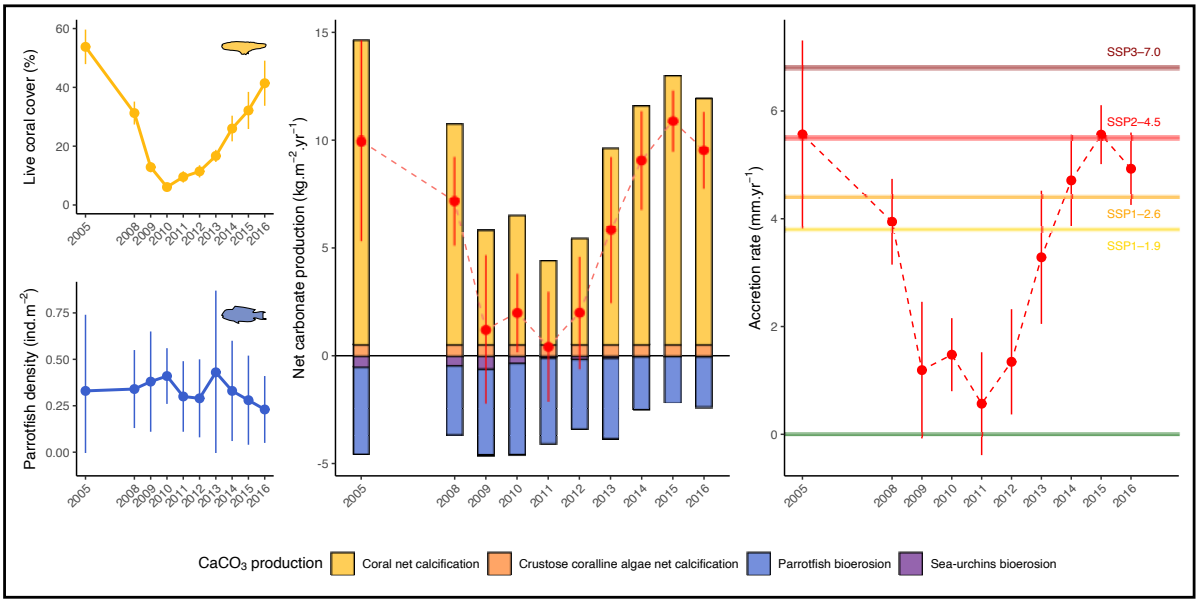


*Figure 6.1 | A. Evolution of live coral cover (%) from 2005 to 2016 on Mo'orea. B. Evolution of the parrotfishes' density (ind m$^{-2}$) from 2005 to 2016 on Mo'orea. C. $CaCO_3$ gains and the losses (kg m$^{-2}$ yr$^{-1}$) from 2005 to 2016 at Mo'orea, with $CaCO_3$ production from corals in gold, $CaCO_3$ production from CCA in orange, bioerosion from parrotfishes in blue and bioerosion from sea-urchins in purple. Red dots represent the $CaCO_3$ budget for each year (±SE). D. Evolution of overall accretion rate (mm yr$^{-1}$) from 2005 to 2016 on Mo'orea (±SE). Horizontal lines represent the Global Mean Sea Level (GMSL) under 4 IPCC's scenarios (i.e., SSP1-1.9 in yellow, SSP1-2.6 in orange, SSP2-4.5 in light red and SSP3-7.0 in dark red)*

## 6.3.2 Mo'orea's carbonate budget and following reef accretion

In recent years, there has been an increasing interest in quantifying the $CaCO_3$ budget for reef islands (Perry *et al.*, 2018; Cornwall *et al.*, 2021). A reef $CaCO_3$ budget represents the balance between the rate at which $CaCO_3$ is produced, minus the rate at which $CaCO_3$ is removed by bioerosion, physical processes or chemical dissolution (Perry, Lange and Januchowski-Hartley, 2018). The main $CaCO_3$ producers are usually scleractinian corals (Perry *et al.*, 2012), and Mo'orea's reefs are no exception (**Figure 6.1C**), with coral production accounting for between 85% and 95% of the overall $CaCO_3$ production. However, coral $CaCO_3$

production was drastically reduced from 2005 to 2011 (respectively 14 kg $m^{-2}$ $yr^{-1}$ to nearly 4 kg $m^{-2}$ $yr^{-1}$) because of *Acanthaster* cf. *solaris* outbreak and the cyclone Oli. Thanks to a high coral recruitment in 2013 (Holbrook *et al.*, 2018), the production of $CaCO_3$ from corals increased again highlighting the high contribution from juvenile corals (*i.e.,* 9.5 kg $m^{-2}$ $yr^{-1}$) (Carlot *et al.*, 2021). However, even when the average coral cover recovered to pre-disturbance levels by 2016, coral $CaCO_3$ production was still reduced by 2 kg $m^{-2}$ $yr^{-1}$ compared to 2005 (Figure 6.1C). At the same time, bioerosion rates remained constant from 2005 to 2013 (*i.e.,* 3.8 ± 0.4 kg $m^{-2}$ $yr^{-1}$) and decreased from 2013 until they were halved by 2016 (*i.e.,* 2.3 ± 1.7 kg $m^{-2}$ $yr^{-1}$). The combined loss of the main bioeroders from 2013 and the overall decrease in parrotfish size explain this decrease in bioerosion rates (see section "Population demographics trends", Figure S6.1).

As a result, Mo'orea's $CaCO_3$ budget reached the highest values of *ca.* 10 kg $m^{-2}$ $yr^{-1}$ in both 2005 and 2015, whereas the lowest value was about 0.4 kg $m^{-2}$ $yr^{-1}$ in 2011, right after the cyclone Oli. Therefore, Mo'orea did not experience a negative $CaCO_3$ budget after extreme disturbances, as it might have been the case in other locations worldwide (Januchowski-Hartley *et al.*, 2017; Perry and Morgan, 2017b). This highlights the resilience of Mo'orea's reefs in the face of disturbances (Adjeroud *et al.*, 2018). Additionally, these results add to previous works which identified Mo'orea as one of the most productive reefs in the world (Perry *et al.*, 2018; Cornwall *et al.*, 2021). However, Mo'orea's $CaCO_3$ budget is lower in 2016 than in 2015, despite an increase in the coral cover and a similar bioerosion rate. This decrease is mainly due to the fact that corals were larger but less abundant (*i.e.,* average loss of 8 coral colonies in $1m^2$, and average gain of 1.3 cm of coral diameter). This decrease might be explained, on the one hand, by the competition between corals for space and light (Connell, 1983) and, on

the other hand, to one of the strongest El Niño events ever recorded, which bleached a significant part of Mo'orea's reefs (Hédouin *et al.*, 2020).

## 6.3.3 Risks in the near future

Using the $CaCO_3$ budget to define reef accretion rate (Perry *et al.*, 2015), we have calculated that in the last 10 years Mo'orea's coral reefs have grown vertically between 0.6 mm $yr^{-1}$ and 5.6 mm $yr^{-1}$, with an average accretion rate of 3.26 ± 1.96 mm $yr^{-1}$ (**Figure 6.1D**). These results are consistent with those reported by Montaggioni *et al.* (1997), confirming that reef accretion rates are commonly lower than 4 mm $yr^{-1}$ in French Polynesia. As a result, our data highlights how Mo'orea's reefs potential accretion rate might decrease due to repeated and intensifying disturbances (Perry and Morgan, 2017a). The minimum accretion rate observed in Mo'orea, occurred at the end of the *Acanthaster* cf. *solaris* outbreak and right after the cyclone Oli in 2011 (*i.e.,* 0.6 mm $yr^{-1}$; **Figure 6.1D**). After 2011, reef accretion rates observed in Mo'orea increased and reached pre-disturbance accretion level rates in 2015 (*i.e.,* 5.6 mm $yr^{-1}$) before slightly decreasing again in 2016 by *ca.* 0.6 mm $yr^{-1}$ (*i.e.,* 4. mm $yr^{-1}$; **Figure 6.1D**) likely due to the strong El Niño event (Hédouin *et al.*, 2020).

We then compared accretion rates with sea level rise estimates. According to the different scenarios defined by the Intergovernmental Panel on Climate Change (IPCC) (IPCC, 2021), Mo'orea's reefs might not have the potential to accrete and protect the coastal population in the future. For example, considering the scenario SSP2-4.5 (*i.e.,* medium scenario), sea-level rise estimates may reach 5.5 mm $yr^{-1}$ by 2100 (Fox-Kemper *et al.*, 2021). Although these predictions are lower than accretion rate levels in both 2005 and 2015, they are still greater than the average potential vertical accretion rates measured across Mo'orea's reefs over 10 years (*i.e.,* 3.26 ± 1.96 mm $yr^{-1}$). Considering one of the most optimistic scenario by the IPCC (*i.e.,* SSP2-4.5), our results suggest

that Mo'orea's reefs might not have the potential to keep up with rising sea levels, which raises concerns for coastal protection on a global scale. These findings are supported by Cornwall et al. (2021), which postulates a worldwide decline in coral reef $CaCO_3$ production by 2100 with the same IPCC scenario (*i.e.,* SSP2-4.5), implying further a decrease of the potential accretion rates estimates (Perry *et al.*, 2018).

In addition, there is consensus that warmer ocean temperatures and higher sea levels will increase the impact of storms, threatening even more Mo'orea's reefs in the future (Christensen *et al.*, 2013). Therefore, to face the rising water levels, Mo'orea's reefs need to accrete efficiently and keep a high structural complexity (Harris *et al.*, 2018). However, previous works also suggested a trend in decreasing overall structural reef complexity in 2016 on Mo'orea (Carlot *et al.*, 2020). Combining the results of previous studies with our findings suggests that the coastal protection barriers of Mo'orea are likely already compromised and will decline even more in the future, raising serious concerns for populations inhabiting these coastal regions.

## 6.4 Data availability

Code and data are available on my Github folder "Reef accretion": https://github.com/JayCrlt/Reef_Accretion.git

## 6.5 Supplementary information

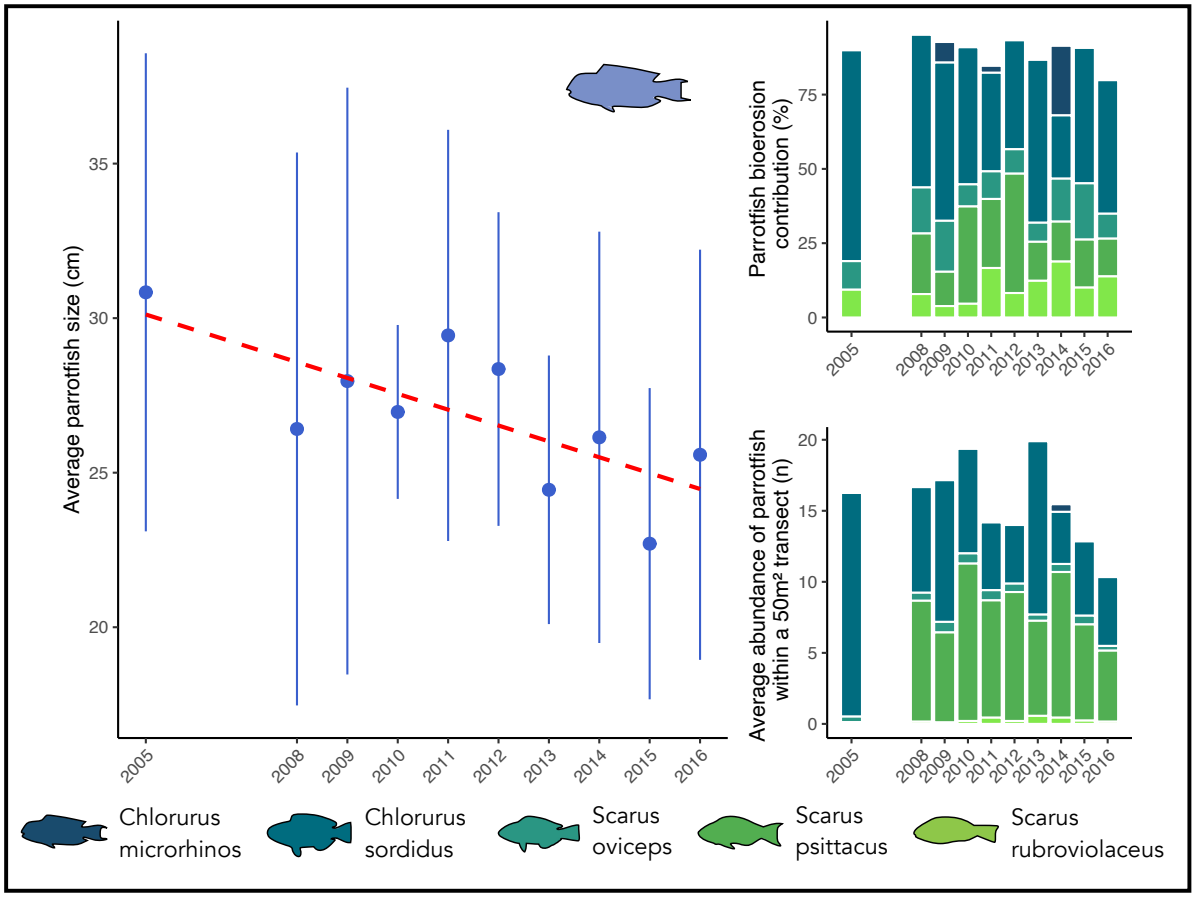


*Figure S6.1 | A. Evolution of the average parrotfish size (cm) from 2005 to 2016 on Mo'orea (±SE). B. Contribution (%) of five main parrotfish species to bioerosion from 2005 to 2016 on Mo'orea. C. Average abundance of parrotfish within a 50m² transect from 2005 to 2016 on Mo'orea.*

# Chapter 7

# General discussion

*Wave dissipation by coral reefs in French Polynesia*

## 7.1 Main advances

Coral reef ecosystems are experiencing ever increasing declines under the influence of anthropogenic and climatic pressures. There is an urgent need to evaluate their capacity to maintain key functions such as reef accretion and waves dissipation. Several studies have begun to address the status of several coral reef ecosystems in the Atlantic and Indian Oceans, but very few have been established in the Pacific. During this thesis, I focused on answering these questions using Mo'orea (French Polynesia) as a case study.

First, I highlighted the relationship between coral cover and structural complexity using different modeling methods (*i.e.,* BRT vs. GLM – see chapter 2). Indeed, despite the rise of photogrammetric techniques, many monitoring programs cannot afford regular photogram-metric monitoring due to a lack of resources (*e.g.,* staff, computing). Although photogram-metric monitoring would indeed allow having a significant amount of information (*i.e.,* demographic data, growth rate, structural complexity, and so on), the priority is still given to traditional monitoring such as Point Intersect Transect (PIT), Line Intersect Transect (LIT), or photo-quadrats. Thanks to my work, I established a link between traditional monitoring methods to assess coral cover and the 3D structural complexity defined according to photogrammetry. Although more data are needed to actually use statistical modeling to infer structural complexity, my work demonstrates that modelling and photogrammetry may be used to infer most basic three-dimensional indicators of reef health. Thus, estimating structural complexity allows to understand recovery trajectory in the face of anthropogenic and climate-related disturbances (Alvarez-Filip *et al.*, 2009), to define functional indicators of reef health (González-Barrios, Cabral-Tena and Alvarez-Filip, 2021), or to define how coral reefs will cope with rising sea levels (Harris *et al.*, 2018).

In the third chapter, I discuss the importance of juveniles and their major contribution to the $CaCO_3$ budgets (see chapter 3). More specifically, I discuss the importance of collecting demographic data to define $CaCO_3$ budgets at the ecosystem scale. Indeed, my results show that juveniles produce much more $CaCO_3$ per unit area than adults. However, current methods for determining $CaCO_3$ budgets are based on average production per species, *i.e.,* without size discrimination (Perry, Lange and Januchowski-Hartley, 2018). More precisely, current $CaCO_3$ budgets are either overestimated in the case of mature communities or underestimated in the case of young communities. Therefore, my work aims to improve the definition of $CaCO_3$ budgets in reef islands, highlighting the need to collect demographic data.

One of the 21$^{st}$ century's biggest challenges is to define how coral reefs will face global changes in the future. To answer this question, I investigated the three main coral functions (*i.e.,* calcification, photosynthesis and respiration – see Chapter 4). I developed a new indicator based on the ratio of photosynthesis minus respiration (*i.e.,* net photosynthesis) divided by the calcification. Basically, this indicator implies that when the balance is lower than 1, the coral species uses most of the energy from photosynthesis for calcification. However, if this result is greater than one, the coral will have significant energy resources to ensure other functions such as reproduction. I suggest that the species that are presently the most abundant in Mo'orea reefs (*i.e., Pocillopora* cf. *verrucosa* and *Montipora verilli*) have the highest ratios. Although this work has important limitations (*i.e.,* small size gradient and single species comparisons), these results may represent a promising approach for the definitions of losers and winners (Loya *et al.*, 2001) in the face of global changes.

The general flattening of coral reefs around the world is also partly due to community change (Jouffray *et al.*, 2015; Smith *et al.*, 2016; Arias-González *et al.*, 2017; Bellwood *et al.*, 2018). One of the most remarkable examples is the

flattening of Caribbean coral reefs due to disease (Alvarez-Filip *et al.*, 2009). This flattening is worrying when considering that coastal protection of reef islands is correlated to the structural complexity of coral assemblages. Indeed, (Harris *et al.*, 2018) demonstrated that ocean wave energy dissipation relies on two factors: reef accretion and structural complexity. In my Chapter 5, I defined the structural complexity of the most ocean wave exposed site at Mo'orea between 2005 and 2016. My results support previous work regarding the 95% dissipation in wave energy (Ferrario *et al.*, 2014) thanks to coral reefs. However, my work also introduces an important point regarding extreme events. Indeed, the loss of structural complexity is not proportional to the increase in waves impacting the reef coast, raising thus global concern for the future of coastal societies in the face of predictions of increasingly powerful storms.

Finally, drawing on my previous work (Chapter 3) I also estimated the second component influencing wave energy dissipation: the reef accretion. I determined the average accretion rate at the Mo'orea between 2005 and 2016. Then, by comparing my results with the latest IPCC assessment (IPCC, 2021), I highlighted that reef accretion rates were strongly compromised due to coral bleaching occurring year after year. As a result, I warn that the average accretion rate at Mo'orea is lower than the global mean sea level (GMSL) under the SSP2-4.5 scenario, one of the most optimistic scenarios.

Key message: To conclude, my PhD exemplifies that coral cover alone is a poor metric for describing ecosystem functioning. On the one hand, Mo'orea reefs have recovered a percentage of coral cover similar to 2005 after two major disturbances (*i.e.,* COTS outbreak and cyclone) and some moderate coral bleaching events. Coral assemblages have changed, resulting in a dominance of the genus *Pocillopora* (see chapter 4). The genus *Pocillopora*, particularly the species *P. verrucosa*, presents a high structural complexity due to its corymbose morphology (see chapter 2). As a result, coral reefs in Mo'orea still

present relatively high structural complexity that can, in theory, efficiently protect coastal populations from extreme events (see chapter 5). However, despite the high potential for $CaCO_3$ production due to the outnumbered coral juveniles following the cyclone (see chapter 3), the reef accretion rate in Mo'orea might not overcome the sea level rise estimated by the IPCC under the SSP2-4.5 scenario or higher (see chapter 6), raising a global concern for coastal societies in the future.

# 7.2 Limits and futures directions

## 7.2.1 Management limits

One of the main limitations of my work lies in its spatial resolution. In order to move from research to the management of coastal erosion (see section 7.3), it is necessary to obtain more accurate spatial data. Indeed, in the near future, it will be crucial to produce high resolution maps that explicitly quantify erosion risks spatially. Moreover, it would be important to carry out coral demographic monitoring (*i.e.,* length, width and height – see chapter 3) at different sites to define coral $CaCO_3$ production in an accurate way. It would be possible, for example, to determine accretion rates in the 13 MPAs around Mo'orea, to leverage the fish monitoring already carried out by the CRIOBE (http://observatoire.criobe.pf). Therefore, a risk map would be defined, helping decision-makers to prioritize the most at-risk areas. Moreover, the structural complexity at Mo'orea differs according to the side of the island studied (see chapter 2). A more detailed hydrodynamic study would allow defining better the risks during extreme events (see chapter 5).

## 7.2.2 Increase Spatial resolution

Although the resolution at the island level is a limitation for local management, it allows to obtain a first quantification of the risks associated to

sea level rise. Indeed, the Reefbudget methodology on which I based my reef accretion estimates (Perry, Lange and Januchowski-Hartley, 2018, see chapter 6) is a universal method, and the improvements I have made to this method can also be applied elsewhere (see chapter 3). Thus, a global study would allow coastal societies worldwide to be better informed on the risks associated with global change (Perry *et al.*, 2018). In this thesis, I focused on the six most abundant coral species in Mo'orea (*i.e., A. hyacinthus, A. curta, M. verrilli, N. irregularis, P. verrucosa* and *P. lutea*). However, to generate a global study, it is necessary to define the $CaCO_3$ production of other coral species from around the world. Although average production by species is already available for many species (Madin *et al.*, 2016), it is crucial to define $CaCO_3$ production along a size gradient (see chapter 3). Thus, with the emergence of photogrammetric monitoring such as the 100 islands challenge monitoring (https://100islandchallenge.org), it would be possible to define coral growth (*i.e.,* $CaCO_3$ production) from one year to another for several coral species. Moreover, thanks to photogrammetric monitoring, demographic data around the world may be defined, in order to determine the overall $CaCO_3$ production from corals for several tropical islands. Later, the fish bioerosion which has been already defined in 585 sites all around the world may be used to define $CaCO_3$ budget (Schiettekatte et al, in review).

## 7.2.3 Considering nutrient releases

Although carbon is never limiting, the unavailability of nitrogen and phosphorus can limit the growth of coral reef organisms (Schiettekatte *et al.*, 2020). Nitrogen and phosphorus concentrations from one tropical island to another differ greatly. More precisely, a recent study found that rat-free islands hosted more seabirds than islands hosting rats (Graham *et al.*, 2018). Seabirds feed in the open ocean and transport large amounts of nutrients to islands, improving the productivity of island flora and fauna (Graham *et al.*, 2018). In turn,

the leaching of these nutrients into the sea enhances the productivity, structure and functioning of adjacent coral reef ecosystems (Benkwitt, Wilson and Graham, 2020; Benkwitt *et al.*, 2021) and reduces the risk of coral bleaching (Morris *et al.*, 2019) when amounts in nitrogen and phosphorous are balanced. It would therefore be interesting to define how coral growth rates change according to different levels of nitrogen and phosphorus. These relationships can be established by performing *ex situ* experiments for different coral species and sizes (see Chapter 4). Then, these relationships may be used for the global study mentioned above (see section 7.2.2) since global maps of nitrogen and phosphorous concentrations are already available (https://www.bio-oracle.org/).

## 7.2.4 Predictions

During this thesis, I defined the reef accretion rates of Mo'orea thanks to the combined use of in situ and ex situ experiments and demographic monitoring. As a result, I did not forecast reef accretion due to the lack of demographic data in the future. To overcome this problem, it is possible to determine the demographic evolution of coral colonies thanks to Integrated Population Models (IPM, see chapter 3). Thus, one new promising three-dimensional functional-structural model may be used (Cresswell *et al.*, 2020). The strength of this model lies in its incorporation of three types of mortality: 1) the mortality due to shading (*i.e.,* competition for space and light), 2) the "background mortality" such as coral bleaching or *Acanthaster* outbreak, and 3) the mortality due to hydrodynamic disturbances (Madin *et al.*, 2016). As a result, setting up many scenarios (*e.g.,* a critical scenario with one mass bleaching event each year reducing coral cover by 60% as in 2016 vs. a unique mass bleaching event every 10 years) would allow to define reef accretion with a relatively high accuracy.

## 7.3 Solutions and recommendations

In this section I would like to propose solutions to reduce the risk of flooding and erosion. For this purpose, I will organize this part in 3 sub-sections: 1) artificial methods (see section 7.3.1), 2) environmental methods (see section 7.3.2) and 3) intermediate methods (see section 7.3.3).

### 7.3.1 Artificialisation

There are two major ways to reduce coastal erosion. One consists in the fixation of the coastline (*i.e.*, "Hard" Method) while the second consists in a more natural approach (*i.e.,* "Soft" Method, see section 7.3.2). Hard methods such as embankments have the main role of protecting immediate issues and fixing the coastline. Thus, embankments in Mo'orea have increased drastically from 12.2% (in 1977) to 56.5% (in 2018), *i.e.,* an increase by 4.5 times over 41 years (Madi Moussa *et al.*, 2019). Similarly, sandy beach areas have decreased from 79.9% (in 1977) to 32% (in 2018), *i.e.,* a decrease by 2.5 times over the same period. Although hard methods have demonstrated their effectiveness, they have many negative aspects in the midterm. Indeed, these interventions affect the dynamics of the environment, often resulting in increased coastal erosion in the proximity of the project area, and they are generally very costly but have a long-life expectancy.

### 7.3.2 Natural protection

• Enhancing the vegetation

Several biotopes can protect coastal populations from ocean waves. For example, among aquatic ecosystems, one of the most effective in reducing ocean wave energy would likely be coral reefs (Ferrario *et al.*, 2014), but at the ocean-

coastal interface, one of the most effective biotopes would likely be mangroves. Indeed, mangroves act as the last natural ramparts to protect shorelines from erosion and reduce wave heights by up to 66% (Spalding, McIvor, *et al.*, 2014). Mangroves in the Pacific Islands represent only 3% of the global extent of mangroves (Gilman, Ellison and Coleman, 2007). In Mo'orea, mangroves are not naturally present, but have been introduced to increase fish recruitment. They are mostly located in the southwest and northeast, covering 3.6 ha (Meyer *et al.*, 2021), and represent less than 1% of the island's surface. Expanding these areas to targeted zones would help to protect the coastal zones. However, this measure can only be considered as a complementary method because the functioning of mangroves is also threatened by global changes (Ward *et al.*, 2016). Indeed, the IPCC (2021) predicts significant regional rainfall variations and temperature changes (IPCC, 2021). The mangrove forests' distribution, extent, and growth rates could then change permanently (Gilman *et al.*, 2008). In addition, mangroves are sensitive to changes in the duration and frequency of flooding that alter salinity levels beyond the species-specific physiological tolerance range (Friess *et al.*, 2012), and may result in the death of mangrove plants (He *et al.*, 2007). Thus, although mangroves represent an effective barrier against waves, they cannot be considered as the only protection method.

• Coral restoration

In the case of significant loss of coral cover resulting from an extreme event (*e.g.,* cyclone), coral restoration can be considered as an option. Thus, corals might be transplanted to a degraded site using three main methods (Edwards and Gomez, 2007). 1) The cheapest way is to harvest corals directly from a healthy or unimpacted reef and transplant them to the degraded area. However, the transplanted individuals must be relatively large (Boström-Einarsson *et al.*, 2020). 2) Smaller fragments can be grown *in situ* (*i.e.,* nurseries) until they are large enough to survive on the reef. 3). Finally, tiny fragments do not present

good survival rates in situ, whereas they can survive and grow *ex situ*. Thus, for a higher cost and a longer culture process, it is possible to create tens of thousands of small colonies from a similar number of fragments (Boström-Einarsson *et al.*, 2020). In the context of coastal protection, a recent study discussed the benefits of coral restoration in reducing coastal flooding (Roelvink *et al.*, 2021). In particular, the authors point out that the more physically robust coral species (*e.g.,* genus *Porites*) should be transplanted to shallower (*i.e.,* more energetic) locations than the more fragile and faster-growing species (*e.g.,* genus *Acropora*). However, corals are also vulnerable to global change, and bleaching events reducing the coral cover are becoming increasingly common. For example, in Bora Bora, from 1996-2000, a coral restoration project (method 1) was carried out, aiming to create a 7200m$^2$ coral garden (Edwards and Gomez, 2007). More than 311 coral colonies were transplanted to 11 artificial structures, and *ca.* 200 large colonies (genera *Acropora* and *Porites*) were placed on the sandy bottom. Unfortunately, massive coral mortality was recorded due to a bleaching event in January 2002, which affected both transplanted corals and natural corals. Thus, coral transplantation cannot be considered as the only protection method such as mangroves (see subsection above), despite a strong potential for protection against ocean waves.

### 7.3.3 Scientific engineering

There is no optimal solution to coastal erosion. Hard methods lead to increased coastal erosion in the targeted areas, while soft methods' applicability is threatened by global changes. It is in this context that new initiatives have emerged. For example, the company Geocorail (http://www.geocorail.com) is working in France to reinforce the sandy bed and to protect coastal societies against erosion. The Geocorail device aims at creating a rock conglomerate around a specially designed grid. The aggregation process works thanks to the natural electrolysis process coming from the seawater and leads to the formation

of a calcareous-magnesian deposit with a thickness of more than 10 cm. Since the device is dependent on natural sediment inputs, each device is unique (nature, color, etc.). Therefore, the Geocorail company proposes a hybrid solution (hard and soft methods) to deal with coastal erosion. Although the coral component is not included in this protection method, other solutions can promote coral settlement. For example, the company Seaboost (https://www.seaboost.fr) is working to find materials that allow better settlement of coral recruits. Thus, combining these two alternatives could improve coral recruitment rates and help to face global changes.

## 7.4 General conclusion

I highlight in this thesis two key results regarding the erosion and flooding risk in Mo'orea. 1) The high structural complexity of Mo'orea due to the high recolonization of the genus *Pocillopora* allows for a better protection against extreme events. These results are encouraging in the face of a likely increase in the intensity of extreme events (*e.g.,* tropical storms); 2) However, reef accretion rates are below IPCC estimates of sea-level rise (SSP2-4.5 scenario and higher), suggesting that even with high structural complexity, the population of Mo'orea may be at risk of coastal erosion. Over the last 40 years, embankments at Mo'orea have increased by a factor of 4.5, protecting about *ca.* 60% of the coastline. However, this development may lead to further destruction of the coastline and adjacent beaches. In parallel, the sustainability of soft solutions is threatened by global changes. Thus, new intermediate methods have emerged to deal with the increasing risk of erosion. Although these solutions are sustainable in the long term, coral reefs remain the best coastal protection mechanism and the best way to conserve them remains in the reduction of our carbon emissions in order to be below the SSP2-4.5 scenario by 2100

# References

1. **ADJEROUD, M. ET AL. (2018)** RECOVERY OF CORAL ASSEMBLAGES DESPITE ACUTE AND RECURRENT DISTURBANCES ON A SOUTH CENTRAL PACIFIC REEF. SCIENTIFIC REPORTS, 8(1), P. 9680. HTTPS://DOI.ORG/10.1038/S41598-018-27891-3.

2. **ADJEROUD, M., MAUGUIT, Q. AND PENIN, L. (2015)** THE SIZE-STRUCTURE OF CORALS WITH CONTRASTING LIFE-HISTORIES: A MULTI-SCALE ANALYSIS ACROSS ENVIRONMENTAL CONDITIONS. MARINE ENVIRONMENTAL RESEARCH, 112, PP. 131–139. HTTPS://DOI.ORG/10.1016/J.MARENVRES.2015.10.004.

3. **AGISOFT, L. (2016)** AGISOFT PHOTOSCAN USER MANUAL : PROFESSIONAL EDITION, VERSION 1.2, USER MANUALS, P. 97. HTTP://WWW.AGISOFT.COM/DOWNLOADS/USER-MANUALS/

4. **ALBERT, S. ET AL. (2016)** INTERACTIONS BETWEEN SEA-LEVEL RISE AND WAVE EXPOSURE ON REEF ISLAND DYNAMICS IN THE SOLOMON ISLANDS. ENVIRONMENTAL RESEARCH LETTERS. IOP PUBLISHING, 11(5). HTTPS://DOI.ORG/10.1088/1748-9326/11/5/054011.

5. **ALLEN, A. P., GILLOOLY, J. F. AND BROWN, J. H. (2005)** LINKING THE GLOBAL CARBON CYCLE TO INDIVIDUAL METABOLISM. FUNCTIONAL ECOLOGY, 19(2), PP. 202–213. HTTPS://DOI.ORG/10.1111/J.1365-2435.2005.00952.X.

6. **ALLEN, M. R. ET AL. (2018)** IPCC: FRAMING AND CONTEXT, GLOBAL WARMING OF 1.5°C. AN IPCC SPECIAL REPORT.

7. **ALLGEIER, J. E. ET AL. (2014)** CONSISTENT NUTRIENT STORAGE AND SUPPLY MEDIATED BY DIVERSE FISH COMMUNITIES IN CORAL REEF ECOSYSTEMS. GLOBAL CHANGE BIOLOGY, 20(8), PP. 2459–2472. HTTPS://DOI.ORG/10.1111/GCB.12566.

8. **ALMOND, R. E. A., GROOTEN, M. AND PETERSEN, T. (2020)** WWF (2020) LIVING PLANET REPORT 2020, BENDING THE CURVE OF BIODIVERSITY LOSS.

9. **ALVARADO, J. J. ET AL. (2016)** BIOEROSION BY THE SEA URCHIN DIADEMA MEXICANUM ALONG EASTERN TROPICAL PACIFIC CORAL REEFS. MARINE ECOLOGY. JOHN WILEY & SONS, LTD, 37(5), PP. 1088–1102. HTTPS://DOI.ORG/10.1111/MAEC.12372.

10. **ALVAREZ-FILIP, L. ET AL. (2009)** FLATTENING OF CARIBBEAN CORAL REEFS: REGION-WIDE DECLINES IN ARCHITECTURAL COMPLEXITY. PROCEEDINGS OF THE ROYAL SOCIETY B: BIOLOGICAL SCIENCES, 276(1669), PP. 3019–3025. HTTPS://DOI.ORG/10.1098/RSPB.2009.0339.

11. **ALVAREZ-FILIP, L. ET AL. (2011)** REGION-WIDE TEMPORAL AND SPATIAL VARIATION IN CARIBBEAN REEF ARCHITECTURE: IS CORAL COVER THE WHOLE STORY? GLOBAL CHANGE BIOLOGY, 17(7), PP. 2470–2477. HTTPS://DOI.ORG/10.1111/J.1365-2486.2010.02385.X.

12. **ANDERSON, K. D. ET AL. (2018)** TEMPORAL AND TAXONOMIC CONTRASTS IN CORAL GROWTH AT DAVIES REEF, CENTRAL GREAT BARRIER REEF, AUSTRALIA. CORAL REEFS, 37(2), PP. 409–421. HTTPS://DOI.ORG/10.1007/S00338-018-1666-1.

13. **ARIAS-GONZALEZ, J. E. ET AL. (2017)** A CORAL-ALGAL PHASE SHIFT IN MESOAMERICA NOT DRIVEN BY CHANGES IN HERBIVOROUS FISH ABUNDANCE. PLOS ONE. PUBLIC LIBRARY OF SCIENCE, 12(4), P. E0174855. HTTPS://DOI.ORG/10.1371/JOURNAL.PONE.0174855.

14. **ARKEMA, K. K. ET AL. (2013)** COASTAL HABITATS SHIELD PEOPLE AND PROPERTY FROM SEA-LEVEL RISE AND STORMS. NATURE CLIMATE CHANGE, 3(10), PP. 913–918. HTTPS://DOI.ORG/10.1038/NCLIMATE1944.

15. **ARONSON, R. B. AND PRECHT, W. F. (2006)** CONSERVATION, PRECAUTION, AND CARIBBEAN REEFS. CORAL REEFS, 25(3), PP. 441–450. HTTPS://DOI.ORG/10.1007/S00338-006-0122-9.

16. **BABCOCK, R. C. ET AL. (2003)** IDENTIFICATION OF SCLERACTINIAN CORAL RECRUITS FROM INDO-PACIFIC REEFS. ZOOLOGICAL STUDIES. CITESEER, 42(1), PP. 211–226.

17. **BAIRD, A. H. ET AL. (2013)** ACANTHASTER PLANCI IS A MAJOR CAUSE OF CORAL MORTALITY IN INDONESIA. CORAL REEFS, 32(3), PP. 803–812. HTTPS://DOI.ORG/10.1007/S00338-013-1025-1.

18. **BAIRD, A. H., GUEST, J. R. AND WILLIS, B. L. (2009)** SYSTEMATIC AND BIOGEOGRAPHICAL PATTERNS IN THE REPRODUCTIVE BIOLOGY OF SCLERACTINIAN CORALS. ANNUAL REVIEW OF ECOLOGY, EVOLUTION, AND SYSTEMATICS, 40(1), PP. 551–571. HTTPS://DOI.ORG/10.1146/ANNUREV.ECOLSYS.110308.120220.

19. **BAKER, D. M. ET AL. (2018)** CLIMATE CHANGE PROMOTES PARASITISM IN A CORAL SYMBIOSIS. THE ISME JOURNAL, 12(3), PP. 921–930. HTTPS://DOI.ORG/10.1038/S41396-018-0046-8.

20. **BARBIER, E. B. ET AL. (2011)** THE VALUE OF ESTUARINE AND COASTAL ECOSYSTEM SERVICES. ECOLOGICAL MONOGRAPHS, 81(2), PP. 169–193. HTTPS://DOI.ORG/10.1890/10-1510.1.

21. **BARNECHE, D. R. ET AL. (2014)** SCALING METABOLISM FROM INDIVIDUALS TO REEF-FISH COMMUNITIES AT BROAD SPATIAL SCALES. ECOLOGY LETTERS, 17(9), PP. 1067–1076. DOI: HTTPS://DOI.ORG/10.1111/ELE.12309.

22. **BARNES, R. D. (1987)** INVERTEBRATE ZOOLOGY, FIFTH EDIT. ED. HARCOURT BRACE JOVANOVICH COLLEGE PUBLISHERS, FORT WORTH, TX.

23. **BARNES, R. S. K. AND HUGHES, R. N. (1999)** AN INTRODUCTION TO MARINE ECOLOGY. JOHN WILEY & SONS.

24. **BECK, M. W. ET AL. (2018)** THE GLOBAL FLOOD PROTECTION SAVINGS PROVIDED BY CORAL REEFS. NATURE COMMUNICATIONS, 9(1), P. 2186. HTTPS://DOI.ORG/10.1038/S41467-018-04568-Z.

25. **BELLWOOD, D. R. ET AL. (2004)** CONFRONTING THE CORAL REEF CRISIS. NATURE, 429(6994), PP.827–833. HTTPS://DOI.ORG/10.1038/NATURE02691.

26. **BELLWOOD, D. R. ET AL. (2018)** THE ROLE OF THE REEF FLAT IN CORAL REEF TROPHODYNAMICS: PAST, PRESENT, AND FUTURE, ECOLOGY AND EVOLUTION. JOHN WILEY & SONS, LTD, 8(8), PP. 4108–4119. HTTPS://DOI.ORG/10.1002/ECE3.3967.

27. **BELLWOOD, D. R. AND CHOAT, J. H. (1990)** A FUNCTIONAL ANALYSIS OF GRAZING IN PARROTFISHES (FAMILY SCARIDAE): THE ECOLOGICAL IMPLICATIONS. ALTERNATIVE LIFE-HISTORY STYLES OF FISHES. SPRINGER, PP. 189–214.

28. **BENKWITT, C. E. ET AL. (2021)** RAT ERADICATION RESTORES NUTRIENT SUBSIDIES FROM SEABIRDS ACROSS TERRESTRIAL AND MARINE ECOSYSTEMS. CURRENT BIOLOGY, 31(12), PP. 2704-2711.E4. HTTPS://DOI.ORG/10.1016/J.CUB.2021.03.104.

29. **BENKWITT, C. E., WILSON, S. K. AND GRAHAM, N. A. J. (2020)** BIODIVERSITY INCREASES ECOSYSTEM FUNCTIONS DESPITE MULTIPLE STRESSORS ON CORAL REEFS. NATURE ECOLOGY & EVOLUTION, 4(7), PP. 919–926. HTTPS://DOI.ORG/10.1038/S41559-020-1203-9.

30. **BERUMEN, M. L. AND PRATCHETT, M. S. (2006)** RECOVERY WITHOUT RESILIENCE: PERSISTENT DISTURBANCE AND LONG-TERM SHIFTS IN THE STRUCTURE OF FISH AND CORAL COMMUNITIES AT TIAHURA REEF, MO'OREA. CORAL REEFS, 25(4), PP. 647–653. HTTPS://DOI.ORG/10.1007/S00338-006-0145-2.

31. **BIRKELAND, C. (1997)** LIFE AND DEATH OF CORAL REEFS. SPRINGER SCIENCE & BUSINESS MEDIA.

32. **BLUNDEN, J. AND BOYER, T. (2021)** STATE OF THE CLIMATE IN 2020, BULLETIN OF THE AMERICAN METEOROLOGICAL SOCIETY. BOSTON MA, USA: AMERICAN METEOROLOGICAL SOCIETY, 102(8), PP. S1–S475. HTTPS://DOI.ORG/10.1175/2021BAMSSTATEOFTHECLIMATE.1.

33. **VAN DEN BOOGAART, K. G. AND TOLOSANA-DELGADO, R. (2013)** ANALYZING COMPOSITIONAL DATA WITH R, PP. 1–258. HTTPS://DOI.ORG/10.1007/978-3-642-36809-7.

34. **BOSSERELLE, P. ET AL. (2014)** GUIDE DIDENTIFICATION DES CORAUX DE MO'OREA. CRIOBE.

35. **BOSTRÖM-EINARSSON, L. ET AL. (2020)** CORAL RESTORATION – A SYSTEMATIC REVIEW OF CURRENT METHODS, SUCCESSES, FAILURES AND FUTURE DIRECTIONS. PLOS ONE. PUBLIC LIBRARY OF SCIENCE, 15(1), P. E0226631. HTTPS://DOI.ORG/10.1371/JOURNAL.PONE.0226631.

36. **BRANDL, S., RASHER, D. B., ET AL. (2019)** CORAL REEF ECOSYSTEM FUNCTIONING: EIGHT CORE PROCESSES AND THE ROLE OF BIODIVERSITY. FRONTIERS IN ECOLOGY AND THE ENVIRONMENT. JOHN WILEY & SONS, LTD, 17(8), PP. 445–454. HTTPS://DOI.ORG/10.1002/FEE.2088.

37. **BRANDL, S., TORNABENE, L., ET AL. (2019)** DEMOGRAPHIC DYNAMICS OF THE SMALLEST MARINE VERTEBRATES FUEL CORAL REEF ECOSYSTEM FUNCTIONING. SCIENCE, 364(6446), PP. 1189 LP – 1192. HTTPS://DOI.ORG/10.1126/SCIENCE.AAV3384.

38. **BRIDGES, E. M. AND OLDEMAN, L. R. (2019)** FOOD PRODUCTION AND ENVIRONMENTAL DEGRADATION, IN RESPONSE TO LAND DEGRADATION. CRC PRESS, PP. 36–43.

39. **BRUNO, J. F. AND SELIG, E. R. (2007)** REGIONAL DECLINE OF CORAL COVER IN THE INDO-PACIFIC: TIMING, EXTENT, AND SUBREGIONAL COMPARISONS. PLOS ONE. PUBLIC LIBRARY OF SCIENCE, 2(8), PP. 1–8. HTTPS://DOI.ORG/10.1371/JOURNAL.PONE.0000711.

40. **BRUNO, J. F., STACHOWICZ, J. J. AND BERTNESS, M. D. (2003)** INCLUSION OF FACILITATION INTO ECOLOGICAL THEORY. TRENDS IN ECOLOGY & EVOLUTION, 18(3), PP. 119–125. HTTPS://DOI.ORG/10.1016/S0169-5347(02)00045-9.

41. **BRYSON, M. ET AL. (2017)** CHARACTERIZATION OF MEASUREMENT ERRORS USING STRUCTURE-FROM-MOTION AND PHOTOGRAMMETRY TO MEASURE MARINE HABITAT STRUCTURAL

COMPLEXITY. ECOLOGY AND EVOLUTION. JOHN WILEY AND SONS INC., 7(15), PP. 5669–5681. HTTPS://DOI.ORG/10.1002/ECE3.3127.

42. **BURKE, L. ET AL. (2011)** REEFS AT RISK REVISITED. WORLD RESOURCES INSTITUTE.

43. **BÜRKNER, P.-C. (2017A)** ADVANCED BAYESIAN MULTILEVEL MODELING WITH THE R PACKAGE BRMS.

44. **BÜRKNER, P.-C. (2017B)** BRMS: AN R PACKAGE FOR BAYESIAN MULTILEVEL MODELS USING STAN, JOURNAL OF STATISTICAL SOFTWARE; VOL 1, ISSUE 1 (2017). HTTPS://DOI.ORG/10.18637/JSS.V080.I01.

45. **BURNS, J. ET AL. (2015)** INTEGRATING STRUCTURE-FROM-MOTION PHOTOGRAMMETRY WITH GEOSPATIAL SOFTWARE AS A NOVEL TECHNIQUE FOR QUANTIFYING 3D ECOLOGICAL CHARACTERISTICS OF CORAL REEFS. PEERJ, 3, P. 19. HTTPS://DOI.ORG/10.7717/PEERJ.1077.

46. **CAFARO, P. AND CRIST, E. (2012)** LIFE ON THE BRINK: ENVIRONMENTALISTS CONFRONT OVERPOPULATION. UNIVERSITY OF GEORGIA PRESS.

47. **CAMERON, D. ET AL. (2015)** A SUSTAINABLE MODEL FOR INTENSIVE AGRICULTURE, GRANTHAM CENTRE BRIEFING NOTE, (DECEMBER).

48. **CARDINI, U. ET AL. (2014)** BENTHIC N2 FIXATION IN CORAL REEFS AND THE POTENTIAL EFFECTS OF HUMAN-INDUCED ENVIRONMENTAL CHANGE, ECOLOGY AND EVOLUTION. JOHN WILEY & SONS, LTD, 4(9), PP. 1706–1727. HTTPS://DOI.ORG/10.1002/ECE3.1050.

49. **CARLOT, J. ET AL. (2020)** COMMUNITY COMPOSITION PREDICTS PHOTOGRAMMETRY-BASED STRUCTURAL COMPLEXITY ON CORAL REEFS. CORAL REEFS, 39(4), PP. 967–975. HTTPS://DOI.ORG/10.1007/S00338-020-01916-8.

50. **CARLOT, J. ET AL. (2021)** JUVENILE CORALS UNDERPIN CORAL REEF CARBONATE PRODUCTION AFTER DISTURBANCE. GLOBAL CHANGE BIOLOGY, 27(11), PP. 2623–2632. HTTPS://DOI.ORG/10.1111/GCB.15610.

51. **CARROLL, A., HARRISON, P. AND ADJEROUD, M. (2006)** SEXUAL REPRODUCTION OF ACROPORA REEF CORALS AT MO'OREA , FRENCH POLYNESIA. CORAL REEFS, 25, PP. 93–97. HTTPS://DOI.ORG/10.1007/S00338-005-0057-6.

52. **CASELLA, E. ET AL. (2017)** MAPPING CORAL REEFS USING CONSUMER-GRADE DRONES AND STRUCTURE FROM MOTION PHOTOGRAMMETRY TECHNIQUES. CORAL REEFS. SPRINGER BERLIN HEIDELBERG, 36(1), PP. 269–275. HTTPS://DOI.ORG/10.1007/S00338-016-1522-0.

53. **CASTRO, P. (1988)** ANIMAL SYMBIOSES IN CORAL REEF COMMUNITIES: A REVIEW, SYMBIOSIS (PHILADELPHIA, PA), 5(3).

54. **CEBALLOS, G., EHRLICH, P. R. AND RAVEN, P. H. (2020)** VERTEBRATES ON THE BRINK AS INDICATORS OF BIOLOGICAL ANNIHILATION AND THE SIXTH MASS EXTINCTION. PROCEEDINGS OF THE NATIONAL ACADEMY OF SCIENCES. NATIONAL ACADEMY OF SCIENCES, 117(24), PP. 13596–13602. HTTPS://DOI.ORG/10.1073/PNAS.1922686117.

55. **CHAZDON, R. L. (2014)** SECOND GROWTH, THE PROMISE OF TROPICAL FOREST REGENERATION IN AN AGE OF DEFORESTATION, THE UNIVERSITY OF CHICAGO PRESS. HTTPS://DOI.ORG/10.1007/BF02394968.

56. **CHAZOTTES, V. ET AL. (2002)** THE EFFECTS OF EUTROPHICATION-RELATED ALTERATIONS TO CORAL REEF COMMUNITIES ON AGENTS AND RATES OF BIOEROSION (REUNION ISLAND, INDIAN OCEAN). CORAL REEFS, 21(4), PP. 375–390. HTTPS://DOI.ORG/10.1007/S00338-002-0259-0.

57. **CHAZOTTES, V., CAMPION-ALSUMARD, T. L. AND PEYROT-CLAUSADE, M. (1995)** BIOEROSION RATES ON CORAL REEFS: INTERACTIONS BETWEEN MACROBORERS, MICROBORERS AND GRAZERS (MO'OREA, FRENCH POLYNESIA). PALAEOGEOGRAPHY, PALAEOCLIMATOLOGY, PALAEOECOLOGY, 113(2), PP. 189–198. HTTPS://DOI.ORG/10.1016/0031-0182(95)00043-L.

58. **CHRISTENSEN, J. H. ET AL. (2013)** CLIMATE PHENOMENA AND THEIR RELEVANCE FOR FUTURE REGIONAL CLIMATE CHANGE. CLIMATE CHANGE 2013 THE PHYSICAL SCIENCE BASIS. UNITED KINGDOM: CAMBRIDGE UNIVERSITY PRESS, PP. 1217–1308. HTTPS://DOI.ORG/10.1017/CBO9781107415324.028.

59. **CHURCH, J. A. ET AL. (2013)** 2013: SEA LEVEL CHANGE, CLIMATE CHANGE 2013: THE PHYSICAL SCIENCE BASIS. CONTRIBUTION OF WORKING GROUP I TO THE FIFTH ASSESSMENT REPORT OF THE INTERGOVERNMENTAL PANEL ON CLIMATE CHANGE.

60. **CINNER, J. E. ET AL. (2020)** MEETING FISHERIES, ECOSYSTEM FUNCTION, AND BIODIVERSITY GOALS IN A HUMAN-DOMINATED WORLD. SCIENCE. AMERICAN ASSOCIATION FOR THE ADVANCEMENT OF SCIENCE, 368(6488), PP. 307–311. HTTPS://DOI.ORG/10.1126/SCIENCE.AAX9412.

61. **COLE, A. J. ET AL. (2011)** CHRONIC CORAL CONSUMPTION BY BUTTERFLYFISHES. CORAL REEFS, 30(1), PP. 85–93. HTTPS://DOI.ORG/10.1007/S00338-010-0674-6.

62. **CONNELL, J. H. (1983)** ON THE PREVALENCE AND RELATIVE IMPORTANCE OF INTERSPECIFIC COMPETITION: EVIDENCE FROM FIELD EXPERIMENTS. THE AMERICAN NATURALIST. UNIVERSITY OF CHICAGO PRESS, 122(5), PP. 661–696.

63. **CORNWALL, C. E. ET AL. (2021)** GLOBAL DECLINES IN CORAL REEF CALCIUM CARBONATE PRODUCTION UNDER OCEAN ACIDIFICATION AND WARMING. PROCEEDINGS OF THE NATIONAL ACADEMY OF SCIENCES. NATIONAL ACADEMY OF SCIENCES, 118(21). HTTPS://DOI.ORG/10.1073/PNAS.2015265118.

64. **COSTANZA, R. ET AL. (2014)** CHANGES IN THE GLOBAL VALUE OF ECOSYSTEM SERVICES. GLOBAL ENVIRONMENTAL CHANGE, 26, PP. 152–158. HTTPS://DOI.ORG/10.1016/J.GLOENVCHA.2014.04.002.

65. **CRESSWELL, A. K. ET AL. (2020)** FREQUENT HYDRODYNAMIC DISTURBANCES DECREASE THE MORPHOLOGICAL DIVERSITY AND STRUCTURAL COMPLEXITY OF 3D SIMULATED CORAL COMMUNITIES. CORAL REEFS, 39(4), PP. 1147–1161. HTTPS://DOI.ORG/10.1007/S00338-020-01947-1.

66. **DARLING, E. S. ET AL. (2012)** EVALUATING LIFE-HISTORY STRATEGIES OF REEF CORALS FROM SPECIES TRAITS. ECOLOGY LETTERS. JOHN WILEY & SONS, LTD, 15(12), PP. 1378–1386. HTTPS://DOI.ORG/10.1111/J.1461-0248.2012.01861.X.

67. **DARLING, E. S. ET AL. (2019)** SOCIAL–ENVIRONMENTAL DRIVERS INFORM STRATEGIC MANAGEMENT OF CORAL REEFS IN THE ANTHROPOCENE. NATURE ECOLOGY & EVOLUTION, 3(9), PP. 1341–1350. HTTPS://DOI.ORG/10.1038/S41559-019-0953-8.

68. **DARWIN, C. (1839)** THE VOYAGE OF THE BEAGLE. PENGUIN BOOKS, LONDON.

69. **DAVIES, S. W. ET AL. (2020)** CLADOCOPIUM COMMUNITY DIVERGENCE IN TWO ACROPORA CORAL HOSTS ACROSS MULTIPLE SPATIAL SCALES. BIORXIV. COLD SPRING HARBOR LABORATORY. HTTPS://DOI.ORG/10.1101/575183.

70. **DEATH, G. ET AL. (2012)** THE 27–YEAR DECLINE OF CORAL COVER ON THE GREAT BARRIER REEF AND ITS CAUSES. PROCEEDINGS OF THE NATIONAL ACADEMY OF SCIENCES, 109(44), PP. 17995 LP – 17999. HTTPS://DOI.ORG/10.1073/PNAS.1208909109.

71. **DECARLO, T. M. ET AL. (2015)** CORAL MACROBIOEROSION IS ACCELERATED BY OCEAN ACIDIFICATION AND NUTRIENTS. GEOLOGY. GEOLOGICAL SOCIETY OF AMERICA, 43(1), PP. 7–10.

72. **DICKSON, A., SABINE, C. AND CHRISTIAN, J. (2007)** GUIDE TO BEST PRACTICES FOR OCEAN CO2 MEASUREMENTS. NORTH PACIFIC MARINE SCIENCE ORGANIZATION.

73. **DIETZEL, A. ET AL. (2020)** LONG-TERM SHIFTS IN THE COLONY SIZE STRUCTURE OF CORAL POPULATIONS ALONG THE GREAT BARRIER REEF. PROCEEDINGS OF THE ROYAL SOCIETY B: BIOLOGICAL SCIENCES. ROYAL SOCIETY, 287(1936), P. 20201432. HTTPS://DOI.ORG/10.1098/RSPB.2020.1432.

74. **DONE, T. J. ET AL. (2010)** CORAL GROWTH ON THREE REEFS : DEVELOPMENT OF RECOVERY BENCHMARKS USING A SPACE FOR TIME APPROACH. CORAL REEFS, 29, PP. 815–833. HTTPS://DOI.ORG/10.1007/S00338-010-0637-Y.

75. **DONEY, S. C. ET AL. (2009)** OCEAN ACIDIFICATION: THE OTHER CO2 PROBLEM. ANNUAL REVIEW OF MARINE SCIENCE. ANNUAL REVIEWS, 1(1), PP. 169–192. HTTPS://DOI.ORG/10.1146/ANNUREV.MARINE.010908.163834.

76. **DORNELAS, M. ET AL. (2017)** ALLOMETRIC GROWTH IN REEF-BUILDING CORALS. PROCEEDINGS OF THE ROYAL SOCIETY B: BIOLOGICAL SCIENCES. ROYAL SOCIETY, 284(1851), P. 20170053. HTTPS://DOI.ORG/10.1098/RSPB.2017.0053.

77. **DOROPOULOS, C. ET AL. (2012)** INTERACTIONS AMONG CHRONIC AND ACUTE IMPACTS ON CORAL RECRUITS: THE IMPORTANCE OF SIZE-ESCAPE THRESHOLDS. ECOLOGY, 93(10), PP. 2131–2138. HTTPS://DOI.ORG/10.1890/12-0495.1.

78. **DUFAULT, A. M. ET AL. (2013)** THE ROLE OF LIGHT IN MEDIATING THE EFFECTS OF OCEAN ACIDIFICATION ON CORAL CALCIFICATION. JOURNAL OF EXPERIMENTAL BIOLOGY, 216(9), PP. 1570–1577. HTTPS://DOI.ORG/10.1242/JEB.080549.

79. **DUSTAN, P. (1975)** GROWTH AND FORM IN THE REEF-BUILDING CORAL MONTASTREA ANNULARIS. MARINE BIOLOGY. SPRINGER, 33(2), PP. 101–107.

80. **EDMUNDS, P. J. ET AL. (2014)** EVALUATING THE CAUSAL BASIS OF ECOLOGICAL SUCCESS WITHIN THE SCLERACTINIA: AN INTEGRAL PROJECTION MODEL APPROACH. MARINE BIOLOGY, 161(12), PP. 2719–2734. HTTPS://DOI.ORG/10.1007/S00227-014-2547-Y.

81. **EDMUNDS, P. J. (2017)** UNUSUALLY HIGH CORAL RECRUITMENT DURING THE 2016 EL NIÑO IN MO'OREA, FRENCH POLYNESIA. PLOS ONE. PUBLIC LIBRARY OF SCIENCE, 12(10), P. E0185167. HTTPS://DOI.ORG/10.1371/JOURNAL.PONE.0185167.

82. **EDMUNDS, P. J. AND BURGESS, S. C. (2016)** SIZE-DEPENDENT PHYSIOLOGICAL RESPONSES OF THE BRANCHING CORAL POCILLOPORA VERRUCOSA TO ELEVATED TEMPERATURE AND PCO2. JOURNAL OF EXPERIMENTAL BIOLOGY. THE COMPANY OF BIOLOGISTS LTD, 219(24), PP. 3896–3906. HTTPS://DOI.ORG/10.1242/JEB.146381.

83. **EDMUNDS, P. J. AND BURGESS, S. C. (2017)** COLONY SIZE AND TURBULENT FLOW SPEED MODULATE THE CALCIFICATION RESPONSE OF THE CORAL POCILLOPORA VERRUCOSA TO TEMPERATURE. MARINE BIOLOGY, 165(1), P. 13. HTTPS://DOI.ORG/10.1007/S00227-017-3257-Z.

84. **EDMUNDS, P. J. AND RIEGL, B. (2020)** URGENT NEED FOR CORAL DEMOGRAPHY IN A WORLD WHERE CORALS ARE DISAPPEARING, MARINE ECOLOGY PROGRESS SERIES, 635, PP. 233–242. HTTPS://WWW.INT-RES.COM/ABSTRACTS/MEPS/V635/P233-242/.

85. **EDWARDS, A. J. AND GOMEZ, E. D. (2007)** REEF RESTORATION CONCEPTS AND DE PUBLICATION : GUIDELINES: MAKING SENSIBLE MANAGEMENT CHOICES IN THE FACE OF UNCERTAINTY, CORAL REEF TARGETED RESEARCH & CAPACITY BUILDING FOR MANAGEMENT PROGRAMME: ST LUCIA, AUSTRALIA, P. 38.

86. **EDWARDS, C. A. (1991)** ADVANCES IN SOIL SCIENCE. VOLUME 11: SOIL DEGRADATION . R. LAL ,B. A. STEWART, THE QUARTERLY REVIEW OF BIOLOGY, 66(2). HTTPS://DOI.ORG/10.1086/417205.

87. **ELAHI, R. AND EDMUNDS, P. J. (2007)** TISSUE AGE AFFECTS CALCIFICATION IN THE SCLERACTINIAN CORAL MADRACIS MIRABILIS, THE BIOLOGICAL BULLETIN. MARINE BIOLOGICAL LABORATORY, 212(1), PP. 20–28.

88. **ELITH, J., LEATHWICK, J. R. AND HASTIE, T. (2008)** A WORKING GUIDE TO BOOSTED REGRESSION TREES. JOURNAL OF ANIMAL ECOLOGY, 77, PP. 802–813. HTTPS://DOI.ORG/10.1111/J.1365-2656.2008.01390.X.

89. **ELLISON, J. C., HAN, P. AND LEWIS, T. W. (2019)** CARBONATE BEACH SAND OF ABAIANG ATOLL, KIRIBATI: GEOCHEMISTRY, BIOGENIC SOURCES, AND PROPERTIES. ATOLL RESEARCH BULLETIN. SMITHSONIAN INSTITUTION PRESS, (621), PP. 1–21.

90. **ENGLISH, S., WILKINSON, C. AND BAKER, V. (1997)** SURVEY MANUAL FOR TROPICAL MARINE RESOURCES.

91. **ESWARAN, H., LAL, R. AND REICH, P. F. (2001)** LAND DEGRADATION AN OVERVIEW IN BRIDGES RESPONSES TO LAND DEGRADATION.

92. **FALKOWSKI, P. G. ET AL. (1984)** LIGHT AND THE BIOENERGETICS OF A SYMBIOTIC CORAL. BIOSCIENCE, 34(11), PP. 705–709. HTTPS://DOI.ORG/10.2307/1309663.

93. **FERRARIO, F. ET AL. (2014)** THE EFFECTIVENESS OF CORAL REEFS FOR COASTAL HAZARD RISK REDUCTION AND ADAPTATION. NATURE COMMUNICATIONS, 5(1), P. 3794. HTTPS://DOI.ORG/10.1038/NCOMMS4794.

94. **FIGUEIRA, W. ET AL. (2015)** ACCURACY AND PRECISION OF HABITAT STRUCTURAL COMPLEXITY METRICS DERIVED FROM UNDERWATER PHOTOGRAMMETRY. REMOTE SENSING, 7, PP. 16883–16900. HTTPS://DOI.ORG/10.3390/RS71215859.

95. **FITT, W. K. ET AL. (2001)** CORAL BLEACHING: INTERPRETATION OF THERMAL TOLERANCE LIMITS AND THERMAL THRESHOLDS IN TROPICAL CORALS. CORAL REEFS, 20(1), PP. 51–65. HTTPS://DOI.ORG/10.1007/S003380100146.

96. **FLOWER, J. ET AL. (2017)** INTERPRETING CORAL REEF MONITORING DATA: A GUIDE FOR IMPROVED MANAGEMENT DECISIONS. ECOLOGICAL INDICATORS, 72, PP. 848–869. HTTPS://DOI.ORG/10.1016/J.ECOLIND.2016.09.003.

97. **FOX-KEMPER, B. ET AL. (2021)** OCEAN, CRYOSPHERE AND SEA LEVEL CHANGE, CAMBRIDGE UNIVERSITY PRESS.

98. **DE FRAITURE, C. AND GIORDANO, M. (2014)** SMALL PRIVATE IRRIGATION: A THRIVING BUT OVERLOOKED SECTOR. AGRICULTURAL WATER MANAGEMENT, 131, PP. 167–174. HTTPS://DOI.ORG/10.1016/J.AGWAT.2013.07.005.

99. **FRIEDMAN, A. ET AL. (2012)** MULTI-SCALE MEASURES OF RUGOSITY, SLOPE AND ASPECT FROM BENTHIC STEREO IMAGE RECONSTRUCTIONS. PLOS ONE, 7(12), P. 14. HTTPS://DOI.ORG/10.1371/JOURNAL.PONE.0050440.

100. **FRIESS, D. A. ET AL. (2012)** ARE ALL INTERTIDAL WETLANDS NATURALLY CREATED EQUAL? BOTTLENECKS, THRESHOLDS AND KNOWLEDGE GAPS TO MANGROVE AND SALTMARSH ECOSYSTEMS. BIOLOGICAL REVIEWS. JOHN WILEY & SONS, LTD, 87(2), PP. 346–366. HTTPS://DOI.ORG/10.1111/J.1469-185X.2011.00198.X.

101. **GARDNER, T. A. ET AL. (2003)** LONG-TERM REGION-WIDE DECLINES IN CARIBBEAN CORALS. SCIENCE. AMERICAN ASSOCIATION FOR THE ADVANCEMENT OF SCIENCE, 301(5635), PP. 958–960. HTTPS://DOI.ORG/10.1126/SCIENCE.1086050.

102. **GATTUSO, J.-P. ET AL. (1998)** EFFECT OF CALCIUM CARBONATE SATURATION OF SEAWATER ON CORAL CALCIFICATION. GLOBAL AND PLANETARY CHANGE, 18(1), PP. 37–46. DOI: HTTPS://DOI.ORG/10.1016/S0921-8181(98)00035-6.

103. **GELMAN, A., RUBIN, D. B. AND AL. (1992)** INFERENCE FROM ITERATIVE SIMULATION USING MULTIPLE SEQUENCES, STATISTICAL SCIENCE. INSTITUTE OF MATHEMATICAL STATISTICS, 7(4), PP. 457–472.

104. **GILMAN, E., ELLISON, J. AND COLEMAN, R. (2007)** ASSESSMENT OF MANGROVE RESPONSE TO PROJECTED RELATIVE SEA-LEVEL RISE AND RECENT HISTORICAL RECONSTRUCTION OF SHORELINE POSITION. ENVIRONMENTAL MONITORING AND ASSESSMENT, 124(1), PP. 105–130. HTTPS://DOI.ORG/10.1007/S10661-006-9212-Y.

105. **GILMAN, E. L. ET AL. (2008)** THREATS TO MANGROVES FROM CLIMATE CHANGE AND ADAPTATION OPTIONS: A REVIEW. AQUATIC BOTANY, 89(2), PP. 237–250. HTTPS://DOI.ORG/10.1016/J.AQUABOT.2007.12.009.

106. **GILMOUR, J. P. ET AL. (2013)** RECOVERY OF AN ISOLATED CORAL REEF SYSTEM FOLLOWING SEVERE DISTURBANCE. SCIENCE, 340(6128), PP. 69 LP – 71. HTTPS://DOI.ORG/10.1126/SCIENCE.1232310.

107. **GONZÁLEZ-BARRIOS, F. J., CABRAL-TENA, R. A. AND ALVAREZ-FILIP, L. (2021)** RECOVERY DISPARITY BETWEEN CORAL COVER AND THE PHYSICAL FUNCTIONALITY OF REEFS WITH IMPAIRED CORAL ASSEMBLAGES. GLOBAL CHANGE BIOLOGY, 27(3), PP. 640–651. HTTPS://DOI.ORG/10.1111/GCB.15431.

108. **GRAHAM, N. A. J. ET AL. (2015)** PREDICTING CLIMATE-DRIVEN REGIME SHIFTS VERSUS REBOUND POTENTIAL IN CORAL REEFS. NATURE. NATURE PUBLISHING GROUP, 518(7537), P. 7. HTTPS://DOI.ORG/10.1038/NATURE14140.

109. **GRAHAM, N. A. J. ET AL. (2018)** SEABIRDS ENHANCE CORAL REEF PRODUCTIVITY AND FUNCTIONING IN THE ABSENCE OF INVASIVE RATS. NATURE, 559(7713), PP. 250–253. HTTPS://DOI.ORG/10.1038/S41586-018-0202-3.

110. **GRAHAM, N. A. J. AND NASH, K. L. (2013)** THE IMPORTANCE OF STRUCTURAL COMPLEXITY IN CORAL REEF ECOSYSTEMS. CORAL REEFS, 32(2), PP. 315–326. HTTPS://DOI.ORG/10.1007/S00338-012-0984-Y.

111. **GRATWICKE, B. AND SPEIGHT, M. R. (2005)** EFFECTS OF HABITAT COMPLEXITY ON CARIBBEAN MARINE FISH ASSEMBLAGES. MARINE ECOLOGY PROGRESS SERIES, 292, PP. 301–310. HTTPS://DOI.ORG/10.3354/MEPS292301.

112. **GROTTOLI, A. G. ET AL. (2021)** INCREASING COMPARABILITY AMONG CORAL BLEACHING EXPERIMENTS. ECOLOGICAL APPLICATIONS, 31(4), P. E02262. HTTPS://DOI.ORG/10.1002/EAP.2262.

113. **GROTTOLI, A. G. AND WELLINGTON, G. M. (1999)** EFFECT OF LIGHT AND ZOOPLANKTON ON SKELETAL Δ13C VALUES IN THE EASTERN PACIFIC CORALS PAVONA CLAVUS AND PAVONA GIGANTEA. CORAL REEFS, 18(1), PP. 29–41. HTTPS://DOI.ORG/10.1007/S003380050150.

114. **HALFORD, A. ET AL. (2004)** RESILIENCE TO LARGE-SCALE DISTURBANCE IN CORAL AND FISH ASSEMBLAGES ON THE GREAT BARRIER REEF. ECOLOGICAL SOCIETY OF AMERICA, 85(7), PP. 1892–1905.

115. **HARBORNE, A. R. ET AL. (2017)** MULTIPLE STRESSORS AND THE FUNCTIONING OF CORAL REEFS. ANNUAL REVIEW OF MARINE SCIENCE, 9(1), PP. 445–468. HTTPS://DOI.ORG/0.1146/ANNUREV-MARINE-010816-060551.

116. HARRIOTT, V. J. (1999) CORAL GROWTH IN SUBTROPICAL EASTERN AUSTRALIA. CORAL REEFS, 18(3), PP. 281–291. HTTPS://DOI.ORG/10.1007/S003380050195.

117. HARRIS, D. L. ET AL. (2015) SPATIAL VARIATIONS IN WAVE TRANSFORMATION AND SEDIMENT ENTRAINMENT ON A CORAL REEF SAND APRON. MARINE GEOLOGY, 363, PP. 220–229. DOI: HTTPS://DOI.ORG/10.1016/J.MARGEO.2015.02.010.

118. HARRIS, D. L. ET AL. (2018) CORAL REEF STRUCTURAL COMPLEXITY PROVIDES IMPORTANT COASTAL PROTECTION FROM WAVES UNDER RISING SEA LEVELS. SCIENCE ADVANCES, 4(2), P. EAAO4350. HTTPS://DOI.ORG/10.1126/SCIADV.AAO4350.

119. HARWIN, S., LUCIEER, A. AND OSBORN, J. (2015) THE IMPACT OF THE CALIBRATION METHOD ON THE ACCURACY OF POINT CLOUDS DERIVED USING UNMANNED AERIAL VEHICLE MULTI-VIEW STEREOPSIS. REMOTE SENSING, 7(9), PP. 11933–11953. HTTPS://DOI.ORG/10.3390/RS70911933.

120. HASLETT, S. (2009) COASTAL SYSTEMS, 2ND EDITION. ROUTLEDGE.

121. HE, B. ET AL. (2007) COMPARISON OF FLOODING-TOLERANCE IN FOUR MANGROVE SPECIES IN A DIURNAL TIDAL ZONE IN THE BEIBU GULF. ESTUARINE, COASTAL AND SHELF SCIENCE, 74(1), PP. 254–262. HTTPS://DOI.ORG/10.1016/J.ECSS.2007.04.018.

122. HÉDOUIN, L. ET AL. (2020) CONTRASTING PATTERNS OF MORTALITY IN POLYNESIAN CORAL REEFS FOLLOWING THE THIRD GLOBAL CORAL BLEACHING EVENT IN 2016. CORAL REEFS, 39(4), PP. 939–952. HTTPS://DOI.ORG/10.1007/S00338-020-01914-W.

123. HEINO AND KAITALA (1999) EVOLUTION OF RESOURCE ALLOCATION BETWEEN GROWTH AND REPRODUCTION IN ANIMALS WITH INDETERMINATE GROWTH. JOURNAL OF EVOLUTIONARY BIOLOGY, 12(3), PP. 423–429. DOI: HTTPS://DOI.ORG/10.1046/J.1420-9101.1999.00044.X.

124. HERON, S. F. ET AL. (2016) WARMING TRENDS AND BLEACHING STRESS OF THE WORLDS CORAL REEFS 1985-2012. SCIENTIFIC REPORTS, 6, P. 14. HTTPS://DOI.ORG/10.1038/SREP38402.

125. HERON, S. F. ET AL. (2017) IMPACTS OF CLIMATE CHANGE ON WORLD HERITAGE CORAL REEFS. HTTPS://REPOSITORY.LIBRARY.NOAA.GOV/VIEW/NOAA/16386.

126. HILL, J. J., WILKINSON, C. C. R. AND AL. (2004) METHODS FOR ECOLOGICAL MONITORING OF CORAL REEFS: A RESOURCE FOR MANAGERS. AUSTRALIAN INSTITUTE OF MARINE SCIENCE. HTTPS://DOI.ORG/10.1017/CBO9781107415324.004.

127. HILMI, N., SAFA, A. AND REYNAUD, S. (2012) CORAL REEFS AND TOURISM IN EGYPTS RED SEA. TOPICS IN MIDDLE EASTERN AND NORTH AFRICAN ECONOMIES. MIDDLE EAST ECONOMIC ASSOCIATION AND LOYOLA UNIVERSITY CHICAGO, 14.

128. HINKEL, J. ET AL. (2019) MEETING USER NEEDS FOR SEA LEVEL RISE INFORMATION: A DECISION ANALYSIS PERSPECTIVE. EARTHS FUTURE. JOHN WILEY & SONS, LTD, 7(3), PP. 320–337. HTTPS://DOI.ORG/10.1029/2018EF001071.

129. **HIROSE, M., KINZIE, R. AND HIDAKA, M. (2001)** TIMING AND PROCESS OF ENTRY OF ZOOXANTHELLAE INTO OOCYTES OF HERMATYPIC CORALS. CORAL REEFS, 20(3), PP. 273–280. HTTPS://DOI.ORG/10.1007/S003380100171.

130. **HOBSON, R. D. (2019)** SURFACE ROUGHNESS IN TOPOGRAPHY: QUANTITATIVE APPROACH, IN SPATIAL ANALYSIS IN GEOMORPHOLOGY. ROUTLEDGE, PP. 221–246.

131. **HOEGH-GULDBERG, O. (1999)** CLIMATE CHANGE, CORAL BLEACHING AND THE FUTURE OF THE WORLD S CORAL REEFS. MARINE AND FRESHWATER RESEARCH, 50(8), PP. 839–866.

132. **HOEGH-GULDBERG, O. ET AL. (2007)** CORAL REEFS UNDER RAPID CLIMATE CHANGE AND OCEAN ACIDIFICATION. SCIENCE, 318(5857), PP. 1737 LP – 1742. HTTPS://DOI.ORG/10.1126/SCIENCE.1152509.

133. **HOEGH-GULDBERG, O. (2011)** CORAL REEF ECOSYSTEMS AND ANTHROPOGENIC CLIMATE CHANGE. REGIONAL ENVIRONMENTAL CHANGE, 11(1), PP. 215–227. HTTPS://DOI.ORG/10.1007/S10113-010-0189-2.

134. **HOEGH-GULDBERG, O., PENDLETON, L. AND KAUP, A. (2019)** PEOPLE AND THE CHANGING NATURE OF CORAL REEFS. REGIONAL STUDIES IN MARINE SCIENCE, 30, P. 100699. HTTPS://DOI.ORG/10.1016/J.RSMA.2019.100699.

135. **HOLBROOK, S. J. ET AL. (2018)** RECRUITMENT DRIVES SPATIAL VARIATION IN RECOVERY RATES OF RESILIENT CORAL REEFS. SCIENTIFIC REPORTS, 8(1), P. 7338. HTTPS://DOI.ORG/10.1038/S41598-018-25414-8.

136. **HOOGENBOOM, M. O. AND ANTHONY, K. R. N. (2006)** ENERGETIC COST OF PHOTOINHIBITION IN CORALS. MARINE ECOLOGY PROGRESS SERIES, 313, PP. 1–12. HTTPS://WWW.INT-RES.COM/ABSTRACTS/MEPS/V313/P1-12/.

137. **VAN HOOIDONK, R. ET AL. (2016)** LOCAL-SCALE PROJECTIONS OF CORAL REEF FUTURES AND IMPLICATIONS OF THE PARIS AGREEMENT. SCIENTIFIC REPORTS, 6(1), P. 39666. HTTPS://DOI.ORG/10.1038/SREP39666.

138. **HOWARD, J. ET AL. (2017)** CLARIFYING THE ROLE OF COASTAL AND MARINE SYSTEMS IN CLIMATE MITIGATION. FRONTIERS IN ECOLOGY AND THE ENVIRONMENT, 15(1), PP. 42–50. HTTPS://DOI.ORG/10.1002/FEE.1451.

139. **HUGHES, T. P. ET AL. (2003)** CLIMATE CHANGE, HUMAN IMPACTS, AND THE RESILIENCE OF CORAL REEFS. SCIENCE, 301, PP. 929–933. HTTPS://DOI.ORG/10.1117/12.850389.

140. **HUGHES, T. P., BARNES, M. L., ET AL. (2017)** CORAL REEFS IN THE ANTHROPOCENE. NATURE, 546(7656), PP. 82–90. HTTPS://DOI.ORG/10.1038/NATURE22901.

141. **HUGHES, T. P., KERRY, J. T., ET AL. (2017)** GLOBAL WARMING AND RECURRENT MASS BLEACHING OF CORALS. NATURE. NATURE PUBLISHING GROUP, 543(7645), PP. 373–377. HTTPS://DOI.ORG/10.1038/NATURE21707

142. **HUGHES, T. P. ET AL. (2018)** SPATIAL AND TEMPORAL PATTERNS OF MASS BLEACHING OF CORALS IN THE ANTHROPOCENE. SCIENCE, 83(JANUARY 2018), PP. 80–83. HTTPS://DOI.ORG/10.1126/SCIENCE.AAN8048

143. **HUGHES, T. P. ET AL. (2019)** GLOBAL WARMING IMPAIRS STOCK–RECRUITMENT DYNAMICS OF CORALS. NATURE, 568(7752), PP. 387–390. HTTPS://DOI.ORG/10.1038/S41586-019-1081-Y.

144. **HUGHES, T. P. AND TANNER, J. E. (2000)** RECRUITMENT FAILURE, LIFE HISTORIES, AND LONG-TERM DECLINE OF CARIBBEAN CORALS, ECOLOGY. JOHN WILEY & SONS, LTD, 81(8), PP. 2250–2263. HTTPS://DOI.ORG/10.1890/0012-9658(2000)081[2250:RFLHAL]2.0.CO;2.

145. **IPBES (2019)** GLOBAL ASSESSMENT REPORT ON BIODIVERSITY AND ECOSYSTEM SERVICES, GLOBAL ASSESSMENT SUMMARY FOR POLICYMAKERS.

146. **IPCC (1990)** THE IPCC SCIENTIFIC ASSESSMENT, HOUGHTON JT, JENKINS G, EPHRAUMS JJ EDS. CAMBRIDGE: CAMBRIDGE UNIVERSITY PRESS, 1, P. 990.

147. **IPCC (2021)** ASSESSMENT REPORT 6 CLIMATE CHANGE 2021: THE PHYSICAL SCIENCE BASIS. HTTPS://WWW.IPCC.CH/REPORT/AR6/WG1/.

148. **JANUCHOWSKI-HARTLEY, F. A. ET AL. (2017)** DRIVERS AND PREDICTIONS OF CORAL REEF CARBONATE BUDGET TRAJECTORIES. PROCEEDINGS OF THE ROYAL SOCIETY B: BIOLOGICAL SCIENCES, 284(1847), P. 20162533. HTTPS://DOI.ORG/10.1098/RSPB.2016.2533.

149. **JOKIEL, P. L., JURY, C. P. AND KUFFNER, I. B. (2016)** CORAL CALCIFICATION AND OCEAN ACIDIFICATION. CORAL REEFS AT THE CROSSROADS. SPRINGER NETHERLANDS, PP. 7–45. HTTPS://DOI.ORG/10.1007/978-94-017-7567-0.

150. **JOKIEL, P. L. AND MORRISSEY, J. I. (1986)** INFLUENCE OF SIZE ON PRIMARY PRODUCTION IN THE REEF CORAL POCILLOPORA DAMICORNIS AND THE MACROALGA ACANTHOPHORA SPICIFERA. MARINE BIOLOGY, 91(1), PP. 15–26. HTTPS://DOI.ORG/10.1007/BF00397566.

151. **JONSSON, I. G. (2021)** WAVE BOUNDARY LAYERS AND FRICTION FACTORS. COASTAL ENGINEERING 1966. (PROCEEDINGS), PP. 127–148. HTTPS://DOI.ORG/DOI:10.1061/9780872620087.010.

152. **JORISSEN, H. ET AL. (2020)** CONTRASTING EFFECTS OF CRUSTOSE CORALLINE ALGAE FROM EXPOSED AND SUBCRYPTIC HABITATS ON CORAL RECRUITS. CORAL REEFS, 39(6), PP. 1767–1778. HTTPS://DOI.ORG/10.1007/S00338-020-02002-9.

153. **JOUFFRAY, J.-B. ET AL. (2015)** IDENTIFYING MULTIPLE CORAL REEF REGIMES AND THEIR DRIVERS ACROSS THE HAWAIIAN ARCHIPELAGO. PHILOSOPHICAL TRANSACTIONS OF THE ROYAL SOCIETY B: BIOLOGICAL SCIENCES. ROYAL SOCIETY, 370(1659), P. 20130268. HTTPS://DOI.ORG/10.1098/RSTB.2013.0268.

154. **KAPPES, H., SUNDERMANN, A. AND HAASE, P. (2010)** HIGH SPATIAL VARIABILITY BIASES THE SPACE-FOR-TIME APPROACH IN ENVIRONMENTAL MONITORING. ECOLOGICAL INDICATORS. ELSEVIER LTD, 10(6), PP. 1202–1205. HTTPS://DOI.ORG/10.1016/J.ECOLIND.2010.03.012.

155. KARAMBAS, T. V. AND KOUTITAS, C. (2002) SURF AND SWASH ZONE MORPHOLOGY EVOLUTION INDUCED BY NONLINEAR WAVES. JOURNAL OF WATERWAY, PORT, COASTAL, AND OCEAN ENGINEERING. AMERICAN SOCIETY OF CIVIL ENGINEERS, 128(3), PP. 102–113. HTTPS://DOI.ORG/10.1061/(ASCE)0733-950X(2002)128:3(102).

156. KAYAL, M. ET AL. (2012) PREDATOR CROWN-OF-THORNS STARFISH (ACANTHASTER PLANCI) OUTBREAK, MASS MORTALITY OF CORALS, AND CASCADING EFFECTS ON REEF FISH AND BENTHIC COMMUNITIES, PLOS ONE. PUBLIC LIBRARY OF SCIENCE, 7(10), P. E47363. HTTPS://DOI.ORG/10.1371/JOURNAL.PONE.0047363.

157. KAYAL, M. ET AL. (2015) SEARCHING FOR THE BEST BET IN LIFE-STRATEGY: A QUANTITATIVE APPROACH TO INDIVIDUAL PERFORMANCE AND POPULATION DYNAMICS IN REEF-BUILDING CORALS. ECOLOGICAL COMPLEXITY, 23, PP. 73–84. HTTPS://DOI.ORG/10.1016/J.ECOCOM.2015.07.003.

158. KAYAL, M. ET AL. (2018) PREDICTING CORAL COMMUNITY RECOVERY USING MULTI-SPECIES POPULATION DYNAMICS MODELS. ECOLOGY LETTERS. JOHN WILEY & SONS, LTD, 21(12), PP. 1790–1799. HTTPS://DOI.ORG/10.1111/ELE.13153.

159. KENNEDY, A. B. ET AL. (2000) BOUSSINESQ MODELING OF WAVE TRANSFORMATION, BREAKING, AND RUNUP. I: 1D. JOURNAL OF WATERWAY, PORT, COASTAL, AND OCEAN ENGINEERING. AMERICAN SOCIETY OF CIVIL ENGINEERS, 126(1), PP. 39–47. HTTPS://DOI.ORG/10.1061/(ASCE)0733-950X(2000)126:1(39).

160. KENNEDY, E. V ET AL. (2013) AVOIDING CORAL REEF FUNCTIONAL COLLAPSE REQUIRES LOCAL AND GLOBAL ACTION. CURRENT BIOLOGY, 23(10), PP. 912–918. HTTPS://DOI.ORG/10.1016/J.CUB.2013.04.020.

161. KNOWLTON, N. ET AL. (1981) EVIDENCE FOR DELAYED MORTALITY IN HURRICANE-DAMAGED JAMAICAN STAGHORN CORALS. NATURE, 294(5838), PP. 251–252. HTTPS://DOI.ORG/10.1038/294251A0.

162. KOHLER, K. E. AND GILL, S. M. (2006) CORAL POINT COUNT WITH EXCEL EXTENSIONS (CPCE): A VISUAL BASIC PROGRAM FOR THE DETERMINATION OF CORAL AND SUBSTRATE COVERAGE USING RANDOM POINT COUNT METHODOLOGY. COMPUTERS AND GEOSCIENCES, 32(9), PP. 1259–1269. HTTPS://DOI.ORG/10.1016/J.CAGEO.2005.11.009.

163. KOLB, R. W. (2018) NATIONAL AMBIENT AIR QUALITY STANDARDS (NAAQS). THE SAGE ENCYCLOPEDIA OF BUSINESS ETHICS AND SOCIETY. SAGE PUBLICATIONS, INC. HTTPS://DOI.ORG/10.4135/9781483381503.N817.

164. KORNDER, N. A., RIEGL, B. M. AND FIGUEIREDO, J. (2018) THRESHOLDS AND DRIVERS OF CORAL CALCIFICATION RESPONSES TO CLIMATE CHANGE. GLOBAL CHANGE BIOLOGY, 24(11), PP. 5084–5095. HTTPS://DOI.ORG/10.1111/GCB.14431.

165. KUFFNER, I. B., HICKEY, T. D. AND MORRISON, J. M. (2013) CALCIFICATION RATES OF THE MASSIVE CORAL SIDERASTREA SIDEREA AND CRUSTOSE CORALLINE ALGAE ALONG THE FLORIDA KEYS (USA) OUTER-REEF TRACT. CORAL REEFS, 32(4), PP. 987–997. HTTPS://DOI.ORG/10.1007/S00338-013-1047-8.

166. KWIATKOWSKI, L. ET AL. (2015) CORAL BLEACHING UNDER UNCONVENTIONAL SCENARIOS OF CLIMATE WARMING AND OCEAN ACIDIFICATION. NATURE CLIMATE CHANGE, 5(8), PP. 777–781. HTTPS://DOI.ORG/10.1038/NCLIMATE2655.

167. LAJEUNESSE, T. C. ET AL. (2018) SYSTEMATIC REVISION OF SYMBIODINIACEAE HIGHLIGHTS THE ANTIQUITY AND DIVERSITY OF CORAL ENDOSYMBIONTS. CURRENT BIOLOGY, 28(16), PP. 2570-2580.E6. HTTPS://DOI.ORG/10.1016/J.CUB.2018.07.008.

168. LAMY, T. ET AL. (2016) THREE DECADES OF RECURRENT DECLINES AND RECOVERIES IN CORALS BELIE ONGOING CHANGE IN FISH ASSEMBLAGES. CORAL REEFS. SPRINGER BERLIN HEIDELBERG, 35(1), PP. 293–302. HTTPS://DOI.ORG/10.1007/S00338-015-1371-2.

169. LANGDON, C. AND ATKINSON, M. J. (2005) EFFECT OF ELEVATED PCO2 ON PHOTOSYNTHESIS AND CALCIFICATION OF CORALS AND INTERACTIONS WITH SEASONAL CHANGE IN TEMPERATURE/IRRADIANCE AND NUTRIENT ENRICHMENT. JOURNAL OF GEOPHYSICAL RESEARCH: OCEANS, 110(C9). HTTPS://DOI.ORG/10.1029/2004JC002576.

170. LANGE, I. D. ET AL. (2020) SITE-LEVEL VARIATION IN PARROTFISH GRAZING AND BIOEROSION AS A FUNCTION OF SPECIES-SPECIFIC FEEDING METRICS. DIVERSITY, 12(10). HTTPS://DOI.ORG/10.3390/D12100379.

171. LAVY, A. ET AL. (2015) A QUICK , EASY AND NON-INTRUSIVE METHOD FOR UNDERWATER VOLUME AND SURFACE AREA EVALUATION OF BENTHIC ORGANISMS BY 3D COMPUTER MODELLING, METHODS IN ECOLOGY AND EVOLUTION, 6, PP. 521–531. HTTPS://DOI.ORG/10.1111/2041-210X.12331.

172. LEICHTER, J. J. ET AL. (2013) BIOLOGICAL AND PHYSICAL INTERACTONS ON A TROPICAL ISLAND CORAL REEF: TRANSPORT, AND RETENTION PROCESSES ON MO'OREA, FRENCH POLYNESIA. OCEANOGRAPHY, 26(3), PP. 52–63. HTTPS://DOI.ORG/10.5670/OCEANOG.2012.49.

173. LENIHAN, H. S. ET AL. (2008) REEF STRUCTURE REGULATES SMALL-SCALE SPATIAL VARIATION IN CORAL BLEACHING. MARINE ECOLOGY PROGRESS SERIES, 370, PP. 127–141. HTTPS://WWW.INT-RES.COM/ABSTRACTS/MEPS/V370/P127-141/.

174. LEON, J. X. ET AL. (2015) MEASURING CORAL REEF TERRAIN ROUGHNESS USING "STRUCTURE-FROM-MOTION" CLOSE-RANGE PHOTOGRAMMETRY. GEOMORPHOLOGY. ELSEVIER B.V., 242, PP. 21–28. HTTPS://DOI.ORG/10.1016/J.GEOMORPH.2015.01.030.

175. LERAY, M. ET AL. (2012) ACANTHASTER PLANCI OUTBREAK: DECLINE IN CORAL HEALTH, CORAL SIZE STRUCTURE MODIFICATION AND CONSEQUENCES FOR OBLIGATE DECAPOD ASSEMBLAGES. PLOS ONE. PUBLIC LIBRARY OF SCIENCE, 7(4), P. E35456. HTTPS://DOI.ORG/10.1371/JOURNAL.PONE.0035456.

176. LEUZINGER, S., ANTHONY, K. R. N. AND WILLIS, B. L. (2003) REPRODUCTIVE ENERGY INVESTMENT IN CORALS: SCALING WITH MODULE SIZE. OECOLOGIA. SPRINGER, 136(4), PP. 524–531.

177. LEWIS, B., KENNEDY, E. AND DIAZ-PULIDO, G. (2017) SEASONAL GROWTH AND CALCIFICATION OF A REEF-BUILDING CRUSTOSE CORALLINE ALGA ON THE GREAT BARRIER REEF. MARINE ECOLOGY PROGRESS SERIES, 568, PP. 73–86. HTTPS://WWW.INT-RES.COM/ABSTRACTS/MEPS/V568/P73-86/.

178. **LIANG, J. ET AL. (2015)** BIODIVERSITY INFLUENCES PLANT PRODUCTIVITY THROUGH NICHE EFFICIENCY. PROCEEDINGS OF THE NATIONAL ACADEMY OF SCIENCES. NATIONAL ACADEMY OF SCIENCES, 112(18), PP. 5738–5743. HTTPS://DOI.ORG/10.1073/PNAS.1409853112.

179. **LINNÉR, B. O. AND SELIN, H. (2013)** THE UNITED NATIONS CONFERENCE ON SUSTAINABLE DEVELOPMENT: FORTY YEARS IN THE MAKING. ENVIRONMENT AND PLANNING C: GOVERNMENT AND POLICY, 31(6). HTTPS://DOI.ORG/10.1068/C12287.

180. **LOUGH, J. M. (2008)** CORAL CALCIFICATION FROM SKELETAL RECORDS REVISITED. MARINE ECOLOGY PROGRESS SERIES, 373, PP. 257–264. HTTPS://WWW.INT-RES.COM/ABSTRACTS/MEPS/V373/P257-264/.

181. **LOYA, Y. ET AL. (2001)** CORAL BLEACHING: THE WINNERS AND THE LOSERS. ECOLOGY LETTERS. JOHN WILEY & SONS, LTD, 4(2), PP. 122–131. HTTPS://DOI.ORG/10.1046/J.1461-0248.2001.00203.X.

182. **MACARTHUR, R. H. AND WILSON, E. O. (1967)** THE THEORY OF ISLAND BIOGEOGRAPHY. THE JOURNAL OF WILDLIFE MANAGEMENT. HTTPS://DOI.ORG/10.2307/3799353.

183. **MACHOVINA, B., FEELEY, K. J. AND RIPPLE, W. J. (2015)** BIODIVERSITY CONSERVATION: THE KEY IS REDUCING MEAT CONSUMPTION. SCIENCE OF THE TOTAL ENVIRONMENT, 536, PP. 419–431. HTTPS://DOI.ORG/10.1016/J.SCITOTENV.2015.07.022.

184. **MADI MOUSSA, R. ET AL. (2019)** LONG-TERM COASTLINE MONITORING ON A CORAL REEF ISLAND (MO'OREA, FRENCH POLYNESIA). OCEAN & COASTAL MANAGEMENT, 180, P. 104928. HTTPS://DOI.ORG/10.1016/J.OCECOAMAN.2019.104928.

185. **MADIN, J. ET AL. (2018)** CUMULATIVE EFFECTS OF CYCLONES AND BLEACHING ON CORAL COVER AND SPECIES RICHNESS AT LIZARD ISLAND. MARINE ECOLOGY PROGRESS SERIES, 604, PP. 263–268. HTTPS://WWW.INT-RES.COM/ABSTRACTS/MEPS/V604/P263-268/.

186. **MADIN, J. S. ET AL. (2014)** MECHANICAL VULNERABILITY EXPLAINS SIZE-DEPENDENT MORTALITY OF REEF CORALS. ECOLOGY LETTERS. JOHN WILEY & SONS, LTD, 17(8), PP. 1008–1015. HTTPS://DOI.ORG/10.1111/ELE.12306.

187. **MADIN, J. S. ET AL. (2016)** THE CORAL TRAIT DATABASE, A CURATED DATABASE OF TRAIT INFORMATION FOR CORAL SPECIES FROM THE GLOBAL OCEANS. SCIENTIFIC DATA, 3(1), P. 160017. HTTPS://DOI.ORG/10.1038/SDATA.2016.17.

188. **MADIN, J. S. ET AL. (2020)** PARTITIONING COLONY SIZE VARIATION INTO GROWTH AND PARTIAL MORTALITY. BIOLOGY LETTERS. ROYAL SOCIETY, 16(1), P. 20190727. HTTPS://DOI.ORG/10.1098/RSBL.2019.0727.

189. **MADIN, J. S. AND CONNOLLY, S. R. (2006)** ECOLOGICAL CONSEQUENCES OF MAJOR HYDRODYNAMIC DISTURBANCES ON CORAL REEFS. NATURE, 444(7118), PP. 477–480. HTTPS://DOI.ORG/10.1038/NATURE05328.

190. **MCCLANAHAN, T. R. AND GRAHAM, N. A. J. (2005)** RECOVERY TRAJECTORIES OF CORAL REEF FISH ASSEMBLAGES WITHIN KENYAN MARINE PROTECTED AREAS. MARINE ECOLOGY PROGRESS SERIES, 294, PP. 241–248.

191. MCCORMICK, M. I. (1994) COMPARISON OF FIELD METHODS FOR MEASURING SURFACE TOMOGRAPHY AND THEIR ASSOCIATIONS WITH A TROPICAL REEF FISH ASSEMBLAGE. MARINE ECOLOGY PROGRESS SERIES, 112, PP. 87–96. HTTPS://DOI.ORG/10.3354/MEPS112087.

192. MCGRANAHAN, G., BALK, D. AND ANDERSON, B. (2007) THE RISING TIDE: ASSESSING THE RISKS OF CLIMATE CHANGE AND HUMAN SETTLEMENTS IN LOW ELEVATION COASTAL ZONES. ENVIRONMENT AND URBANIZATION, 19(1), PP. 17–37. HTTPS://DOI.ORG/10.1177/0956247807076960.

193. MCWILLIAM, M. ET AL. (2020) DEFICITS IN FUNCTIONAL TRAIT DIVERSITY FOLLOWING RECOVERY ON CORAL REEFS. PROCEEDINGS OF THE ROYAL SOCIETY B: BIOLOGICAL SCIENCES, 287(1918), P. 20192628. HTTPS://DOI.ORG/10.1098/RSPB.2019.2628.

194. MEYER, J.-Y. ET AL. (2021) INTRODUCED MANGROVES IN THE SOCIETY ISLANDS, FRENCH POLYNESIA (SOUTH PACIFIC): INVASIVE SPECIES OR NOVEL ECOSYSTEM? BIOLOGICAL INVASIONS, 23(8), PP. 2527–2539. HTTPS://DOI.ORG/10.1007/S10530-021-02520-9.

195. MONTAGGIONI, L. F. ET AL. (1997) CONTINUOUS RECORD OF REEF GROWTH OVER THE PAST 14 KY ON THE MID-PACIFIC ISLAND OF TAHITI. GEOLOGY. GEOLOGICAL SOCIETY OF AMERICA, 25(6), PP. 555–558.

196. MONTAGGIONI, L. F. (2005) HISTORY OF INDO-PACIFIC CORAL REEF SYSTEMS SINCE THE LAST GLACIATION: DEVELOPMENT PATTERNS AND CONTROLLING FACTORS. EARTH-SCIENCE REVIEWS, 71(1), PP. 1–75. HTTPS://DOI.ORG/10.1016/J.EARSCIREV.2005.01.002.

197. MOON, T. A. ET AL. (2020) ARCTIC REPORT CARD 2020: GREENLAND ICE SHEET. HTTPS://DOI.ORG/10.25923/MS78-G612.

198. MORAIS, R. A., CONNOLLY, S. R. AND BELLWOOD, D. R. (2020) HUMAN EXPLOITATION SHAPES PRODUCTIVITY–BIOMASS RELATIONSHIPS ON CORAL REEFS. GLOBAL CHANGE BIOLOGY, 26(3), PP. 1295–1305. HTTPS://DOI.ORG/10.1111/GCB.14941.

199. MORAN, P. J. (1988) THE ACANTHASTER PHENOMENON. MONOGRAPH SERIES-AUSTRALIAN INSTITUTE OF MARINE SCIENCE (AUSTRALIA). AUSTRALIAN INSTITUTE OF MARINE SCIENCE.

200. MORGAN, K. M. AND KENCH, P. S. (2012) SKELETAL EXTENSION AND CALCIFICATION OF REEF-BUILDING CORALS IN THE CENTRAL INDIAN OCEAN, MARINE ENVIRONMENTAL RESEARCH, 81, PP. 78–82. HTTPS://DOI.ORG/10.1016/J.MARENVRES.2012.08.001.

201. MORRIS, L. A. ET AL. (2019) NUTRIENT AVAILABILITY AND METABOLISM AFFECT THE STABILITY OF CORAL–SYMBIODINIACEAE SYMBIOSES. TRENDS IN MICROBIOLOGY. ELSEVIER, 27(8), PP. 678–689. HTTPS://DOI.ORG/10.1016/J.TIM.2019.03.004.

202. MUMBY, P. J. (2009) HERBIVORY VERSUS CORALLIVORY: ARE PARROTFISH GOOD OR BAD FOR CARIBBEAN CORAL REEFS? CORAL REEFS, 28(3), PP. 683–690. HTTPS://DOI.ORG/10.1007/S00338-009-0501-0.

203. MUMBY, P. J. AND HARBORNE, A. R. (2010) MARINE RESERVES ENHANCE THE RECOVERY OF CORALS ON CARIBBEAN REEFS, PLOS ONE. PUBLIC LIBRARY OF SCIENCE, 5(1), P. E8657. HTTPS://DOI.ORG/10.1371/JOURNAL.PONE.0008657.

204. **MUSCATINE, L. (1990)** THE ROLE OF SYMBIOTIC ALGAE IN CARBON AND ENERGY FLUX IN REEF CORALS. CORAL REEFS, 25(1.29), PP. 75–87.

205. **MUSCATINE, L. AND PORTER, J. W. (1977)** REEF CORALS: MUTUALISTIC SYMBIOSES ADAPTED TO NUTRIENT-POOR ENVIRONMENTS. BIOSCIENCE, 27(7), PP. 454–460. DOI: HTTPS://DOI.ORG/10.2307/1297526.

206. **MYHRE, G. ET AL. (2013)** IPCC AR5 (2013) CHAPTER 8: ANTHROPOGENIC AND NATURAL RADIATIVE FORCING, IN CLIMATE CHANGE 2013: THE PHYSICAL SCIENCE BASIS. CONTRIBUTION OF WORKING GROUP I TO THE FIFTH ASSESSMENT REPORT OF THE INTERGOVERNMENTAL PANEL ON CLIMATE CHANGE.

207. **NAKAMURA, T. AND NAKAMORI, T. (2009)** ESTIMATION OF PHOTOSYNTHESIS AND CALCIFICATION RATES AT A FRINGING REEF BY ACCOUNTING FOR DIURNAL VARIATIONS AND THE ZONATION OF CORAL REEF COMMUNITIES ON REEF FLAT AND SLOPE: A CASE STUDY FOR THE SHIRAHO REEF, ISHIGAKI ISLAND, SOUTHWEST JAPAN. CORAL REEFS, 28(1), PP. 229–250. HTTPS://DOI.ORG/10.1007/S00338-008-0454-8.

208. **NAUGHTON, P. ET AL. (2015)** SCALING THE ANNOTATION OF SUBTIDAL MARINE HABITATS. PROCEEDINGS OF THE 10TH INTERNATIONAL CONFERENCE ON UNDERWATER NETWORKS & SYSTEMS, PP. 1–5. HTTPS://DOI.ORG/10.1145/2831296.2831342.

209. **NEUMANN, B. ET AL. (2015)** FUTURE COASTAL POPULATION GROWTH AND EXPOSURE TO SEA-LEVEL RISE AND COASTAL FLOODING - A GLOBAL ASSESSMENT. PLOS ONE. PUBLIC LIBRARY OF SCIENCE, 10(3), PP. 1–34. HTTPS://DOI.ORG/10.1371/JOURNAL.PONE.0118571.

210. **NEWMAN, S. P. ET AL. (2015)** REEF FLATTENING EFFECTS ON TOTAL RICHNESS AND SPECIES RESPONSES IN THE CARIBBEAN. JOURNAL OF ANIMAL ECOLOGY, 84(6), PP. 1678–1689. HTTPS://DOI.ORG/10.1111/1365-2656.12429.

211. **NIKURADSE, J. (1933)** STROMUNGSGESETZE IN RAUHEN ROHREN, VDI-FORSCHUNGSHEFT, 361, P. 1.

212. **NUNN, P., KOHLER, A. AND KUMAR, R. (2017)** IDENTIFYING AND ASSESSING EVIDENCE FOR RECENT SHORELINE CHANGE ATTRIBUTABLE TO UNCOMMONLY RAPID SEA-LEVEL RISE IN POHNPEI, FEDERATED STATES OF MICRONESIA, NORTHWEST PACIFIC OCEAN. JOURNAL OF COASTAL CONSERVATION, 21(6), PP. 719–730. HTTPS://DOI.ORG/10.1007/S11852-017-0531-7.

213. **VAN OPPEN, M. J. H. AND LOUGH, J. M. (2009)** CORAL BLEACHING PATTERNS, PROCESSES, CAUSES AND CONSEQUENCES. SPRINGER. EDITED BY E. S. 205. HTTPS://DOI.ORG/10.1007/978-3-319-75393-5.

214. **OPPENHEIMER, M. ET AL. (2019)** SEA LEVEL RISE AND IMPLICATIONS FOR LOW LYING ISLANDS, COASTS AND COMMUNITIES., IPCC SPECIAL REPORT ON THE OCEAN AND CRYOSPHERE IN A CHANGING CLIMATE, 355(6321), PP. 126–129.

215. **PARRAVICINI, V. ET AL. (2006)** A METHOD TO MEASURE THREE-DIMENSIONAL SUBSTRATUM RUGOSITY FOR ECOLOGICAL STUDIES: AN EXAMPLE FROM THE DATE-MUSSEL FISHERY DESERTIFICATION IN THE NORTH-WESTERN MEDITERRANEAN. JOURNAL OF THE MARINE BIOLOGICAL ASSOCIATION OF THE UNITED KINGDOM, 86(4), PP. 689–690.

216. **PARRAVICINI, V. ET AL. (2013)** GLOBAL PATTERNS AND PREDICTORS OF TROPICAL REEF FISH SPECIES RICHNESS. ECOGRAPHY, 36, PP. 1254–1262. HTTPS://DOI.ORG/10.1111/J.1600-0587.2013.00291.X.

217. **PEARCE, F. (2018)** WHEN THE RIVERS RUN DRY, FULLY REVISED AND UPDATED EDITION: WATER-THE DEFINING CRISIS OF THE TWENTY-FIRST CENTURY. BEACON PRESS.

218. **PENIN, L. ET AL. (2007)** HIGH SPATIAL VARIABILITY IN CORAL BLEACHING AROUND MO'OREA (FRENCH POLYNESIA): PATTERNS ACROSS LOCATIONS AND WATER DEPTHS, COMPTES RENDUS BIOLOGIES, 330(2), PP. 171–181. HTTPS://DOI.ORG/HTTPS://DOI.ORG/10.1016/J.CRVI.2006.12.003.

219. **PENIN, L. ET AL. (2010)** EARLY POST-SETTLEMENT MORTALITY AND THE STRUCTURE OF CORAL ASSEMBLAGES, MARINE ECOLOGY PROGRESS SERIES, 408, PP. 55–64. HTTPS://WWW.INT-RES.COM/ABSTRACTS/MEPS/V408/P55-64/.

220. **PENIN, L. ET AL. (2011)** EFFECTS OF PREDATORS AND GRAZERS EXCLUSION ON EARLY POST-SETTLEMENT CORAL MORTALITY, HYDROBIOLOGIA, 663(1), PP. 259–264. HTTPS://DOI.ORG/10.1007/S10750-010-0569-0.

221. **PERERA, A. T. D. ET AL. (2020)** QUANTIFYING THE IMPACTS OF CLIMATE CHANGE AND EXTREME CLIMATE EVENTS ON ENERGY SYSTEMS, NATURE ENERGY, 5(2), PP. 150–159. HTTPS://DOI.ORG/10.1038/S41560-020-0558-0.

222. **PERRY, C. T. ET AL. (2012)** ESTIMATING RATES OF BIOLOGICALLY DRIVEN CORAL REEF FRAMEWORK PRODUCTION AND EROSION: A NEW CENSUS-BASED CARBONATE BUDGET METHODOLOGY AND APPLICATIONS TO THE REEFS OF BONAIRE, CORAL REEFS, 31(3), PP. 853–868. HTTPS://DOI.ORG/10.1007/S00338-012-0901-4.

223. **PERRY, C. T. ET AL. (2015)** REMOTE CORAL REEFS CAN SUSTAIN HIGH GROWTH POTENTIAL AND MAY MATCH FUTURE SEA-LEVEL TRENDS. SCIENTIFIC REPORTS, 5(1), P. 18289. HTTPS://DOI.ORG/10.1038/SREP18289.

224. **PERRY, C. T. ET AL. (2018)** LOSS OF CORAL REEF GROWTH CAPACITY TO TRACK FUTURE INCREASES IN SEA LEVEL. NATURE, 558(7710), PP. 396–400. HTTPS://DOI.ORG/10.1038/S41586-018-0194-Z.

225. **PERRY, C. T. AND HEPBURN, L. J. (2008)** SYN-DEPOSITIONAL ALTERATION OF CORAL REEF FRAMEWORK THROUGH BIOEROSION, ENCRUSTATION AND CEMENTATION: TAPHONOMIC SIGNATURES OF REEF ACCRETION AND REEF DEPOSITIONAL EVENTS. EARTH-SCIENCE REVIEWS, 86(1), PP. 106–144. HTTPS://DOI.ORG/10.1016/J.EARSCIREV.2007.08.006.

226. **PERRY, C. T., LANGE, I. AND JANUCHOWSKI-HARTLEY, F. A. (2018)** REEFBUDGET INDO-PACIFIC: ONLINE RESOURCE AND METHODOLOGY, HTTP://GEOGRAPHY.EXETER.AC.UK/REEFBUDGET/.

227. **PERRY, C. T. AND MORGAN, K. M. (2017A)** BLEACHING DRIVES COLLAPSE IN REEF CARBONATE BUDGETS AND REEF GROWTH POTENTIAL ON SOUTHERN MALDIVES REEFS. SCIENTIFIC REPORTS, 7(1), P. 40581. HTTPS://DOI.ORG/10.1038/SREP40581.

228. PERRY, C. T. AND MORGAN, K. M. (2017B) POST-BLEACHING CORAL COMMUNITY CHANGE ON SOUTHERN MALDIVIAN REEFS: IS THERE POTENTIAL FOR RAPID RECOVERY? CORAL REEFS, 36(4), PP. 1189–1194. HTTPS://DOI.ORG/10.1007/S00338-017-1610-9.

229. PEYROT-CLAUSADE, M. ET AL. (2000) SEA URCHIN AND FISH BIOEROSION ON LA RÉUNION AND MO'OREA REEFS. BULLETIN OF MARINE SCIENCE, 66(2), PP. 477–485.

230. PICKETT, S. T. A. (1989) SPACE-FOR-TIME SUBSTITUTION AS AN ALTERNATIVE TO LONG-TERM STUDIES. LONG-TERM STUDIES IN ECOLOGY, PP. 110–135.

231. PINHEIRO, J. ET AL. (2013) NLME: LINEAR AND NONLINEAR MIXED EFFECTS MODELS, R PACKAGE VERSION, 3(1), P. 111.

232. PLUMPTRE, A. J. ET AL. (2021) WHERE MIGHT WE FIND ECOLOGICALLY INTACT COMMUNITIES? FRONTIERS IN FORESTS AND GLOBAL CHANGE, 4, P. 26. HTTPS://DOI.ORG/10.3389/FFGC.2021.626635.

233. PRATCHETT, M. S. ET AL. (2015) SPATIAL, TEMPORAL AND TAXONOMIC VARIATION IN CORAL GROWTH-IMPLICATIONS FOR THE STRUCTURE AND FUNCTION OF CORAL REEF ECOSYSTEMS. OCEANOGRAPHY AND MARINE BIOLOGY: AN ANNUAL REVIEW. CRC PRESS, PP. 215–295. HTTPS://DOI.ORG/10.1201/B18733.

234. PRATCHETT, M. S. ET AL. (2017) THIRTY YEARS OF RESEARCH ON CROWN-OF-THORNS STARFISH (1986–2016): SCIENTIFIC ADVANCES AND EMERGING OPPORTUNITIES. DIVERSITY, 9(4). HTTPS://DOI.ORG/10.3390/D9040041.

235. PRATCHETT, M. S. ET AL. (2021) RECURRENT MASS-BLEACHING AND THE POTENTIAL FOR ECOSYSTEM COLLAPSE ON AUSTRALIAS GREAT BARRIER REEF. ECOSYSTEM COLLAPSE AND CLIMATE CHANGE. SPRINGER, PP. 265–289.

236. PUTNAM, H. M. ET AL. (2012) ENDOSYMBIOTIC FLEXIBILITY ASSOCIATES WITH ENVIRONMENTAL SENSITIVITY IN SCLERACTINIAN CORALS. PROCEEDINGS OF THE ROYAL SOCIETY B: BIOLOGICAL SCIENCES, 279(1746), PP. 4352–4361. HTTPS://DOI.ORG/10.1098/RSPB.2012.1454.

237. R CORE TEAM (2019) R: A LANGUAGE AND ENVIRONMENT FOR STATISTICAL COMPUTING. VIENNA, AUSTRIA.

238. RÄDECKER, N. ET AL. (2015) NITROGEN CYCLING IN CORALS: THE KEY TO UNDERSTANDING HOLOBIONT FUNCTIONING? TRENDS IN MICROBIOLOGY, 23(8), PP. 490–497. HTTPS://DOI.ORG/10.1016/J.TIM.2015.03.008.

239. RAZAK, T. B. ET AL. (2020) GROWTH RESPONSES OF BRANCHING VERSUS MASSIVE CORALS TO OCEAN WARMING ON THE GREAT BARRIER REEF, AUSTRALIA. SCIENCE OF THE TOTAL ENVIRONMENT, 705, P. 135908. HTTPS://DOI.ORG/10.1016/J.SCITOTENV.2019.135908.

240. REAKA-KUDLA, M. L. (1997) THE GLOBAL BIODIVERSITY OF CORAL REEFS: A COMPARISON WITH RAIN FORESTS. BIODIVERSITY II: UNDERSTANDING AND PROTECTING OUR BIOLOGICAL RESOURCES. JOSEPH HENRY PRESS WASHINGTON, DC, 2, P. 551.

241. **RICHARDSON, L. E., GRAHAM, N. A. J. AND HOEY, A. S. (2017)** CROSS-SCALE HABITAT STRUCTURE DRIVEN BY CORAL SPECIES COMPOSITION ON TROPICAL REEFS. SCIENTIFIC REPORTS. SPRINGER US, 7, P. 11. HTTPS://DOI.ORG/10.1038/S41598-017-08109-4.

242. **RICHMOND, R. (1987)** ENERGETIC RELATIONSHIPS AND BIOGEOGRAPHICAL DIFFERENCES AMONG FECUNDITY, GROWTH AND REPRODUCTION IN THE REEF CORAL POCILLOPORA DAMICORNIS. BULLETIN OF MARINE SCIENCE, 41(2).

243. **RIGNOT, E. ET AL. (2008)** MASS BALANCE OF THE GREENLAND ICE SHEET FROM 1958 TO 2007. GEOPHYSICAL RESEARCH LETTERS. JOHN WILEY & SONS, LTD, 35(20). HTTPS://DOI.ORG/10.1029/2008GL035417.

244. **RINKEVICH, B. (1989)** THE CONTRIBUTION OF PHOTOSYNTHETIC PRODUCTS TO CORAL REPRODUCTION. MARINE BIOLOGY, 101(2), PP. 259–263. HTTPS://DOI.ORG/10.1007/BF00391465.

245. **RIPPLE, W. J. ET AL. (2017)** WORLD SCIENTISTS WARNING TO HUMANITY: A SECOND NOTICE, BIOSCIENCE. HTTPS://DOI.ORG/10.1093/BIOSCI/BIX125.

246. **RISK, M. J. (1972)** FISH DIVERSITY ON A CORAL REEF IN THE VIRGIN ISLANDS. ATOLL RESEARCH BULLETIN.

247. **RITSON-WILLIAMS, R. ET AL. (2009)** NEW PERSPECTIVES ON ECOLOGICAL MECHANISMS AFFECTING CORAL RECRUITMENT ON REEFS. SMITHSONIAN CONTRIBUTIONS TO THE MARINE SCIENCES, (38), PP. 437–457. HTTPS://DOI.ORG/10.5479/SI.01960768.38.437.

248. **ROBERT, M. M. (1988)** HOW MANY SPECIES ARE THERE ON EARTH? SCIENCE. AMERICAN ASSOCIATION FOR THE ADVANCEMENT OF SCIENCE, 241(4872), PP. 1441–1449. HTTPS://DOI.ORG/10.1126/SCIENCE.241.4872.1441.

249. **ROELVINK, F. E. ET AL. (2021)** CORAL REEF RESTORATIONS CAN BE OPTIMIZED TO REDUCE COASTAL FLOODING HAZARDS. FRONTIERS IN MARINE SCIENCE, 8, P. 440. HTTPS://DOI.ORG/10.3389/FMARS.2021.653945.

250. **ROGERS, A., BLANCHARD, J. L. AND MUMBY, P. J. (2014)** VULNERABILITY OF CORAL REEF FISHERIES TO A LOSS OF STRUCTURAL COMPLEXITY. CURRENT BIOLOGY, 24(9), PP. 1000–1005. HTTPS://DOI.ORG/10.1016/J.CUB.2014.03.026.

251. **ROTJAN, R. AND LEWIS, S. (2008)** IMPACT OF CORAL PREDATORS ON TROPICAL REEFS. MARINE ECOLOGY PROGRESS SERIES, 367, PP. 73–91. HTTPS://WWW.INT-RES.COM/ABSTRACTS/MEPS/V367/P73-91/.

252. **ROUSSEL, J.-R. ET AL. (2020)** LIDR: AN R PACKAGE FOR ANALYSIS OF AIRBORNE LASER SCANNING (ALS) DATA. REMOTE SENSING OF ENVIRONMENT, 251, P. 112061. HTTPS://DOI.ORG/10.1016/J.RSE.2020.112061.

253. **ROUSSEL, J.-R. AND AUTY, D. (2021)** AIRBORNE LIDAR DATA MANIPULATION AND VISUALIZATION FOR FORESTRY APPLICATIONS. HTTPS://CRAN.R-PROJECT.ORG/PACKAGE=LIDR.

254. **ROUZÉ, H. ET AL. (2019)** UNIQUE QUANTITATIVE SYMBIODINIACEAE SIGNATURE OF CORAL COLONIES REVEALED THROUGH SPATIO-TEMPORAL SURVEY IN MO'OREA. SCIENTIFIC REPORTS, 9(1). HTTP://DX.DOI.ORG/10.1038/S41598-019-44017-5.

255. **SCHÄFFER, H. A., MADSEN, P. A. AND DEIGAARD, R. (1993)** A BOUSSINESQ MODEL FOR WAVES BREAKING IN SHALLOW WATER, COASTAL ENGINEERING, 20(3), PP. 185–202. HTTPS://DOI.ORG/10.1016/0378-3839(93)90001-O.

256. **SCHIETTEKATTE, N. M. D. ET AL. (2020)** NUTRIENT LIMITATION, BIOENERGETICS AND STOICHIOMETRY: A NEW MODEL TO PREDICT ELEMENTAL FLUXES MEDIATED BY FISHES. FUNCTIONAL ECOLOGY, 34(9), PP. 1857–1869. HTTPS://DOI.ORG/10.1111/1365-2435.13618.

257. **SCHNEIDER, C. A., RASBAND, W. S. AND ELICEIRI, K. W. (2012)** NIH IMAGE TO IMAGEJ: 25 YEARS OF IMAGE ANALYSIS. NATURE METHODS, 9(7), PP. 671–675. HTTPS://DOI.ORG/10.1038/NMETH.2089.

258. **SCOTT, B. D. AND JITTS, H. R. (1977)** PHOTOSYNTHESIS OF PHYTOPLANKTON AND ZOOXANTHELLAE ON A CORAL REEF. MARINE BIOLOGY, 41(4), PP. 307–315. HTTPS://DOI.ORG/10.1007/BF00389097.

259. **SMITH, J. E. ET AL. (2016)** RE-EVALUATING THE HEALTH OF CORAL REEF COMMUNITIES: BASELINES AND EVIDENCE FOR HUMAN IMPACTS ACROSS THE CENTRAL PACIFIC. PROCEEDINGS OF THE ROYAL SOCIETY B: BIOLOGICAL SCIENCES. ROYAL SOCIETY, 283(1822), P. 20151985. HTTPS://DOI.ORG/10.1098/RSPB.2015.1985.

260. **SMITH, L. D. AND HUGHES, T. P. (1999)** AN EXPERIMENTAL ASSESSMENT OF SURVIVAL, RE-ATTACHMENT AND FECUNDITY OF CORAL FRAGMENTS. JOURNAL OF EXPERIMENTAL MARINE BIOLOGY AND ECOLOGY, 235(1), PP. 147–164. HTTPS://DOI.ORG/HTTPS://DOI.ORG/10.1016/S0022-0981(98)00178-6.

261. **SMITH, L. W., BARSHIS, D. AND BIRKELAND, C. (2007)** PHENOTYPIC PLASTICITY FOR SKELETAL GROWTH, DENSITY AND CALCIFICATION OF PORITES LOBATA IN RESPONSE TO HABITAT TYPE. CORAL REEFS, 26(3), PP. 559–567. HTTPS://DOI.ORG/10.1007/S00338-007-0216-Z.

262. **SMITH, S. V AND KEY, G. S. (1975)** CARBON DIOXIDE AND METABOLISM IN MARINE ENVIRONMENTS. LIMNOLOGY AND OCEANOGRAPHY, 20(3), PP. 493–495. HTTPS://DOI.ORG/10.4319/LO.1975.20.3.0493.

263. **SPALDING, M., MCIVOR, A., ET AL. (2014)** MANGROVES FOR COASTAL DEFENCE, WETLANDS INTERNATIONAL AND THE NATURE CONSERVANCY, P. 42.

264. **SPALDING, M., RUFFO, S., ET AL. (2014)** THE ROLE OF ECOSYSTEMS IN COASTAL PROTECTION: ADAPTING TO CLIMATE CHANGE AND COASTAL HAZARDS, OCEAN & COASTAL MANAGEMENT, 90, PP. 50–57. HTTPS://DOI.ORG/10.1016/J.OCECOAMAN.2013.09.007.

265. **STACHOWICZ, J. J. (2001)** MUTUALISM, FACILITATION, AND THE STRUCTURE OF ECOLOGICAL COMMUNITIES: POSITIVE INTERACTIONS PLAY A CRITICAL, BUT UNDERAPPRECIATED, ROLE IN ECOLOGICAL COMMUNITIES BY REDUCING PHYSICAL OR BIOTIC STRESSES IN EXISTING HABITATS AND BY CREATING NEW HABITATS. BIOSCIENCE, 51(3), PP. 235–246. HTTPS://DOI.ORG/10.1641/0006-3568(2001)051[0235:MFATSO]2.0.CO;2.

266. **STAT, M., MORRIS, E. AND GATES, R. D. (2008)** FUNCTIONAL DIVERSITY IN CORAL DINOFLAGELLATE SYMBIOSIS. PROCEEDINGS OF THE NATIONAL ACADEMY OF SCIENCES. NATIONAL ACADEMY OF SCIENCES. HTTPS://DOI.ORG/10.1073/PNAS.0801328105.

267. **STAT, M., YOST, D. M. AND GATES, R. D. (2015)** GEOGRAPHIC STRUCTURE AND HOST SPECIFICITY SHAPE THE COMMUNITY COMPOSITION OF SYMBIOTIC DINOFLAGELLATES IN CORALS FROM THE NORTHWESTERN HAWAIIAN ISLANDS. CORAL REEFS, 34(4), PP. 1075–1086. HTTPS://DOI.ORG/10.1007/S00338-015-1320-0.

268. **STEINFELD, H. ET AL. (2006)** LIVESTOCKS LONG SHADOW: ENVIRONMENTAL ISSUES AND OPTIONS. FOOD \& AGRICULTURE ORG.

269. **STORLAZZI, C. D. ET AL. (2016)** END OF THE CHAIN? RUGOSITY AND FINE-SCALE BATHYMETRY FROM EXISTING UNDERWATER DIGITAL IMAGERY USING STRUCTURE-FROM-MOTION (SFM) TECHNOLOGY. CORAL REEFS. SPRINGER BERLIN HEIDELBERG, 35(3), PP. 889–894. HTTPS://DOI.ORG/10.1007/S00338-016-1462-8.

270. **SWART, D. H. (1974)** OFFSHORE SEDIMENT TRANSPORT AND EQUILIBRIUM BEACH PROFILES. WD MEINEMA.

271. **TEBALDI, C., STRAUSS, B. H. AND ZERVAS, C. E. (2012)** MODELLING SEA LEVEL RISE IMPACTS ON STORM SURGES ALONG US COASTS. ENVIRONMENTAL RESEARCH LETTERS. IOP PUBLISHING, 7(1), P. 14032. HTTPS://DOI.ORG/10.1088/1748-9326/7/1/014032.

272. **TEMMERMAN, S. ET AL. (2013)** ECOSYSTEM-BASED COASTAL DEFENCE IN THE FACE OF GLOBAL CHANGE. NATURE, 504(7478), PP. 79–83. HTTPS://DOI.ORG/10.1038/NATURE12859.

273. **TRAPON, M. L. ET AL. (2013)** POST-SETTLEMENT GROWTH AND MORTALITY RATES OF JUVENILE SCLERACTINIAN CORALS IN MO'OREA, FRENCH POLYNESIA VERSUS TRUNK REEF, AUSTRALIA. MARINE ECOLOGY PROGRESS SERIES, 488, PP. 157–170.

274. **LE TREUT, H., CUBASCH, U. AND ALLEN, M. (2005)** HISTORICAL OVERVIEW OF CLIMATE CHANGE SCIENCE, NOTES, 16.

275. **TRISOS, C. H., MEROW, C. AND PIGOT, A. L. (2020)** THE PROJECTED TIMING OF ABRUPT ECOLOGICAL DISRUPTION FROM CLIMATE CHANGE. NATURE, 580(7804), PP. 496–501. HTTPS://DOI.ORG/10.1038/S41586-020-2189-9.

276. **ULLMAN, S. (1979)** THE INTERPRETATION OF STRUCTURE FROM MOTION. PROCEEDINGS OF THE ROYAL SOCIETY OF LONDON. SERIES B, CONTAINING PAPERS OF A BIOLOGICAL CHARACTER. ROYAL SOCIETY (GREAT BRITAIN), 203(1153), PP. 405–426. HTTPS://DOI.ORG/10.1098/RSPB.1979.0006.

277. **UN GENERAL ASSEMBLY (2015)** TRANSFORMING OUR WORLD: THE 2030 AGENDA FOR SUSTAINABLE DEVELOPMENT UNITED NATIONS UNITED NATIONS, UNITED NATIONS.

278. **UNITED NATIONS (1972)** REPORT ON THE UNITED NATIONS CONFERENCE ON THE HUMAN ENVIRONMENT DECLARATION, STOCKHOLM, 5-16 JUNE 1972, IN.

279. **UNITED NATIONS (1992)** REPORT OF THE UNITED NATIONS CONFERENCE ON ENVIRONMENT AND DEVELOPMENT, RIO DE JANEIRO, 3-14 1992.

280. **UNITED NATIONS (2010)** MILLENNIUM DECLARATION, COMPENDIUM OF SUSTAINABLE ENERGY LAWS, (SEPTEMBER), HTTPS://DOI.ORG/10.1017/CBO9780511664885.009.

281. **UNITED NATIONS (2012)** REPORT OF THE UNITED NATIONS CONFERENCE ON SUSTAINABLE DEVELOPMENT, RIO DE JANEIRO, BRAZIL, 20-22 JUNE 2012. HTTPS://DOI.ORG/10.1111/J.1745-6606.1967.TB00808.X.

282. **VECSEI, A. (2004)** A NEW ESTIMATE OF GLOBAL REEFAL CARBONATE PRODUCTION INCLUDING THE FORE-REEFS. GLOBAL AND PLANETARY CHANGE, 43(1), PP. 1–18. HTTPS://DOI.ORG/10.1016/J.GLOPLACHA.2003.12.002.

283. **VENTI, A., ANDERSSON, A. AND LANGDON, C. (2014)** MULTIPLE DRIVING FACTORS EXPLAIN SPATIAL AND TEMPORAL VARIABILITY IN CORAL CALCIFICATION RATES ON THE BERMUDA PLATFORM. CORAL REEFS, 33(4), PP. 979–997. HTTPS://DOI.ORG/10.1007/S00338-014-1191-9.

284. **VERCELLONI, J. ET AL. (2019)** EXPOSURE, VULNERABILITY, AND RESILIENCY OF FRENCH POLYNESIAN CORAL REEFS TO ENVIRONMENTAL DISTURBANCES. SCIENTIFIC REPORTS, 9(1), P. 1027. HTTPS://DOI.ORG/10.1038/S41598-018-38228-5.

285. **VIVIANI, J. (2019)** EVOLUTIONNARY DYNAMICS OF THE DENTITION IN RELATIONSHIP WITH HABITAT, BEHAVIOUR AND DIET IN PARROTFISHES (SCARINAE, LABRIFORMES). UNIVERSITE DE LYON. HTTPS://TEL.ARCHIVES-OUVERTES.FR/TEL-02994614.

286. **VOGEL, K. ET AL. (2000)** EXPERIMENTAL STUDIES ON MICROBIAL BIOEROSION AT LEE STOCKING ISLAND, BAHAMAS AND ONE TREE ISLAND, GREAT BARRIER REEF, AUSTRALIA: IMPLICATIONS FOR PALEOECOLOGICAL RECONSTRUCTIONS, LETHAIA, 33(3), PP. 190–204. HTTPS://DOI.ORG/10.1080/00241160025100053.

287. **VOLLMER, S. V AND EDMUNDS, P. J. (2000)** ALLOMETRIC SCALING IN SMALL COLONIES OF THE SCLERACTINIAN CORAL SIDERASTREA SIDEREA (ELLIS AND SOLANDER). THE BIOLOGICAL BULLETIN. MARINE BIOLOGICAL LABORATORY, 199(1), PP. 21–28.

288. **DE VOS, J. M. ET AL. (2015)** ESTIMATING THE NORMAL BACKGROUND RATE OF SPECIES EXTINCTION. CONSERVATION BIOLOGY, 29(2), PP. 452–462. HTTPS://DOI.ORG/10.1111/COBI.12380.

289. **VOUSDOUKAS, M. I. ET AL. (2012)** FIELD OBSERVATIONS AND MODELING OF WAVE ATTENUATION OVER COLONIZED BEACHROCKS, CONTINENTAL SHELF RESEARCH, 48, PP. 100–109. HTTPS://DOI.ORG/10.1016/J.CSR.2012.08.015.

290. **VOUSDOUKAS, M. I. ET AL. (2020)** SANDY COASTLINES UNDER THREAT OF EROSION. NATURE CLIMATE CHANGE, 10(3), PP. 260–263. HTTPS://DOI.ORG/10.1038/S41558-020-0697-0.

291. **WALL, K. R. AND STALLINGS, C. D. (2018)** SUBTROPICAL EPIBENTHOS VARIES WITH LOCATION, REEF TYPE, AND GRAZING INTENSITY, JOURNAL OF EXPERIMENTAL MARINE BIOLOGY AND ECOLOGY, 509, PP. 54–65. HTTPS://DOI.ORG/10.1016/J.JEMBE.2018.09.005.

292. **WARD, R. D. ET AL. (2016)** IMPACTS OF CLIMATE CHANGE ON MANGROVE ECOSYSTEMS: A REGION BY REGION OVERVIEW, ECOSYSTEM HEALTH AND SUSTAINABILITY. TAYLOR & FRANCIS, 2(4), P. E01211. HTTPS://DOI.ORG/10.1002/EHS2.1211.

293. **WATSON, J. E. M. ET AL. (2018)** PROTECT THE LAST OF THE WILD. NATURE, 563, PP. 27–30.

294. **WEI, G. AND KIRBY, J. T. (1995)** TIME-DEPENDENT NUMERICAL CODE FOR EXTENDED BOUSSINESQ EQUATIONS. JOURNAL OF WATERWAY, PORT, COASTAL, AND OCEAN ENGINEERING. AMERICAN SOCIETY OF CIVIL ENGINEERS, 121(5), PP. 251–261. HTTPS://DOI.ORG/10.1061/(ASCE)0733-950X(1995)121:5(251).

295. **WESTOBY, M. J. ET AL. (2012)** "STRUCTURE-FROM-MOTION" PHOTOGRAMMETRY: A LOW-COST, EFFECTIVE TOOL FOR GEOSCIENCE APPLICATIONS, GEOMORPHOLOGY. ELSEVIER B.V., 179, PP. 300–314. HTTPS://DOI.ORG/10.1016/J.GEOMORPH.2012.08.021.

296. **WIEBE, W. J., JOHANNES, R. E. AND WEBB, K. L. (1975)** NITROGEN FIXATION IN A CORAL REEF COMMUNITY. SCIENCE. AMERICAN ASSOCIATION FOR THE ADVANCEMENT OF SCIENCE, 188(4185), PP. 257–259. HTTPS://DOI.ORG/10.1126/SCIENCE.188.4185.257.

297. **WILKINSON, C. (2008)** STATUS OF CORAL REEFS OF THE WORLD: 2008 GLOBAL CORAL REEF MONITORING NETWORK AND REEF AND RAINFOREST RESEARCH CENTRE, CORAL REEFS, (3).

298. **WILLIS, T. J. AND ANDERSON, M. J. (2003)** STRUCTURE OF CRYPTIC REEF FISH ASSEMBLAGES: RELATIONSHIPS WITH HABITAT CHARACTERISTICS AND PREDATOR DENSITY. MARINE ECOLOGY PROGRESS SERIES, 257, PP. 209–221. HTTP://DX.DOI.ORG/10.1016/B978-0-08-026482-0.50017-7.

299. **WILSON, M. C. ET AL. (2016)** HABITAT FRAGMENTATION AND BIODIVERSITY CONSERVATION: KEY FINDINGS AND FUTURE CHALLENGES. LANDSCAPE ECOLOGY, 31(2), PP. 219–227. HTTPS://DOI.ORG/10.1007/S10980-015-0312-3.

300. **WOESIK, R. VAN ET AL. (2011)** REVISITING THE WINNERS AND THE LOSERS A DECADE AFTER CORAL BLEACHING. MARINE ECOLOGY PROGRESS SERIES, 434, PP. 67–76. HTTPS://DOI.ORG/10.3354/MEPS09203.

301. **WOODHEAD, A. J. ET AL. (2019)** CORAL REEF ECOSYSTEM SERVICES IN THE ANTHROPOCENE. FUNCTIONAL ECOLOGY, 33(6), PP. 1023–1034. HTTPS://DOI.ORG/10.1111/1365-2435.13331.

302. **WOODROFFE, C. D. AND WEBSTER, J. M. (2014)** CORAL REEFS AND SEA-LEVEL CHANGE. MARINE GEOLOGY, 352, PP. 248–267. HTTPS://DOI.ORG/10.1016/J.MARGEO.2013.12.006.

303. **WORLD POPULATION DATA SHEET (2020)** HTTPS://WWW.PRB.ORG/WP-CONTENT/UPLOADS/2020/07/LETTER-BOOKLET-2020-WORLD-POPULATION.PDF.

# Annexes

*Besides my thesis, I had the chance to interact with a great team on several side projects. In this section, I compile three of these projects that are already published but that cannot be presented as a PhD chapter.*

# 8.1 Otholitometry study

www.nature.com/scientificdata

SCIENTIFIC DATA

Check for updates

OPEN

DATA DESCRIPTOR

## Individual back-calculated size-at-age based on otoliths from Pacific coral reef fish species

Fabien Morat[1,2,7✉], Jérémy Wicquart[1,2,7], Nina M. D. Schiettekatte[1,2], Guillemette de Sinéty[1,2], Jean Bienvenu[1,2], Jordan M. Casey[1,2], Simon J. Brandl[1,2,3,4], Jason Vii[1,2], Jérémy Carlot[1,2], Samuel Degregori[5], Alexandre Mercière[1,2], Pauline Fey[6], René Galzin[1,2], Yves Letourneur[2,6], Pierre Sasal[1,2] & Valeriano Parravicini[1,2✉]

**Somatic growth is a critical biological trait for organismal, population, and ecosystem-level processes. Due to its direct link with energetic demands, growth also represents an important parameter to estimate energy and nutrient fluxes. For marine fishes, growth rate information is most frequently derived from sagittal otoliths, and most of the available data stems from studies on temperate species that are targeted by commercial fisheries. Although the analysis of otoliths is a powerful tool to estimate individual growth, the time-consuming nature of otolith processing is one barrier for collection of comprehensive datasets across multiple species. This is especially true for coral reef fishes, which are extremely diverse. Here, we provide back-calculated size-at-age estimates (including measures of uncertainty) based on sagittal otoliths from 710 individuals belonging to 45 coral reef fish species from French Polynesia. In addition, we provide Von Bertalanffy growth parameters which are useful to predict community level biomass production.**

### Background & Summary

Anthropogenic disturbances, such as resource exploitation, pollution, and climate change, can significantly alter the structure and function of marine ecosystems[1–3]. Species differ in their contributions to ecological processes[4,5]; thus, accurately gauging the susceptibility of ecosystems to disturbances requires high-resolution data on life history traits across a broad suite of species, especially in highly diverse ecosystems[1,6,7]. Somatic growth, the increase of size (and weight) over time, is a critical trait to gauge biological processes that range from individuals to entire ecosystems. For fishes, this trait is particularly important because it links past, present, and future population trajectories in the context of fisheries and stock management; thus, it directly pertains to the provision of ecosystem services. Moreover, somatic growth rate is directly correlated with the energetic demands of organisms. As such, it underlies bioenergetic models that quantify energetic fluxes from individuals to ecosystems[8–10], such as biomass production[11–13] and nutrient cycling[14,15]. Quantifying somatic growth offers an opportunity to examine ecosystem function based on rates of ecological processes rather than employing traditional variables such as abundance or standing biomass[12,16]. Numerous temperate species have been extensively studied due to their commercial importance, but less information exists for the majority of coral reef species[17]. Reef fishes are extremely diverse, display a wide range of life history strategies, and provide an invaluable food source to millions of people in the world's tropics. Therefore, a detailed understanding of reef fish growth rates is critical.

Fish growth parameters can be estimated using several approaches, but those that link age to body size are the most common. Growth can be measured from features preserved in hard structures, such as scales, vertebrae, fin spines, cleithra, opercula, and otoliths[18]. For teleost fishes, the most commonly used and reliable approach to estimate age is the analysis of growth rings found on otoliths. Otoliths are calcified structures of the inner ear that

[1]PSL Université Paris: EPHE-UPVD-CNRS, USR 3278 CRIOBE, Université de Perpignan, 52 Avenue Paul Alduy, 66860, Perpignan, Cedex, France. [2]Laboratoire d'Excellence "CORAIL", EPHE, Perpignan, France. [3]Department of Biological Sciences, Simon Fraser University, Burnaby, BC, V5A 1S6, Canada. [4]CESAB-FRB (Centre de synthèse et d'analyse sur la biodiversité), Institut Bouisson Bertrand, 5 rue de l'école de médecine, 34000, Montpellier, France. [5]Department of Ecology and Evolutionary Biology, University of California Los Angeles, Los Angeles, United States. [6]Université de la Nouvelle-Calédonie, Institut ISEA, BP R4, 98851, Nouméa Cedex, New Caledonia. [7]These authors contributed equally: Fabien Morat, Jérémy Wicquart. ✉e-mail: fabien.morat@univ-perp.fr; valeriano.parravicini@ephe.psl.eu

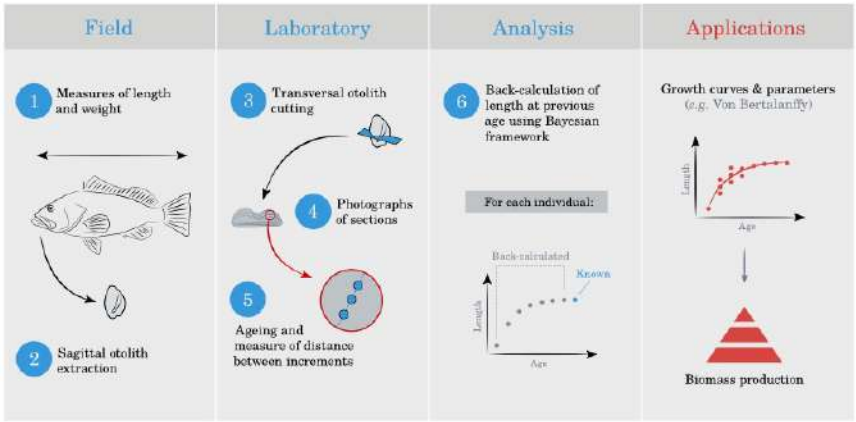


Fig. 1 Illustration of the different steps that allowed the production of the dataset associated to this article.

grow with the deposition of successive calcium carbonate layers, which respond to both circadian and seasonal rhythms[19–22]. Fish growth parameters can then be obtained with various models such as Gompertz, Logistic, or Von Bertalanffy (with the latter being the most commonly used approach)[23]. Such growth models can only be fitted based on a large number of individuals that cover the complete size range of the study species. However, due to the required sample sizes and the need for lethal sampling, obtaining such datasets is time consuming. Further, the raw data that permit size-at-age estimates are often unpublished, available only from technical reports, and/or available for a limited suite of commercial species. Multi-species growth curve comparisons are particularly rare, especially across a wide range of environmental conditions that may influence individual growth rates. Therefore, a back-calculation model that estimates fish size across previous ages based on otoliths represents an alternative to model growth[24].

Here, we provide a comprehensive dataset of raw otolith reads (51 species, 855 individuals) for corals reef fishes, collected across six islands in French Polynesia. Further, we provide the back-calculated size-at-age by species (45 species, 710 individuals); and by species across multiple locations (44 species, 669 individuals) using a Bayesian back-calculation model inspired by Vigliola and Meekan[24]. The inclusion of back-calculated size-at-age values alongside the raw data allows users to fit any regression model in line with their scientific question (Fig. 1). Finally, we provide Von Bertalanffy growth parameters estimated with Bayesian framework both by species and by species across multiple locations (when possible).

## Methods

**Study locations.** Extending over 2,500,000 km$^2$, French Polynesia includes 118 islands spread across five archipelagos: the Society Islands, Tuamotus, Marquesas, Austral Islands and Gambiers. We collected data across four archipelagos, including six distinct islands: Mo'orea and Manuae (Society Islands), Hao and Mataiva (Tuamotus), Mangareva (Gambiers), and Nuku Hiva (Marquesas) (Fig. 2). All fishes were collected in the lagoon and/or reef slope, depending on the accessibility of the respective habitats. Sea surface temperatures (SST) substantially varies around these six islands distributed across French Polynesia (Table 1).

**Sampling design.** Fishes were collected from Mo'orea (March 2016, March 2018, July 2018, and November 2018), Manuae (December 2014), and Nuku Hiva (August 2016 and March 2017) by spearfishing and clove oil, while fishes were collected from Hao (March 2017 and July 2017) and Mangareva (June 2018) only by spearfishing. Additional fishes from Mataiva were bought at the fish market in Tahiti. All applicable international, national, and/or institutional guidelines for the care and use of animals were followed.

*Taxonomy and systematics.* Fishes were identified using Bacchet *et al.*[25] and Moore and Colas[26].

*Permits.* Sample collection was permitted by the French Polynesian government (authorization number: 681MCE/ENV).

**Research methods.** *Field/Laboratory.* In the laboratory, total length (TL) was measured to the nearest millimeter, and fishes were weighed to the nearest 0.1 grams. Then, pairs of sagittae (the largest otoliths of the inner ear) were extracted, cleaned with distilled water, dried, and stored in microtubes.

For each species, otoliths were cut transversely, using a diamond disc saw (Presi Mecatome T210) to obtain a section of 500 µm. Sections were then fixed on a glass side with thermoplastic glue (Crystalbond TM). Small otoliths were directly embedded in the thermoplastic glue and polished to obtain a transversal section. Otoliths were

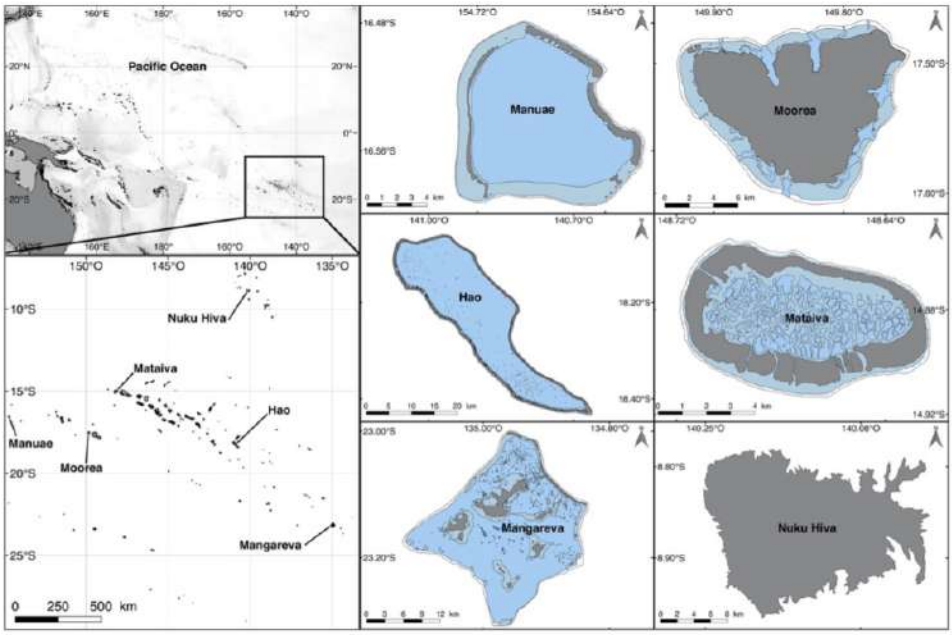


Fig. 2 Map of sampling locations in French Polynesia.

| Island | Minimum | Mean | Maximum |
|---|---|---|---|
| Hao | 25.72 | 27.53 | 29.26 |
| Mangareva | 23.20 | 25.44 | 27.74 |
| Manuae | 26.83 | 28.39 | 29.78 |
| Mataiva | 27.26 | 28.60 | 29.66 |
| Moorea | 26.62 | 28.29 | 30.94 |
| Nuku Hiva | 27.41 | 28.21 | 29.33 |

Table 1. Minimum, mean, and maximum monthly average temperatures (°C) from 2002–2009, across the six locations where fishes were collected. Temperatures are based on Bio-Oracle data[36].

sanded with abrasive discs of decreasing grain size (2,400 and 1,200 grains $cm^{-2}$) and polished with a 0.25 µm diamond suspension to reach the nucleus. All sections were photographed under a Leica DM750 light microscope with a Leica ICC50 HD microscope camera and LAS software (Leica Microsystems). When sections were too large for a single photograph, multiple photographs were taken and assembled with the software Photostitch (Canon).

A standardized transect across the otoliths (from the nucleus to the edge) was chosen for each species. On this transect, fish age was estimated and distances between annual growth increments were measured using the software ImageJ (Supplementary File 1). The age estimation was performed twice by two independent researchers to prevent biases induced by a single observer. When the coefficient of variation between the two observers was greater than 5%, a common reading was assessed for each section[21].

*Back-calculation.* We then used a back-calculation procedure[24] to estimate fish length at previous ages, which we modified to also quantify the uncertainty around the obtained length estimates. This method requires an examination of the shape of the relationship between the length at capture ($L_{cpi}$) and the radius of the otolith at capture across all samples ($R_{cpi}$) as follows:

$$L_{cpi} = L_{0p} - bR_{0p}^{c} + bR_{cpi}^{c} \quad (1)$$

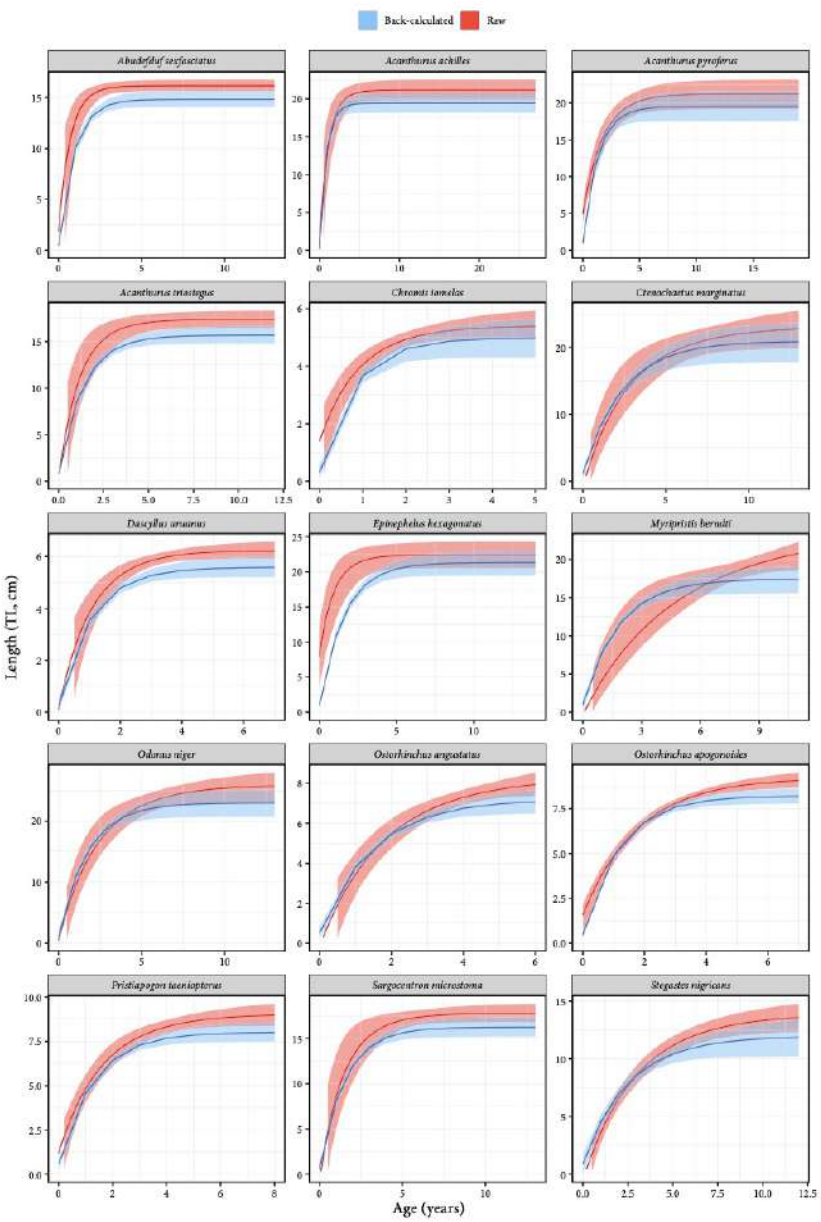


**Fig. 3** Comparison of Von Bertalanffy growth curves fitted on back-calculated size-at-age data (by species across multiple locations) to those fitted on raw data. The 15 species correspond to those with a sufficient number of individuals to fit the model on raw data.

where $L_{0_b}$ and $R_{0_b}$ are the fish size and radius of the otolith at hatching. The regression parameters $b$ and $c$ were estimated by fitting Bayesian models with RStan[27]. We used informative priors for both parameters [$b \sim$ normal (200, 200) and $c \sim$ normal (1, 1)].

| Column | Variable identity | Variable definition | Unit | Storage type | Range |
|---|---|---|---|---|---|
| 1 | *Family* | Family names according to fishbase (https://www.fishbase.de/search.php) | — | Factor | — |
| 2 | *Genus* | Genus names according to fishbase (https://www.fishbase.de/search.php) | — | Factor | — |
| 3 | *Species* | Species names according to fishbase (https://www.fishbase.de/search.php) | — | Factor | — |
| 4 | *ID* | Unique code identifying each individual | — | Factor | — |
| 5 | $Age_i$ | Age *i* | years | Integer | 0–30 |
| 6 | $R_i$ | Otolith radius at age *i* | mm | Numeric | 0.008–3.784 |
| 7 | $Age_{cpt}$ | Age at capture | years | Integer | 0–30 |
| 8 | $R_{cpt}$ | Otolith radius at capture | mm | Numeric | 0.152–3.859 |
| 9 | $L_{cpt}$ | Total length at capture | mm | Numeric | 28.11–984.69 |
| 10 | $L_{0p}$ | Total length at hatching | mm | Numeric | 1.45–4.25 |
| 11 | $R_{0p}$ | Otolith radius at hatching | mm | Numeric | 0.008–0.136 |
| 12 | *Li_sp_m* | Total length (mean) at age *i* calculated by species | mm | Numeric | 1.45–949.65 |
| 13 | *Li_sp_sd* | Standard deviation around the value of *Li_sp_m* | mm | Numeric | 0–81.87 |
| 14 | *Li_sploc_m* | Total length (mean) at age *i* calculated by species and location | mm | Numeric | 1.45–948.67 |
| 15 | *Li_sploc_sd* | Standard deviation around the value of *Li_sploc_m* | mm | Numeric | 0–87.42 |
| 16 | *Weight* | Wet body mass at capture | g | Numeric | 0.4–12,950 |
| 17 | *Location* | Island or archipelago of the sampling | — | Factor | — |
| 18 | *Observer* | Name of person that made the otolith reading | — | Factor | — |

**Table 2.** Description of the variables included in the dataset.

For some individuals, it was not possible to measure the $R_{0p}$ value. Nevertheless, these individuals were still included in the back-calculation model. To do so, we included all missing $R_{0p}$ values as parameters in the model that are estimated in the posterior[28]. Specifically, these missing $R_{0p}$ values were simultaneously modelled with the known $R_{0p}$ values, so that their prior distribution was defined by the distribution of the known $R_{0p}$ values. These prior distributions were then updated with the information provided by the aforementioned relationship (Eq. 1). Consequently, each missing $R_{0p}$ value had a unique posterior distribution.

For all 4,000 iterations used to fit the models, we used parameters *b* and *c* (Eq. 1), to then quantify another parameter, the parameter *a*, combining both (Eq. 2).

$$a[i] = L_{0p} - b \times R_{0p}[i]^c \tag{2}$$

Next, the back-calculation with the Modified Fry (MF) model (Eq. 3)[29] was applied to quantify fish lengths at all ages for each individual, using parameter *a* for each iteration.

$$\text{MF model: } L_i = a + exp\left(ln(L_{0p} - a) + \frac{[ln(L_{cpt} - a) - ln(L_{0p} - a)]\,[ln(R_i) - ln(R_{0p})]}{[ln(R_{cpt}) - ln(R_{0p})]}\right) \tag{3}$$

where $L_i$ and $R_i$ are the fish length and otolith radius at age *i*, $L_{0p}$ and $R_{0p}$ are the fish size and radius of otolith at hatching. $L_{0p}$ is provided for each species (Online-only Table 1).

We calculated $L_i$ for the species that had sufficient replicates, and when possible also per species in each location separately. The estimation of parameters *b* and *c* (Eq. 1) required at least two values of $R_{0p}$, so the back-calculation was not carried out when only one $R_{0p}$ was available for a given species (or a given species in a certain location).

Individuals with estimated age at capture of one year where not used for back-calculation.

Finally, we reported the averages and standard deviations of those length estimates based on the 4,000 iterations. As such, the back-calculated estimates include a measure of uncertainty that can be integrated in the future applications.

*Von bertalanffy growth curves.* The Von Bertalanffy growth model (Eq. 4) is the most frequently used model to describe fish growth. This model is defined as:

$$Lt = L_\infty(1 - e^{-K(t-t_0)}) \tag{4}$$

where *Lt* is the average length at age *i*, $L_\infty$ is the asymptotic average length, *K* is the growth rate coefficient, and $t_0$ is the age when the average length was zero. In order to validate the accuracy of our back-calculated size-at-age data,

we compared growth curves fitted with raw data (total length at capture and estimated age at capture) to those fitted with back-calculated data. As back-calculated size-at-age data within individuals are highly auto-correlated, we designed a Bayesian hierarchical model that takes this auto-correlation into account by fitting individual growth curves as well as an average population-level growth curve. The model was applied on back-calculated data with at least five individuals and for individuals with an age at capture that was greater than two years.

We fitted models both for each species and for each species per location. In all models, we used informative priors for growth parameters extracted from FishBase (https://www.fishbase.se/search.php). We ran models with 2,000 iterations and a warmup of 1,000. When the $\hat{R}$ was above one, indicating non-convergence of the Markov Chains Monte Carlo (MCMC), we ran models again augmenting iterations to 4,000 with a warmup of 2,000. If despite that, model convergence was still not achieved, we use MCMC chain plots of the model parameters to remove the individual(s) responsible for non-convergence.

As a comparison, we also ran a general non-linear Bayesian model on the raw data (*i.e.* using size and age at capture only). Back-calculated data contains more points (multiple points for each individual) than raw data (one point by individual), so the comparison was limited to the species with a sufficient number of individuals ($n > 10$) and age range in the raw data. These models were run using the package *brms*[30].

All analyses were done with the software R v.3.6.3[31] and the packages *rstan* (2.19.3), *tidyverse* (1.3.0)[32], *plyr* (1.8.6)[33], rfishbase (3.0.4)[34], and *brms* (2.13.0)[30].

## Data Records

The dataset is publicly accessible in the permanent figshare repository (https://doi.org/10.6084/m9.figshare.12156159.v5)[35]. This dataset consists of:

1. 855 individuals from 51 fish species in 15 families collected across six locations in French Polynesia,
2. Fish total length and weight (when measured) for each individual,
3. Age estimations and back-calculated size-at-age for each individual, by species (45 species and 710 individuals) and by species across multiple locations (44 species, and 669 individuals).

## Technical Validation

- The validity of fish names and families were verified on the World Register of Marine Species (WoRMS; http://www.marinespecies.org/index.php) and FishBase (https://www.fishbase.in/search.php).
- Each otolith was read twice by two readers to limit observer biases for age estimations. When the coefficient of variation between observers was greater than 5%, a common reading was assessed for each section[21]. Moreover, for each species, we provide a photograph of an otolith section with annual increments and reading axes (Supplementary File 1).
- To validate the accuracy of back-calculated data, growth curves fitted on back-calculated size-at-age were compared to those from raw data (total length at capture and estimated age at capture) (Fig. 3). This comparison was not possible for a species when the number of collected individuals was too low to fit a growth curve. Comparisons were possible for fifteen species, and for each of them, the 95% credible intervals overlapped between growth curves fitted on back-calculated data *versus* raw data, suggesting negligible differences between the two approaches (Fig. 3). Moreover, for all species, the curves from back-calculated data were always below those from raw data, indicating no overestimation of $L_\infty$. Further, because the back-calculated lengths also include the lengths at age zero, the length at hatching is more realistically represented in the regression models from the back-calculated data. Consequently, when using back-calculation, estimates of $K$ tend to be higher and $L_\infty$ tend to be lower. The Von Bertalanffy growth parameters from our back-calculated size-at-age data by species and species across multiple locations are available online (Online-Only Table 2).
- Further, Von Bertalanffy growth parameters estimated from otoliths were extracted from published articles, book chapters, reports and Ph.D. theses and compared to back-calculated parameters from our study (Online-only Table 3). For most species, the growth parameters from our study were similar to those in the literature. Differences may stem from different geographical locations (different temperatures, primary productivity, etc.), the number of analyzed fishes, different length measurements (standard, fork, or total length), or variations in modeling approaches.
- Finally, we compared our age estimates to the maximum ages reported in the literature (Online-only Table 3). Comparisons were possible for species with available data (seventeen species). Only five species were above the maximum reported age (*Caranx melanpygus, Cephalopholis urodeta, Chlorurus spilurus, Epinephelus merra, Plectropomus laevis*).

## Usage Notes

The dataset is provided as a csv file, which can be directly used by most statistical software. It contains eighteen variables, as described in Table 2. Additional growth parameters can be obtained by fitting other growth models (*e.g.* Gompertz model) using the variables '$Age_i$' and '*Li_sp_m*' (species across all locations) or '*Li_sploc_m*' (species by location).

Back-calculated data are highly auto-correlated, so we recommend using a hierarchical structure to fit growth models.

Within the dataset, 'NA' indicates a missing value. Missing values are present for the variables '$R_i$' ($n = 387$), '$R_{0p}$' ($n = 2{,}811$), '*Li_sp_m*' ($n = 410$), '*Li_sp_sd*' ($n = 410$), '*Li_sploc_m*' ($n = 757$), '*Lp_sploc_sd*' ($n = 757$), and '*Weight*' ($n = 603$). For the variable '$R_i$', missing values correspond to individuals for which it was impossible to estimate the radius at hatching from photographs. The '$R_{0p}$' values correspond to '$R_i$' values where '$Age_i$' is equal to zero. Because the '$R_{0p}$' value is the same for all '$Age_i$' of a given individual ('ID'), a large number of NAs arises as soon as the '$R_i$' value

is missing (where '*Age*,' is equal to zero). For the variables '*Li_sp_m*', '*Li_sp_sd*', '*Li_sploc_m*', and '*Lp_sploc_sd*', missing values correspond to values with insufficient numbers of individuals or known '$R_{0p}$' measurements to accurately fit the Bayesian back-calculation model. The number of NAs for the variables '*Li_sp_m*' and '*Li_sp_sd*' (estimates by species) is lower than the number of NAs for the variables '*Li_sploc_m*' and '*Lp_sploc_sd*' (estimates for species by location). Finally, for the variable '*Weight*', missing values are the result of missing sampling measurements.

## Code availability

The code to generate the back-calculated size-at-age data is available at https://github.com/JWicquart/fish_growth.

Received: 21 April 2020; Accepted: 5 October 2020;
Published online: 27 October 2020

## References

1. Dulvy, N. K., Metcalfe, J. D., Glanville, J., Pawson, M. G. & Reynolds, J. D. Fishery stability, local extinctions, and shifts in community structure in skates. *Conserv. Biol.* **14**, 283–293, https://doi.org/10.1046/j.1523-1739.2000.98540.x (2000).
2. Hoegh-Guldberg, O. & Bruno, J. F. The Impact of Climate Change on the World's Marine Ecosystems. *Science* **328**, 1523–1528, https://doi.org/10.1126/science.1189930 (2010).
3. Jackson, J. B. C. *et al.* Historical Overfishing and the Recent Collapse of Coastal Ecosystems. *Science* **293**, 629–637, https://doi.org/10.1126/science.1059199 (2001).
4. William, W. L. C., Reg, W., Telmo, M., Tony, J. P. & Daniel, P. Intrinsic vulnerability in the global fish catch. *Mar. Ecol. Prog. Ser.* **333**, 1–12 (2007).
5. Graham, N. A. J. *et al.* Extinction vulnerability of coral reef fishes. *Ecol. Lett.* **14**, 341–348, https://doi.org/10.1111/j.1461-0248.2011.01592.x (2011).
6. Dulvy, N. K., Sadovy, Y. & Reynolds, J. D. Extinction vulnerability in marine populations. *Fish. Fish.* **4**, 25–64 (2003).
7. Cheung, W. W., Pitcher, T. J. & Pauly, D. A fuzzy logic expert system to estimate intrinsic extinction vulnerabilities of marine fishes to fishing. *Biol. Conserv.* **124**, 97–111 (2005).
8. Frost, P. C. *et al.* Threshold elemental ratios of carbon and phosphorus in aquatic consumers. *Ecol. Lett.* **9**, 774–779 (2006).
9. Schindler, D. E. & Eby, L. A. Stoichiometry of fishes and their prey: implications for nutrient recycling. *Ecology* **78**, 1816–1831 (1997).
10. Schreck, C. B. & Moyle, P. B. *Methods for fish biology*. Schreck, Carl B. & Moyle, Peter B. edn, (American fisheries society, 1990).
11. Brandl, S. J. *et al.* Demographic dynamics of the smallest marine vertebrates fuel coral reef ecosystem functioning. *Science* **364**, 1189–1192 (2019).
12. Depczynski, M., Fulton, C. J., Marnane, M. J. & Bellwood, D. R. Life history patterns shape energy allocation among fishes on coral reefs. *Oecologia* **153**, 111–120 (2007).
13. Morais, R. A. & Bellwood, D. R. Pelagic Subsidies Underpin Fish Productivity on a Degraded Coral Reef. *Curr. Biol.* **29**, 1521–1527. e1526 (2019).
14. Barneche, D. R. & Allen, A. P. Embracing general theory and taxon-level idiosyncrasies to explain nutrient recycling. *Proc. Natl. Acad. Sci. U. S. A.* **112**, 6248–6249 (2015).
15. Barneche, D. R. & Allen, A. P. The energetics of fish growth and how it constrains food-web trophic structure. *Ecol. Lett.* **21**, 836–844 (2018).
16. Brandl, S. J. *et al.* Coral reef ecosystem functioning: eight core processes and the role of biodiversity. *Front. Ecol. Environ.* **17**, 445–454 (2019).
17. Taylor, B., Rhodes, K., Marshell, A. & McIlwain, J. Age-based demographic and reproductive assessment of orangespine *Naso lituratus* and bluespine *Naso unicornis* unicornfishes. *J. Fish. Biol.* **85**, 901–916, https://doi.org/10.1111/jfb.12479 (2014).
18. Campana, S. Accuracy, precision and quality control in age determination, including a review of the use and abuse of age validation methods. *J. Fish. Biol.* **59**, 197–242 (2001).
19. Jolivet, A., Bardeau, J., Fablet, R., Paulet, Y. & de Pontual, H. Understanding otolith biomineralization processes: new insights into mircoscale spatial distribution of organic and mineral fractions from Raman microspectrometry. *Anal. Bioanal. Chem.* **392**, 551–560 (2008).
20. Jolivet, A., Bardeau, J.-F., Fablet, R., Paulet, Y.-M. & de Pontual, H. How do the organic and mineral fractions drive the opacity of fish otoliths? Insights using Raman microspectrometry. *Can. J. Fish. Aq. Sci.* **70**, 711–719, https://doi.org/10.1139/cjfas-2012-0298 (2013).
21. Panfili, J., de Pontual, H., Troadec, H. & Wright, P. J. *Manuel de sclérochronologie des poissons*. Coédition Ifremer-IRD, Panfili, J., de Pontual, H., Troadec, H. & Wright, P. J. (eds). France, 464 pp edn (2002).
22. Pannella, G. Fish otolith: daily growth layers and periodical patterns. *Science* **173**, 1124–1126, https://doi.org/10.1126/science.173.4002.1124 (1971).
23. Katsanevakis, S. Modelling fish growth: model selection, multi-model inference and model selection uncertainty. *Fish. Res.* **81**, 229–235 (2006).
24. Vigliola, L. & Meekan, M. G. In *Tropical fish otoliths: information for assessment, management and ecology Methods and technologies in fish biology and fisheries* Ch. The back-calculation of fish growth from otoliths., 174-211 (Spinger, 2009).
25. Bacchet, P., Zysman, T. & Lefèvre, Y. *Guide des poissons de Tahiti et ses îles*. (Au vent des îles, 2006).
26. Moore, B. & Colas, B. *Identification guide to the common coastal food fishes of the Pacific Islands region*. (2016).
27. RStan: the R interface to Stan. R package version 2.19.2. http://mc-stan.org/ (2018).
28. Stan Modeling Language Users Guide and Reference Manual, Version 2.18.0, http://mc-stan.org (2018).
29. Vigliola, L., Harmelin-Vivien, M. & Meekan, M. G. Comparison of techniques of back-calculation of growth and settlement marks from the otoliths of three species of *Diplodus* from the Mediterranean Sea. *Can. J. Fish. Aq. Sci.* **57**, 1291–1299 (2000).
30. Bürkner, P.-C. brms: An R Package for Bayesian Multilevel Models Using Stan. *J. Stat. Softw.* **80**, 28, https://doi.org/10.18637/jss.v080.i01 (2017).
31. R: a Language and environment for statistical computing. R Foundation for Statistical Computing (Austria, Vienna, 2019).
32. Wickham, H. *et al.* Welcome to the Tidyverse. *J. Open Source Softw.* **4**, 1686, https://doi.org/10.21105/joss.01686 (2019).
33. Wickham, H. The split-apply-combine strategy for data analysis. *J. Stat. Softw.* **40**, 1–29 (2011).
34. Boettiger, C., Lang, D. T. & Wainwright, P. rfishbase: exploring, manipulating and visualizing FishBase data from R. *J. Fish. Biol.* **81**, 2030–2039, https://doi.org/10.1111/j.1095-8649.2012.03464.x (2012).
35. Morat, F. *et al.* Individual back-calculated size-at-age based on otoliths from Pacific coral reef fish species. *figshare* https://doi.org/10.6084/m9.figshare.12156159.v5 (2020).
36. Tyberghein, L. *et al.* Bio-ORACLE: a global environmental dataset for marine species distribution modelling. *Glob. Ecol. Biogeogr.* **21**, 272–281 (2012).
37. Shadrin, A. & Emel'yanova, N. Embryonic-larval development and some data on the reproductive biology of *Abudefduf sexfasciatus* (Pomacentridae: Perciformes). *J. Ichthyol.* **47**, 67–80 (2007).

38. McCormick, M. I. Delayed metamorphosis of a tropical reef fish (*Acanthurus triostegus*): a field experiment. *Mar. Ecol. Prog. Ser.* **176**, 25–38 (1999).
39. Leis, J. M. & Carson-Ewart, B. M. *The larvae of Indo-Pacific coastal fishes: an identification guide to marine fish larvae*. Vol. 2 (Brill, 2000).
40. Hutapea, J. H. & Slamet, B. Morphological development of Napoleon wrasse, *Cheilinus undulatus* larvae. *Indonesian Aquaculture J.* **1**, 145–151 (2006).
41. Westneat, M. W. & Alfaro, M. E. Phylogenetic relationships and evolutionary history of the reef fish family Labridae. *Mol. Phylogenet. Evol.* **36**, 370–390, https://doi.org/10.1016/j.ympev.2005.02.001 (2005).
42. Choat, J. H., Klanten, O. S., Van Herwerden, L., Robertson, D. R. & Clements, K. D. Patterns and processes in the evolutionary history of parrotfishes (Family Labridae). *Biol. J. Linnean Soc.* **107**, 529–557, https://doi.org/10.1111/j.1095-8312.2012.01959.x (2012).
43. Emel'yanova, N., Pavlov, D. & Thuan, L. Hormonal stimulation of maturation and ovulation, gamete morphology, and raising of larvae in *Dascyllus trimaculatus* (Pomacentridae). *J. Ichthyol.* **49**, 249–263 (2009).
44. Kawabe, K. & Kohno, H. Morphological development of larval and juvenile blacktip grouper, *Epinephelus fasciatus*. *Fish. Sci.* **75**, 1239–1251 (2009).
45. Hussain, N. A. & Higuchi, M. Larval rearing and development of the brown spotted grouper, *Epinephelus tauvina* (Forskål). *Aquaculture* **19**, 339–350 (1980).
46. Ukawa, M., Higuchi, M. & Mito, S. Spawning habits and early life history of a serranid fish, *Epinephelus akaara* (Temminck et Schlegel). *Jpn. J. Ichthyol.* **13**, 156–161 (1966).
47. Lim, L. Larviculture of the greasy grouper *Epinephelus tauvina* F. and the brown-marbled grouper *E. fuscoguttatus* F. in Singapore. *J. World Aquacult. Soc.* **24**, 262–274 (1993).
48. Colin, P., Koenig, C. & Laroche, W. In *Biology, fisheries and culture of tropical groupers and snappers. ICLARM Conf. Proc.* Vol. 48 (eds F. Arreguín-Sánchez, J.L. Munro, M.C. Balgos, & D. Pauly) 399-414 (1996).
49. Duray, M. N., Estudillo, C. B. & Alpasan, L. G. The effect of background color and rotifer density on rotifer intake, growth and survival of the grouper (*Epinephelus suillus*) larvae. *Aquaculture* **146**, 217–224 (1996).
50. Duray, M. N., Estudillo, C. B. & Alpasan, L. G. Larval rearing of the grouper *Epinephelus suillus* under laboratory conditions. *Aquaculture* **150**, 63–76 (1997).
51. James, C., Al-Thobaiti, S., Rasem, B. & Carlos, M. Breeding and larval rearing of the camouflage grouper *Epinephelus polyphekadion* (Bleeker) in the hypersaline waters of the Red Sea coast of Saudi Arabia. *Aquac. Res.* **28**, 671–681 (1997).
52. Glamuzina, B., Glavic, N., Tutman, P., Kozul, V. & Skaramuca, B. Egg and early larval development of laboratory reared goldblotch grouper, *Epinephelus costae* (Steindachner, 1878)(Pisces, Serranidae). *Sci. Mar.* **64**, 341–345 (2000).
53. Glamuzina, B. *et al.* Egg and early larval development of laboratory reared dusky grouper, *Epinephelus marginatus* (Lowe, 1834) (Picies, Serranidae). *Sci. Mar.* **62**, 373–378 (1998).
54. Leu, M.-Y., Liou, C.-H. & Fang, L.-S. Embryonic and larval development of the malabar grouper, *Epinephelus malabaricus* (Pisces: Serranidae). *J. Mar. Biol. Assoc. U.K.* **85**, 1249 (2005).
55. Jagadis, I., Ignatius, B., Kandasami, D. & Khan, M. A. Embryonic and larval development of honeycomb grouper *Epinephelus merra* Bloch. *Aquac. Res.* **37**, 1140–1145 (2006).
56. Yoseda, K. *et al.* Effects of temperature and delayed initial feeding on the growth of Malabar grouper (*Epinephelus malabaricus*) larvae. *Aquaculture* **256**, 192–200 (2006).
57. Ma, Z., Guo, H., Zhang, N. & Bai, Z. State of art for larval rearing of grouper. *Intern. J. Aquac.* **3**, 63–72, https://doi.org/10.5376/ija.2013.03.0013 (2013).
58. Kimura, S. & Kiriyama, T. Development of eggs, larvae and juveniles of the labrid fish, *Halichoeres poecilopterus*, reared in the laboratory. *Jpn. J. Ichthyol.* **39**, 371–377 (1993).
59. Suzuki, K. & Hioki, S. Spawning behavior, eggs, and larvae of the lutjanid fish, *Lutjanus kasmira*, in an aquarium. *Jpn. J. Ichthyol.* **26**, 161–166 (1979).
60. Pavlov, D., Emel'yanova, N., Thuan, L. T. B. & Ha, V. T. Reproduction and initial development of manybar goatfish *Parupeneus multifasciatus* (Mullidae). *J. Ichthyol.* **51**, 604 (2011).
61. Masuma, S., Tezuka, N. & Teruya, K. Embryonic and morphological development of larval and juvenile coral trout, *Plectropomus leopardus*. *Jpn. J. Ichthyol.* **40**, 333–342 (1993).
62. May, R. C., Popper, D. & McVEY, J. P. Rearing and larval development of *Siganus canaliculatus* (Park)(Pisces: Siganidae). *Micronesica* **10**, 285–298 (1974).
63. Popper, D., May, R. & Lichatowich, T. An experiment in rearing larval *Siganus vermiculatus* (Valenciennes) and some observations on its spawning cycle. *Aquaculture* **7**, 281–290 (1976).
64. Bryan, P. G. & Madraisau, B. B. Larval rearing and development of *Siganus lineatus* (Pisces: Siganidae) from hatching through metamorphosis. *Aquaculture* **10**, 243–252 (1977).
65. Hara, S., Duray, M. N., Parazo, M. & Taki, Y. Year-round spawning and seed production of the rabbitfish, *Siganus guttatus*. *Aquaculture* **59**, 259–272 (1986).
66. Choat, J. H. & Robertson, D. R. In *Coral reef fishes: dynamics and diversity in a complex ecosystem*. (ed Academic Press. San Diego. California. USA) Ch. 3: Age-based studies, 57–80 (2002).
67. Craig, P. C., Choat, J. H., Axe, L. M. & Saucerman, S. Population biology and harvest of the coral reef surgeonfish *Acanthurus lineatus* in American Samoa. *Fish. Bull.* **95**, 680–693 (1997).
68. Gust, N., Choat, J. & Ackerman, J. Demographic plasticity in tropical reef fishes. *Mar. Biol.* **140**, 1039–1051, https://doi.org/10.1007/s00227-001-0773-6 (2002).
69. Ralston, S. & Williams, H. A. Age and growth of *Lutjanus kasmira, Lethrinus rubrioperculatus, Acanthurus lineatus*, and *Ctenochaetus striatus* from American Samoa. (Southwest Fisheries Center, Honolulu Laboratory, National Marine Fisheries, 1988).
70. Sudekum, A. E., Parrish, J. D., Radtke, R. L. & Ralston, S. Life history and ecology of large jacks in undisturbed, shallow, oceanic communities*. *Fish. Bull.* **89**, 493–513 (1991).
71. Donovan, M. K., Friedlander, A. M., DeMartini, E. E., Donahue, M. J. & Williams, I. D. Demographic patterns in the peacock grouper (*Cephalopholis argus*), an introduced Hawaiian reef fish. *Environ. Biol. Fishes* **96**, 981–994, https://doi.org/10.1007/s10641-012-0095-1 (2013).
72. Mapleston, A. *et al.* Comparative biology of key inter-reefal serranid species on the Great Barrier Reef. *Project Milestone Report to the Marine and Tropical Sciences Research Facility*. 55 pp (Reef and Rainforest Research Centre Limited, Cairns 2009).
73. Mehanna, S. F., Osman, Y. A. A., Khalil, M. T. & Hassan, A. Age and growth, mortality and exploitation ratio of *Epinephelus summana* (Forsskål, 1775) and *Cephalopholis argus* (Schneider, 1801) from the Egyptian Red Sea coast, Hurghada fishing area. *Egypt. J. Aquat. Biol. Fish.* **23**, 65–75, https://doi.org/10.21608/ejabf.2019.52050 (2019).
74. Pears, R. J. *Comparative demography and assemblage structure of serranid fishes: implications for conservation and fisheries management* Ph.D thesis, James Cook University, (2005).
75. Moore, B. *et al.* Monitoring the Vulnerability and Adaptation of Coastal Fisheries to Climate Change: Pohnpei, Federated States of Micronesia. *Report No. Assement Report N°2, February-March* **2014**, 116 (2015).
76. Payet, S. D. *et al.* Hybridisation among groupers (genus Cephalopholis) at the eastern Indian Ocean suture zone: taxonomic and evolutionary implications. *Coral Reefs* **35**, 1157–1169, https://doi.org/10.1007/s00338-016-1482-4 (2016).
77. Fry, G., Brewer, D. & Venables, W. Vulnerability of deepwater demersal fishes to commercial fishing: Evidence from a study around a tropical volcanic seamount in Papua New Guinea. *Fish. Res.* **81**, 126–141, https://doi.org/10.1016/j.fishres.2006.08.002 (2006).

78. DeMartini, E. E. *et al.* Comparative growth, age at maturity and sex change, and longevity of Hawaiian parrotfishes, with bomb radiocarbon validation. *Can. J. Fish. Aq. Sci.* **75**, 580–589, https://doi.org/10.1139/cjfas-2016-0523 (2018).
79. Taylor, B. M. & Choat, J. H. Comparative demography of commercially important parrotfish species from Micronesia. *J. Fish. Biol.* **84**, 383–402, https://doi.org/10.1111/jfb.12294 (2014).
80. Trip, E. L., Choat, J. H., Wilson, D. T. & Robertson, D. R. Inter-oceanic analysis of demographic variation in a widely distributed Indo-Pacific coral reef fish. *Mar. Ecol. Prog. Ser.* **373**, 97–109, https://doi.org/10.3354/meps07755 (2008).
81. Fidler, R. Y., Carroll, J., Rynerson, K. W., Matthews, D. F. & Turingan, R. G. Coral reef fishes exhibit beneficial phenotypes inside marine protected areas. *PLoS ONE* 13, e0193426, https://doi.org/10.1371/journal.pone.0193426 (2018).
82. Ochavillo, D., Tofaeono, S., Sabater, M. & Trip, E. L. Population structure of *Ctenochaetus striatus* (Acanthuridae) in Tutuila, American Samoa: The use of size-at-age data in multi-scale population size surveys. *Fish. Res.* **107**, 14–21, https://doi.org/10.1016/j.fishres.2010.10.001 (2011).
83. Moore, B., Alefaio, S. & Siaosi, F. Monitoring the Vulnerability and Adaptation of Coastal Fisheries to Climate Change: Funafuti Atoll, Tuvalu. *Report No. Assessment Report N°2, April-May* **2013**, 100 (2014).
84. Moore, B. *et al.* Monitoring the Vulnerability and Adaptation of Coastal Fisheries to Climate Change: Majuro Atoll, Republic of the Marshall Islands. *Report No. Assement Report N°2, July-August* **2013**, 112 (2014).
85. Moore, B. *et al.* Monitoring the Vulnerability and Adaptation of Coastal Fisheries to Climate Change: Northern Manus Outer Islands, Papua New Guinea. Report No. Assessment Report N°2, April-June 2014, 119 (2015).
86. Hubble, M. *The ecological significance of body size in tropical wrasses (Pisces: Labridae)*, James Cook University. (2003).
87. Pothin, K., Letourneur, Y. & Lecomte-Finiger, R. Age, growth and mortality of the tropical grouper *Epinephelus merra* (Pisces, Serranidae) on Réunion Island, SW Indian ocean. *Vie Milieu* **54**, 193–202 (2004).
88. Rhodes, K. L., Taylor, B. M. & McIlwain, J. L. Detailed demographic analysis of an *Epinephelus polyphekadion* spawning aggregation and fishery. *Mar. Ecol. Prog. Ser.* **421**, 183–198, https://doi.org/10.3354/meps08904 (2011).
89. Grandcourt, E. Demographic characteristics of selected epinepheline groupers (family: Serranidae; subfamily: Epinephelinae) from Aldabra Atoll, Seychelles. *Atoll Res. Bull.*, https://doi.org/10.5479/si.00775630.539.199 (2005).
90. Ohta, I., Akita, Y., Uehara, M. & Ebisawa, A. Age-based demography and reproductive biology of three Epinephelus groupers, *E. polyphekadion, E. tauvina*, and *E. howlandi* (Serranidae), inhabiting coral reefs in Okinawa. *Environ. Biol. Fishes* **100**, 1451–1467, https://doi.org/10.1007/s10641-017-0655-5 (2017).
91. Shimose, T. & Nanami, A. Age, growth, and reproductive biology of blacktail snapper, *Lutjanus fulvus*, around the Yaeyama Islands, Okinawa, Japan. *Ichthyol. Res.* **61**, 322–331, https://doi.org/10.1007/s10228-014-0401-3 (2014).
92. Mehanna, S., Osman, A., Farrag, M. & Osman, Y. Age and growth of three common species of goatfish exploited by artisanal fishery in Hurghada fishing area, Egypt. *J. Appl. Ichthyol.* **34**, 917–921, https://doi.org/10.1111/jai.13590 (2018).
93. Heupel, M. R. *et al.* Demography of a large exploited grouper, *Plectropomus laevis*: Implications for fisheries management. *Mar. Freshw. Res.* **61**, 184–195, https://doi.org/10.1071/MF09056 (2010).
94. Taylor, B. M., Gourley, J. & Trianni, M. S. Age, growth, reproductive biology and spawning periodicity of the forktail rabbitfish (*Siganus argenteus*) from the Mariana Islands. *Mar. Freshw. Res.* **68**, 1088–1097, https://doi.org/10.1071/MF16169 (2017).



## Acknowledgements

We thank the French Polynesian Urban Planning Department for providing the GIS shape files for the Polynesian coastline. The project was supported by the BNP Paribas Foundation (REEF SERVICES project), the Agence Nationale de la Recherche (ANR-17-CE32-006), the Fondation de France, a Make Our Planet Great Again Postdoctoral Grant (mopga-pdf-0000000144), and "Direction des ressources marines" (convention number 09419).


## Author contributions

This study was designed by F.M., J.W. and V.P. Field collections were made by F.M., S.J.B., J.C., J.M.C., S.D., P.F., R.G., A.M., Y.L., P.S., N.M.D.S. and V.P. Otolith analyses were conducted by F.M., J.W., G.D.S. and J.B. Funds were obtained by V.P., P.S., Y.L. and J.M.C. Statistical analyses were conducted by J.W. and N.M.D.S. Temperature data were compiled by J.V. (http://www.bio-oracle.org/).

## Competing interests

The authors declare no competing interests.

## Additional information

**Supplementary information** is available for this paper at https://doi.org/10.1038/s41597-020-00711-y.

**Correspondence** and requests for materials should be addressed to F.M. or V.P.

**Reprints and permissions information** is available at www.nature.com/reprints.

**Publisher's note** Springer Nature remains neutral with regard to jurisdictional claims in published maps and institutional affiliations.

# 8.2 Gut contents study

PLOS BIOLOGY

METHODS AND RESOURCES

## Delineating reef fish trophic guilds with global gut content data synthesis and phylogeny

**Valeriano Parravicini[1,2☯*], Jordan M. Casey[1,2,3☯], Nina M. D. Schiettekatte[1,2], Simon J. Brandl[1,2,3,4], Chloé Pozas-Schacre[1,2], Jérémy Carlot[1,2], Graham J. Edgar[5], Nicholas A. J. Graham[6], Mireille Harmelin-Vivien[7], Michel Kulbicki[8], Giovanni Strona[9], Rick D. Stuart-Smith[4]**

**1** PSL Université Paris: EPHE-UPVD-CNRS, USR 3278 CRIOBE, Université de Perpignan, Perpignan, France, **2** Laboratoire d'Excellence "CORAIL," Perpignan, France, **3** Department of Marine Science, University of Texas at Austin, Marine Science Institute, Port Aransas, Texas, United States of America, **4** Centre for the Synthesis and Analysis of Biodiversity (CESAB), Institut Bouisson Bertrand, Montpellier, France, **5** Institute for Marine and Antarctic Studies, University of Tasmania, Hobart, Tasmania, Australia, **6** Lancaster Environment Centre, Lancaster University, Lancaster, United Kingdom, **7** Aix-Marseille Université, Institut Méditerranéen d'Océanologie, CNRS/INSU, Marseille, France, **8** UMR Entropie, LabEx Corail, IRD, Université de Perpignan, Perpignan, France, **9** University of Helsinki, Department of Bioscience, Helsinki, Finland

☯ These authors contributed equally to this work.
* valeriano.parravicini@ephe.psl.eu



OPEN ACCESS

**Citation:** Parravicini V, Casey JM, Schiettekatte NMD, Brandl SJ, Pozas-Schacre C, Carlot J, et al. (2020) Delineating reef fish trophic guilds with global gut content data synthesis and phylogeny. PLoS Biol 18(12): e3000702. https://doi.org/10.1371/journal.pbio.3000702

**Academic Editor:** Pedro Jordano, Estacion Biologica de Doñana CSIC, SPAIN

**Received:** February 13, 2020

**Accepted:** December 3, 2020

**Published:** December 28, 2020



**Data Availability Statement:** All methods are described within the paper and its Supporting Information files. The data and the R code are available at the GitHub repository https://github.com/valerianoparravicini/Trophic_Fish_2020.

**Funding:** This research was funded by the BNP Paribas Foundation (Reef Services Project) and the French National Agency for Scientific Research (ANR; REEFLUX Project; ANR-17-CE32-0006). This research is product of the SCORE-REEF group funded by the Centre de Synthèse et d'Analyse sur

## Abstract

Understanding species' roles in food webs requires an accurate assessment of their trophic niche. However, it is challenging to delineate potential trophic interactions across an ecosystem, and a paucity of empirical information often leads to inconsistent definitions of trophic guilds based on expert opinion, especially when applied to hyperdiverse ecosystems. Using coral reef fishes as a model group, we show that experts disagree on the assignment of broad trophic guilds for more than 20% of species, which hampers comparability across studies. Here, we propose a quantitative, unbiased, and reproducible approach to define trophic guilds and apply recent advances in machine learning to predict probabilities of pairwise trophic interactions with high accuracy. We synthesize data from community-wide gut content analyses of tropical coral reef fishes worldwide, resulting in diet information from 13,961 individuals belonging to 615 reef fish. We then use network analysis to identify 8 trophic guilds and Bayesian phylogenetic modeling to show that trophic guilds can be predicted based on phylogeny and maximum body size. Finally, we use machine learning to test whether pairwise trophic interactions can be predicted with accuracy. Our models achieved a misclassification error of less than 5%, indicating that our approach results in a quantitative and reproducible trophic categorization scheme, as well as high-resolution probabilities of trophic interactions. By applying our framework to the most diverse vertebrate consumer group, we show that it can be applied to other organismal groups to advance reproducibility in trait-based ecology. Our work thus provides a viable approach to account for the complexity of predator–prey interactions in highly diverse ecosystems.

la Biodiversité (CESAB) of the Foundation pour la Recherche sur la Biodiversité (FRB) and the Agence Nationale de la Biodiversité (AFB). VP was supported by the Institut Universitaire de France (IUF), JMC was supported by a Make Our Planet Great Again Postdoctoral Grant (mopga-pdf-0000000144) and JC was supported by the French Polynesian Government (RisqueRecif project). The funders had no role in study design, data collection and analysis, decision to publish, or preparation of the manuscript.

**Competing interests:** The authors have declared that no competing interests exist.

**Abbreviations:** AUC, area under the receiver operating characteristic curve; HMD, herbivores, microvores, and detritivores; TSS, true skills statistics.

## Introduction

A fundamental goal in ecology is to understand the mechanisms behind the maintenance of biodiversity and ecosystem functioning [1,2]. Understanding the ecological niches of species and their role in ecosystems is central to this endeavor [3,4]. In fact, the degree of niche overlap among species can be a major determinant of relationships among species richness [5], ecosystem productivity [6–8], and vulnerability [9] since limited functional redundancy can make ecosystems more prone to lose entire energetic pathways [10–12]. With growing threats to flora and fauna worldwide, the need to quantify the impact of biodiversity loss has amplified the use of functional groups, which group species (and life history stages) that share common ecological characteristics and are often defined by coarse, categorical descriptors of species traits [13–16].

Natural systems are inherently complex, with almost innumerable, non-random linkages across an intricate network of ecological interactions [17]. Accounting for such complexity is critical to define energetic pathways and, ultimately, ecosystem functioning [18]. However, our understanding of even basic predator–prey interactions is limited for many ecosystems, and expert opinion does not adequately fill this knowledge gap [19]. To overcome this limitation, scientists have developed methods to infer the probability of ecological interactions based on species' evolutionary history and ecological traits [20–23]. However, predicting trophic interactions across the entire spectrum of potential predator–prey interactions often remains unresolved in hyperdiverse ecosystems. In these cases, categorical traits are frequently used as proxy of both ecosystem functioning and trophic structure [24].

Delineating the ecological niche with discrete categories has several operational advantages. First, grouping species into categories helps decompose highly complex ecosystems into comprehensible units, while traditional taxonomic analyses may be difficult to interpret. Second, ecological predictions tied to species are restricted to the geographic range of the species, whereas predictions of functional groups can be globally comparable. Third, the use of functional groups enables the quantification of functional metrics (e.g., functional richness and functional redundancy) from a standard community data matrix without complex manipulative experiments [25–27]. The promise of "user-friendly" metrics for functional ecology has encouraged the employment of trait-based data in community ecology; even with a paucity of empirical information, it is often assumed that experts can achieve accurate descriptions of the ecological niche of species [25,28,29].

Coral reefs, one of the most diverse ecosystems on Earth, have inspired a plethora of studies that assess ecosystem functioning. However, only few studies have attempted to categorize fluxes on a continuous gradient across an entire food web [30], and most studies use expert opinion to define simple functional groups. Indeed, recent efforts have compiled trait-based datasets for 2 major components of this ecosystem: corals and fishes [31,32]. For some traits, such as maximum body size in fishes, the compilation process is simple and accurate because unidimensional, quantitative data (e.g., maximum total length) are compiled in publicly accessible databases; however, when it comes to species' diet or behavior, obtaining consensual data is much more difficult. For example, dietary data are multidimensional (i.e., various prey items can be recorded across individuals), influenced by ontogenetic and spatio-temporal variables (i.e., life history, time, and location can incur dietary shifts), and prone to methodological differences and thus observer bias. Therefore, while some exceptions exist [30,33], our capacity to define coral reef trophic interactions still largely depends on discrete trophic categories defined by expert opinion [27].

Although experts sometimes agree on relevant traits to define trophic categories, there is often an implicit disagreement. Across the coral reef literature, the number and resolution of

reef fish trophic guilds substantially differs. Studies commonly define 3 [34] to 8 [35] trophic guilds, with particular ambivalence on the resolution at which to define herbivores and invertivores [36–39]. Among all trait classification schemes for reef fishes, only a few are openly accessible (e.g., [39,40]). Consequently, different research groups tend to employ proprietary classifications, with little possibility to cross-check and compare assigned traits. The classification of species into functional groups has advantages for our understanding of ecological patterns [42,43]. However, the lack of agreement and the limited transparency of trait-based datasets can conjure skepticism and inhibit the emergence of general patterns.

Here, we quantify expert agreement in the definition of coral reef fish trophic guilds and propose a novel, quantitative framework to delineate trophic guilds. Moreover, we test whether machine learning allows us to go beyond the definition of discrete categories, accurately predicting individual trophic interactions in hyperdiverse ecosystems. We compiled all quantitative, community-wide dietary analyses from several locations across the Indo-Pacific and the Caribbean. Then, we used network analysis to quantitatively define modules that correspond to trophic guilds and machine learning to infer pairwise trophic interactions. We then examined phylogenetic niche conservatism between species to predict trophic guilds and probabilities of pairwise trophic interactions for the global pool of coral reef fishes. Our framework is fully reproducible and can be extended and updated as new data become available.

## Materials and methods

### Assessment of expert agreement

We systematically searched Google Scholar, including papers since 2000, using the following keywords: "coral reefs" AND "reef fish" AND ("fish community" OR "fish assemblage") AND "diet" AND ("functional group" OR "functional trait" OR "functional entity" OR "trophic guild" OR "trophic group"). The search yielded 856 papers, which were individually assessed. We only kept studies performed at the community level that targeted all trophic levels. Most studies were excluded because they only included specific families or groups, or the data were not provided with the publication. When the data were not provided with the publications, we contacted authors with trophic classifications used widely used across the literature. We often found redundant results, with groups publishing several papers using the same classification scheme. In those cases, only the most recent reference was retained. Of the 856 papers, 163 papers were inaccessible (i.e., non-English language and/or data inaccessibility despite contacting the first author). Thus, 182 studies met the criteria of our initial assessment, which ultimately yielded 33 papers with independent trophic classifications (S1 Table).

The classifications were not uniform in terms of the number and nature of trophic guilds. In order to compare trophic guilds across publications, we first standardized the schemes by converting the original trophic categories into 5 broad trophic guilds: "herbivores and detritivores," "invertivores," "omnivores," "planktivores," and "piscivores." All classification schemes could be attributed to these categories with the exception of 8 papers that did not include either "omnivores" or "piscivores" as a category. In these cases, the comparison was only made across the 4 comparable guilds.

In order to assess expert agreement, we compared each possible pair of classifications that shared at least 50 species, generated a confusion matrix (also known as an error matrix; [50]), and measured agreement as the proportion of species with matching trophic guild assignments. We then calculated the average agreement between classification pairs for each trophic guild. Simplifying categories into 5 comparable, broad trophic guilds therefore reduced the number of trophic categories and naturally inflated agreement among authors; thus, our estimates of author agreement are conservative.

## Data collection on fish gut contents

To provide a quantitative definition of trophic guilds for reef fishes, we collected gut content data across the literature at the individual or species level for Elasmobranchii (i.e., cartilaginous fishes) and Actinopterygii (i.e., ray-finned fishes). We obtained dietary information from 5 published works: Hiatt and Strasburg (1960) for the Marshall Islands [51], Randall (1967) for Puerto Rico and the Virgin Islands [52], Hobson (1974) for Hawaii [53], Harmelin-Vivien (1979) for Madagascar [54], and Sano and colleagues (1984) for Okinawa [55]. In addition, we provide hitherto unpublished data on the gut contents of 3,015 individuals of 111 species collected in New Caledonia from 1984 to 2000.

All dietary information was based on visual gut content analysis that reported prey ingestion as a volumetric percentage or frequency. The data were standardized and analyzed as proportions. To our knowledge, the compiled dataset represents the first detailed synthesis of community-wide visual gut content analyses to infer the structure of coral reef food webs across ocean basins. A total of 13,961 non-empty fish guts belonging to 615 species were analyzed, and more than 1,200 different prey items were described across the original datasets.

First, fish species and family names were taxonomically verified and corrected with the R package *rfishbase* [56]. Only species with at least 10 non-empty guts were kept for further analysis. The taxonomic classification of each prey item was then obtained, and all non-informative and redundant items were discarded (e.g., unidentified fragments; "crustacea fragments" when co-occurring with an item already identified to a lower taxonomic level such as "shrimp"). Prey identification was highly heterogeneous across the 6 datasets, differing in taxonomic level and the use of common or scientific names (e.g., crabs versus Brachyura). In order to make the 6 datasets comparable, prey items were grouped into 38 ecologically informative prey groups (S2 Table). Items were generally assigned to groups corresponding to their phylum or class. Due to the high diversity and detailed descriptions of crustaceans, they were assigned to the level of order or superorder. Most groups follow official taxonomic classifications except for "detritus," "inorganic," and "zooplankton." In the West Indies dataset [52], items labelled as "Algae & Detritus" were assigned to both of the categories "detritus" and "benthic autotroph," and the percentage was equally divided in 2. The category "zooplankton" includes all eggs and larvae regardless of taxonomy.

## Definition of trophic guilds with network analysis

Of the 615 species with dietary information, 516 were present in only 1 location, 66 were collected in 2 locations, 25 in 3 locations, 7 in 4 locations, and only 1 across 5 locations. We tested whether there was a strong dietary difference in species present in more than 1 location by creating a quantitative bipartite network [57] where fish species at each location were linked to the 38 prey groups. This network was weighted so that edge weights represent the proportional contribution of each prey group to the diet of a species at a given location.

In order to identify network modules that correspond to reef fish trophic guilds and their ingested prey, we used the maximization of the weighted network modularity based on weighted bipartite networks [58]. Due to the high occurrence of accidental predation in reef fishes, we used weighted networks to define modules so that rare or accidental prey would not drive the definition of trophic guilds.

Since the modularity maximization algorithm has an initial random step, it may converge to different (although similar) suboptimal solutions each time the analysis is performed, which is common across several optimization algorithms, such as simulated annealing [59]. To guarantee reproducibility and reduce the risk of basing our analysis on an outlier, we performed the modularity maximization 500 times and retained the medoid solution, which was

identified as the solution with the highest similarity to the other 499 modules. Similarity between classifications was assessed as the variation of information, which is an accepted metric to compare multiple clustering results [60]. Overall, 68% of the species found in more than 1 location belonged to the same module. Therefore, we considered the regional effect to be minor and performed the analysis on the global network, ignoring regional variability and increasing the number of individuals per species.

## Phylogenetic conservatism of trophic guilds

We extracted the phylogenetic position of the 615 species used for the definition of trophic guilds through the Fish Tree of Life [61]. A total of 603 out of 615 species were available in the Fish Tree of Life, but only 535 species had verified phylogenetic information. For the taxa available in the Fish Tree of Life without verified phylogenetic information, we retrieved the pseudo-posterior distribution of 100 synthetic stochastically resolved phylogenies where missing taxa were placed according to taxonomy using the function *fishtree_complete_phylogeny()* in the R package *fishtree* [62].

We quantified the phylogenetic conservatism of trophic guilds by calculating the phylogenetic statistic δ, which uses a Bayesian approach for discrete variables [63]. The δ statistic can be arbitrarily large with a high level of variation, depending on the number of species and trait levels. To evaluate the significance of the δ statistic, we applied a bootstrapping approach where we quantified δ 100 times after randomly shuffling the trait values.

We then fitted a multinomial phylogenetic regression to predict fish trophic guild according to phylogeny and body size with the R package *brms* [64]. We used a multinomial logit link function. As such, the probability of a particular trophic guild is computed as follows:

$$Pr(k|mu_1, mu_2, \ldots, mu_k) = \frac{mu_k}{\sum_1^k \exp(mu_i)} \quad (1)$$

with $mu_k$ defined as

$$mu_1 = 0, mu_{k[2:8} = \beta_{0k} + \beta_{1k}\log(\text{sizemax}) + \gamma_{0\text{phy}\times k}, \quad (2)$$

where $\beta_{0k}$ is the category-specific fixed-effect intercept, $\beta_{1k}$ is the slope for the natural transformed maximum body size for each category $k$, and $\gamma_{0\text{phy}\times k}$ is the matrix of random effect coefficients that account for intercept variation based on relatedness as described by the phylogeny for each diet category $k$. We used uninformative priors and ran the model for 3 chains, each with 6,000 iterations and a warm-up of 1,000 iterations. We visualized the fitted probabilities for each trophic guild with a phylogenetic tree, including the 535 species with verified phylogenetic positions using the R package *ggtree* [63]. Next, we used our model to predict the most likely trophic guild for the global pool of reef fish species. For the extrapolation, we selected all species within reef fish families with more than 1 representative species (but we also included *Zanclus cornutus*, which is the only species in the family Zanclidae), which resulted in 50 families. Further, we only selected species with a maximum length greater than 3 cm, which was the maximum size of the smallest fish in our compiled database. This selection process resulted in a list of 4,554 reef fish species.

Currently, no streamlined method exists to predict traits for new species from a phylogenetic regression model. We circumvented this issue by extracting draws of the phylogenetic effect ($\gamma_{0\text{phy}\times k}$) for each species included in the model. We subsequently predicted the phylogenetic effects for missing species with the help of the function *phyEstimate* from the R package *picante* [65]. This function uses phylogenetic ancestral state estimation to infer trait values for new species on a phylogenetic tree by re-rooting the tree to the parent edge to predict the node [66]. We repeated this inference across 2,000 draws. Per draw, we randomly sampled 1 of the

100 trees. Then, we predicted the probability of each species to be assigned to each diet category by combining the predicted phylogenetic effects with the global intercept and slopes for maximum body size for each draw. Finally, we summarized all diet category probabilities per species by taking the mean and standard deviation across all 2,000 draws.

We quantified the total standard deviation (i.e., the square root of the quadratic sum of the standard deviations in each category) and the negentropy value, a measure of certainty calculated by subtracting 1 from the entropy value (i.e., uncertainty). Thus, the negentropy value lies between 0 and 1, and the higher the value, the higher the certainty for trophic guild assignment (i.e., if a given species has a high probability of assignment to a dietary category, the negentropy value will be high).

Finally, we conducted a cross validation to validate our extrapolation of trophic guilds to the global pool of fish species. Specifically, we repeated the extrapolation approach (as described above) 535 times, each time leaving out 1 species and predicting the trophic guild of that species. We then compared this prediction to the original assigned trophic guild and calculated the accuracy of each of the 8 trophic guild predictions.

### Prediction of trophic interactions with machine learning

To complement the assignment of discrete trophic guilds, we also modeled pairwise trophic interactions. In accordance with previous studies that infer trophic interactions by matching species traits or phylogenetic position [19,21,23,67,68], we predicted the probability of pairwise trophic interactions between the 535 reef fish species and the 38 prey categories in our dataset. Building on Laigle and colleagues [21], we developed a new machine learning approach to extract the reef fish phylogenetic tree from the Fish Tree of Life [61] and obtain phylogenetic eigenvector maps for each species, which were used as explanatory variables in our models [69]. We then predicted the probability of trophic interactions between fish species and prey categories based on phylogenetic position and maximum body size. Specifically, using the R package *h2o* [70], we employed an ensemble modeling approach based on 3 models calibrated with 10-fold cross validation: extreme gradient boosting [71], boosted regression trees [72], and random forest [73]. A cross-validated general linear model was used as a super-learner to create an optimal weighted average (i.e., an ensemble) of the predictions from the 3 models. The 3 models were implemented using 2,000 regression trees and default settings to reduce overfitting. Model performance was assessed using the area under the receiver operating characteristic curve (AUC) and true skills statistics (TSS) [74].

In addition to applying this analysis to our dataset, we also tested whether this technique could reliably predict pairwise trophic interactions for new species and locations. To this aim, we calibrated the models with only 5 locations, excluding the dataset from New Caledonia. We then used the New Caledonia dataset to assess model performance. As detailed above, after cross validation, we used our model to predict probabilities of pairwise trophic interactions between the 4,554 reef fish species and the 38 prey categories.

## Results

### Assessment of expert agreement

We evaluated expert agreement among 33 distinct and independent trophic guild classifications by comparing the classification schemes in pairs. Considering the broadness of the expert-assigned categories, we found low agreement. The median agreement between pairs, expressed as the proportion of species with matching trophic group assignments, was 78% (Fig 1). For approximately 50% of the pairwise comparisons, at least a quarter of the species were attributed to different trophic groups. In the most severe disagreement, the proportion of

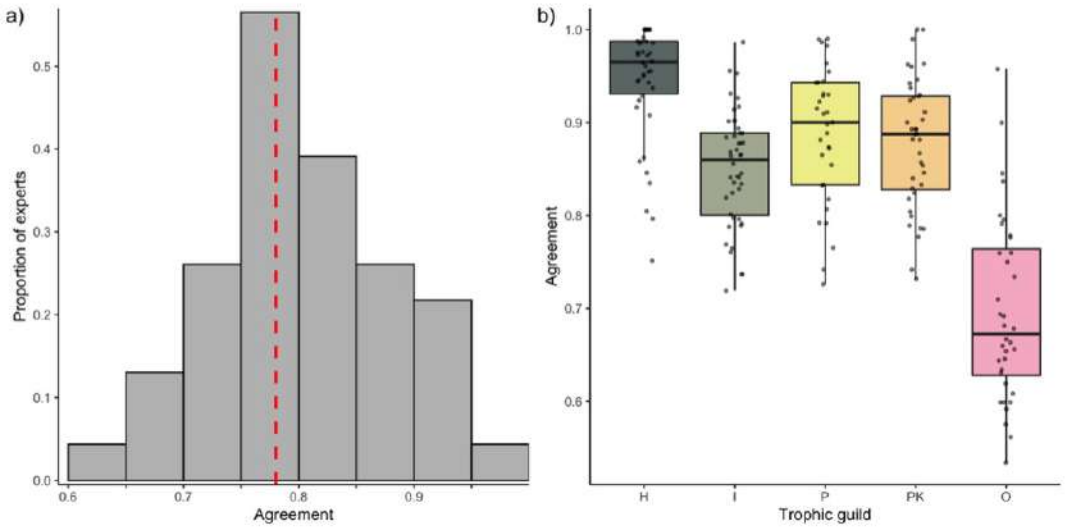


**Fig 1. Expert agreement on trophic guild assignment.** (A) The distribution of the agreement (i.e., proportion of species assigned to the same trophic category) across the 32 comparisons between pairs of experts. The red dotted line represents the median. (B) Agreement between pairs of experts by trophic category. The data underlying this figure may be found in https://github.com/valerianoparravicini/Trophic_Fish_2020. *H*, herbivores and detritivores; *I*, invertivores; *O*, omnivores; *P*, piscivores; *PK*, planktivores.

https://doi.org/10.1371/journal.pbio.3000702.g001

mismatched assignments reached 38%. In addition, expert agreement differed depending on the trophic group. Expert disagreement on the classification of "herbivores and detritivores" was low, with an average expert agreement of 95% and pairs of expert disagreement only reaching 20% (Fig 1B). In contrast, "omnivores" showed the highest mismatch, with experts agreeing on an average of only 70% of the species and peaks of disagreement between expert pairs reaching 47% (Fig 1B).

Expert agreement was variable and often homogeneously distributed around the mean for all the trophic categories. Therefore, the high agreement between a few combinations of experts did not necessarily exclude peaks of disagreement (Fig 1B). The analysis of individual confusion matrices between pairs of experts revealed high heterogeneity (Fig 2). For example, Morais and Bellwood were generally in agreement with Mouillot and colleagues [36] (across 89% of the 515 species in common), while Mouillot and colleagues [36] agreed with Stuart-Smith and colleagues [39] across only 68% of the 2,211 species in common.

Surprisingly, there was also a high heterogeneity in groups with high disagreement (i.e., multiple alternative assignments for species not assigned to the same trophic group). Species classified as "invertivores" according to 1 expert were considered "omnivores," "piscivores," or "planktivores" according to other classification schemes (Fig 2). Similarly, species considered "omnivores" by 1 expert were alternatively considered "invertivores," "herbivores and detritivores," or "planktivores" by another expert.

## Definition of trophic guilds with network analysis

We defined trophic guilds by identifying modules (i.e., combinations of predators and prey) that maximize the weighted modularity of the global network [58]. Our analysis robustly

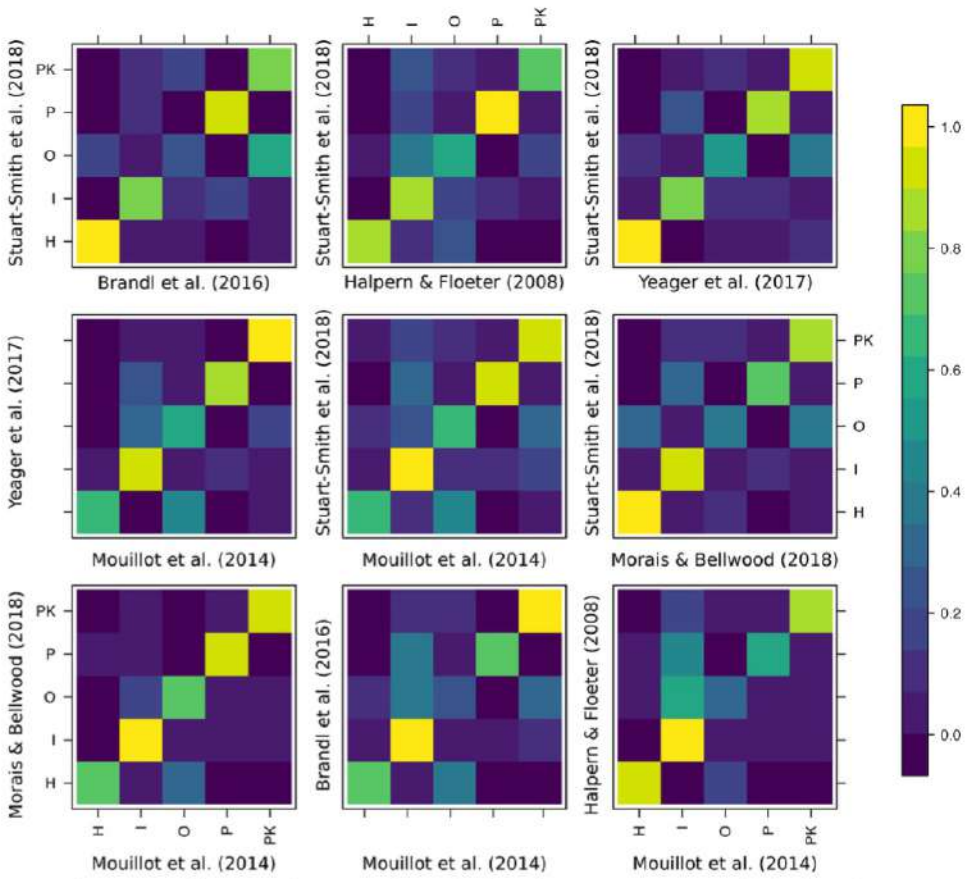


**Fig 2. Confusion matrices of the agreement between pairs of experts that share at least 200 species in common and define all 5 trophic categories.** Colors represent proportions of species in each trophic guild as classified by experts. The data underlying this figure may be found in https://github.com/valerianoparravicini/Trophic_Fish_2020. *H*, herbivores and detritivores; *I*, invertivores; *O*, omnivores; *P*, piscivores; *PK*, planktivores.

https://doi.org/10.1371/journal.pbio.3000702.g002

identified 8 distinct modules that correspond to different trophic guilds (Fig 3). We identified these trophic guilds as

1. "Sessile invertivores": species predominantly feeding on Asteroidea, Bryozoa, Cirripedia, Holothuroidea, Porifera, and Tunicata;
2. "Herbivores, microvores, and detritivores (HMD)": species primarily feeding on autotrophs, detritus, inorganic material, foraminifera, and phytoplankton;
3. "Corallivores": species predominantly feeding on Anthozoa and Medusozoa;
4. "Piscivores": species primarily feeding on Actinopterygii and Cephalopoda;

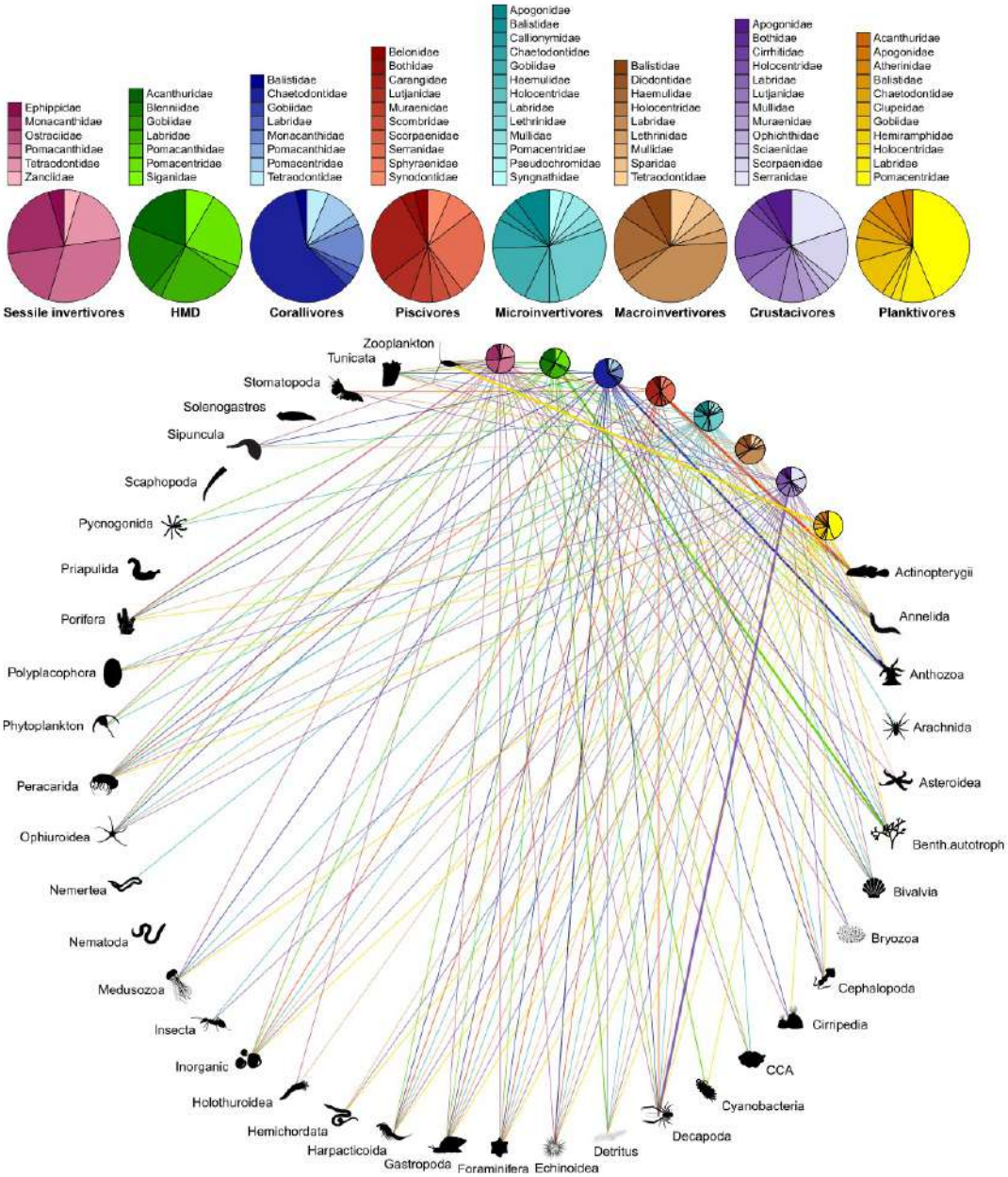
Ephippidae
Monacanthidae
Ostraciidae
Pomacanthidae
Tetraodontidae
Zanclidae
Sessile invertivores
Acanthuridae
Blenniidae
Gobiidae
Labridae
Pomacanthidae
Pomacentridae
Siganidae
HMD
Balistidae
Chaetodontidae
Gobiidae
Labridae
Monacanthidae
Pomacanthidae
Pomacentridae
Tetraodontidae
Corallivores
Belonidae
Bothidae
Carangidae
Lutjanidae
Muraenidae
Scombridae
Scorpaenidae
Serranidae
Sphyraenidae
Synodontidae
Piscivores
Apogonidae
Balistidae
Callionymidae
Chaetodontidae
Gobiidae
Haemulidae
Holocentridae
Labridae
Lethrinidae
Mullidae
Pomacentridae
Pseudochromidae
Syngnathidae
Microinvertivores
Balistidae
Diodontidae
Haemulidae
Holocentridae
Labridae
Lethrinidae
Mullidae
Sparidae
Tetraodontidae
Macroinvertivores
Apogonidae
Bothidae
Cirrhitidae
Holocentridae
Labridae
Lutjanidae
Mullidae
Muraenidae
Ophichthidae
Sciaenidae
Scorpaenidae
Serranidae
Crustacivores
Acanthuridae
Apogonidae
Atherinidae
Balistidae
Chaetodontidae
Clupeidae
Gobiidae
Hemiramphidae
Holocentridae
Labridae
Pomacentridae
Planktivores
Zooplankton
Tunicata
Stomatopoda
Solenogastres
Sipuncula
Scaphopoda
Pycnogonida
Priapulida
Porifera
Polyplacophora
Phytoplankton
Peracarida
Ophiuroidea
Nemertea
Nematoda
Medusozoa
Insecta
Inorganic
Holothuroidea
Hemichordata
Harpacticoida
Gastropoda
Foraminifera
Echinoidea
Detritus
Decapoda
Cyanobacteria
CCA
Cirripedia
Cephalopoda
Bryozoa
Bivalvia
Benth.autotroph
Asteroidea
Arachnida
Anthozoa
Annelida
Actinopterygii

**Fig 3. Bipartite network including 615 fish species (grouped into 8 trophic guilds) and their prey items (grouped into 38 categories; see S1 Table).** The relative proportion of each prey category consumed by each trophic guild corresponds with the width of each interaction bar. The pie charts show the relative proportion of fish families within each trophic guild. The data underlying this figure may be found in https://github.com/valerianoparravicini/Trophic_Fish_2020. HMD, herbivores, microvores, and detritivores.

https://doi.org/10.1371/journal.pbio.3000702.g003

5. "Microinvertivores": species primarily feeding on Arachnida, Pycnogonida, small Crustacea (Peracarida), and worms (Annelida, Hemichordata, Nematoda, Nemertea, and Sipuncula);
6. "Macroinvertivores": species primarily feeding on Mollusca (Bivalvia, Gastropoda, Polyplacophora, and Scaphopoda), Echinoidea, and Ophiuroidea;
7. "Crustacivores": species primarily feeding on large Crustacea (Decapoda and Stomatopoda);
8. "Planktivores": species mainly feeding on zooplankton, cyanobacteria and Harpacticoida.

## Phylogenetic conservatism of trophic guilds

To evaluate the significance of the phylogenetic statistic value ($\delta = 9.37$), we applied a bootstrapping approach and quantified $\delta$ after randomly shuffling the trait values 100 times. The median $\delta$ of these null models was 0.000199 (95% confidence interval [0.000196, 0.000204]), indicating a strong phylogenetic signal associated with the 8 trophic guilds.

Phylogeny and maximum body size were sufficient to correctly predict the trophic guild of 97% of the species in our dataset. For most families, there was strong phylogenetic conservatism, which resulted in the high confidence of these predictions (Fig 4). Within some families, however, closely related species displayed distinct dietary preferences, as showcased by high negentropy values for families such as Balistidae, Diodontidae, and Labridae.

Given its high predictive performance, we used our Bayesian phylogenetic model to extrapolate the probability of all reef fish species belonging to the 8 trophic guilds and assigned the trophic guild with the highest probability (S3 Table). Using leave-one-out cross validation, the final accuracy of this approach was 65%, which is comparable with other phylogenetically extrapolated traits applications, such as those involving microbial traits [75].

By inspecting the confusion matrix of the leave-one-out cross validation, we obtained more detailed information on the accuracy of the trophic guild predictions (S1 Fig). Most categories were well predicted with our extrapolation approach. In particular, the "sessile invertivores," "HMD", and "piscivores" trophic guilds were predicted with high accuracy (77%, 75%, and 73% correct predictions, respectively). The confusion matrix also provided information on incorrectly assigned categories. For example, when "piscivores" were incorrectly assigned, they were mostly classified as "crustacivores." However, the network plot revealed that the fishes classified as "piscivores" also fed on crustaceans (mostly decapods), so this "incorrect assignment" was grounded in ecological reality and reflected uncertainty within the model. Additionally, the "microinvertivores" trophic guild had the highest proportion of inaccurate predictions (52% correct predictions). Here, species were often misclassified as "crustacivores" or "planktivores."

## Prediction of trophic interactions with machine learning

Using machine learning, our model achieved high predictive performance in quantifying probabilities of pairwise trophic interactions (AUC = 0.99; TSS = 0.94). After calibration with 535 fish species and 3,479 trophic interactions, our model accurately identified 3,410 of these interactions, demonstrating an exceptionally low rate of false negative interactions. In addition, the model accurately predicted absent trophic interactions, with a false positive

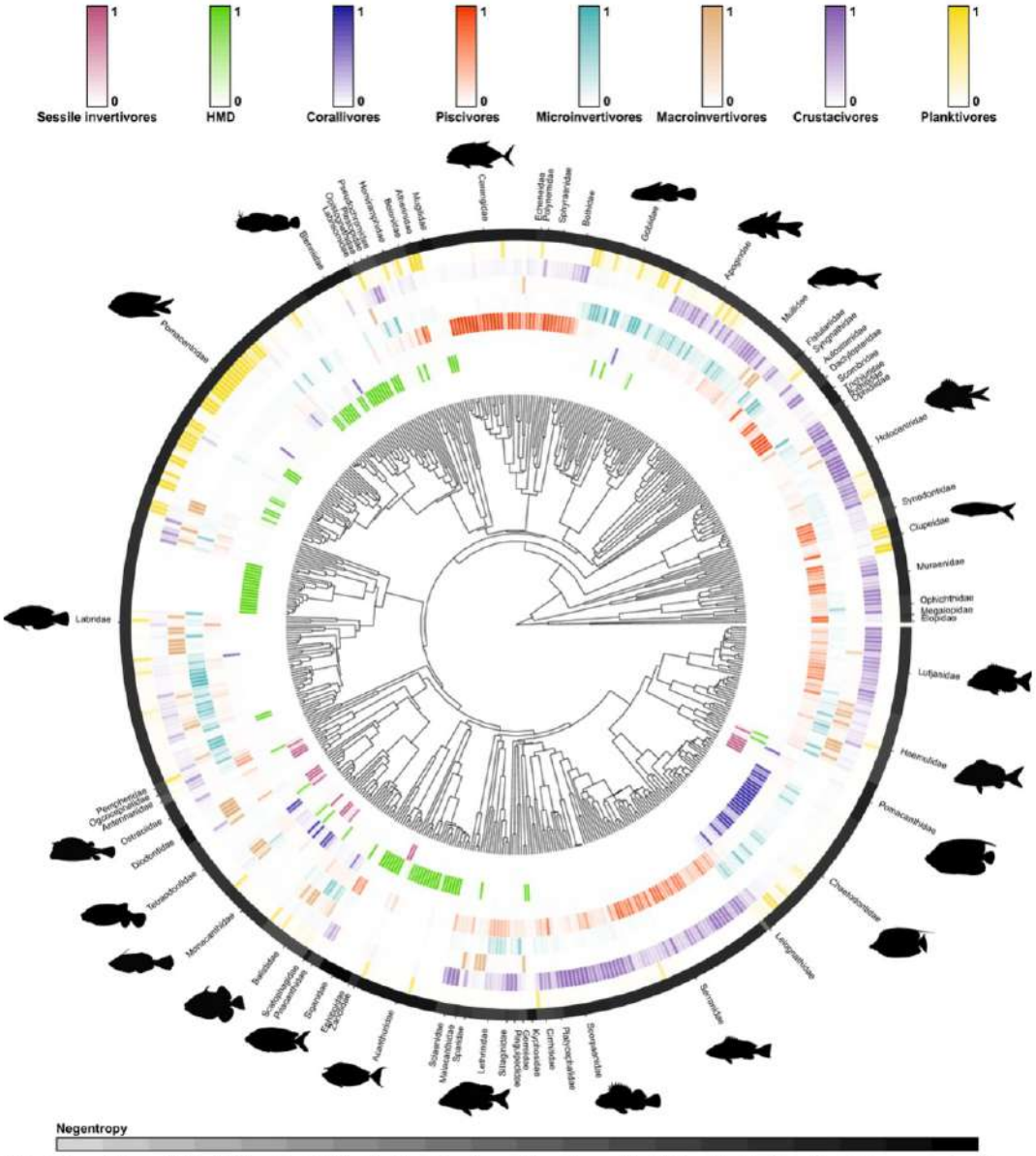


**Fig 4. Phylogenetic tree of 535 reef fish species with fitted trophic guild assignments based on empirical dietary data.** Trophic guild predictions were made with a Bayesian multinomial phylogenetic regression. The probability of trophic guild assignments for each species is visualized with color scales (depicted above the

phylogenetic tree), with darker colors indicating a higher probability of assignment. In the outer black ring, each distinct segment represents a fish family (with silhouettes included for the most speciose families). Uncertainty of overarching trophic guild assignment for each fish family is visualized with negentropy values (i.e., reverse entropy); thus, darker shades indicate a higher degree of certainty of trophic guild assignment. Fish shapes are available at https://github.com/simonjbrandl/fishape/tree/master/shapes. The data underlying this figure may be found in https://github.com/valerianoparravicini/Trophic_Fish_2020.

https://doi.org/10.1371/journal.pbio.3000702.g004

interaction rate of only 3.6%. When the model was calibrated with only 5 locations, excluding the data from New Caledonia, the model still performed well (AUC = 0.82; TSS = 0.52). The model correctly detected 82% of the trophic interactions in the New Caledonia dataset, with a false positive interaction rate of 27%. Based on the high predictive performance of the model, we used the full model with all 6 locations to predict the probability of pairwise trophic interactions on a continuous spectrum between the 4,554 reef fish species with available phylogenetic information and our 38 prey categories (S4 Table).

## Discussion

Functional ecology requires standardized and reproducible classification schemes to characterize species' niches [76–78]. Rather than relying on expert opinion for the assignment of trophic groups, which often results in variable assignments, we demonstrate that the categorization of discrete trophic guilds and pairwise trophic interactions can be achieved with a quantitative, reproducible framework grounded in empirical data across biogeographic regions. We employed network analysis to partition 535 tropical coral reef fish species into 8 trophic guilds based on a synthesis of globally distributed, community-wide fish dietary analyses, and then we applied a Bayesian phylogenetic model that predicts trophic guilds based on phylogeny and body size, attaining a 5% misclassification error. Moreover, using a machine learning approach, we demonstrate that a continuous spectrum of trophic interactions can also be accurately predicted based on phylogeny and body size. Our framework represents the first implementation of a quantifiable classification scheme for coral reef fishes, which form some of the most diverse vertebrate communities worldwide.

Unlike traditional trophic guilds based on expert opinion [36,37,39,44–49], our trophic approaches are reproducible, provide uncertainty estimates, and can be updated and improved in the future with additional dietary information. In an effort to encourage new, accessible benchmarks to categorize fish trophic guilds, our classification of discrete trophic guilds and probabilities of pairwise trophic interactions are publicly available with this publication. Given the growing number of trait-based studies that assign trophic guilds to understand and monitor ecosystem functioning in our changing world, it is imperative that we establish comparable and reproducible trophic classification frameworks.

Our findings highlight the discordance of expert opinion in the assignment of trophic guilds and the necessity to develop quantifiable and reproducible classification schemes that are accessible to the wider scientific community (c.f. [79]). Despite broad similarities between the trophic guilds reported in the literature and the groups identified by our analysis, our classification scheme reveals a higher level of partitioning among invertebrate-feeding fishes as compared to previously proposed trophic guilds. In the past, invertebrate-feeding fishes were generally considered "sessile invertivores," "mobile invertivores," or "omnivores" (e.g., [37,38,48]), but we identify 5 distinct invertebrate-feeding groups: "corallivores," "sessile invertivores," "microinvertivores," "macroinvertivores," and "crustacivores." Given the extreme numerical dominance of invertebrates in coral reef environments [80], the collapse of all invertebrate-feeders into 2 or 3 trophic groups was possibly an artefact of expert oversight, and the expansion of invertebrate-feeding trophic guilds to 5 groups stands to improve ecological resolution of fishes feeding on invertebrate prey.

In contrast to the high resolution achieved within invertebrate-feeding groups, our classification achieved limited resolution among the nominally herbivorous species, "HMD." Across the literature, past classification schemes often separate macroalgal feeders, turf algae croppers, and detritivores (e.g., [36,37,40,41]). The lack of precision in our framework is rooted in the difficulty in distinguishing algae, microbes, and detritus within the alimentary tract of fishes, resulting in the pooling of these ingested items during the visual assessment of fish gut contents. Consequently, species classified as "HMD" may have fundamentally different foraging strategies, dietary preferences, and evolutionary histories [81], which can greatly impact their functional role on coral reefs (e.g., [82]). Thus, while our identified trophic guilds promise increased resolution for fishes that consume animal prey, our identified groupings may not adequately capture consumer–producer dynamics on coral reefs. Emerging techniques, such as gut content metabarcoding, may provide the additional resolution needed to further discriminate prey items in this group [83,84]. Alternatively, coupling diet categorization with other traits, such as feeding behavior, may help to pinpoint the variety of feeding modes that exist within the "HMD" trophic guild.

While our delineation of trophic guilds is applicable to functional studies that employ discrete categories, the continuous output of trophic interaction probabilities holds promise for a variety of other approaches, such as trophic network analyses. On coral reefs, previous studies have employed network analysis to examine human impacts on coral reef food webs [30,33]. However, these studies only incorporate local fish gut content data, which limits their spatial application. Larger-scale network analyses exist (e.g. [85]), but they are predominantly based on co-occurrence patterns and solely consider piscivores, thus neglecting a large portion of marine food webs, which are typically dominated by invertebrate-feeders. Therefore, our demonstrated ability to predict trophic interactions based on phylogeny and body size opens new avenues for marine food web research. Moreover, the high performance of the reduced model to predict pairwise trophic interactions in New Caledonia confirms the potential of our approach to predict probabilities of local trophic interactions for entire food webs.

Our findings add to recent evidence that evolutionary history (i.e., phylogenetic relatedness) is essential to evaluate the ecological traits of fishes (c.f. [86–88]). Recently, taxonomy and body size have been revealed as important predictors of fish diet composition and size structure [89,90], and in the highest resolution analyses of coral reef fish diet, taxonomic family was a better predictor of fish diet than broad trophic guilds [83]. Given the exceedingly low rate of misclassification error in our predictions, we posit that phylogeny is a critical variable that should be consistently considered in the assignment of trophic guilds for reef fishes. Across a plethora of organismal groups (e.g., birds [91], reptiles [92], fishes [93,94], insects [95], parasites [96], and plants [97]), phylogenetic niche conservatism has been alternately supported and dismissed. In our case, when examining fish trophic guilds using 38 prey categories, phylogenetic conservatism is readily apparent at a relatively coarse dietary resolution and may allow us to extrapolate trophic assignments to closely related consumer species and potentially extend this framework to fishes inhabiting other habitats. However, with increasing dietary resolution beyond what is detailed in the present study, phylogenetic signals may weaken [98] since even closely related species may exhibit dietary specialization [83,99]. In the future, with the availability of higher resolution of dietary information, phylogenetic niche conservatism can be easily examined within our framework.

With ongoing environmental and ecological change, a firm grasp on shifts in ecosystem functioning will depend on the reliable assignment of organismal traits [15] and the comparability of trait-based approaches across space, time, and independent studies [77]. Especially in complex, hyperdiverse environments such as coral reefs, it is imperative to standardize how we measure and report these traits to prevent idiosyncratic results based on subjective trait

assignments [27,100]. Trophic guilds are among the most commonly applied trait to assess ecosystem functioning because they directly relate to energy and nutrient fluxes across trophic levels. Thus, our standardized framework represents a major step forward for coral reef functional ecology, while heeding the call for openly accessible, reproducible trait databases [31,78,101]. As trait-based ecology continues to be used to examine disturbances and implement management strategies, our cohesive and accessible framework can provide key insights into the trajectory of coral reef communities.

Further, our results can serve as the foundation for an online platform that permits researchers to collate, update, and utilize trait-based data on coral reef fishes. Similar to current initiatives across the entire tree of life [78], the creation of an online, user-maintained dietary database will facilitate collaboration and traceability in trait-based reef fish research. One challenge will lie in merging visual fish gut content analysis databases with molecular data, such as gut content DNA metabarcoding (e.g., [83]), and biochemical data, such as stable isotope analysis (e.g., [102]), and short-chain fatty acid profiles (e.g., [103]), which indicate nutritional assimilation rather than the simple ingestion of prey items [81]. Despite this challenge, accessibility to a large breadth of reef fish dietary information would improve our framework. Our proposed trophic guilds and probabilities of trophic interactions are model predictions, so they are only as reliable as the underlying dietary data. In addition, these predictions may suffer from extrapolation biases; for example, if limited dietary information exists across species within a taxonomic group, extrapolations to closely related species are more likely to be assigned erroneous trophic guilds. Consequently, an ongoing, extensive compilation of dietary traits across coral reef fishes will continuously improve our predicted trophic guild assignments and pairwise trophic interactions.

Finally, our proposed framework is not limited to coral reef fishes; indeed, trophic guild assignments can be quantifiable, reproducible, and transparent, with the inclusion of uncertainty metrics, across many organismal groups. However, the standardization of trophic guilds is sorely lacking across the ecological literature [79], especially based on quantitative data (e.g., [104]). We posit that a similar approach can be readily applied across a multitude of organisms and environments. In fact, given the paucity of dietary information available for coral reef fishes in comparison to other organisms, particularly birds and mammals, building rigorous, global trophic classification schemes for many other organisms should be readily achievable within our framework. With a quantitative, transparent trophic classification scheme that can be augmented over time and is applicable across ecological systems, our framework represents a significant advancement for trait-based ecology and a viable approach to monitor ecosystem dynamics into the future [78].

## Supporting information

**S1 Fig. Confusion matrix showcasing the accuracy of the 8 trophic guild predictions from the leave-one-out cross validation based on the extrapolation of the Bayesian phylogenetic model.** Trophic guilds include (1) "sessile invertivores," (2) "herbivores, microvores, and detritivores," (3) "corallivores," (4) "piscivores," (5) "microinvertivores," (6) macroinvertivores, (7) "crustacivores," and (8) "planktivores." The data underlying this figure may be found in https://github.com/valerianoparravicini/Trophic_Fish_2020.
(PNG)

**S1 Table. Prey categories used to define the trophic guilds of coral reef fishes.**
(CSV)

**S2 Table. Summary of the 33 papers used to evaluate expert agreement on reef fish trophic guilds.** The column named "Fishes" refers to the number of fish species included in that study.
(CSV)

**S3 Table. Global extrapolation to infer the probability of each of the 4554 reef fish species to belong to the 8 trophic guilds.** The mean and the standard deviation (e.g., p1-8_m, and p1-8_sd) of the posterior probabilities are reported alongside with the mean and standard deviation of the negentropy.
(CSV)

**S4 Table. Probability of trophic interaction between the 4554 reef fish species and the 38 prey categories according to the extrapolation performed by the machine learning approach.**
(CSV)

## Acknowledgments

We thank the Centre de Recherche Insulaires et Observatoire de l'Environnement (CRIOBE) in Perpignan, France and all the researchers who have made their fish gut content data and/or trait-based fish trophic guild assignments publicly available for use by the wider scientific community

## Author Contributions

**Conceptualization:** Valeriano Parravicini, Jordan M. Casey, Nina M. D. Schiettekatte.

**Data curation:** Valeriano Parravicini, Jordan M. Casey, Nina M. D. Schiettekatte, Chloé Pozas-Schacre.

**Formal analysis:** Valeriano Parravicini, Nina M. D. Schiettekatte.

**Funding acquisition:** Valeriano Parravicini.

**Investigation:** Valeriano Parravicini, Jordan M. Casey, Nina M. D. Schiettekatte, Simon J. Brandl, Chloé Pozas-Schacre, Jérémy Carlot, Graham J. Edgar, Nicholas A. J. Graham, Mireille Harmelin-Vivien, Michel Kulbicki, Giovanni Strona, Rick D. Stuart-Smith.

**Methodology:** Valeriano Parravicini, Jordan M. Casey, Nina M. D. Schiettekatte, Simon J. Brandl, Chloé Pozas-Schacre.

**Project administration:** Valeriano Parravicini.

**Supervision:** Valeriano Parravicini, Jordan M. Casey.

**Visualization:** Valeriano Parravicini, Jordan M. Casey, Nina M. D. Schiettekatte, Simon J. Brandl.

**Writing – original draft:** Valeriano Parravicini, Jordan M. Casey.

**Writing – review & editing:** Valeriano Parravicini, Jordan M. Casey, Nina M. D. Schiettekatte, Simon J. Brandl, Chloé Pozas-Schacre, Jérémy Carlot, Graham J. Edgar, Nicholas A. J. Graham, Mireille Harmelin-Vivien, Michel Kulbicki, Giovanni Strona, Rick D. Stuart-Smith.

## References

1. Tilman D, Isbell F, Cowles JM. Biodiversity and Ecosystem Functioning. Annu Rev Ecol Evol Syst. 2014; 45:471–93. https://doi.org/10.1146/annurev-ecolsys-120213-091917

2. Reiss J, Bridle JR, Montoya JM, Woodward G. Emerging horizons in biodiversity and ecosystem functioning research. Trends Ecol Evol. 2009; 24:505–14. https://doi.org/10.1016/j.tree.2009.03.018 PMID: 19595476
3. Whittaker RH, Levin SA, Root RB. Niche, Habitat, and Ecotope. Am Nat. 1973; 107:321–38.
4. Finke DL, Snyder WE. Niche partitioning increases resource exploitation by diverse communities. Science. 2008; 321:1488–90. https://doi.org/10.1126/science.1160854 PMID: 18787167
5. Levine JM, HilleRisLambers J. The importance of niches for the maintenance of species diversity. Nature. 2009; 461:254–7. https://doi.org/10.1038/nature08251 PMID: 19675568
6. Poisot T, Mouquet N, Gravel D. Trophic complementarity drives the biodiversity-ecosystem functioning relationship in food webs. Ecol Lett. 2013; 16:853–61. https://doi.org/10.1111/ele.12118 PMID: 23692591
7. Loreau M, Naeem S, Inchausti P, Bengtsson J, Grime JP, Hector A, et al. Biodiversity and Ecosystem Functioning: Current Knowledge and Future Challenges. Science. 2001; 294:804. https://doi.org/10.1126/science.1064088 PMID: 11679658
8. Terborgh JW. Toward a trophic theory of species diversity. Proc Natl Acad Sci U S A. 2015; 112:11415. https://doi.org/10.1073/pnas.1501070112 PMID: 26374788
9. Mouillot D, Bellwood DR, Baraloto C, Chave J, Galzin R, Harmelin-Vivien M, et al. Rare Species Support Vulnerable Functions in High-Diversity Ecosystems. Mace GM, editor. PLoS Biol. 2013; 11: e1001569. https://doi.org/10.1371/journal.pbio.1001569 PMID: 23723735
10. Rosenfeld JS. Functional redundancy in ecology and conservation. Oikos. 2002; 98:156–62. https://doi.org/10.1034/j.1600-0706.2002.980116.x
11. Wohl DL, Arora S, Gladstone JR. Functional redundancy supports biodiversity and ecosystem function in a closed and constant environment. Ecology. 2004; 85:1534–40. https://doi.org/10.1890/03-3050
12. Brandl SJ, Bellwood DR. Individual-based analyses reveal limited functional overlap in a coral reef fish community. Hays G, editor. J Anim Ecol. 2014; 83:661–70. https://doi.org/10.1111/1365-2656.12171 PMID: 24164060
13. Wilman H, Belmaker J, Simpson J, de la Rosa C, Rivadeneira MM, Jetz W. EltonTraits 1.0: Species-level foraging attributes of the world's birds and mammals. Ecology. 2014; 95:2027–7. https://doi.org/10.1890/13-1917.1
14. Kraft NJB, Valencia R, Ackerly DD. Functional traits and niche-based tree community assembly in an Amazonian forest. Science. 2008; 322:580. https://doi.org/10.1126/science.1160662 PMID: 18948539
15. McGill B, Enquist B, Weiher E, Westoby M. Rebuilding community ecology from functional traits. Trends Ecol Evol. 2006; 21:178–85. https://doi.org/10.1016/j.tree.2006.02.002 PMID: 16701083
16. De Deyn GB, Cornelissen JHC, Bardgett RD. Plant functional traits and soil carbon sequestration in contrasting biomes. Ecol Lett. 2008; 11:516–31. https://doi.org/10.1111/j.1461-0248.2008.01164.x PMID: 18279352
17. Jordano P. Chasing Ecological Interactions. PLoS Biol. 2016; 14:e1002559. https://doi.org/10.1371/journal.pbio.1002559 PMID: 27631692
18. Thompson RM, Brose U, Dunne JA, Hall RO, Hladyz S, Kitching RL, et al. Food webs: reconciling the structure and function of biodiversity. Trends Ecol Evol. 2012; 27:689–97. https://doi.org/10.1016/j.tree.2012.08.005 PMID: 22959162
19. Gravel D, Poisot T, Albouy C, Velez L, Mouillot D. Inferring food web structure from predator-prey body size relationships. Freckleton R, editor. Methods Ecol Evol. 2013; 4:1083–90. https://doi.org/10.1111/2041-210X.12103
20. Sander EL, Wootton JT, Allesina S. Ecological Network Inference From Long-Term Presence-Absence Data. Sci Rep. 2017; 7. https://doi.org/10.1038/s41598-017-07009-x PMID: 28769079
21. Laigle I, Aubin I, Digel C, Brose U, Boulangeat I, Gravel D. Species traits as drivers of food web structure. Oikos. 2018; 127:316–26. https://doi.org/10.1111/oik.04712
22. Pichler M, Boreux V, Klein A, Schleuning M, Hartig F. Machine learning algorithms to infer trait-matching and predict species interactions in ecological networks. Carvalheiro L, editor. Methods Ecol Evol. 2020; 11:281–93. https://doi.org/10.1111/2041-210X.13329
23. Dalla Riva GV, Stouffer DB. Exploring the evolutionary signature of food webs' backbones using functional traits. Oikos. 2016; 125:446–56. https://doi.org/10.1111/oik.02305
24. Flynn DFB, Mirotchnick N, Jain M, Palmer MI, Naeem S. Functional and phylogenetic diversity as predictors of biodiversity–ecosystem-function relationships. Ecology. 2011; 92:1573–81. https://doi.org/10.1890/10-1245.1 PMID: 21905424

25. Schmera D, Podani J, Heino J, Erős T, Poff NL. A proposed unified terminology of species traits in stream ecology. Freshwater Science. 2015; 34:823–30. https://doi.org/10.1086/681623

26. Belmaker J, Parravicini V, Kulbicki M. Ecological traits and environmental affinity explain Red Sea fish introduction into the Mediterranean. Glob Chang Biol. 2013; 19:1373–82. https://doi.org/10.1111/gcb.12132 PMID: 23505033

27. Brandl SJ, Rasher DB, Côté IM, Casey JM, Darling ES, Lefcheck JS, et al. Coral reef ecosystem functioning: eight core processes and the role of biodiversity. Front Ecol Environ. 2019; 17:445–54. https://doi.org/10.1002/fee.2088

28. Nash KL, Watson RA, Halpern BS, Fulton EA, Blanchard JL. Improving understanding of the functional diversity of fisheries by exploring the influence of global catch reconstruction. Sci Rep. 2017; 7:10746. https://doi.org/10.1038/s41598-017-10723-1 PMID: 28878250

29. Aubin I, Venier L, Pearce J, Moretti M. Can a trait-based multi-taxa approach improve our assessment of forest management impact on biodiversity? Biodivers Conserv. 2013; 22:2957–75. https://doi.org/10.1007/s10531-013-0565-6

30. Gilarranz LJ, Mora C, Bascompte J. Anthropogenic effects are associated with a lower persistence of marine food webs. Nat Commun. 2016; 7. https://doi.org/10.1038/ncomms10737 PMID: 26867790

31. Madin JS, Anderson KD, Andreasen MH, Bridge TCL, Cairns SD, Connolly SR, et al. The Coral Trait Database, a curated database of trait information for coral species from the global oceans. Scientific Data. 2016; 3:160017. https://doi.org/10.1038/sdata.2016.17 PMID: 27023900

32. Stuart-Smith RD, Bates AE, Lefcheck JS, Duffy JE, Baker SC, Thomson RJ, et al. Integrating abundance and functional traits reveals new global hotspots of fish diversity. Nature. 2013; 501:539–42. https://doi.org/10.1038/nature12529 PMID: 24067714

33. Bascompte J, Melian CJ, Sala E. Interaction strength combinations and the overfishing of a marine food web. Proc Natl Acad Sci. 2005; 102:5443–7. https://doi.org/10.1073/pnas.0501562102 PMID: 15802468

34. McClanahan TR. A coral reef ecosystem-fisheries model: impacts of fishing intensity and catch selection on reef structure and processes. Ecol Model. 1995; 80:1–19. https://doi.org/10.1016/0304-3800(94)00042-G

35. Ferreira CEL, Floeter SR, Gasparini JL, Ferreira BP, Joyeux JC. Trophic structure patterns of Brazilian reef fishes: a latitudinal comparison. J Biogeogr. 2004; 31:1093–106. https://doi.org/10.1111/j.1365-2699.2004.01044.x

36. Mouillot D, Villeger S, Parravicini V, Kulbicki M, Arias-Gonzalez JE, Bender M, et al. Functional over-redundancy and high functional vulnerability in global fish faunas on tropical reefs. Proc Natl Acad Sci. 2014; 111:13757–62. https://doi.org/10.1073/pnas.1317625111 PMID: 25225388

37. Parravicini V, Villéger S, McClanahan TR, Arias-González JE, Bellwood DR, Belmaker J, et al. Global mismatch between species richness and vulnerability of reef fish assemblages. Byers JJ, editor. Ecol Lett. 2014; 17:1101–10. https://doi.org/10.1111/ele.12316 PMID: 24985880

38. Micheli F, Mumby PJ, Brumbaugh DR, Broad K, Dahlgren CP, Harborne AR, et al. High vulnerability of ecosystem function and services to diversity loss in Caribbean coral reefs. Biol Conserv. 2014; 171:186–94. https://doi.org/10.1016/j.biocon.2013.12.029

39. Stuart-Smith RD, Brown CJ, Ceccarelli DM, Edgar GJ. Ecosystem restructuring along the Great Barrier Reef following mass coral bleaching. Nature. 2018; 560:92–6. https://doi.org/10.1038/s41586-018-0359-9 PMID: 30046108

40. Bejarano S, Pardede S, Campbell SJ, Hoey AS, Ferse SCA. Herbivorous fish rise as a destructive fishing practice falls in an Indonesian marine national park. Ecol Appl. 2019; 29. https://doi.org/10.1002/eap.1981 PMID: 31349375

41. Siqueira AC, Bellwood DR, Cowman PF. The evolution of traits and functions in herbivorous coral reef fishes through space and time. Proc R Soc B Biol Sci. 2019; 286:20182672. https://doi.org/10.1098/rspb.2018.2672 PMID: 30963846

42. Mouillot D, Graham NAJ, Villéger S, Mason NWH, Bellwood DR. A functional approach reveals community responses to disturbances. Trends Ecol Evol. 2013; 28:167–77. https://doi.org/10.1016/j.tree.2012.10.004 PMID: 23141923

43. Mason NWH, de Bello F. Functional diversity: a tool for answering challenging ecological questions. J Veg Sci. 2013; 24:777–80. https://doi.org/10.1111/jvs.12097

44. Brandl SJ, Emslie MJ, Ceccarelli DM, T. Richards Z. Habitat degradation increases functional originality in highly diverse coral reef fish assemblages. Ecosphere. 2016; 7. https://doi.org/10.1002/ecs2.1557

45. Halpern BS, Floeter SR. Functional diversity responses to changing species richness in reef fish communities. Mar Ecol Prog Ser. 2008; 364:147–56.

46. Graham NAJ, Chabanet P, Evans RD, Jennings S, Letourneur Y, Aaron MacNeil M, et al. Extinction vulnerability of coral reef fishes: Reef fish extinction vulnerability. Ecol Lett. 2011; 14:341–8. https://doi.org/10.1111/j.1461-0248.2011.01592.x PMID: 21320260

47. Morais RA, Bellwood DR. Global drivers of reef fish growth. Fish Fish. 2018; 19:874–89. https://doi.org/10.1111/faf.12297

48. Yeager LA, Deith MCM, McPherson JM, Williams ID, Baum JK. Scale dependence of environmental controls on the functional diversity of coral reef fish communities. Glob Ecol Biogeogr. 2017; 26:1177–89. https://doi.org/10.1111/geb.12628

49. Newman MJH, Paredes GA, Sala E, Jackson JBC. Structure of Caribbean coral reef communities across a large gradient of fish biomass. Ecol Lett. 2006; 9:1216–27. https://doi.org/10.1111/j.1461-0248.2006.00976.x PMID: 17040324

50. Stehman SV. Selecting and interpreting measures of thematic classification accuracy. Remote Sens Environ. 1997; 62:77–89. https://doi.org/10.1016/S0034-4257(97)00083-7

51. Hiatt RW, Strasburg DW. Ecological relationships of the fish fauna on coral reefs of the Marshall Islands. Ecol Monogr. 1960; 30:65–127. https://doi.org/10.2307/1942181

52. Randall JE. Food habits of reef fishes of the West Indies. Hawaii Institute of Marine Biology. 1967:1–94.

53. Hobson ES. Feeding relationships of teleostean fishes on coral reefs in Kona. Hawaii Fishery Bulletin. 1974; 72:915–1031.

54. Harmelin-Vivien M. Ichtyofaune des recifs coralliens de Tulear (Madagascar): ecologie et relations trophiques. L'Université d'Aix-Marseille II. 1979.

55. Sano M, Shimizu M, Nose Y. Food habits of teleostean reef fishes in Okinawa Island, southern Japan. The University of Tokyo; 1984.

56. Boettiger C, Lang DT, Wainwright PC. rfishbase: exploring, manipulating and visualizing FishBase data from R. J Fish Biol. 2012; 81:2030–9. https://doi.org/10.1111/j.1095-8649.2012.03464.x PMID: 23130696

57. Barrat A, Barthelemy M, Pastor-Satorras R, Vespignani A. The architecture of complex weighted networks. Proc Natl Acad Sci. 2004; 101:3747–52. https://doi.org/10.1073/pnas.0400087101 PMID: 15007165

58. Beckett SJ. Improved community detection in weighted bipartite networks. R Soc Open Sci. 2016; 3:140536. https://doi.org/10.1098/rsos.140536 PMID: 26909160

59. Serafini P. Simulated Annealing for Multi Objective Optimization Problems. In: Tzeng G, Wang H, Wen U, Yu P, editors. Multiple Criteria Decision Making. New York: Springer; 1994. pp. 283–292.

60. Meilă M. Comparing clusterings—an information based distance. J Multivar Anal. 2007; 98:873–95. https://doi.org/10.1016/j.jmva.2006.11.013

61. Rabosky DL, Chang J, Title PO, Cowman PF, Sallan L, Friedman M, et al. An inverse latitudinal gradient in speciation rate for marine fishes. Nature. 2018; 559:392–5. https://doi.org/10.1038/s41586-018-0273-1 PMID: 29973726

62. Chang J, Rabosky DL, Smith SA, Alfaro ME. An R package and online resource for macroevolutionary studies using the ray-finned fish tree of life. Methods Ecol Evol. 2019. https://doi.org/10.1111/2041-210X.13182

63. Yu G, Smith DK, Zhu H, Guan Y, Lam TT-Y. ggtree: an R package for visualization and annotation of phylogenetic trees with their covariates and other associated data Methods in Ecology and Evolution. 2017; 8:28–36. https://doi.org/10.1111/2041-210X.12628

64. Bürkner P-C. brms: An R Package for Bayesian Multilevel Models Using Stan. J Stat Softw; Vol 1, Issue 1 (2017). 2017. Available: https://www.jstatsoft.org/v080/i01

65. Kembel SW, Cowan PD, Helmus MR, Cornwell WK, Morlon H, Ackerly DD, et al. Picante: R tools for integrating phylogenies and ecology. Bioinformatics. 2010; 26:1463–4. https://doi.org/10.1093/bioinformatics/btq166 PMID: 20395285

66. Garland T, Ives AR. Using the Past to Predict the Present: Confidence Intervals for Regression Equations in Phylogenetic Comparative Methods.: 19.

67. Morales-Castilla I, Matias MG, Gravel D, Araújo MB. Inferring biotic interactions from proxies. Trends Ecol Evol. 2015; 30:347–56. https://doi.org/10.1016/j.tree.2015.03.014 PMID: 25922148

68. Pomeranz JPF, Thompson RM, Poisot T, Harding JS. Inferring predator–prey interactions in food webs. Lecomte N, editor. Methods in Ecology and Evolution. 2018 [cited 3 Aug 2020]. https://doi.org/10.1111/2041-210X.13125

69. Guénard G, Legendre P, Peres-Neto P. Phylogenetic eigenvector maps: a framework to model and predict species traits. Freckleton R, editor. Methods Ecol Evol. 2013; 4:1120–31. https://doi.org/10.1111/2041-210X.12111

70. LeDell E, Gill N, Aiello S, Fu A, Candel A, Click C, et al. h2o: R Interface for the "H2O" Scalable Machine Learning Platform. 2020. Available: https://CRAN.R-project.org/package=h2o

71. Chen T, Guestrin C. XGBoost: A Scalable Tree Boosting System. Proceedings of the 22nd ACM SIGKDD International Conference on Knowledge Discovery and Data Mining. 2016; 785–794. https://doi.org/10.1145/2939672.2939785

72. Elith J, Leathwick JR, Hastie T. A working guide to boosted regression trees. J Anim Ecol. 2008; 77:802–13. https://doi.org/10.1111/j.1365-2656.2008.01390.x PMID: 18397250

73. Breiman L. Random forests. Mach Learn. 2001; 45:5–32.

74. Allouche O, Tsoar A, Kadmon R. Assessing the accuracy of species distribution models: prevalence, kappa and the true skill statistic (TSS): Assessing the accuracy of distribution models. J Appl Ecol. 2006; 43:1223–32. https://doi.org/10.1111/j.1365-2664.2006.01214.x

75. Goberna M, Verdú M. Predicting microbial traits with phylogenies. ISME J. 2016; 10:959–67. https://doi.org/10.1038/ismej.2015.171 PMID: 26371406

76. Schneider FD, Fichtmueller D, Gossner MM, Güntsch A, Jochum M, König-Ries B, et al. Towards an ecological trait-data standard. Methods Ecol Evol. 2019; 10:2006–19. https://doi.org/10.1111/2041-210X.13288

77. Weiss KCB, Ray CA. Unifying functional trait approaches to understand the assemblage of ecological communities: synthesizing taxonomic divides. Ecography. 2019; 42:2012–20. https://doi.org/10.1111/ecog.04387

78. Gallagher R, Falster DS, Maitner B, Salguero-Gomez R, Vandvik V, Pearse W, et al. The Open Traits Network: Using Open Science principles to accelerate trait-based science across the Tree of Life. https://doi.org/10.32942/osf.io/kac45

79. Cano-Barbacil C, Radinger J, García-Berthou E. Reliability analysis of fish traits reveals discrepancies among databases. Freshwater Biology. 2020 [cited 11 Feb 2020]. https://doi.org/10.1111/fwb.13469

80. Glynn PW, Enochs IC. Invertebrates and Their Roles in Coral Reef Ecosystems. In: Dubinsky Z, Stambler N, editors. Coral Reefs: An Ecosystem in Transition. Dordrecht: Springer Netherlands; 2011. pp. 273–325.

81. Clements KD, German DP, Piché J, Tribollet A, Choat JH. Integrating ecological roles and trophic diversification on coral reefs: multiple lines of evidence identify parrotfishes as microphages. Biol J Linn Soc. 2016. https://doi.org/10.1111/bij.12914

82. Brandl SJ, Bellwood DR. Microtopographic refuges shape consumer-producer dynamics by mediating consumer functional diversity. Oecologia. 2016; 182:203–17. https://doi.org/10.1007/s00442-016-3643-0 PMID: 27147547

83. Casey JM, Meyer CP, Morat F, Brandl SJ, Planes S, Parravicini V. Reconstructing hyperdiverse food webs: Gut content metabarcoding as a tool to disentangle trophic interactions on coral reefs. Mahon A, editor. Methods Ecol Evol. 2019; 10:1157–70. https://doi.org/10.1111/2041-210X.13206

84. Brandl SJ, Casey JM, Meyer CP. Dietary and habitat niche partitioning in congeneric cryptobenthic reef fish species. Coral Reefs. 2020 [cited 28 Jan 2020]. https://doi.org/10.1007/s00338-020-01892-z

85. Albouy C, Archambault P, Appeltans W, Araújo MB, Beauchesne D, Cazelles K, et al. The marine fish food web is globally connected. Nature Ecology & Evolution. 2019; 3:1153–61. https://doi.org/10.1038/s41559-019-0950-y PMID: 31358950

86. Westoby M. Phylogenetic ecology at world scale, a new fusion between ecology and evolution. Ecology. 2006; 87:S163–5. https://doi.org/10.1890/0012-9658(2006)87[163:peawsa]2.0.co;2 PMID: 16922311

87. Floeter SR, Bender MG, Siqueira AC, Cowman PF. Phylogenetic perspectives on reef fish functional traits: Evolution of functional traits. Biol Rev. 2018; 93:131–51. https://doi.org/10.1111/brv.12336 PMID: 28464469

88. Siqueira AC, Morais RA, Bellwood DR, Cowman PF. Trophic innovations fuel reef fish diversification. Nat Commun. 2020; 11. https://doi.org/10.1038/s41467-020-16498-w PMID: 32472063

89. Soler G, Thomson R, Stuart-Smith R, Smith A, Edgar G. Contributions of body size, habitat and taxonomy to predictions of temperate Australian fish diets. Mar Ecol Prog Ser. 2016; 545:239–49. https://doi.org/10.3354/meps11584

90. Soler GA, Edgar GJ, Stuart-Smith RD, Smith ADM, Thomson RJ. Predicting the diet of coastal fishes at a continental scale based on taxonomy and body size. J Exp Mar Biol Ecol. 2016; 480:1–7. https://doi.org/10.1016/j.jembe.2016.03.017

91. Lovette IJ, Hochachka WM. Simultaneous effects of phylogenetic niche conservatism and competition on avian community structure. Ecology. 2006; 87:S14–28. https://doi.org/10.1890/0012-9658(2006)87[14:seopnc]2.0.co;2 PMID: 16922299

92. Knouft JH, Losos JB, Glor RE, Kolbe JJ. Phylogenetic analysis of the evolution of the niche in lizards of the Anolis sagrei group. Ecology. 2006; 87:S29–38. https://doi.org/10.1890/0012-9658(2006)87[29:paoteo]2.0.co;2 PMID: 16922300

93. Peres-Neto PR. Patterns in the co-occurrence of fish species in streams: the role of site suitability, morphology and phylogeny versus species interactions. Oecologia. 2004; 140:352–60. https://doi.org/10.1007/s00442-004-1578-3 PMID: 15138880

94. Gajdzik L, Aguilar-Medrano R, Frédérich B. Diversification and functional evolution of reef fish feeding guilds. Ecol Lett. 2019. https://doi.org/10.1111/ele.13219 PMID: 30648337

95. Weiblen GD, Webb CO, Novotny V, Basset Y, Miller SE. Phylogenetic dispersion of host use in a tropical insect herbivore community. Ecology. 2006; 87:S62–75. https://doi.org/10.1890/0012-9658(2006)87[62:pdohui]2.0.co;2 PMID: 16922303

96. Mouillot D. R. Krasnov B, I. Shenbrot G, J. Gaston K, Poulin R. Conservatism of host specificity in parasites. Ecography. 2006; 29:596–602. https://doi.org/10.1111/j.0906-7590.2006.04507.x

97. Silvertown J, Dodd M, Gowing D, Lawson C, McConway K. Phylogeny and the hierarchical organization of plant diversity. Ecology. 2006; 87:S39–49. https://doi.org/10.1890/0012-9658(2006)87[39:pathoo]2.0.co;2 PMID: 16922301

98. Mazel F, Pennell MW, Cadotte MW, Diaz S, Dalla Riva GV, Grenyer R, et al. Prioritizing phylogenetic diversity captures functional diversity unreliably. Nat Commun. 2018; 9. https://doi.org/10.1038/s41467-018-05126-3 PMID: 30038259

99. Leray M, Alldredge AL, Yang JY, Meyer CP, Holbrook SJ, Schmitt RJ, et al. Dietary partitioning promotes the coexistence of planktivorous species on coral reefs. Mol Ecol. 2019; 28:2694–710. https://doi.org/10.1111/mec.15090 PMID: 30933383

100. Bellwood DR, Streit RP, Brandl SJ, Tebbett SB. The meaning of the term 'function' in ecology: A coral reef perspective. Funct Ecol. 2019; 33:948–61. https://doi.org/10.1111/1365-2435.13265

101. Jeliazkov A, Mijatovic D, Chantepie S, Andrew N, Arlettaz R, Barbaro L, et al. A global database for metacommunity ecology, integrating species, traits, environment and space. Scientific Data. 2020; 7. https://doi.org/10.1038/s41597-019-0344-7 PMID: 31913312

102. Eurich J, McCormick M, Jones G. Habitat selection and aggression as determinants of fine-scale partitioning of coral reef zones in a guild of territorial damselfishes. Mar Ecol Prog Ser. 2018; 587:201–15. https://doi.org/10.3354/meps12458

103. Choat HJ, Clements KD, Robbins WD. The trophic status of herbivorous fishes on coral reefs: I. Dietary analyses Marine Biology. 2002; 140:613–23. https://doi.org/10.2527/2002.80102726x PMID: 12413096

104. González-Salazar C, Martínez-Meyer E, López-Santiago G. A hierarchical classification of trophic guilds for North American birds and mammals. Revista Mexicana de Biodiversidad. 2014; 85:931–41. https://doi.org/10.7550/rmb.38023

## 8.3 Science popularisation (French)

# Les derniers gardiens de la côte

*Jérémy Carlot, Mélanie Biausque, Alessio Rovere, Emmanuel Dormy & Valeriano Parravicini*

Plus de 275 millions de personnes vivent à moins de 10 kilomètres des côtes et à moins de 30 kilomètres des récifs coralliens. Les populations en bord de littoral peuvent ainsi jouir d'une protection côtière plus ou moins efficace grâce aux assemblages coralliens situés au large. En effet, les récifs agissent comme des brise-lames submergés et cassent les vagues, dissipant ainsi l'énergie venue du large, avant qu'elles n'inondent les communautés côtières. De récentes études montrent que pour que l'énergie des vagues soit dissipée, la combinaison de deux facteurs géomorphologiques est indispensable. D'une part, plus l'espace entre la vague et le récif est faible, plus l'énergie sera dissipée. D'autre part, plus le récif possède de relief – on parle alors de complexité structurelle – plus il sera à même de contrer l'énergie provenant des vagues. Un récif optimal à l'obstruction de l'énergie houlomotrice sera donc un récif haut et complexe.

Hélas cette protection est menacée par les activités anthropiques et le changement climatique. Une augmentation moyenne du niveau de la mer de plus de 83 centimètres est attendue pour la fin du siècle. Cette élévation augmente l'espace entre la vague à la surface et les récifs coralliens sur les fonds. Si la croissance corallienne n'est pas suffisante, l'énergie provenant des vagues ne sera plus dissipée, conduisant à des épisodes d'inondation lors de fortes tempêtes. Le changement climatique entraîne également une augmentation de la température des océans et leur acidification. C'est ainsi que nous assistons à des phénomènes de blanchissements coralliens de plus en plus soutenus. En 2016, par exemple, l'épisode de blanchissement le plus long et le plus destructeur jamais enregistré a eu lieu. Pendant cette période, plus de 70 % des récifs coralliens du monde entier ont été endommagés, ce qui a considérablement diminué leur complexité structurelle.

Ainsi, plusieurs études amènent à penser que la hauteur des vagues post-récifs (c'est-à-dire celles, de taille bien plus modeste, se reformant derrière les récifs en direction de la côte grâce aux résidus énergétiques) seront plus importantes à l'avenir, ce qui pourrait amener à des épisodes d'inondations ou de réduction de l'espace littoral. Par exemple, de nouvelles prédictions envisagent, avec une probabilité de 50 %, qu'avec nos conditions actuelles – diminution de la couverture corallienne couplée à une élévation du niveau de la mer – la hauteur des vagues post-récifs de Teahupo'o (l'un des sites de surf les plus connus au monde, en Polynésie française) pourrait augmenter d'un facteur 1,5 d'ici 2100. Ces mêmes estimations prédisent par la suite la perte de près de 50 % des plages sableuse d'ici la fin du siècle.

Cette menace croissante a entraîné au cours des deux dernières décennies la construction de structures de défense contre l'érosion côtière comme des digues, des enrochements ou des revêtements. Cependant, des interdictions ou des restrictions importantes concernant l'artificialisation du littoral ont été mises en place dû au fait que les aménagements artificiels pourraient endommager les habitats adjacents ou nuire aux espèces qui y vivent. Les récifs en bonne santé apparaissent alors comme le meilleur mécanisme de protection côtière et il devient plus que primordial de les conserver.

## RÉSUMÉ

L'augmentation des températures de surface à l'échelle mondiale a agi comme un effet boule de neige, augmentant à son tour le niveau moyen marin. De plus, l'augmentation combinée de la température et du niveau de la mer menace les récifs coralliens. Les blachissements sont de plus en plus fréquents et intenses et agissent à grande échelle. Par conséquent, les couvertures coralliennes dans le monde entier diminuent, menaçant l'avenir des populations côtières. Dans ce doctorat, je quantifie l'impact du changement climatique sur les récifs coralliens de Mo'orea (Polynésie française). Je définis 1) comment la topographie (aussi appelée complexité structurelle) évolue et 2) le taux d'accrétion potentiel des récifs coralliens entre 2005 et 2016. Mes résultats montrent que la complexité structurelle moyenne à Mo'orea a retrouvé son niveau d'avant la perturbation en 2016. Malheureusement, je démontre également que les taux d'accrétion restent inférieurs aux prévisions du GIEC concernant l'élévation du niveau de la mer (scénario 4.5), menaçant les populations côtières de Mo'orea d'ici 2100 si nos émissions de carbone ne diminuent pas drastiquement

## MOTS-CLÉS

Protection côtière, montée des eaux, récifs coralliens, Polynésie française, taux d'accrétion, scénarios du GIEC, changements globaux.

## ABSTRACT

The increase in global surface temperatures has acted as a snowball effect, increasing, in turn, the global mean sea level (GMSL). More worryingly, the combined rise in temperature and sea level threatens coral reefs, one of the most diverse and productive ecosystems worldwide. Indeed, coral cover is being reduced by various stresses such as cyclones and bleaching events. The latter are becoming increasingly frequent and intense, acting on large scales. As a result, coral covers worldwide are declining, threatening the future of coastal populations. In this Ph.D., I quantify the impact of climate change on coral reefs in Mo'orea (French Polynesia). I define 1) how the topography (also called structural complexity) evolves and 2) the potential accretion rate of coral reefs between 2005 and 2016. My results show that average structural complexity in Mo'orea recovered to pre-disturbance levels by 2016. Unfortunately, I also demonstrate that accretion rates remain below the IPCC's predictions for sea-level rise (scenario 4.5), threatening Mo'orea's coastal populations by 2100 if our carbon emissions do not decrease drastically.

## KEYWORDS

Coastal protection, sea level rise, coral reefs, French Polynesia, accretion rate, IPCC scenarios, global changes.